

Effect of alkali, aluminium and equilibration time on calcium-silicate-hydrates

Présentée le 29 juin 2022

Faculté des sciences et techniques de l'ingénieur
Laboratoire des matériaux de construction
Programme doctoral en science et génie des matériaux

pour l'obtention du grade de Docteur ès Sciences

par

Yiru YAN

Acceptée sur proposition du jury

Dr J. C. Plummer, président du jury
Prof. K. Scrivener, Prof. B. Lothenbach, directrices de thèse
Dr M. Zajac, rapporteur
Dr S. Grangeon, rapporteur
Dr J. Tits, rapporteur

Acknowledgements

The first acknowledgments go to my Ph.D. supervisors, Barbara Lothenbach, and Karen Scrivener.

Barbara, thank you for giving me the opportunity to pursue my Ph.D. at Empa. Thank you for all the guidance, encouragement and support during my PhD. Thank you for sharing with me the knowledge about cement and particularly the thermodynamics. Your enthusiasm, passion, vision and hardworking in research always helped me to go through the challenges in my study, your genuineness and cheerful personality inspired me of being a better human being. It was a great privilege and honor to work with you, and a special thank you for the support at the end of the thesis for correcting and commenting my thesis or the paper drafts. Thank you for everything!

Karen, thank you also for giving me the opportunity to carry out this thesis. I'm very grateful for your continuous support, wealth of knowledge, constant encouragement and all the valuable discussions during these four years and took the time to read and give me comments on the journal manuscripts.

I am also very grateful to being a part of CASH II project. A profound thanks to Dr. Dimitrii Kulik and Dr. George-Dan Miron for their help and constructive suggestions about thermodynamic modelling. A particular acknowledgement goes to Dr. Jørgen Skibsted and Dr. Sheng-Yu Yang for their valuable discussion and for always finding time to help on the solid state NMR analysis. Dr. Christian Ludwig is acknowledged for insightful discussions in the CASH II meetings during the last four years.

I would like to thank Dr. Thomas Huthwelker and Dr. Camelia Borca for their help during SLS beamtime. I also thank Dr. Guoqing Geng, Dr. Daniel Jansen, Dr. Krassimir Garbev and Dr. Jiaqi Li for helpful discussion about XANES, crystallography and Raman of C-S-H.

I am highly obliged to my colleagues at Empa for their presence, company and contributions to shaping this amazing four years. I am so lucky to be part of this team. Love you all. Special thanks go to Prof. Pietro Lura for his financial support of my last year's study and his concerns during my PhD as the department leader. To Dr. Frank Winnefeld for his guidance on XRD especially on profile fitting and Rietveld analysis as well as the language corrections

Acknowledgements

of the manuscripts, to Dr. Andreas Leeman for his valuable discussion about Raman. To Dr. Andreas Borgschulte, Dr. Rico Muff and Beatrice Fischer for their help with Raman and FTIR experiments. Thank you Dr. Daniel Rentsch for your help in solid state NMR. To Dr. Bin Ma, whom I would like to thank for his contribution to one of the sub-projects of my PhD work, and for his constant willingness to share his knowledge. To Dr. Zhenguo Shi for the helpful discussions about C-S-H and ASR. To Dr. Ellina Bernard for the introduction of CEC, help on NMR analysis, fruitful discussions about C-S-H and her encouraging conversations. And to Dr. Malene Thostrup Pedersen, my former office mate, for her help on XRD Rietveld analysis and NMR and also her supportive attitude. To Dr. Ines Collings for her contribution to crystallite size analysis and the helpful discussions, to Alessio Di Giacomo and Dr. Emilie L'Hôpital for their efforts in preparing the C-A-S-H samples and providing valuable experimental data. I would also thank Inga Mathilde Tangen for all the nice work done about AI sorption isotherms and reversibility in C-S-H. To Serena and Rosa, I would like to thank you for always supporting me and sharing feelings with me, also thanks for the nice hiking moments in Switzerland. To Alexander German, Lei Lyu, Zhenyin Piao, Alexandru Pirvan, Raphael Kuhn, for the useful discussions about our research, PhD life as well as the lunch time together. Special thanks goes to my Chinese female friends: Zhangli and Biwan, my former flatmates, and Ye, my current office mate, for their helpful discussion on C-S-H and comprehensive scientific topics, also for many nights they accompanied and their regular concern about my study and life. I'm very happy to have you all not only as colleagues but also as friends. Specific thankyou's go to Luigi, Boris, Janis, Nik, Daniel, Seb and Marcel for their help in the lab. To everyone else at Empa, thank you for showing me the best research environment that I have been a part of.

Thank you to everyone else that I have worked with, met or learned from over these years, from those that I have seen present at scientific conferences to those that I have only learned from via their publications.

My deep thanks to my boyfriend, Pengpeng. You are my solid backing who always support me, encourage me and take care of me. Your innocent soul, optimistic nature and meticulous attitude to work inspire me to be a better me. I feel very lucky to have you.

Lastly, I would like to thank my family and my friends for all their love, encouragement and support.

Abstract

Calcium silicate hydrate (C-S-H) is the main hydration product in Portland and blended cements, and greatly affects durability and mechanical properties of the hydrated cement. In the presence of Al-rich supplementary cementitious materials (SCMs), C-(A-)S-H can contain more Al than C-S-H in plain Portland cements. The use of SCMs in cementitious system not only lowers CO₂ emission, but may also enhance the mechanical properties in the long term, its durability and can help to suppress alkali silica reaction. However, important questions regarding the effect of Al, alkali and equilibration time on C-(A-)S-H structure and solubility are still not fully understood. This thesis focuses on the interplay between aluminium, alkali hydroxides in solution, the structure of C-A-S-H and aluminium, alkali uptake by C-A-S-H and kinetics of C-(A-)S-H formation.

For aluminium free C-S-H, both KOH and NaOH have a similar effect, they increase pH values and silicon concentrations, and decrease calcium concentrations. At higher alkali hydroxide concentrations, more portlandite precipitates, while amorphous silica dissolves. This increases the Ca/Si_{C-S-H} at low Ca/Si_{target} but lowers the maximum Ca/Si_{C-S-H} from 1.5 to 1.2 in 1 M KOH/NaOH. The amount of alkalis bound in C-S-H increases with increasing alkali hydroxide concentrations and is higher at low Ca/Si_{C-S-H}. KOH/NaOH lead to a structural rearrangement in C-S-H, increasing the interlayer distance, number of layers stacked in c direction and shortening the silica chains. The mean chain lengths (MCL) estimated from FTIR and Raman spectroscopy agree well with the trends from ²⁹Si-NMR. Comparison with the independently developed CASH+ thermodynamic model showed a good agreement between the observed and modelled changes, including the shortening of the MCL.

For C-(A-)S-H with Ca/Si = 1, the presence of Al led to higher amounts of secondary phases, larger interlayer distance, longer silicate chain, higher dissolved Al and Si, and lower Ca concentrations. The amount of secondary phases is reduced at higher pH; strätlingite and Al(OH)₃ dominate at lower pH, and katoite at higher pH values. High pH is also associated with shortened silicate chain length, increased Al and Si concentrations, maximum Al/Si_{C-S-H} and lower Ca concentrations. The Al uptake in C-A-S-H increased with aluminum concentration in solution, indicating the predominance of a common Al sorption mechanism

Abstract

independent of dissolved Al concentration or pH values. XANES data showed the presence of both Al(IV) and Al(VI) with different chemical environments in C-S-H.

The effect of equilibration time on C-A-S-H was investigated from 6 hours to 3 years. Rapid changes within the first day were observed in both the solid phase and the aqueous phase. Portlandite was formed in all samples with different Ca/Si and its amount decreased rapidly within the first day and remained stable after more than 7 days. A zeolitic phase (gismondine-P1) precipitated between 1 and 3 years and destabilized the C-A-S-H phases at target Ca/Si 0.6. In the solid phase, the Al migration from secondary phases to C-A-S-H and an increasing fraction of Al(V) and Al(VI) in C-S-H were observed with longer equilibration time. The Ca/Si ratio of C-S-H played an important role on the extent of changes in aqueous concentration: an increasing of Al concentrations with time was observed in C-A-S-H with $\text{Ca/Si}_{\text{target}} = 0.6$, while a decrease was observed for C-A-S-H with $\text{Ca/Si}_{\text{target}} \geq 1.0$. The uptake of Al and Na in C-A-S-H was observed to decrease after 4 days and 1 day separately, which indicates a rearrangement of C-A-S-H phases with time.

Keywords: C-S-H, uptake, aluminium, alkali, equilibration time, pH, Ca/Si

Résumé

Le silicate de calcium hydraté (C-S-H) est le principal produit d'hydratation des ciments de Portland et des ciments composés, et il affecte considérablement la durabilité et les propriétés mécaniques des pâtes ciment hydratées. En présence d'ajouts cimentaires riches en Al, le C-(A-)S-H peut contenir plus d'aluminium que le C-S-H des ciments de Portland. L'utilisation d'ajouts cimentaires dans un système cimentaire permet non seulement de réduire les émissions de CO₂, mais aussi d'améliorer les propriétés mécaniques à long terme, la durabilité et de supprimer la réaction alcalino-siliceuse. Cependant, des questions importantes concernant l'effet de l'aluminium, des alcalins et du temps d'équilibre sur la structure et la solubilité de C-(A-)S-H ne sont pas encore totalement comprises. Cette thèse se concentre sur l'interaction entre l'aluminium, les alcalins (KOH et NaOH) en solution, la structure de C-A-S-H et de l'aluminium, l'absorption d'alcalin par C-A-S-H et la cinétique de la formation du C-(A-)S-H.

En ce qui concerne le C-S-H sans aluminium, KOH et NaOH ont tous deux un effet similaire: ils augmentent les valeurs de pH et les concentrations en silicium, et diminuent les concentrations en calcium. À des concentrations plus élevées d'hydroxyde de sodium ou de potassium, davantage de portlandite précipite, tandis que la silice amorphe se dissout. Cela augmente le rapport Ca/Si dans le C-S-H à faible Ca/Si mais abaisse le rapport maximum Ca/Si dans les C-S-H de 1,5 à 1,2 dans 1 M KOH/NaOH. La quantité d'alcalin incorporée dans le C-S-H augmente avec l'augmentation des concentrations d'hydroxydes de sodium ou de potassium et est plus élevée pour des C-S-H à faible Ca/Si. Le KOH ou le NaOH conduit à un réarrangement structurel dans le C-S-H, augmentant la distance de l'interfeuille mais aussi le nombre de couches empilées dans la direction c et raccourcissant les chaînes de silice. Les longueurs moyennes des chaînes (MCL) estimées à partir des résultats de spectroscopie (infrarouge ou Raman) correspondent bien aux tendances de la RMN du silicium. La comparaison avec le modèle thermodynamique CASH+ développé indépendamment montre une bonne concordance entre les changements observés et modélisés, y compris le raccourcissement de la MCL.

Pour le C-(A-)S-H avec Ca/Si = 1, la présence d'aluminium conduit à des quantités plus importantes de phases secondaires, à une plus grande distance entre les couches et à une

chaîne silicatée plus longue. De plus, une plus grande quantité d'aluminium et de silicium dissous et à des concentrations de Ca plus faibles sont observées. La quantité de phases secondaires est réduite à un pH plus élevé; les quantités de strätlingite et de $\text{Al}(\text{OH})_3$ dominant à un faible pH tandis que la quantité de katoite domine à un pH élevé. Un pH élevé est également associé à des plus courtes chaînes de silicate, à une augmentation des concentrations d'aluminium et de silicium, à un rapport maximum Al/Si dans les C-S-H et à des concentrations de Ca plus faibles. L'absorption d'aluminium dans C-A-S-H augmente avec la concentration d'aluminium en solution, indiquant la prédominance d'un mécanisme commun de sorption d'Al indépendant de la concentration d'Al dissous ou des valeurs de pH. Les données de XANES ont montré la présence de Al(IV) et de Al(VI) avec des environnements chimiques différents dans le C-S-H.

L'effet du temps d'équilibration sur C-A-S-H a aussi été étudié de 6 heures à 3 ans. Des changements rapides au cours du premier jour ont été observés à la fois dans la phase solide et dans la phase aqueuse. La portlandite se forme dans tous les échantillons avec différents rapports Ca/Si et sa quantité diminue rapidement au cours du premier jour et reste stable après plus de 7 jours. Une phase zéolitique (Gismondie-P1) précipite entre 1 et 3 ans et déstabilise le C-A-S-H avec un rapport cible Ca/Si de 0,6. En phase solide, on observe la migration d'aluminium initialement dans les phases secondaires vers le C-A-S-H et une fraction croissante de Al(V) et Al(VI) dans le C-S-H avec le temps. Le rapport Ca/Si du C-S-H joue un rôle important sur les changements de concentration en solution: une augmentation des concentrations d'aluminium avec le temps a été observée pour le C-A-S-H avec un rapport initial Ca/Si de 0,6, tandis qu'une diminution d'aluminium a été observée pour le C-A-S-H avec des rapports Ca/Si plus grand que 1,0. L'absorption d'aluminium et de sodium dans le C-A-S-H diminue après 4 jours et 1 jour indépendamment, ce qui indique un réarrangement de la structure du C-A-S-H avec le temps.

Mots clés : C-S-H, absorption, aluminium, alcali, temps d'équilibre, pH, Ca/Si.

Contents

Acknowledgements	i
Abstract	iii
Résumé.....	v
List of Figures	ix
List of Tables.....	xv
Glossary	xvii
CHAPTER 1: Introduction.....	18
1.1. Portland and blended cement	19
1.2. Calcium (aluminium) silicate hydrate.....	19
1.2.1. Alkali uptake in C-S-H.....	21
1.2.2. Aluminium uptake in C-S-H.....	22
1.2.3. Effect of equilibration time.....	24
1.3. Secondary phases	25
1.4. Objectives of the thesis	26
CHAPTER 2: Materials and methods	29
2.1. Materials and Synthesis	29
2.2. Analytical methods	29
2.2.1. Ionic chromatography (IC) and pH measurements	29
2.2.2. Thermogravimetric analyses (TGA)	30
2.2.3. X-ray diffractometry (XRD).....	30
2.2.4. Nuclear magnetic resonance (NMR).....	31
2.2.5. Fourier Transformation-Infrared (FTIR).....	32
2.2.6. Raman spectroscopy	32
2.2.7. Aluminum K-edge (1559 eV) XANES measurements	33
2.2.8. C-S-H composition.....	33
2.2.9. Thermodynamic modelling.....	34
CHAPTER 3: Effect of alkali hydroxide on calcium silicate hydrate (C-S-H)	35
3.1. Introduction	35
3.2. Results and discussion	36
3.2.1. Effect of Ca/Si on liquid and solid phase composition.....	36
3.2.2. Effect of NaOH / KOH on the aqueous phase.....	43
3.2.3. Effect of NaOH / KOH on C-S-H	45
3.2.3.1. Alkali uptake in C-S-H.....	45
3.2.3.2. Water content in C-S-H.....	47
3.2.3.3. Basal spacing and crystallite size	49
3.2.3.4. Composition of C-(N,K-)S-H	55
3.3. Effect of pH on silica sites in C-S-H	56
3.4. Conclusion	62
CHAPTER 4: Al uptake in calcium silicate hydrate (C-S-H) and the effect of pH	65
4.1. Introduction	65
4.2. Results and discussion	66

4.2.1. Influence of aluminium	66
4.2.2. Influence of NaOH and KOH.....	80
4.3. Conclusions	89
CHAPTER 5: Effect of time on Al uptake in calcium silicate hydrate	91
5.1. Introduction	91
5.2. Results and discussion	91
5.2.1. Effect of time on solid phases	91
5.2.1.1. Solids present	91
5.2.1.2. C-A-S-H structure	96
5.2.2. Effect of time on aqueous phases.....	100
5.2.3. Al uptake in C-S-H	103
5.2.4. Na uptake in C-S-H.....	108
5.2.5. Effect of Ca/Si on kinetics of C-A-S-H.....	109
5.3. Conclusion	112
CHAPTER 6: Conclusions and outlook.....	115
6.1. Effect of alkali hydroxide on C-S-H	115
6.2. Effect of alkali hydroxide on Al uptake in C-S-H with Ca/Si = 1.....	115
6.3. Effect of time on Al uptake in C-S-H.....	116
6.4. Outlook.....	117
Appendix	119
Appendix A Mixing proportions used to prepared C-(A-)S-H.....	120
Appendix B Dissolved concentration.....	123
Appendix C Saturation indices	127
Appendix D C-(A-)S-H compositions.....	130
Appendix E Secondary phase quantification.....	134
Appendix F Silicate main chain length and Q ¹ species determined by FTIR, Raman and ²⁹ Si NMR	138
Appendix G FTIR and Raman spectra of C-(N,K-)S-H and C-N-(A-)S-H.....	139
Appendix H NMR spectra.....	142
Appendix I Pawley fits of the tobermorite 11 Å and 14 Å (for 1.0 M KOH) model to the C-(N,K-)S-H	146
Appendix J XRD and TGA.....	147
Appendix K Al K-edge XANES.....	150
Appendix L Concentrations of Ca, Si and Al in solutions	152
References	154
Yiru Yan	163

List of Figures

Figure 1. Energy consumption and CO ₂ emission from cement manufacturing [4].	18
Figure 2 Schematic structure of C-A-S-H. Spheres of blue, golden, turquoise, yellow red and white colors represent Si, Al, Ca, Na, O and H respectively. The dashed circles are Si tetrahedra vacancies in bridging sites. Q ⁿ : n indicates the numbers of Si tetrahedral neighbors, b: bridging position, p: pairing position.	20
Figure 3. Contour plots of ²⁷ Al MQMAS NMR spectra recorded at 22.3 T (νR = 25.0 kHz) with sum projections in both dimensions for the C-(A)-S-H sample with Ca/Si of 1.0 and relative ²⁷ Al NMR intensities for the different Al(IV) sites as a function of the Ca/Si ratio. Adapted from [45].	23
Figure 4. Effect of dissolved aluminium concentrations in the aqueous solution on the aluminium uptake in C-S-H [18].	24
Figure 5 Concentrations of Ca, Si and OH ⁻ in solutions equilibrated with C-S-H samples as a function of the Ca/Si ratios in C-S-H. Yellow triangles: OH ⁻ , red squares: Ca and blue circles: Si. Solid lines: simulated using the thermodynamic CASH+ model [61,62]. The estimated absolute errors of Ca/Si _{C-S-H} are smaller than ±0.05 units in the Ca/Si ratios. The estimated relative uncertainty of the IC measurements is ±10%, which is smaller than the size of the symbols.	37
Figure 6. (a) XRD diffractograms of the C-S-H samples synthesized in water and C-S-H schema for C-S-H with low Ca and high Ca. (b) ²⁹ Si NMR spectra, (c) FTIR and (d) Raman spectra of C-S-H with Ca/Si _{C-S-H} from 0.75 to 1.44, after an equilibration time of 3 months. C: C-(K)-S-H; P: portlandite.	42
Figure 7 Silicate main chain length determined by FTIR, Raman, ²⁹ Si NMR, and thermodynamic CASH+ model.	43
Figure 8. pH values, Si and Ca concentrations in the solutions of the C-(N,K)-S-H samples as a function of Ca/Si ratios in C-(N,K)-S-H. The estimated absolute errors are ≤ ±0.05 units in the Ca/Si ratios and ±0.2 in pH. The estimated relative uncertainty of the IC measurements is ±10%. Grey symbols: synthetic C-S-H data from [18,40,42,98]; colored symbols: C-(N,K)-S-H from this study; red triangles: C-S-H in water; orange circles: C-(N,K)-S-H with 0.1 M alkali hydroxide solution, light green diamonds: C-(N,K)-S-H with 0.5 M alkali hydroxide solution, dark green squares: C-(N,K)-S-H with 1 M alkali hydroxide solution; filled symbol: C-(N,K)-S-H with NaOH solution; empty symbol: C-(N,K)-S-H with KOH solution. Lines: simulated using the thermodynamic CASH+ model [61,62].	45
Figure 9. Alkali uptake in C-(N,K)-S-H as a function of the Ca/Si ratio, for samples synthesized with NaOH (filled symbols) and KOH (empty symbols) equilibrated for 3 months determined by the direct method. Orange circles: C-(N,K)-S-H synthesized with 0.1 M alkali hydroxide; green diamonds: C-(N,K)-S-H synthesized with 0.5 M alkali hydroxide. Lines: simulated using the thermodynamic CASH+ model [61,62]. The estimated absolute errors were ±0.08 units in the (Na, K)/Si ratios of the C-(N,K)-S-H products synthesized with 0.5 M alkali hydroxide and ±0.04 units of the C-(N,K)-S-H products synthesized with 0.1 M alkali hydroxide. The estimate errors of Ca/Si _{C-S-H} were smaller than ±0.05. The values determined indirectly by mass balance at 0.1 M (grey triangles) are given for comparison.	47

Figure 10. TGA of C-(K-)S-H with target Ca/Si=1.2 after an equilibration time of 3 months at different KOH concentrations. C: C-(K-)S-H ; P: portlandite. *P: The weight loss between 300 and 400 °C in 1 M KOH is tentatively assigned to finely dispersed portlandite. Similar weight losses have also been observed for C-N-S-H.48

Figure 11. H₂O/Si ratios of the C-(N,K-)S-H as functions of the Ca/Si ratio, for samples synthesized with water, 0.1 M, 0.5 M and 1 M NaOH (filled symbols) or KOH (empty symbols) solutions equilibrated for three months. The estimated absolute errors are ±0.05 units in the Ca/Si ratios and ±0.2 in the H₂O/Si ratios of the C-(N,K-)S-H products. The estimate error of Ca/Si_{C-S-H} is smaller than 0.05.49

Figure 12. XRD diffractograms of C-(K-)S-H with target Ca/Si=1.2 after an equilibration time of 3 months at different KOH concentrations. C: C-(K-)S-H, P: portlandite50

Figure 13. Variation of the mean basal spacing as a function of the total Ca/Si ratio in C-(N,K-)S-H solid after an equilibration time of 3 months. Grey symbol: C-S-H from L'Hôpital [26]; colored symbol: C-(N,K-)S-H from this study; triangles: C-S-H with water; circles: C-(N,K-)S-H with 0.1 M alkali hydroxide solution, squares: C-(N,K-)S-H with 1 M alkali hydroxide solution; filled symbols: C-(N,K-)S-H with NaOH solution; empty symbols: C-(N,K-)S-H with KOH solution.52

Figure 14 (a) Variation of mean basal spacing and crystallite size along the c-axis as a function of the initial alkali concentration for C-S-H with Ca/Si = 1.0 after an equilibration time of 3 months, solid symbols: mean basal spacing, empty symbol: crystallite size calculated based on the tobermorite model. Grey symbols: C-S-H from L'Hôpital et al. [26]; colored symbol: C-S-H from this study; triangle. (b) FWHM of the d₀₀₁ reflection of C-(N,K-)S-H with target Ca/Si = 1.0 as a function of initial alkali concentration after an equilibration time of 3 months. Triangles: C-S-H synthesized with water, squares: C-(N, K-)S-H synthesized with NaOH solutions, circles: C-(N, K-)S-H synthesized with KOH solutions. The symbol marked with * stands for the second basal peak. The grey region is shown only as an eye-guide.55

Figure 15. Chemical compositions (units in molar fraction) of the C-(N, K-) S-H products of different target Ca/Si and with different NaOH or KOH concentration projected in ternary diagram.56

Figure 16 ²⁹Si NMR spectra of C-(N,K-)S-H a) with Ca/Si_{target} = 1.2 after an equilibration time of 3 months at different KOH concentrations.58

Figure 17 (a) FTIR and (b) Raman spectra of C-(N,K-)S-H with target Ca/Si=1.2 after an equilibration time of 3 months at different KOH concentrations.60

Figure 18. Calculated main chain length (MCL) of C-(N,K-)S-H from Gems compared with MCL values reported from ²⁹Si NMR. The estimated absolute errors are less than 30%. The error limits for the MCL from NMR is ± 0.05. Solid and empty symbols: MCL from NMR; red triangles: C-S-H with MilliQ water; orange circles: C-(N,K-)S-H with 0.1 M alkali hydroxide solution, light green diamonds: C-(N,K-)S-H with 0.5 M alkali hydroxide solution, grey symbols: C-(N,K-)S-H with 0.5 M – 1M alkali hydroxide solution adapted from [42,48,120,121]. Lines: simulated using the thermodynamic CASH+ model.62

Figure 19 XRD and TGA of C-N,K-(A-)S-H with target Ca/Si=1.0 synthesized in NaOH 0.5 M with different initial Al/Si, equilibrated for 1 year. C: C-N,K-(A-)S-H, K: katoite (Ca₃Al₂(OH)₆, PDF# 00-024-0217), Hc: Hemicarbonate (Ca₄Al₂(OH)₁₂(OH)(CO₃)_{0.5}(H₂O)₅, PDF# 00-029-0285), Mc: monocarbonate (Ca₄Al₂(OH)₁₂(OH)(CO₃)(H₂O)₅, PDF# 00-029-0285). *: The weight loss between 300 and 400 °C in (b) is tentatively assigned to C-N-A-S-H.68

Figure 20. Effect of pH on Al solubility of microcrystalline Al(OH) ₃ , strätlingite and katoite (all solids 1 mol/L) at equilibrium conditions. Above pH 13.7, the formation of portlandite is calculated in the presence of katoite.....	69
Figure 21 Variation of the mean basal spacing as a function of Al/Si in C-(N,K-)A-S-H and (Al-)tobermorite [65,135–140] . C-A-S-H with Ca/Si _{target} at 1.0. * indicates two reflections. The dash lines are shown only as an eye-guide	70
Figure 22 (a) FTIR and second derivative and (b) Raman spectra of C-N-(A-)S-H with target Ca/Si=1.0 after an equilibration time of 1 year with different initial Al/Si, synthesized in 0.5 M NaOH. Normalized to the most intensive band at ~ 970 cm ⁻¹ of FTIR and ~ 670 of Raman. *, †: unidentified peaks from secondary phases.	73
Figure 23 (a) Al K-edge XANES spectra for C-A-S-H synthesized in NaOH 0.1 M and reference spectra for CA, C ₃ AH ₆ and CO ₃ -AFm. Black and red lines: experimental spectra; blue lines: ITFA fits. (b) Comparison between selected experimental Al K-edge XANES spectra (with fitting curves in blue) and calculated spectra for tetrahedral and octahedral Al with different chemical environments.	76
Figure 24. Comparison between component fraction from ITFA analysis and Al fraction from Rietveld quantification.	77
Figure 25 Measured (symbols) and calculated (lines) concentrations of Ca, Si and Al in solutions equilibrated with target Ca/Si=1.0 in KOH 0.5 M as a function of (a) Al/Si ratios and (b) Ca/(Al+Si). The equilibration time is 3 months. Orange squares: Ca, blue triangles: Si and red diamonds: Al, empty ones are C-A-S-H samples and the filled ones are C-S-H samples from [141]. The estimated relative uncertainty of the IC measurements is ±10%. . Lines: simulated using the thermodynamic CASH+ model[61–63], dashed lines: simulated C-A-S-H and solid lines: simulated C-S-H without Al	79
Figure 26 Al fraction in C-A-S-H, aqueous phase and different secondary phases for target Ca/Si = 1.0 after 3 months and 1 year equilibration in the presence of 0.5 M alkali hydroxide. Empty symbols: sample synthesized for 3 months and equilibrated in 0.5 M Na OH, solid symbols: sample synthesized for 1 year and equilibrated in 0.5 M NaOH, patterned symbols: sample synthesized for 3 months and equilibrated in 0.5 M KOH. The dash lines are shown only as an eye-guide.....	79
Figure 27 (a) XRD, (b) TGA, (c) FTIR and second derivative of FTIR and (d) Raman of C-A-S-H with a target Ca/Si of 1.0 and target Al/Si of 0.2 synthesized in NaOH from 0.1 M to 1 M after an equilibration time of 1 year. C: C-(K-)A-S-H; K: katoite, S:strätlingite, Cc: carbonates *: unidentified peak from secondary phase.	83
Figure 28 K-edge XANES spectra for C-A-S-H equilibrated for 1 year in NaOH 0.1 M, C-A-S-H equilibrated for 3 months in NaOH 1 M and calculated Al(IV) and Al(VI) spectra.....	84
Figure 29 Al, Si and Ca concentrations in the solutions of the C-(A-)S-H samples as a function of Al/Si ratios in solid phase. The estimated absolute errors are ≤ ±0.01 units in the Al/Si ratios and the estimated relative uncertainty of the IC measurements is ±10%. Grey symbols: C-(A)-S-H data from [40,48]; colored symbols: C-(A-)S-H from this study; diamonds: C-A-S-H in water; triangles: C-(N,K-)A-S-H with 0.1 M alkali hydroxide solution; circles: C-(N,K-)A-S-H with 0.5 M alkali hydroxide solution, squares: C-(N,K-)A-S-H with 1 M alkali hydroxide solution. Lines: simulated using the thermodynamic CASH+ model [61–63].....	86
Figure 30 Al sorption isotherm on C-A-S-H for target Ca/Si = 1.0 synthesized in different alkali hydroxide and recorded after different equilibration times. Colorful symbols: C-A-S-H from this study, grey symbols. C-A-S-H data adapted from [40,48]	87

Figure 31. Effect of pH on the K_d values of Al on C-S-H with Ca/Si = 1.....	88
Figure 32. XRD and TGA of C-A-S-H with (a) and (b) target Ca/Si=0.6, (c) and (d) target Ca/Si=1.0, (e) and (f) target Ca/Si=1.4 synthesized in NaOH 0.5 M with initial Al/Si 0.1, equilibrated for different time from 0.25 day to 1350 day. C: C-N,K-(A-)S-H, K: katoite ($\text{Ca}_3\text{Al}_2(\text{OH})_6$, PDF# 00-024-0217), Hc: hemicarbonat ($\text{Ca}_4\text{Al}_2(\text{OH})_{12}(\text{OH})(\text{CO}_3)_{0.5}(\text{H}_2\text{O})_5$, PDF# 00-029-0285), Mc: monocarbonat ($\text{Ca}_4\text{Al}_2(\text{OH})_{12}(\text{OH})(\text{CO}_3)(\text{H}_2\text{O})_5$, PDF# 00-029-0285). G: gismondine-P1 ($\text{Na}_6\text{Al}_6\text{Si}_{10}\text{O}_{32}\cdot 12\text{H}_2\text{O}$), P: portlandite; \blacklozenge : unidentified phase. \heartsuit : The weight loss from C-A-S-H Ca/Si = 0.6 and 1.0 at later ages is tentatively assigned to C-N-A-S-H, as portlandite is absent in XRD and FTIR, and the solutions are strongly undersaturated with respect to portlandite. \ddagger : The weight loss from C-A-S-H synthesized for 90 day* between 850 and 900 °C in (d) is assigned to phase transformation of C-N-A-S-H to wollastonite. C-A-S-H equilibrated for 0.25- 90 days: synthesized with water/solid = 45, C-A-S-H equilibrated for 90*, 450* and 1350* days: synthesized with water/solid = 40.....	96
Figure 33. Portlandite content evolution in solid phases.....	96
Figure 34. FTIR and second derivative spectra of C-A-S-H with $\text{Ca/Si}_{\text{target}}$ = (a) 0.6, (b) 1.0 and (c) 1.4 after different equilibration time synthesized in 0.5 M NaOH. Normalized to the most intensive band at $\sim 970\text{ cm}^{-1}$ of FTIR. C-A-S-H equilibrated for 0.25- 90 days: synthesized with water/solid = 45, C-A-S-H equilibrated for 90*, 450* and 1350* days: synthesized with water/solid = 40.....	99
Figure 35. Effect of time on the ^{27}Al MAS NMR of the C-A-S-H with $\text{Ca/Si}_{\text{target}}$ = 1.0 synthesized in 0.5 M NaOH. C-A-S-H equilibrated for 0.25- 90 days: synthesized with water/solid = 45, C-A-S-H equilibrated for 90*, 450* and 1350* days: synthesized with water/solid = 40.....	100
Figure 36. The evolution of dissolved Al, Si and Ca concentrations in solution for $\text{Ca/Si}_{\text{target}}$ ratios of (a) 0.6, (b) 1.0 and (c) 1.4 synthesized in NaOH 0.5 M with initial Al/Si 0.1 equilibrated for different time. Two series were studied: Series A: filled symbols: in w/s = 40; Series B: symbols with black border: w/s = 45. The error of the dissolved concentrations are 10% and the error bars are smaller than the symbols. (j): outlier Ca concentration after 3 months and 1 year. Lines are only for eye-guides.....	103
Figure 37. Al fraction in C-A-S-H, aqueous phase and different secondary phases for target Ca/Si = (a) 0.6, (b) 1.0 and (c) 1.4 after different equilibration time in the presence of 0.5 M NaOH. Symbols without border: C-A-S-H samples synthesized in a vessel and stopped hydration after certain equilibration time; symbols with border: C-A-S-H samples synthesized independently.....	105
Figure 38. Effect of time on the Al sorption in C-A-S-H: (a) Al bound per g C-S-H, (b) Al/Si in C-S-H and (c) Al/Si in solid. The shade area after 6 hours and 1 days indicates the potential underestimation of Al in secondary phases.....	106
Figure 39 Effect of equilibration time on the K_d values of Al on C-S-H synthesized in NaOH 0.5 M. #: gismondine formation observed after 3 years at Ca/Si = 0.6.....	107
Figure 40. Effect of time on the Na absorption in C-A-S-H.....	109
Figure 41. Al, Ca and Si concentrations in the solutions of the C-A-S-H samples in 0.5 M NaOH with different equilibration time as a function of Ca/Si ratios in solid. The estimated absolute errors are $\leq \pm 0.05$ units in the Ca/Si ratios. The estimated relative uncertainty of the IC measurements is $\pm 10\%$. Symbols with color filled from light to dark: synthetic C-A-S-H data with equilibration time from 0.25 day to 1350 days. Solid lines: calculated concentrations using the thermodynamic CASH+ model, suppressing the formation of zeolitic phases, which form only slowly. dashed lines: considering the possible formation of gismondine-P1	

($\text{Na}_6\text{Al}_6\text{Si}_{10}\text{O}_{32}\cdot 12\text{H}_2\text{O}$). C-A-S-H equilibrated for 0.25- 90 days: synthesized with water/solid = 45, C-A-S-H equilibrated for 90*, 450* and 1350* days: synthesized with water/solid = 40. 111

Figure 42. Calculated \log_{10} IAP values for hypothetical C-(A-)S-H and Al-tobermorite with different equilibration time, normalised to $\text{SiO}_2+\text{Al}_2\text{O}_3 = 1$. The approximate uncertainty in the \log_{10} (IAP) values are ± 0.3 . Colored circles: C-A-S-H from this study; patterned circles: C-A-S-H from Myers et al. and Barzgar et al. [47,50], and triangles: Al-tobermorite with $\text{Ca}/(\text{Al}+\text{Si}) = 0.83$ from Lothenbach et al. [65]. Data from this study and [47,50] are calculated from oversaturation condition and [65] is calculated from undersaturation condition..... 112

Figure 43. Silicate main chain length and Q^1 species determined by FTIR, Raman and ^{29}Si NMR. Filled symbols: silicate main chain length, empty symbols: Q^1 species..... 138

Figure 44. FTIR spectra water region of C-(N,K-)S-H with target $\text{Ca}/\text{Si}=1.2$ after an equilibration time of 3 months at different KOH concentrations 139

Figure 45. FTIR spectra of C-(N,K-)S-H with $\text{Ca}/\text{Si}_{\text{target}} = 0.6$ after an equilibration time of 3 months at different KOH concentrations..... 139

Figure 46. (a) FTIR -OH region and (b) Raman -OH region of C-N-(A-)S-H with target $\text{Ca}/\text{Si}=1.0$ after an equilibration time of 1 year with different initial Al/Si, synthesized in 0.5 M NaOH. Three FTIR peaks are observed at 2881, 2933 and 2975 cm^{-1} corresponding to symmetric C-H stretching modes, $\nu_s(\text{CH}_2)$, $\nu_s(\text{CH}_3)$, and $\nu'_s(\text{CH}_3)$ of ethanol molecules [149] on the surface which were not removed during freeze-drying. A Raman peak at 2432 cm^{-1} increasing with the intensity of peak at 477 cm^{-1} , which could indicate the presence of ethanol or water molecules captured in a 4-membered ring..... 140

Figure 47. FTIR and second derivative of C-N-(A-)S-H with target $\text{Ca}/\text{Si}=1.0$ after an equilibration time of 1 year with different initial Al/Si, synthesized in (a), (b) 0.1 M NaOH, and (c), (d) 1 M NaOH. Normalized to the most intensive band at $\sim 970 \text{ cm}^{-1}$ 141

Figure 48. ^{29}Si NMR spectra of C-(N,K-)S-H synthesized in different NaOH and concentrations after an equilibration time of 3 months. The dashed line located at ~ -70 ppm indicates the Q^0 signal. 143

Figure 49. Detailed ^{27}Al NMR deconvolution result in C-A-S-H with Ca/Si 1.0 equilibrated from 0.25 day to 1350 days (target Al/Si = 0.1). C-A-S-H equilibrated for 0.25- 90 days: synthesized with water/solid = 45, C-A-S-H equilibrated for 90*, 450* and 1350* days: synthesized with water/solid = 40. 145

Figure 50. Pawley fits of the tobermorite 11 Å and 14 Å (for 1.0 M KOH) model to the C-(N,K-)S-H powder patterns with $\text{Ca}/\text{Si}_{\text{target}} = 1.0$. Experimental data are shown as black points, red line as the fit, grey line the data-fit curve, and the blue hkl tick marks for tobermorite reflections. In the case of 1.1 M KOH, an additional impurity phase of $\text{K}_2\text{CO}_3\cdot 1.5\text{H}_2\text{O}$ (PDF# 00-011-0655) was present, which was Rietveld refined with the pink hkl tick marks indicating the reflections. For the 1.0 M NaOH synthesis condition, two reflections are visible for the first diffraction peak, therefore two tobermorite 11 Å models were used to fit the data (shown by the blue and red hkl tick marks). These have different c-axis and crystallite size along the c-direction parameters, but all other parameters are kept equal between the two phases. In addition, the portlandite impurity phase was present and was Rietveld refined with the green hkl tick marks indicating the reflection positions. 146

Figure 51 XRD and TGA of C-N,K-(A-)S-H with target $\text{Ca}/\text{Si}=1.0$ and different initial Al/Si, synthesized in (a), (b) NaOH 0.1 M; (c), (d) NaOH 1 M, equilibrated for 1 year; (e), (f) KOH 0.5 M, equilibrated for 3 months. S: strätlingite ($\text{Ca}_2\text{Al}(\text{AlSi})_{1.1}\text{O}_2(\text{OH})_{12}(\text{H}_2\text{O})_8$, PDF# 00-041-0221), K: katoite ($\text{Ca}_3\text{Al}_2(\text{OH})_6$, PDF# 00-024-0217), P: portlandite ($\text{Ca}(\text{OH})_2$, PDF# 00-004-733), Hc:

Hemicarbonate ($\text{Ca}_4\text{Al}_2(\text{OH})_{12}(\text{OH})(\text{CO}_3)_{0.5}(\text{H}_2\text{O})_5$, PDF# 00-029-0285), Mc: monocarbonate ($\text{Ca}_4\text{Al}_2(\text{OH})_{12}(\text{OH})(\text{CO}_3)(\text{H}_2\text{O})_5$, PDF# 00-029-0285), Cc: Carbonates. */P: The weight loss at around 450 °C in (d) is tentatively assigned to C-N-A-S-H and/or portlandite. The d_{001} reflections of $\text{Al}/\text{Si}_{\text{target}} = 0.15$ and 0.2, NaOH 0.1 M are hidden because of the overlap with strätlingite.	147
Figure 52. Variation of the mean basal spacing as a function of the $\text{H}_2\text{O}/\text{Si}$ in C-(N,K-)A-S-H with $\text{Ca}/\text{Si}_{\text{target}}$ at 1.0.	148
Figure 53. FWHM ($\sim 3.1 \text{ \AA}$) vs Al/Si in C-A-S-H. A weak increase of the FWHM (full width at half maximum) of the main peak at $\sim 3.1 \text{ \AA}$ ($\sim 29^\circ 2\theta \text{ Cu K}\alpha$) is observed with the Al/Si in C-S-H. Several different signals contribute to the peak at $\sim 3.1 \text{ \AA}$: 020, -220, 2-22, 022[100]. The broadening of this peak could indicate a growth of the silicate layer and/or a more disordered structure in the presence of more Al.	148
Figure 54 XRD and TGA of C-A-S-H with (a) and (b) target $\text{Ca}/\text{Si}=0.8$, (c) and (d) target $\text{Ca}/\text{Si}=1.2$, (e) and (f) target $\text{Ca}/\text{Si}=1.6$ synthesized in NaOH 0.5 M with initial Al/Si 0.1, equilibrated for different time from 0.25 day to 1350 day. C: C-N,K-(A-)S-H, K: katoite ($\text{Ca}_3\text{Al}_2(\text{OH})_6$, PDF# 00-024-0217), Hc: Hemicarbonate ($\text{Ca}_4\text{Al}_2(\text{OH})_{12}(\text{OH})(\text{CO}_3)_{0.5}(\text{H}_2\text{O})_5$, PDF# 00-029-0285) , Mc: monocarbonate ($\text{Ca}_4\text{Al}_2(\text{OH})_{12}(\text{OH})(\text{CO}_3)(\text{H}_2\text{O})_5$, PDF# 00-029-0285), Cc: carbonates. ▲: unidentified phase.	149
Figure 55. Al K-edge XANES spectra for C-A-S-H with different initial Al/Si synthesized in NaOH 1 M and reference spectra for CA, C_3AH_6 and $\text{CO}_3\text{-AFm}$	150
Figure 56. Iterative-target transformation factor analysis (ITFA) of Al K-edge XANES spectra. (a) Abstract spectra of the components from the principal component analysis (PCA), with the first three components displaying "spectrum" features more obviously. It indicates that all spectra can be well reproduced with only three components. (b) The three component spectra calculated with the ITFA code, which are identified as CASH, katoite, and AFm-CO3 in sequence.	151
Figure 57. Concentrations of Ca, Si and Al in solutions equilibrated with C-N,K-(A-)S-H samples as a function of Al/Si ratios. C-N,K-(A-)S-H with target $\text{Ca}/\text{Si}=1.0$ synthesized in (a) 0.1 M NaOH, (b) 0.5 M NaOH and (c) 1 M NaOH. The equilibration time is 1 year. Orange squares: Ca, blue triangles: Si and red diamonds: Al. The estimated relative uncertainty of the IC measurements is $\pm 10\%$. Lines: simulated using the thermodynamic CASH+ model [61–63]. The thermodynamic model overestimated the Si concentration at 0.5 M and 1 M NaOH.	152
Figure 58. Chemical compositions (units in molar fraction) of the C-N,K-A-S-H products of target Ca/Si at 1.0 and different target Al/Si and with different NaOH or KOH concentration projected in a ternary diagram.	153

List of Tables

Table 1 Secondary phase quantification and mean silica chain length (MCL) of C-S-H samples without alkali	42
Table 2 Unit cell parameters and domain sizes along the a-, and b-axes (l_a) and the c-axis (l_c) obtained from the Pawley fits in Figure 50 for the different alkali concentrations of C-(N,K-)S-H powder patterns with $Ca/Si_{target} = 1.0$. For the 1.0 M NaOH concentration, two tobermorite unit-cells were used, which differ only in the c-axis length and domain size.....	52
Table 3. Assignments of FTIR spectra for C-A-S-H.....	73
. Table 4. Assignment of Raman spectra for C-A-S-H.....	74
Table 5. Fractions of Al(IV), Al(V), and Al(VI) obtained by deconvolution of the ^{27}Al NMR spectra in C-S-H with $Ca/Si_{target} = 1.0$. C-A-S-H equilibrated for 0.25- 90 days: synthesized with water/solid = 45, C-A-S-H equilibrated for 90*, 450* and 1350* days: synthesized with water/solid = 40.....	100
Table 6. Mixing proportions used to prepared C-(Na,K-)S-H with equilibrium time of 3 months (in g per 180 mL of solution).....	120
Table 7. Mixing proportions used to prepared C-(A-)S-H (in g per 180 mL of solution)	121
Table 8. Mixing proportions used to prepared C-A-S-H (in g per 260 mL of solution for samples with equilibration time from 0.25 day to 90 days and per 180mL for samples with 90*, 450* and 1350* days)	122
Table 9 Aqueous dissolved concentrations and pH results for the C-(N, K)S-H samples.....	123
Table 10. Aqueous dissolved concentrations and pH values for the C-(N, K-)A-S-H samples (target Ca/Si = 1.0)	124
Table 11 Aqueous dissolved concentrations and pH values for the C-(N-)A-S-H samples with different equilibration time (target Al/Si = 0.1). C-A-S-H equilibrated for 0.25- 90 days: synthesized with water/solid = 45, C-A-S-H equilibrated for 90*, 450* and 1350* days: synthesized with water/solid = 40.....	125
Table 12. Saturation indices for the relevant reaction products in C-(A-)S-H synthesized in different alkali hydroxide solutions.....	127
Table 13. Saturation indices for the relevant reaction products in C-(A-)S-H system with $Al/Si_{target} = 0.1$ and different Ca/Si as a function of equilibration time. C-A-S-H equilibrated for 0.25- 90 days: synthesized with water/solid = 45, C-A-S-H equilibrated for 90*, 450* and 1350* days: synthesized with water/solid = 40.....	128
Table 14. Chemical compositions of the C-(N,K-)S-H products, determined from IC, TGA, XRD and pH measurements, The estimated absolute errors are less than ± 0.05 units in the Ca/Si ratios, ± 0.2 units in the H_2O/Si ratios, and ± 0.05 units for the 0.1 M alkali samples in the (Na/K)/Si ratios of the C-(N,K-)S-H products. $Ca/Si^* = target\ Ca/Si$	130
Table 15 Chemical compositions of the C-(N,K-)A-S-H products, determined from Rietveld analysis, mass balance and dissolution experiments. The estimated absolute errors are less than ± 0.02 units in the Ca/Si ratios, ± 0.2 units in the H_2O/Si ratios, and ± 0.05 units for the 0.1 M alkali samples in the Na/Si ratios of the C-(N,K-)A-S-H products.....	131
Table 16. Chemical compositions of the C-N-A-S-H products, determined from Rietveld analysis, TGA, mass balance and dissolution experiments. The estimated absolute errors are	

less than ± 0.05 units in the Ca/Si ratios, ± 0.2 units in the H₂O/Si ratios, and ± 0.05 units for the 0.1 M alkali samples in the Na/Si ratios of the C-N-A-S-H products. C-A-S-H equilibrated for 0.25- 90 days: synthesized with water/solid = 45, C-A-S-H equilibrated for 90*, 450* and 1350* days: synthesized with water/solid = 40. 132

Table 17 Secondary phase quantification and mean silica chain length (MCL) of C-S-H samples without and with alkali hydroxide. 134

Table 18 Solid phase assemblages of the C-(N,K-)A-S-H samples, as determined by XRD / Rietveld analysis. The estimated absolute error is ± 2 wt.%. 135

Table 19. Solid phase assemblages of the C-(N,K-)A-S-H samples, as determined by TGA and XRD Rietveld analysis. The estimated absolute error is ± 2 wt.%. C-A-S-H equilibrated for 0.25- 90 days: synthesized with water/solid = 45, C-A-S-H equilibrated for 90*, 450* and 1350* days: synthesized with water/solid = 40. 136

Table 20 Indicators of theoretical error functions. IND_n shows at n = 2 a minimum, indicating that only 2 components are responsible for the variation of the spectra; RPV_n and REN drop down rapidly and level off above at n = 3, and thus the system contains 3 components; IEN fails to show a inflection point for a minimum and thus to indicate the number of components. 150

Glossary

Cement chemistry notations:

C=CaO

S=SiO₂

A=Al₂O₃

H=H₂O

c= CO₂

N= Na₂O

Hydrated phases:

CA	Calcium aluminate
C-S-H	Calcium silicate hydrate
C-A-S-H	Calcium alumino-silicate hydrate
C ₃ AH ₆	Katoite
C ₂ ASH ₈	Strätlingite
CH	Portlandite (Ca(OH) ₂)
AFm	Al ₂ O ₃ -Fe ₂ O ₃ -mono phase
AFt	Al ₂ O ₃ -Fe ₂ O ₃ -tri phase
Hc	Hemicarbonate (Ca ₄ Al ₂ (OH) ₁₂ (OH)(CO ₃) _{0.5} (H ₂ O) ₅)
Mc	Monocarbonate (Ca ₄ Al ₂ (OH) ₁₂ (OH)(CO ₃)(H ₂ O) ₅)
Cc	Calcium carbonate
GGBFS	Ground granulated blast furnace slag
MK	Metakaolin
FA	Fly ash
SF	Silica fume

Techniques:

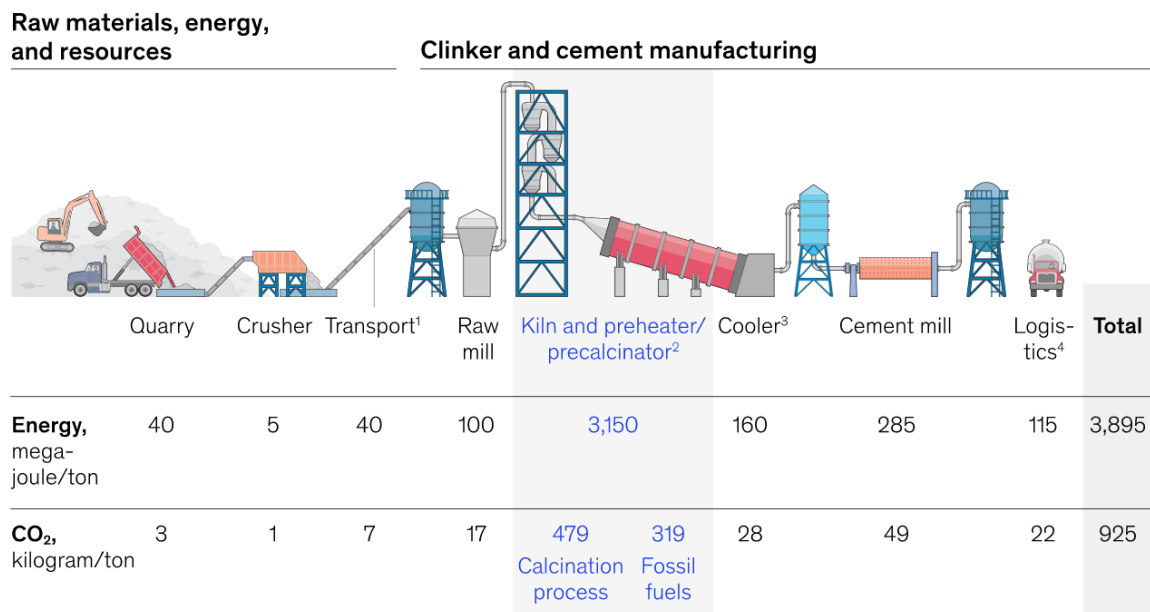
XRD	X-ray diffraction
TGA	Thermogravimetric analysis
DTG	Derivative thermogravimetric analysis
NMR	Nuclear magnetic resonance
FTIR	Fourier-transform infrared spectroscopy
XANES	X-ray absorption near edge structure
IC	Ionic chromatography
GEMS	Gibbs energy minimization software
IAP	Ion activity product

Divers:

OPC	Ordinary Portland cement
SCM	Supplementary cementitious material
ASR	Alkali silica reaction
PE-HD	High-density polyethylene

CHAPTER 1: Introduction

Concrete is the most used construction material globally and is irreplaceable for large scale buildings and transport systems [1]. Most probably concrete will continue to be indispensable and essential for the sustainable development of future societies. Cement, the integral component of concrete that gives the material its binding properties when hydrated, is used in vast amounts: 4.3 Gt of cement were produced in 2019 [2]. The total annual cement consumption is expected to grow up to 4.7 Gt/year by 2050 [3], considering the rising population, continuing urbanization and infrastructure development. Cement production is responsible for roughly 5-7% of the global anthropogenic CO₂, and cement industry is the third largest industrial energy consumer [3]. More than half of the CO₂ emissions from Portland cement (PC) production originate from the calcination of limestone (CaCO₃), which is used as raw material for the manufacturing of clinker as shown in Figure 1.



¹ Assumed with 1kWh/t/100m.
² Assumed global average, data from the Global Cement and Concrete Association, Getting the Numbers Right 2017.
³ Assumed reciprocating grate cooler with 5kWh/t clinker.
⁴ Assumed lorry transportation for average 200km.

Figure 1. Energy consumption and CO₂ emission from cement manufacturing [4].

Thus reducing CO₂ emissions and increasing energy efficiency and environmental friendliness are among the most important and urgent research topics in the cement

community today. One of the greatest potentials for CO₂ footprint reductions in cement production is the (partial) replacement of clinker with appropriate supplementary cementitious materials (SCMs), since it lowers the CO₂ emissions from the raw materials as well as the quantity of fuel used for cement production. An additional benefit of replacing PC clinker with SCMs is the utilization of industrial or agricultural by-products or wastes, such as ground granulated blast furnace slag (GGBFS; a by-product of the pig-iron production), fly ash (FA; a by-product from coal-fired power generation), rice husk ash (an agricultural by-product from rice milling and after burning treatment), or glass based pozzolans (ground recycled glass) [1,5,6]. Natural pozzolans, such as thermally treated volcanic ashes and calcined clays containing metakaolin (MK), are also used as SCM.

1.1. Portland and blended cement

Portland cement (PC) is the most commonly used cement. PC is produced from heating a mixture of finely ground clay and limestone to approximately 1450°C to form so-called clinker, which contains alite ($3\text{CaO}\cdot\text{SiO}_2$ or C_3S in cement shorthand notation), belite (C_2S , $2\text{CaO}\cdot\text{SiO}_2$), aluminite (C_3A , $3\text{CaO}\cdot\text{Al}_2\text{O}_3$), and ferrite ($\text{C}_4\text{A}_x\text{F}_{2-x}$, $4\text{CaO}\cdot(\text{Al}_2\text{O}_3)_x\cdot(\text{Fe}_2\text{O}_3)_{2-x}$) as main components. To produce the cement, the clinker is ground together with some calcium sulphate to regulate the reactivity of aluminite phase. Once PC is mixed with water, the clinker phases and the calcium sulphate react to form different hydrates, such as calcium silicate hydrate (C-S-H) gel, calcium hydroxide (CH), ettringite (AFt) and calcium aluminium (iron) mono (AFm) phases such as monosulfate or monocarbonate.

In blended cements part of the clinker is replaced by SCMs. Typical SCMs are GGBFS, MK, FA and silica fume (SF), which contain a higher amount of silica or alumina compared to Portland cement, such that the use of SCMs influences the amount and kind of hydrates formed, in particular the composition of C-S-H [7–9] and the amount of AFm phases formed. The use of SCMs in cementitious systems not only lowers CO₂ emission [5], but may also enhance the mechanical properties in the long term [6,10], their durability [11,12] and can help to suppress alkali silica reaction [13].

1.2. Calcium (aluminium) silicate hydrate

Calcium silicate hydrate (C-S-H) is the main hydration product in Portland and blended cements, and its composition greatly affects durability and mechanical properties of the hydrated cement. In the presence of Al-rich supplementary cementitious materials (SCMs), higher amounts of Al can be incorporated in C-S-H than in plain Portland cements [14]. C-(A)-S-H has a layered structure, with calcium oxide sheets sandwiched between (alumina)silicate chains in a "dreierketten" arrangement as shown in Figure 2. Within the silicate chains, two "pairing" silicate tetrahedra coordinate with Ca in the main layer, while the third tetrahedron, the bridging silica, links two pairs of silicate units. Aluminium has been observed to substitute silicon in the bridging sites [15–18]. The silicate chain length is influenced by the Ca/Si ratio as demonstrated in several ^{29}Si NMR studies [18–26]. Bridging silicate tetrahedra are mainly present in C-S-H with low Ca/Si and largely absent at high Ca/Si. Between the layers of Ca-O sheets and silicate chains, an interlayer region is present, which contains water molecules, Ca^{2+} , and possibly alkali ions (Na^+ and/or K^+) [18].

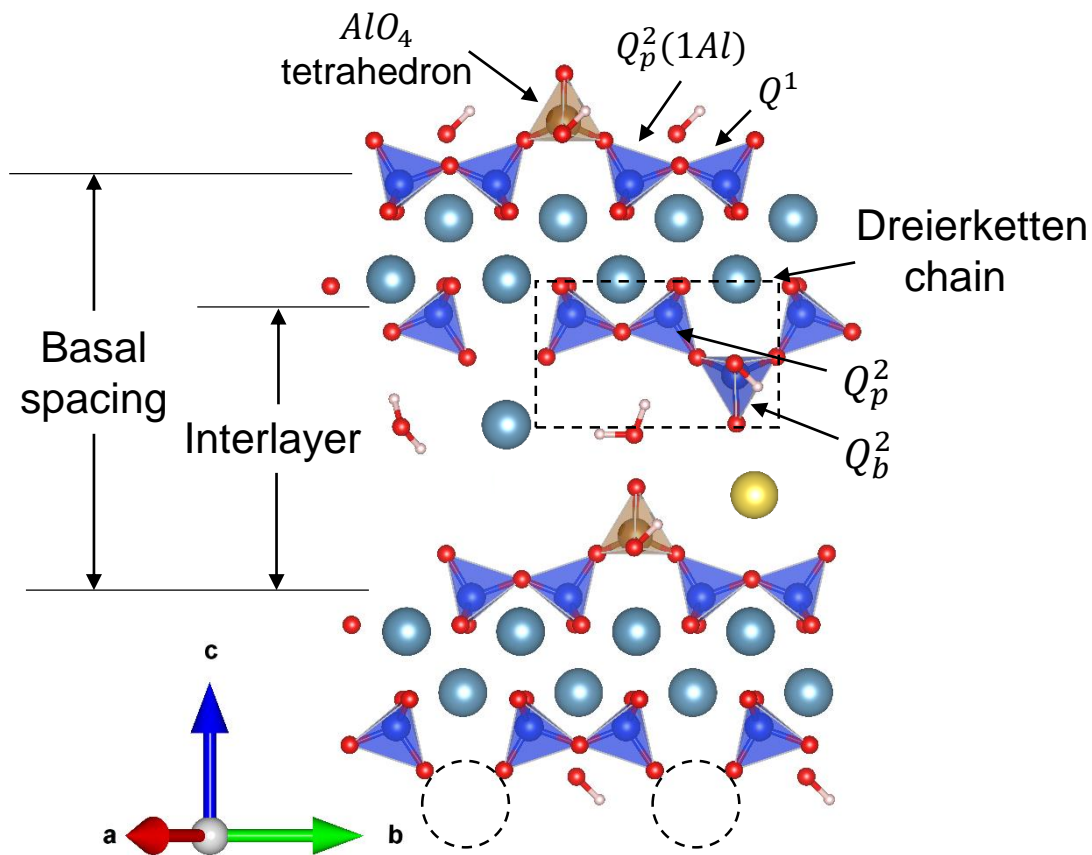


Figure 2 Schematic structure of C-A-S-H. Spheres of blue, golden, turquoise, yellow red and white colors represent Si, Al, Ca, Na, O and H respectively. The dashed circles are Si

tetrahedra vacancies in bridging sites. Q^n : n indicates the numbers of Si tetrahedral neighbors, b : bridging position, p : pairing position

The composition of C-S-H is generally defined according to the Ca/Si mol ratio, which is determined by the ion concentration in aqueous phase, the pH value, the presence of other ions, the equilibration time and the availability of water. In synthetic C-S-H in the presence of sufficient water, Ca/Si ranges from about 0.7 to 1.45. The minimum Ca/Si is limited by the presence of amorphous silica, while the maximum Ca/Si is limited by the precipitation of portlandite. C-S-H formed in Portland cement paste has a Ca/Si of about 1.7 [18].

The water content of C-S-H is difficult to determine precisely, since the measured values depend highly on the drying conditions and on the discrimination between the C-S-H crystal water and the gel water. H_2O/Si in C-S-H has been observed to increase from 1.5 to 2.2, when Ca/Si increases from 0.8 to 1.45 [23,26].

The knowledge of C-S-H composition originates to a large extent from detailed solid state ^{29}Si NMR studies, which allowed to quantify the increase of the mean silica chain length with decreasing Ca/Si [20,27–29]. Also FTIR and Raman spectroscopy have been applied to characterize C-S-H [30–33], however the band assignments of C-S-H are partially contradictory because of a strong overlap of spectral bands, resonance splitting and different factors distorting translational symmetry of real crystals (solid solutions involving different complex anions, alterations of different kinds of stacking of layer. local defects. etc.) [34].

1.2.1. Alkali uptake in C-S-H

The alkali concentration in the pore water of cement-based materials varies strongly depending on the cement composition, from ≈ 0.1 M alkali concentrations in blended cements to 0.3 to 0.5 M in Portland cement, and up to 1 M and even above in alkali-activated cementitious materials [35,36]. The alkali hydroxide concentrations in the pore solution can affect the durability of concrete as the hydroxide concentration has a significant effect on the conductivity of the pore solution as well as on the development of the alkali silicate reaction (ASR) in concrete [37,38]. The alkali hydroxide concentration in solution determines the pH value and thus indirectly also the Ca and Si concentrations. A higher pH value will lower the dissolved Ca concentration and increase Si concentrations [39–42].

Alkali species can be incorporated into the interlayer region and adsorbed on the surface of C-S-H, and they are preferably incorporated in C-S-H with lower Ca/Si [43,44]. The alkali species are thought to compensate the negative charge of deprotonated silanol groups [41,43,44] together with Ca^{2+} in the interlayer [39,41].

There is a lack of consensus on the selectivity of C-S-H for Na or K species. Hong and Glasser [43] and L'Hôpital et al. [41] observed no preference between sodium and potassium, while Bach et al. [39] observed a clear preference of potassium uptake

1.2.2. Aluminium uptake in C-S-H

The incorporation of aluminium in C-S-H has been investigated in several NMR studies. The substitution of aluminium occurs primarily as tetrahedrally coordinated Al(IV) in bridging tetrahedron. In addition to incorporation as Al(IV) into the main silicate chain, a considerable amount of aluminium may also occur in five-fold and octahedral coordination. The amount of Al(IV) in C-S-H decreases with increasing Ca/Si, where a higher fraction of Al(VI) is observed [15,18,28]. About 10% of Al associate with C-S-H is present as Al(V), independent of Ca/Si of the C-S-H.

Al NMR studies have observed multiple Al(IV) signals in C-S-H (Figure 3) and that the relative intensities of some signals (Al(IV)_a and Al(IV)_c) increases, while Al(IV)_d signal decreases with increasing Ca/Si, which indicates the Al(IV) in the bridging sites have different neighbouring cations [28,45].

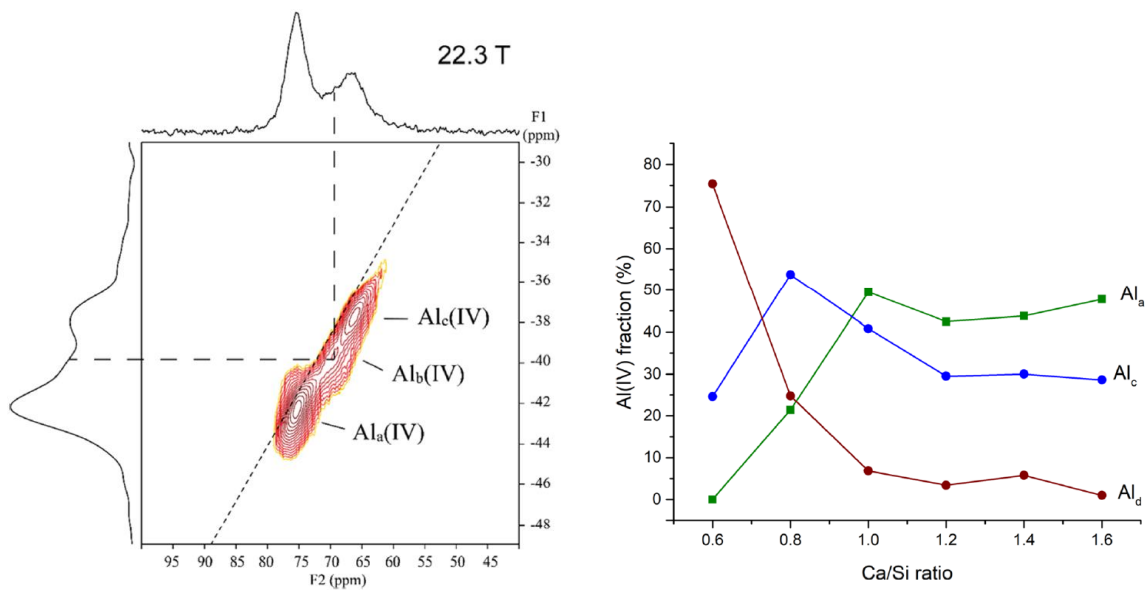


Figure 3. Contour plots of ^{27}Al MQMAS NMR spectra recorded at 22.3 T ($\nu_R = 25.0$ kHz) with sum projections in both dimensions for the C-(A)-S-H sample with Ca/Si of 1.0 and relative ^{27}Al NMR intensities for the different Al(IV) sites as a function of the Ca/Si ratio. Adapted from [45]

The nature of Al(VI) is still under debate. It has been described as third aluminate hydrate (TAH) phase in the C-S-H interlayer or on its surface [17,26], while a recent theoretical and experimental NMR study has suggested that also Al(VI) is present in the bridging site of C-S-H [46], which was recently confirmed by [45] by combined Al and Si NMR analysis.

Al/Si in C-S-H shows a quasi linear relationship with the aluminium concentration in solution, as shown in Figure 4. This trend points towards an Al uptake on one or several types of sorption sites, with a relative high capacity of up to $\text{Al/Si} > 0.2$. A larger interlayer distance has been observed in C-A-S-H than in C-S-H [26,47]. Studies analysing laboratory-synthesised C-A-S-H specimens have shown that also the amount of secondary phases increases as the Al/Si molar ratios of the solid phase increase [42,48,49]. The addition of alkali hydroxide increases the pH values and destabilises strätlingite, aluminium hydroxide and katoite, which leads to higher aluminium concentrations and thus to increased aluminium uptake in C-S-H [40–42,48].

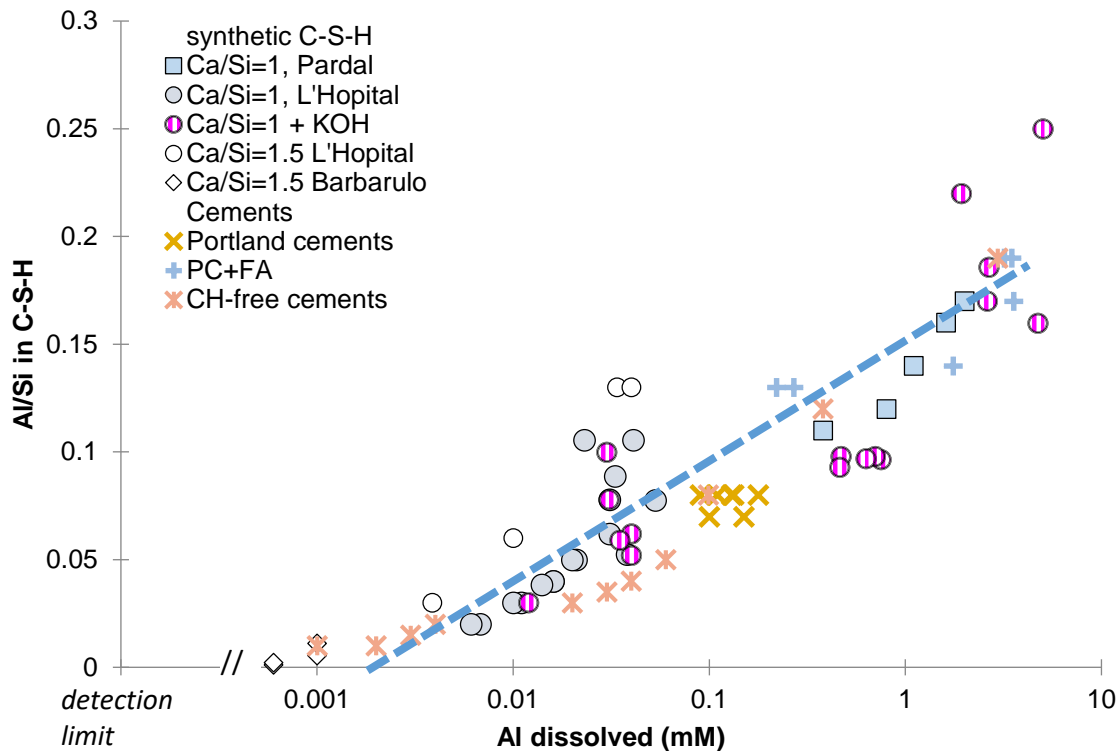


Figure 4. Effect of dissolved aluminium concentrations in the aqueous solution on the aluminium uptake in C-S-H [18].

1.2.3. Effect of equilibration time

The equilibration time can influence the kind of hydrate formed in cementitious systems: Portlandite precipitates first and can be then consumed by reacting with Si or Al rich SCMs; ettringite forms in early hydration and then converts to monosulfate phases if the ratio of calcium sulfate to C_3A is low and carbonate is absent. With 2000 years of equilibrium, phillipsite and Al-tobermorite have been observed in Roman concrete [11]. Also the composition of C(-A)-S-H could be affected by the equilibration time. However, only a limited number of research [48–50] has looked into it. Pardal et al. [49] have studied the evolution of calcium, aluminium and silicon concentrations in the aqueous phase of C-S-H with Ca/Si 0.66 from 0.05 to 20 days but have not characterised the solid phase. L'Hôpital et al. [48] has studied the effect of time on C-A-S-H with target Ca/Si=1.0, on both aqueous phase and solid phase, but only for relatively long equilibration times, from 30 days to 2 years. Very recently, Barzgar et al. [50] has studied the time effect on C-A-S-H on aqueous phase, solid phase of FTIR,

and the C-A-S-H solubility, however the use of two different preparation methods for the short-term and long-term experiments led to considerably scatter in the results.

1.3. Secondary phases

Portlandite

Portlandite is a typical reaction product from Portland cement hydration [35], as the Ca/Si ratio of PC clinker ($\text{Ca/Si} > 2.5$) is much higher than which can be accommodated in C-S-H type phases. Portlandite contains layers of octahedrally-coordinated Ca bound to tetrahedrally-coordinated O atoms [51], and has a trigonal crystal structure. The calcium concentration in equilibrium with portlandite decreases with increasing pH [52].

Hydrogarnet

Katoite, $\text{Ca}_3\text{Al}_2(\text{OH})_{12}$ (C_3AH_6) is a major hydrate formed during the hydration of calcium aluminate cements [53]. It is formed in minor quantities in Portland cement hydrated at ambient temperatures rather hydrogarnet containing iron and silica is formed [51,54]. Hydrogarnet ($\text{Ca}_3(\text{Al,Fe})_2(\text{SiO}_4)_y(\text{OH})_{4(3-y)}$; $0 < y < 3$) includes a group of minerals where the OH^- are partially or completely replaced by $[\text{SiO}_4]^{4-}$ tetrahedra. The Al-containing hydrogarnet includes hydrogrossular ($\text{Ca}_3\text{Al}_2(\text{SiO}_4)_y(\text{OH})_{4(3-y)}$; $0 < y < 3$) with the end member katoite ($\text{Ca}_3\text{Al}_2(\text{OH})_{12}$ or C_3AH_6 in cement notation [53]. Substitution of $[\text{SiO}_4]^{4-}$ for 4OH^- causes expansion of the unit cell volume [52,55]. Katoite has been identified in alkali activated cements [56], and MK blended cements cured at 60°C [57]. It has reported by Dilnesa et al. [53] that in the $\text{CaO-Al}_2\text{O}_3\text{-SiO}_2\text{-H}_2\text{O}$ system at 20°C , hydrogarnet with Si is not formed but only C_3AH_6 and C-A-S-H precipitate, which indicates the formation of iron-free hydrogrossular is kinetically hindered at room temperature.

AFm/AFt

$\text{Al}_2\text{O}_3\text{-Fe}_2\text{O}_3$ -mono and -tri phases (AFm and AFt, respectively), are hydration products of PC. AFm phases have a layered double hydroxide (LDH) type structure. The main portlandite like layer contains Al^{3+} or Fe^{3+} substitutions. The excess positive charge is balanced by an interlayer containing anions and H_2O . The typical anions in AFm phases are OH^- (C_4AH_x , where x depends on the relative humidity [51], and occurs

naturally as the mineral hydrocalumite [58]), SO_4^{2-} (monosulfate: $\text{C}_4\text{AsH}_{12}$), CO_3^{2-} (monocarbonate: $\text{C}_4\text{AcH}_{11}$) and $\text{AlSi}(\text{OH})_8^-$ (strätlingite: C_2ASH_8).

Zeolites

Zeolites or zeolitic precursors are occasionally observed to form at high bulk Al content in laboratory-synthesized C-(N-)A-S-H samples (e.g. heulandite, $\text{CAS}_7\text{H}_{1.7}$) [17], in alkali activated cements (e.g. gismondine, CAS_2H_4) [59]. They have been identified in extremely long-term hydrated Roman concrete (e.g. phillipsite, chabazite) [11] and are also observed in hydrated cements with low Ca content, such as alkali-activated metakaolin/GBFS cements [59]. Zeolites are structural analogues of the alkali aluminosilicate (hydrate) (N-A-S(-H)) gels formed through alkali-activation of low-Ca precursors such as metakaolin and fly ash [60].

1.4. Objectives of the thesis

This PhD thesis aims to investigate the effect of alkali hydroxide, aluminium uptake and equilibration time in C-A-S-H in-depth by combining the aqueous phase measurements and solid phase characterization, including TGA, XRD, spectroscopy methods (FTIR, Raman, NMR and XANES). This thesis had been part of a larger project, in which dedicated NMR spectroscopic investigations (thesis of S.-Y. Yang) had been conducted in addition to detailed experimental investigation of the solubility and structure of C-S-H in two parallel PhDs (thesis of S. Barzgar and the present thesis) and an extended C-A-S-H thermodynamic solid solution model had been developed by D. Miron.

In this thesis, systematic experimental data has been obtained from co-precipitation experiments, and the composition, structure and solubility of synthetic C-(A-)S-H has been determined. C-S-H with different Ca/Si ratios and synthesized in different alkali species and alkali hydroxide concentrations are studied in order to determine the relations between Ca/Si ratios, pH, alkali species and alkali uptake in C-S-H as well as to have a strong experimental database to contribute to the developing thermodynamic model. C-A-S-H with different Al/Si ratios and synthesized in different alkali species and alkali concentrations are also studied in order to understand the relations between aqueous phase concentration, pH and Al uptake in C-S-H. In addition, Al uptake in C-

S-H on different equilibration time from 6 hours to 3 years has been studied to fill the gaps of C-A-S-H formation kinetics.

The objectives of the current study can be summarized as follows:

1. To explain the interplay between aqueous concentrations and C-S-H composition and the influence of KOH and NaOH, and more specifically to study the C-S-H structure by a range of spectroscopic methods and powder X-ray diffraction as well as by comparison to a newly developed thermodynamic model for C-S-H with aluminium and alkali, the CASH+ model [61–63]. Based on detailed comparison of NMR, FTIR and Raman spectra we aimed to establish FTIR and Raman spectroscopy as tools to quantify the silica connectivity and the mean chain length of C-A-S-H (Chapter 3).
2. To understand the interaction between aluminium, alkali hydroxides in solution, the structure of C-A-S-H and aluminium uptake by C-A-S-H. The effect of Al and pH on C-S-H structure was determined by XRD and spectroscopic methods as well as by comparison to the thermodynamic CASH+ model [61–63] as detailed in Chapter 4.
3. To get in-depth knowledge about the kinetics of C-A-S-H formation and the precipitation of secondary phases, chemical evolution of the aqueous phase, C-A-S-H structure and composition evolution, as well as short- and long-term thermodynamic stability of C-A-S-H and secondary phases as summarised in Chapter 5.

In addition to the three main chapters summarising my results, I have also participated in different research projects on calcium silicate hydrates during the last four years, which were not included in the thesis:

Together with Ellina Bernard, we quantified the effective cation exchange capacity of calcium silicate hydrates and found that the effective cation exchange capacity (CEC) decreased at higher Ca/Si in C-S-H [64]. Around 10% of Ca^{2+} are located at exchangeable sites at low Ca/Si (0.8), while at high Ca/Si (1.6), most of Ca^{2+} are not exchangeable. In contrast, Na^+ was present only at exchangeable sites.

With Sheng-Yu Yang the incorporation of sodium and aluminium in C-(A)-S-H phases was studied by ^{23}Na , ^{27}Al , and ^{29}Si MAS NMR spectroscopy [45]: six fold-coordinated and four fold-coordinated Al is observed to present in the bridging sites of the silicate chains.

Chapter 1: Introduction

Together with Barbara Lothenbach and Daniel Jansen I studied the solubility and characterised synthesized Al-tobermorite [65] with $Al/(Al+Si) = 0.1$. A preferential uptake of Al in the branching sites of the silica chains was observed.

CHAPTER 2: Materials and methods

2.1. Materials and Synthesis

Starting materials of calcium oxide (CaO), silica fume (SiO₂) and calcium aluminate (CA: CaO·Al₂O₃) were obtained or chosen following the procedure described in detail in L'Hôpital et al. [26]. The CA contains 99.4% CA and 0.6% C₁₂A₇ as determined by X-ray diffraction and Rietveld refinement analysis using X'Pert HighScore Plus.

In this thesis, all the synthesis were conducted by a one-step protocol where appropriate quantities of CaO, SiO₂ and CA were equilibrated in water, NaOH or KOH solutions with concentrations of 0, 0.1, 0.5 or 1 M at a water/solid ratio of 45 in 180 mL or water/solid ratio of 40 in 260 mL containers.

The targeted molar Ca/Si ratio were $Ca/Si_{\text{target}} = 0.6, 0.8, 1.0, 1.2, 1.4$ and 1.6; the targeted molar Al/Si ratio were $Al/Si_{\text{target}} = 0, 0.01, 0.03, 0.05, 0.1, 0.15, 0.2$. The C-A-S-H samples were equilibrated for 0.25 day to 3 years. For more details about composition, see Appendix A.

The sample preparation, filtration and washing were following the procedure described in detail in L'Hôpital et al. [26]. The samples were freeze-dried for 7 days and then stored in N₂ filled desiccators in the presence of saturated CaCl₂ solutions (RH ≈ 30%) and NaOH as CO₂ trap [26].

For the short-term experiments shown in chapter 5, C-A-S-H samples with Ca/Si ratios of 0.6 to 1.6 and 0.5 M NaOH were synthesized. After equilibrated for 6 hours, 1 day, 3 days, 7 days, 14 days, 28 days and 90 day, 30 mL of total 260 mL homogeneously stirred suspension was filtrated by nylon filter.

2.2. Analytical methods

2.2.1. Ionic chromatography (IC) and pH measurements

The composition of the liquid phase was analyzed by ion chromatography (IC) as soon as possible after filtration in solutions diluted by factor 10, 100 and 1000 with MilliQ water to avoid any carbonation or/and precipitation. The concentrations of Ca, Na, K, Al and Si were quantified using a Dionex DP series ICS-3000 ionic chromatography

system. Independent measurements of solutions with known compositions indicated a measurement error of $\leq 10\%$.

The pH measurements were carried out in a not-diluted fraction of the solution with a Knick pH meter (pHMeter 766) equipped with a Knick SE100 electrode. The pH electrode was calibrated against NaOH or KOH solutions of known concentrations to minimize alkali error using the method detailed in [66]. The pH were measured at laboratory temperature (23 to 24°C) and corrected to 20 °C by adding +0.1 pH unit to take into account the effect of temperature on the pH measurement [48].

2.2.2. Thermogravimetric analyses (TGA)

Thermogravimetric analyses (TGA) were conducted on ground powder (~20–30 mg) under nitrogen atmosphere at a heating rate of 20°C/min from 30 to 980°C with a Mettler Toledo TGA/SDTA 8513 instrument. Mass losses between 30 °C and ~ 600 °C were assigned to dehydration and dehydroxylation of C-(N, K-)S-H and portlandite during heating. Portlandite was quantified based on the weight loss between ~ 350 and ~ 600 °C using the tangential method [67]. Quantification of portlandite by TGA instead of XRD Rietveld analysis was preferred due to the possible presence of nano-crystalline portlandite at high alkali concentrations.

2.2.3. X-ray diffractometry (XRD)

Powder X-ray diffraction (XRD) data were collected using a PANalytical X'Pert Pro MPD diffractometer equipped with rotating sample stage in a θ - 2θ configuration applying Cu radiation ($\lambda=1.54 \text{ \AA}$) at 40 mV voltage and 40 mA, with steps of $0.019^\circ 2\theta$ with a fixed divergence slit size and an anti-scattering slit on the incident beam of 0.25° and $0.5^\circ 2\theta$. The samples were scanned between 5° and $70^\circ 2\theta$ with an X'Celerator detector. Profile fittings are conducted to calculate the d -spacing and the full width at half maximum (FWHM) of the (001) reflection of C-S-H. The diffraction profiles were calculated with Pseudo-Voigt function using the software package Highscore Plus V 3.0e. The observed reflections could all be assigned based on the Powder Diffraction File for portlandite (PDF# 00-044-1481) and tobermorite MDO2 (11 Å structure) from Merlino et al. [68] for C-S-H. In the case of C-S-H with targeted Ca/Si = 1.0 and synthesized in 1.0 M KOH, an additional impurity phase of $\text{K}_2\text{CO}_3 \cdot 1.5\text{H}_2\text{O}$ (PDF# 00-011-0655) was present.

The domain sizes, referred to as crystallite sizes, were calculated by fitting the C-S-H powder XRD patterns using Pawley refinements in Topas [69] with the starting unit cells of tobermorite 11 Å ($a = 6.732(2)$ Å, $b = 7.369(1)$ Å, $c = 22.680(4)$ Å, $\gamma = 123.18(1)^\circ$, space group $B11m$) or 14 Å ($a = 6.735(2)$ Å, $b = 7.425(2)$ Å, $c = 27.987(5)$ Å, $\gamma = 123.25(1)^\circ$, space group $B11b$) [68,70]. A standard sample of CaF₂ was used to account for the instrumental peak broadening. The peak profile parameters, taken from the CaF₂ refinement, were kept fixed for all the C-S-H samples. The additional anisotropic peak broadening arising from the sample as a consequence of different crystallite sizes was refined using the AnisoCS macro [71] where two peak broadening terms were refined: one along the a - and b -axes, and one along the c -direction. In the case of 1.0 M NaOH concentration, two tobermorite phases with different c lattice parameters and different domain size along the c -axis were refined to account for the double d_{001} reflection. All other unit cell parameters and the crystallite size along the ab -directions were kept identical between the two phases.

2.2.4. Nuclear magnetic resonance (NMR)

The ²⁹Si MAS NMR spectra were acquired on a Bruker-400 (9.39 T) spectrometer using a Bruker ¹H - X 4 mm MAS probe and a spinning speed of $\nu_R = 10.0$ kHz. The spectra used single-pulse excitation with a pulse length of 1.75 μs for an rf field strength of $\gamma B_1/2\pi = 71$ kHz, a recycle delay of 30 s, and 2048 scans. The ²⁹Si chemical shifts are referenced to tetramethylsilane (TMS), using an external sample of belite, β-Ca₂SiO₃, at -71.33 ppm as a secondary reference[72].

Deconvolutions were carried out with the dmfit software [73]. The peak shapes were constraint with Lorentzian/Gaussian ratio = 0.5, FWHM ≤ 3.0 ppm for all resonances, following the description in ref. [45]. The structure of the dreierketten silica chains was respected by keeping two pairing tetrahedra (Q_p^2) for one bridging tetrahedron, $I(Q_p^2)/I(Q_b^2) = 2$ (with $I(Q_p^2) = I(Q_{pa}^2) + I(Q_{pb}^2)$). The Q_{pa}^2 and Q_{pb}^2 assignments are discussed in detail in Yang et al. [45]. The Q_{pa}^2 resonance is located at ~ -85 ppm and the Q_{pb}^2 peak at ~ -88 ppm. Q_{pb}^2 is only observed for C-S-H samples with Ca/Si < 1.0, which indicates that the chemical environment of Q_{pa}^2 and Q_{pb}^2 is different. The main chain length (MCL) were calculated using the equation:

$$MCL = \frac{2(Q^1 + Q_p^2 + Q_b^2)}{Q^1} \tag{Eq. 1}$$

²⁷Al MAS NMR measurements were carried out on a Bruker Advance III NMR spectrometer using a 2.5 mm CP/MAS probe. The single-pulse experiments for ²⁷Al MAS NMR were recorded with 104.26 MHz. The parameters used in the present study are 20 kHz spinning speed, 4000 scans, π/12 pulses of 1ms without 1H decoupling,

and 1 s relaxation delays. In order to reference the chemical shifts of the ^{27}Al MAS NMR spectra, 1.0 mol/l $\text{AlCl}_3 \cdot 6\text{H}_2\text{O}$ solution was used at 0 ppm. The ^{27}Al NMR deconvolutions were also conducted with the dmfit software [73]. The peak shape of Al(VI) signal at ~ -11 ppm was constraint with a Lorentzian/Gaussian ratio = 1.0. The Czjzek model was used for the deconvolution of Al(IV), Al(V) and Al(VI) in C-A-S-H, as outlined in detail in [74].

2.2.5. Fourier Transformation-Infrared (FTIR)

Attenuated total reflectance (ATR) Fourier Transformation-Infrared (FTIR) spectra were collected by averaging 32 scans measured on a Bruker Tensor 27 FTIR spectrometer by transmittance between 340 and 4000 cm^{-1} at a resolution of 4 cm^{-1} on ~ 3 mg of powder. The IR spectral data obtained were preprocessed using the software package OPUS (Bruker Optics GmbH, Ettlingen, Germany). Baseline correction and normalization to the intensity of the peak at around 950 cm^{-1} were applied to every recorded spectrum

2.2.6. Raman spectroscopy

The Raman spectra of chapter 3 were recorded using a Raman Bruker Senterra microscope equipped with a Peltier-cooled CCD detector and a 20mW laser. The software Opus 6.5 was used to analyse the spectra. A lens with a magnification of 50x and a green laser with a wavelength of 532 nm were used. The integration time was 10 s and each spectrum was recorded two times at spectrum resolution of 3-5 cm^{-1} . The spectra were background corrected and normalized based on the intensity of the peak at around 670 cm^{-1} .

Raman spectra of chapter 4 were recorded using a WITec Alpha 300 R confocal Raman microscope in backscattering geometry. A diode-pumped green laser with a wavelength of 532 nm laser was used in combination with a 50 \times objective lens. The Rayleigh scattered light was blocked by an edge filter. The backscattered light was coupled to a 400 mm lens-based spectrometer with a grating of 300 g/mm equipped with a cooled deep-depletion CCD. The laser power was set to 20 mW. The C-A-S-H powders were analyzed using quartz glass papillary tubes with a 2.0 mm out diameter and 0.01 mm wall thickness. Raman spectra of the sample filled and empty tubes were recorded, with the spectrum of the empty tube being subsequently subtracted. Each C-A-S-H phase was measured and averaged at 10 spots with an exposition of 10 s

and 10 accumulations for each spectrum. Spectral analysis, including glass tube signal subtraction, individual baseline correction, spectra average and smoothing, was conducted using Spectragryph [75].

2.2.7. Aluminum K-edge (1559 eV) XANES measurements

Aluminum K-edge (1559 eV) XANES measurements were conducted at the Phoenix II, elliptical undulator beamline at the Swiss Light Source (SLS), Paul Scherrer Institute (PSI), Villigen, Switzerland. Energy selection, X-ray energy calibration, sample preparation and measurement were followed as described in [76]

Data integration, reduction, and correction (e.g., fluorescence self-absorption) of X-ray absorption near edge structure (XANES) spectra were performed using the Demeter software package [77]. Al K-edge XANES spectra of samples were interpreted by iterative-target transformation factor analysis (ITFA) to quantify the proportions of Al-containing components [78]. FEFF8.4 [79] was employed to calculate the theoretical Al K-edge XANES spectra of representative Al coordination environments (tetrahedral AlO_4 in bridging site *v.s.* octahedral AlO_6 in interlayer) in C-A-S-H; the corresponding atomic structures were generated using Material Studio (MS) software V7.0.

2.2.8. C-S-H composition

The effective Ca/Si and effective Al/Si in C-S-H ($\text{Ca/Si}_{\text{C-S-H}}$ and $\text{Al/Si}_{\text{C-S-H}}$) was obtained by mass-balance calculations, considering the initial amount of CaO, CA and SiO_2 in the system, the amount of other solids present as well as the fraction of SiO_2 Al_2O_3 and CaO in solution following the procedure outlined in [48].

The amount of alkalis bound in the solid was determined following the **direct method** (i.e. complete re-dissolution of 20 mg of washed and dried C-S-H phase in 10 mL 100 mM HCl). The total amount in the solid was obtained from the measured Ca, Na and K concentrations in the HCl solution as detailed in [41]. The amount of alkali was also obtained indirectly from mass balance calculations using the total amount of alkalis present minus the fraction which remained in the equilibrium solution. This **indirect method** gives comparable results to the direct method up to 0.1 M NaOH and KOH (see also [41]). At higher alkali concentrations, however, the indirect method fails as the deduction of high measured concentrations to obtain a small amount of absorbed alkali ions results in too large errors to allow any meaningful conclusions.

The incorporation of Al into C-S-H phases can also be expressed in terms of a K_d value (distribution coefficient), to quantify the relative affinity for Al to sorb to C-S-H [80]. The K_d values were calculated according to:

$$K_d = \frac{C_{s,eq}}{C_{l,eq}} \approx \frac{(C_0 - C_{l,eq})}{C_{l,eq}} \times \frac{V}{M} \left(\frac{m^3}{kg} \right) \quad Eq. 2$$

where $C_{s,eq}$ is the equilibrium Al concentration sorbed to C-S-H phases [mol/kg] and $C_{l,eq}$ is the equilibrium concentration in solution [mol/m³]. The difference between the initial Al concentration in suspension (C_0) and the concentration determined in the filtrated supernatant ($C_{l,eq}$) corresponds to sorbed Al. M is the dry weight of the C-S-H phase [kg], and V is the volume of solution [m³].

2.2.9. Thermodynamic modelling

Thermodynamic modelling was carried out with the Gibbs free energy minimization program GEM-Selektor v3.7 [81]. GEMS is geochemical modelling code that computes equilibrium speciation of dissolved species and stable solid phases composition using Gibbs free energy minimization algorithms. The thermodynamic data for aqueous, gaseous phases, portlandite and amorphous SiO₂ were taken from the PSI-Nagra thermodynamic database [82], microcrystalline Al(OH)₃, strätlingite, C-S-H and katoite was taken from the Cemdata18 database [83], the zeolites chabazite (CaAl₂Si₄O₁₂·6H₂O) from [84] and gismondine-P1 (Na₆Al₆Si₁₀O₃₂·12H₂O) from [85].

C-S-H and alkali uptake was modelled using the recently developed CASH+ thermodynamic model [61–63], which had been parameterized against experimental data independent of this study. The formation of the CaSiO₂(OH)₂⁰ was described using a formation constant of log K = 4.0 for the equation Ca²⁺ + SiO₂(OH)₂²⁻ ↔ CaSiO₂(OH)₂⁰ [61] instead of the log K of 4.6 from [82].

Ion activity products (IAP) for C-(A)-S-H and saturation indices (SI) for relevant solid phases were calculated from experimentally measured concentrations. Activity coefficients were calculated using the extended Debye-Hückel equation in Truesdell–Jones form with common ion-size parameter $a_i = 3.31 \text{ \AA}$ for NaOH solutions and third parameter $b_y = 0.098 \text{ kg/mol}$; for KOH $a_i = 3.67 \text{ \AA}$ and $b_y = 0.123 \text{ kg/mol}$ [86].

CHAPTER 3: Effect of alkali hydroxide on calcium silicate hydrate (C-S-H)¹

3.1. Introduction

The alkali concentration in cement-based materials varies strongly depending on the cement composition. In the pore solution of blended cements and low alkali cements, ≈ 0.1 M alkali concentrations can be observed, while in most Portland cements alkali concentrations are between 0.3 to 0.5 M, and up to 1 M and even above in alkali-activated cementitious materials [35,36]. The alkali hydroxide concentrations in the pore solution can affect the durability of concrete as the hydroxide concentration has a significant effect on the conductivity of the pore solution as well as on the development of the alkali silicate reaction (ASR) in concrete [37,38].

The alkali hydroxide concentration in solution determines the pH value and thus indirectly also the Ca and Si concentrations. A higher pH value will lower the dissolved Ca concentration and increase Si concentrations [39–42]. The alkali uptake in C-S-H is strongly influenced by the dissolved alkali concentration and Ca/Si of C-S-H. The alkali species are incorporated into the interlayer and on the surface via a charge balance mechanism [16,39,41,42,87]. The silicate chains are negatively charged, depending on pH, which can be compensated by cations, i.e. Ca^{2+} , H_3O^+ and Na^+ or K^+ [64]. The higher the pH value, the higher is the negative charge [87–90]. Bivalent cations such as calcium are strongly preferred compared to monovalent sodium or potassium due to stronger electrostatic interaction [87,90]. Thus less alkalis are taken up at higher Ca/Si, as the alkali ions compete with calcium ions to compensate the negative surface charge of C-S-H. The maximum Na/Si and K/Si reported in the literature are in the range of 0.3-0.7 at $\text{Ca/Si}_{\text{C-S-H}} < 1.0$ [41,42,44,91]. Different approaches are reported in the literature to model thermodynamically the equilibrium between C-S-H and solution as discussed in detail in [18], although only few models are able to describe the incorporation of alkalis in C-S-H. High alkali concentrations result in a shorter mean silica chain length and larger interlayer distances [41,42]. In

¹ This chapter has been published as: Y. Yan, S.Y. Yang, G.D. Miron, I.E. Collings, E. L'Hôpital, J. Skibsted, F. Winnefeld, K. Scrivener, B. Lothenbach, Effect of alkali hydroxide on calcium silicate hydrate (C-S-H), *Cem. Concr. Res.* 151 (2022).

addition, the uptake of alkalis in the interlayer and the surface shifts the ^{29}Si NMR resonances to less negative values [41,42,92].

However, the interplay between alkali hydroxides in solution, the structure of C-S-H and alkali binding by C-S-H is still not fully understood, as most studies focus either on the study of aqueous concentrations [43] or on the characterization of the solid phases [92]. Moreover, there are important discrepancies among the results reported, some research observed a preference of K compared to Na uptake in synthetic C-S-H [39,93–95], while some found a higher sorption of Na than K in hydrated Portland cement [96], and other studies showed no significant difference between Na and K uptake in synthetic C-S-H [41–44,97]. The discrepancies indicate either that a large experimental error is associated with the alkali uptake measurements and/or different mechanisms are responsible for the alkali uptake in C-S-H depending on Ca/Si, equilibration time or the experimental procedure.

The present chapter aims to explain the interplay between aqueous concentrations and C-S-H composition and the influence of KOH and NaOH, and more specifically to study the C-S-H structure by a range of spectroscopic methods and powder X-ray diffraction as well as by comparison to a newly developed thermodynamic model for C-S-H with alkali, the CASH+ model [61,62].

3.2. Results and discussion

3.2.1. Effect of Ca/Si on liquid and solid phase composition

The Ca/Si ratio affects greatly the composition of the equilibrium solutions in the absence of alkali hydroxides as shown in Figure 5, where changes of Ca, Si and OH^- concentrations are plotted as a function of the Ca/Si in C-S-H. The Ca/Si in C-S-H ($\text{Ca/Si}_{\text{C-S-H}}$) varies between ≈ 0.75 -1.44 for $\text{Ca/Si}_{\text{target}}$ from 0.6 to 1.6, as at very low $\text{Ca/Si}_{\text{target}}$ amorphous silica precipitates in addition to C-S-H and at high $\text{Ca/Si}_{\text{target}}$ portlandite [18]. At low $\text{Ca/Si}_{\text{target}}$, the Si and Ca concentrations are in the mM range; the silicon concentrations decrease down to 0.004 mM at high $\text{Ca/Si}_{\text{target}}$, while Ca concentrations increase up to 21 mM in the presence of portlandite. The measured trends and concentrations agree well with other observations reported in the literature as summarized in e.g. the recent review of Walker et al.[98], and with the changes

Chapter 3: Effect of alkali hydroxide on calcium silicate hydrate (C-S-H)

modelled by using the CASH+ thermodynamic model [61], although the model somewhat underestimates the Ca and overestimates the Si concentrations. At the lowest total $\text{Ca}/\text{Si}_{\text{target}}$ of 0.6, the thermodynamic model predicts in addition to low $\text{Ca}/\text{Si}_{\text{C-S-H}}$ C-S-H the presence of a small amount of amorphous SiO_2 (16% of the total silica present in the sample).

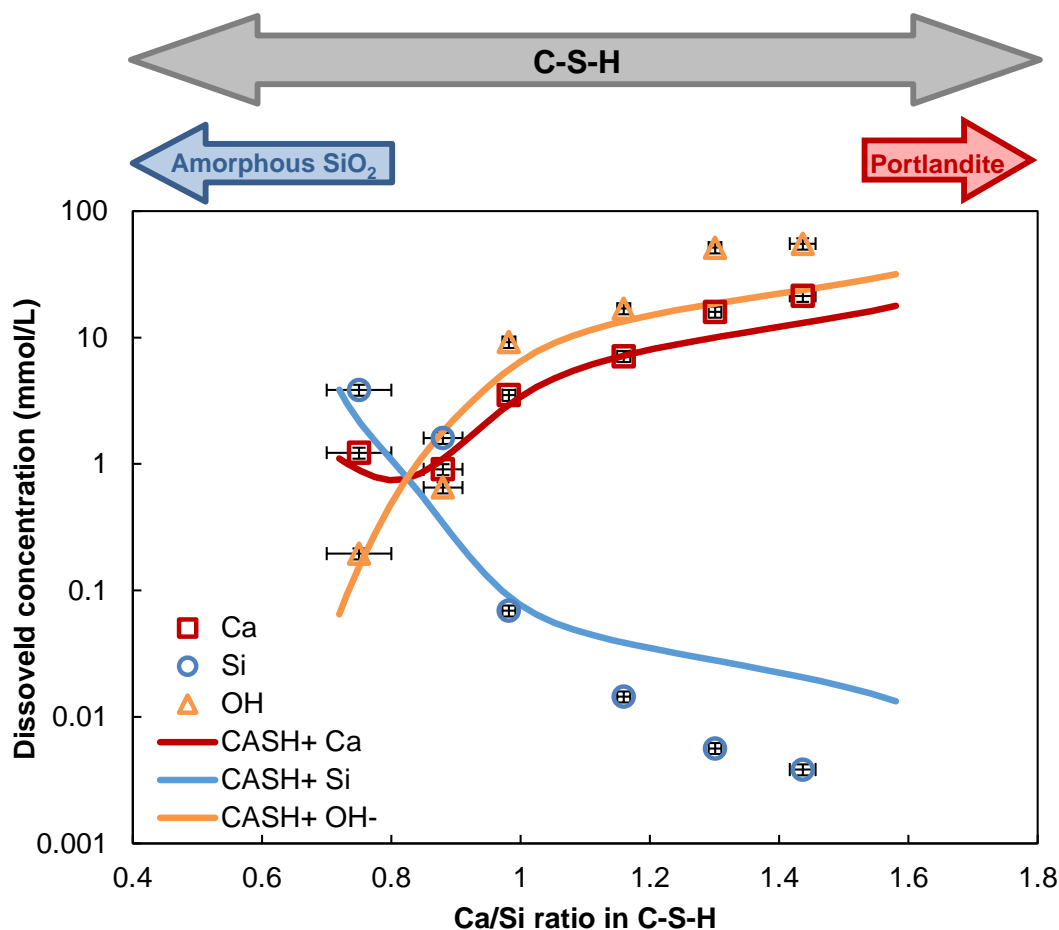


Figure 5 Concentrations of Ca, Si and OH^- in solutions equilibrated with C-S-H samples as a function of the Ca/Si ratios in C-S-H. Yellow triangles: OH^- , red squares: Ca and blue circles: Si. Solid lines: simulated using the thermodynamic CASH+ model [61,62]. The estimated absolute errors of $\text{Ca}/\text{Si}_{\text{C-S-H}}$ are smaller than ± 0.05 units in the Ca/Si ratios. The estimated relative uncertainty of the IC measurements is $\pm 10\%$, which is smaller than the size of the symbols.

C-S-H is the main solid phase observed for every targeted Ca/Si. In addition to C-S-H, portlandite is precipitated at $\text{Ca}/\text{Si}_{\text{target}}=1.6$ (see Figure 6 (a)), while amorphous SiO_2 is observed at $\text{Ca}/\text{Si}_{\text{target}}=0.6$ resulting in effective $\text{Ca}/\text{Si}_{\text{C-S-H}}$ of 0.75 to 1.44. All aqueous concentrations, the effective C-S-H composition and the amount of minor phases are reported in Table 9 and Table 14. A closer inspection of the XRD diffractograms summarized in Figure 6 (a) shows that for high Ca C-S-H the lowest-angle diffraction

peak (d_{001}), indicating the basal spacing of C-S-H, is more distinct and that the interlayer distances are getting smaller. The decrease in basal spacing could be related to the charge balancing effect of Ca^{2+} in the C-S-H interlayer, which may increase the attractive force between the negatively charged main layers [99]. The broad reflection at $\sim 17^\circ 2\theta$ (d -spacing $\sim 5 \text{ \AA}$), which has been assigned to a d_{101} signal and indicates occupation of bridging Si-sites [100], is well visible at low $\text{Ca}/\text{Si}_{\text{C-S-H}}$, where the bridging silica are present and absent at high $\text{Ca}/\text{Si}_{\text{C-S-H}}$, where the bridging sites are empty, which has also been observed in XRD studies on C-S-H [100]. The tendency is in agreement with ^{29}Si NMR studies (e.g. [26], Figure 6 (b)).

The NMR spectra in Figure 6 (b) show resonances between -75 to -90 ppm, which are simulated using four resonances with chemical shifts (δ_{iso}) of ~ -79 ppm (chain-end sites, Q^1), -82 ppm (bridging sites Q_b^2), -85 ppm and -87 ppm (paired sites, Q_{pa}^2 , and Q_{pb}^2) with the restriction that the intensities fulfill the condition, $[I(Q_{pa}^2) + I(Q_{pb}^2)]/I(Q_b^2) = 2$ imposed by the dreierketten model, as discussed in detail by Yang et al. [45]. In C-S-H with low $\text{Ca}/\text{Si}_{\text{C-S-H}}$, mainly Q^2 sites are present indicating the predominance of connected silicate chains and a small number of Q^1 groups from the end of the silica chain. The Q^1 intensity increases with Ca/Si such that at $\text{Ca}/\text{Si}_{\text{C-S-H}} = 1.30$ and 1.44 mainly dimers (Q^1 species) are observed, in agreement with the previous observations [19–22,24,26,42]. The decrease of Q^2 and increase of Q^1 species leads to a decrease of the mean chain length from 76 ± 15 at $\text{Ca}/\text{Si}_{\text{C-S-H}} = 0.75$ to 2.5 ± 0.1 at high $\text{Ca}/\text{Si}_{\text{C-S-H}}$ (see Table 1). The MCL values at low Ca/Si are somewhat larger than those derived earlier for similar samples, which varied from 20 - 37 [20,24–26]. This may reflect differences in equilibration time during synthesis and the fact that the precision in MCL is very sensitive to small intensity variations at low values for the Q^1 intensities (see Eq. (1)).

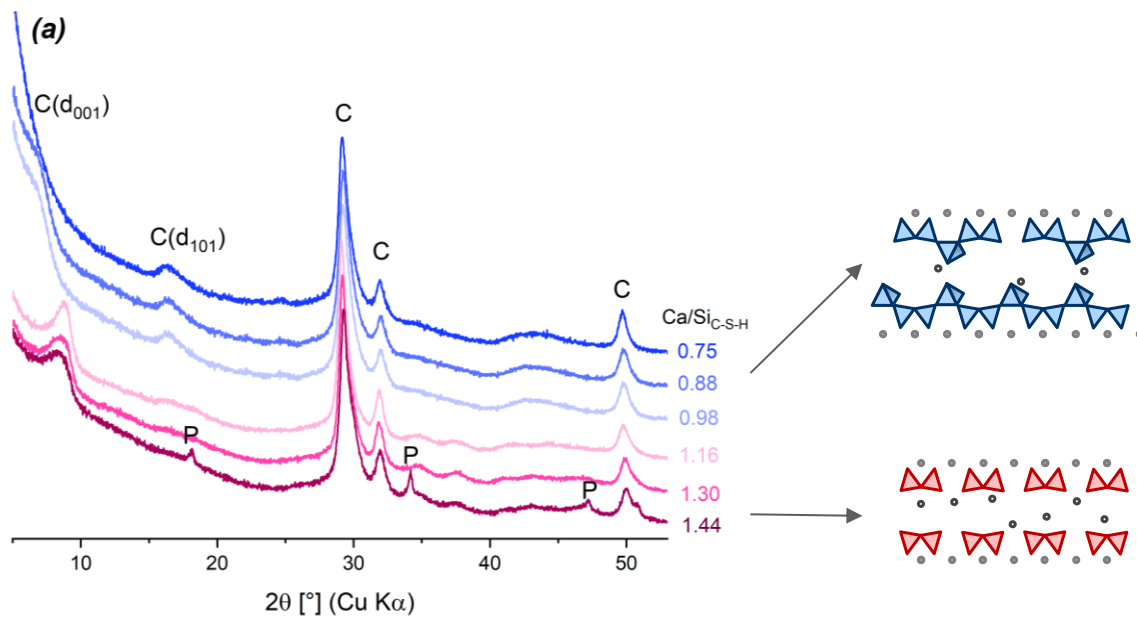
Figure 6 (c and d) show the FTIR and Raman spectra of C-S-H. Since the Si-O bonds are the strongest bonds in the structure with a covalent character, different types of Si-O can be recognized in the infrared spectra; the position of transmittance bands is affected slightly by the ions in the second coordination sphere [101]. From 400 cm^{-1} to 800 cm^{-1} , the spectra have contributions from bending vibrations of the O-Si-O groups in the dreierketten chains and from water librations, while the bands in the region $800\text{--}1200 \text{ cm}^{-1}$ are due to stretching vibration of Si-O [34,102].

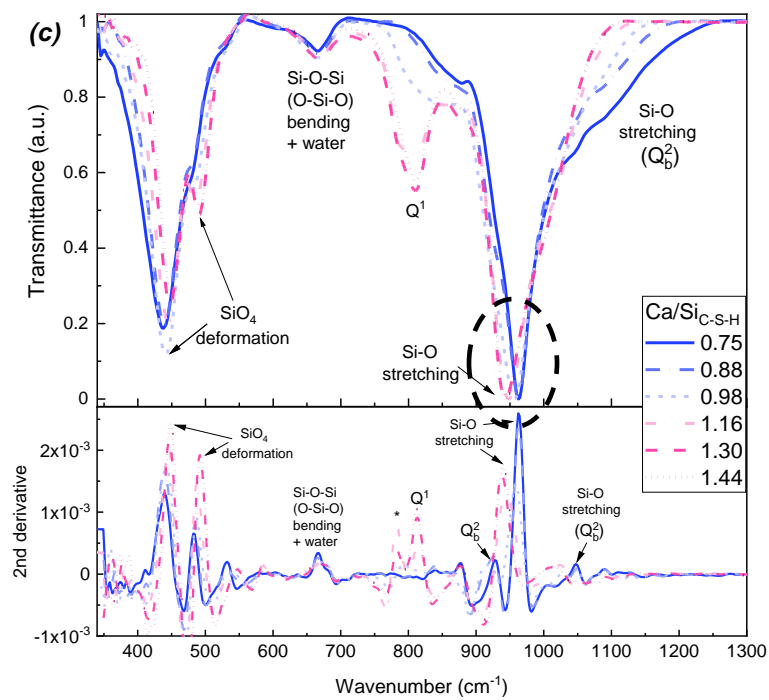
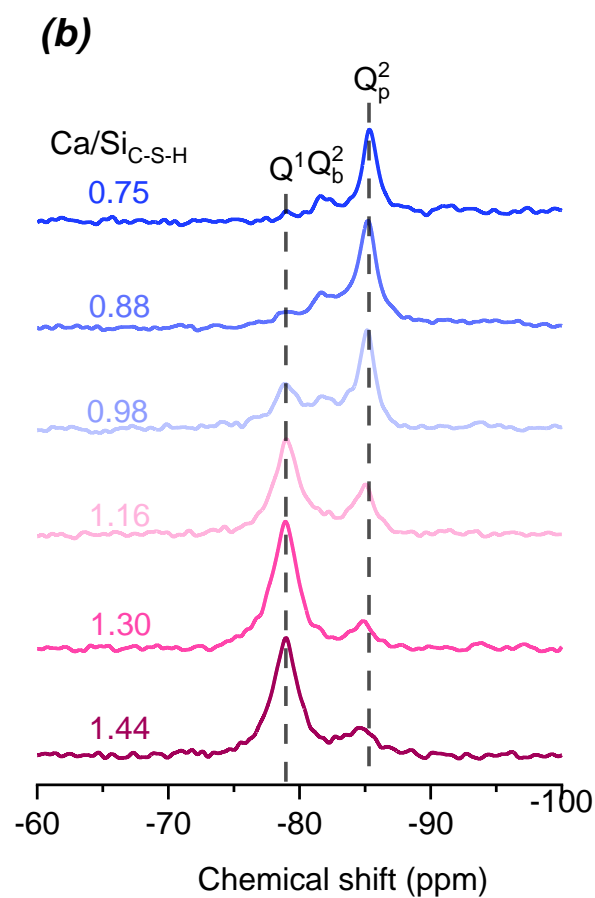
In FTIR the bending vibrations at wavenumbers from 500 to 800 cm^{-1} can be considered as a "fingerprint region" sensitive to the composition and the topological features of the tetrahedral frameworks [34]. The bands observed are consistent with the FTIR spectra of C-S-H at different Ca/Si reported e.g. in Yu et al. [33]. The bands from 400 to 550 cm^{-1} are assigned to deformations of Si tetrahedra [33,102]; the intensity of the shoulder at 480 cm^{-1} increases clearly with Ca/Si_{C-S-H}, which indicates there is also a Q¹ signal hidden under it. The band at 670 cm^{-1} has been related to Si-O-Si (O-Si-O) bending [33,102] and water librations [102] and shows little variation upon an increase of Ca/Si_{C-S-H}. The signal at 810 cm^{-1} is related to Si-O stretching of Q¹ tetrahedra [33]. The strong increase of its intensity at high Ca/Si_{C-S-H} agrees well with the increase of the Q¹ signal reported from Si-NMR studies [25,48] and Figure 6 (b). At 960 cm^{-1} the main peak is observed and is associated with Si-O stretching modes [102]. An increase of the Ca/Si_{C-S-H} leads to a shift to lower wavenumber (940 cm^{-1}), indicating progressive depolymerisation of the silicate chains. A shoulder on the low-frequency side of the Q¹ signal marked as * is also detected in C-S-H with Ca/Si_{C-S-H} from 1.16 to 1.44, while no literature was found to give interpretation of this signal. The main peak of the FTIR spectra located between 940 to 960 cm^{-1} has often been assigned in the literature to Q² vibrations [31,33,103,104], however, its predominance for all Ca/Si_{C-S-H} and the observed shift indicate rather that the band observed is composed of several overlying vibrations including a Q² signal at $\approx 960 \text{ cm}^{-1}$ [105], which results in the observed shift to higher wavenumbers for low Ca/Si_{C-S-H}. A shoulder on the low-frequency side of the main peak located at $\approx 930 \text{ cm}^{-1}$ detected in C-S-H with Ca/Si_{C-S-H} from 0.67 to 0.98 is interpreted as Q_b² due to Si-O stretching modes within OH-SiCa configurations in the bridging tetrahedron [102]. A shoulder on the high-frequency side located at $\approx 1050 \text{ cm}^{-1}$ is also detected arising at increased Ca/Si_{C-S-H} and interpreted as Si-O stretching including Si-O stretching in Q_b² [102].

The Raman spectra in Figure 6 (d) also provide vibrational information; the strongest vibrational modes active in Raman are those that related to the greatest polarizability; symmetric vibrational modes are most Raman active. From 150 cm^{-1} to 400 cm^{-1} , the spectra have contributions from Ca²⁺ motions in the region $< 250 \text{ cm}^{-1}$ [106] and the lattice vibrations of Ca-O at 316-333 cm^{-1} [107]. The intensity of the Ca-O band increases with increasing Ca/Si_{C-S-H} and shifts from 316 cm^{-1} at Ca/Si_{C-S-H} = 0.75 to 333 cm^{-1} at Ca/Si_{C-S-H} = 1.44. A small shoulder 350 cm^{-1} appears at Ca/Si_{C-S-H} = 1.44, which

Chapter 3: Effect of alkali hydroxide on calcium silicate hydrate (C-S-H)

is assigned to portlandite [28,107]. A major band at 445 cm^{-1} is assigned to internal deformation of the Si-tetrahedra [106] or to O-Si-O bending [107]; its intensity increases with Ca/Si. The main Si-O-Si symmetrical bending peak at $\sim 675\text{-}680\text{ cm}^{-1}$ broadens with increasing Ca/Si_{C-S-H}, which agrees with the study of Garbev et al. [107]. The peak has been assigned to Q² symmetrical bending [106,107], however, as this peak is dominant both at high and low Ca/Si_{C-S-H}, further vibrations not related to Q² species contribute to this signal. The Si-O silicate symmetrical stretching (SS) band at $\sim 870\text{-}900\text{ cm}^{-1}$ is assigned to SS Q¹; its intensity increases strongly with Ca/Si and thus the fraction of Q¹ species present. The band at $950\text{-}1010\text{ cm}^{-1}$ has been assigned to SS Q² [22,106–108], however, as its intensity does not decrease at higher Ca/Si_{C-S-H}, a number of other vibrations seem to contribute. The peaks located at 1080 cm^{-1} are attributed to the C-O SS vibrations [28,106,107,109] and are identified in every spectrum as Raman is very sensitive to even small CO₂ contaminations.





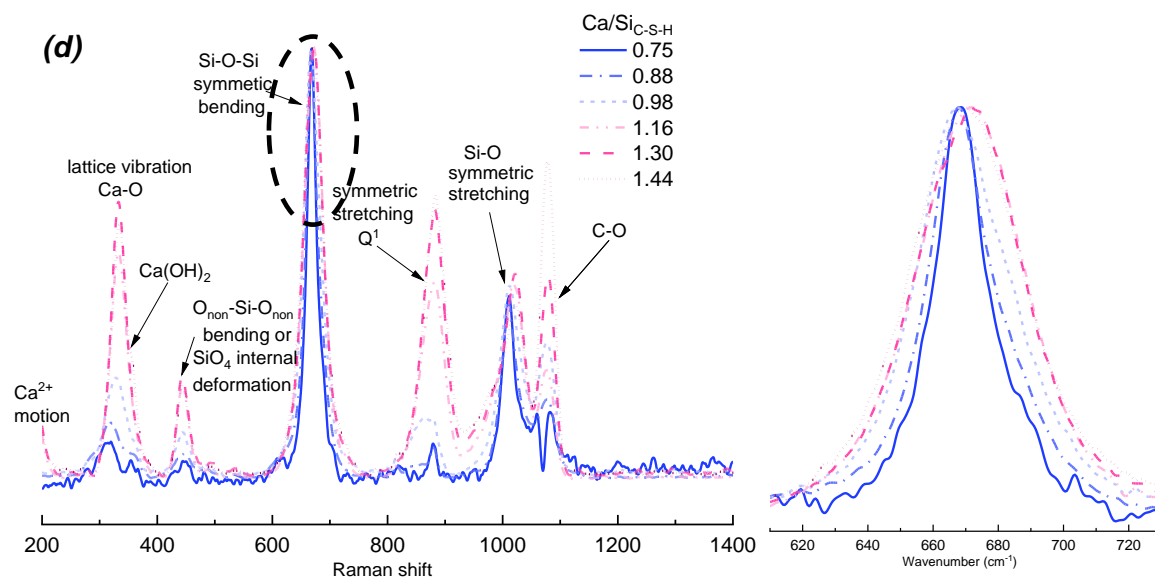


Figure 6. (a) XRD diffractograms of the C-S-H samples synthesized in water and C-S-H schema for C-S-H with low Ca and high Ca. (b) ^{29}Si NMR spectra, (c) FTIR and (d) Raman spectra of C-S-H with $\text{Ca}/\text{Si}_{\text{C-S-H}}$ from 0.75 to 1.44, after an equilibration time of 3 months. C: C-(K)-S-H; P: portlandite.

Table 1 Secondary phase quantification and mean silica chain length (MCL) of C-S-H samples without alkali

$\text{Ca}/\text{Si}_{\text{target}}$	$\text{Ca}/\text{Si}_{\text{C-S-H}}$	SiO_2 amorphous (wt. %) ^a	Portlandite (wt. %) ^b	MCL ^a
0.6	0.75 ± 0.05	10 ± 2	0	76 ± 15
0.8	0.88 ± 0.03	4.0 ± 1.0	0	27 ± 7
1.0	0.98 ± 0.01	0	0	9.1 ± 1.3
1.2	1.16 ± 0.01	0	0	3.5 ± 0.2
1.4	1.30 ± 0.01	0	0	2.55 ± 0.10
1.6	1.44 ± 0.02	0	0.9 ± 0.1	2.56 ± 0.10

^a Amorphous SiO_2 and MCL quantified from ^{29}Si NMR. ^b Portlandite quantified by TGA.

The mean silicate chain length (MCL) calculated from FTIR and Raman as well as thermodynamic CASH+ models are compared with values from ^{29}Si NMR as illustrated in Figure 7. The CASH+ model shows the same trends but a somewhat weaker increase of MCL at low Ca/Si, which is related to higher MCL observed in the present study. The MCL of FTIR and Raman are calculated based on the peak area ratio of the Q¹ signal at ~ 810 and the main peak at ~ 960 cm^{-1} from FTIR, and Q¹ signal at ~ 880 and the main peak at 670 cm^{-1} from Raman. The MCL calculated from FTIR, Raman, and NMR decreases as the $\text{Ca}/\text{Si}_{\text{C-S-H}}$ increases, confirming agreement among the different spectroscopic methods. For C-S-H with every $\text{Ca}/\text{Si}_{\text{C-S-H}}$, FTIR overestimates the MCL because the IR spectrum in the main peak region contains very complicated

series of overlapping bands. Raman shows better agreement with the NMR quantification because the peaks are more separated but for C-S-H with $\text{Ca}/\text{Si}_{\text{C-S-H}} = 0.75$, the signal to noise ratio is lower than the others, which makes the quantification error larger. For C-S-H with $\text{Ca}/\text{Si}_{\text{C-S-H}} > 1.0$, dimers dominate in C-S-H so the MCL is around 2.5. The difference of MCL from FTIR, Raman and NMR is smaller when $\text{Ca}/\text{Si}_{\text{C-S-H}}$ is above 1.15, but the calculation of Q^1 species shows a much greater difference as shown in Figure 43, while this is not well visible in Figure 7.

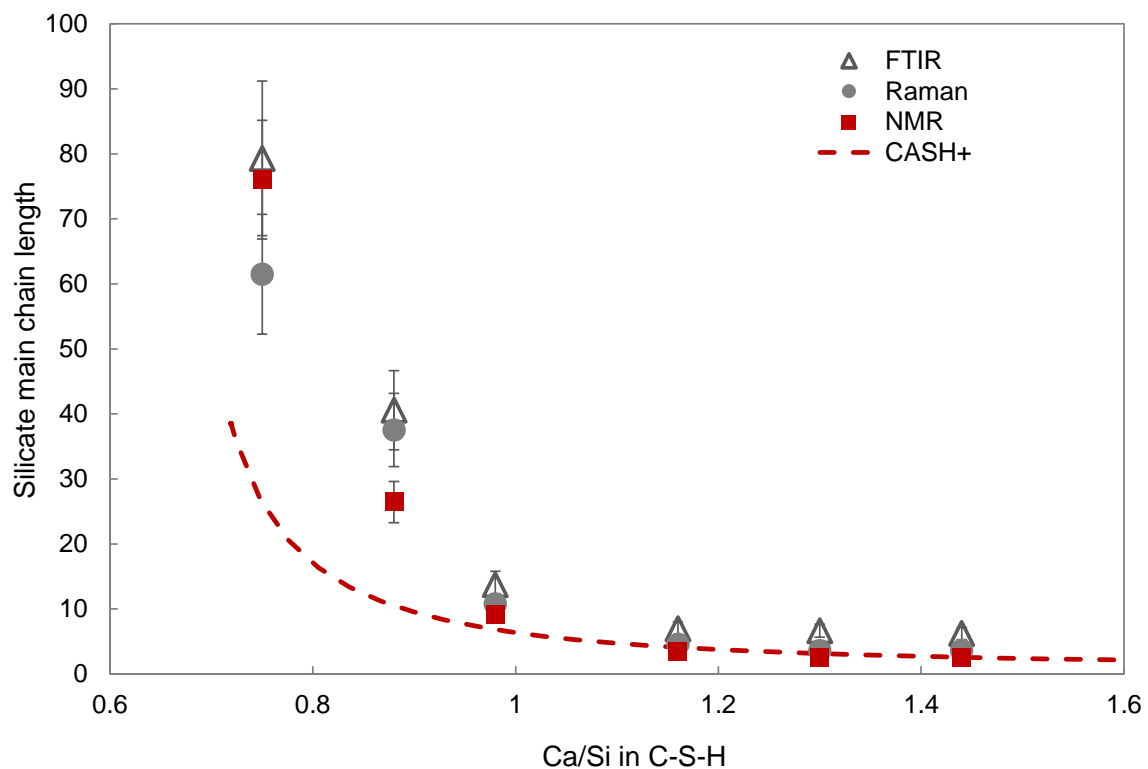


Figure 7 Silicate main chain length determined by FTIR, Raman, ^{29}Si NMR, and thermodynamic CASH+ model.

3.2.2. Effect of NaOH / KOH on the aqueous phase

In the absence of KOH or NaOH, the measured aqueous Ca concentrations and pH values increase with rising $\text{Ca}/\text{Si}_{\text{solid}}$, while the Si concentrations decrease as shown in Figure 5. Figure 8 illustrates that the presence of NaOH or KOH leads to higher pH values and silica concentrations, but lower Ca concentrations; no significant difference was observed between NaOH and KOH. The measured concentrations are consistent with existing solubility measurements in the $\text{CaO-Na}_2\text{O}_3\text{-Na}_2\text{O/K}_2\text{O-SiO}_2\text{-H}_2\text{O}$ systems

Chapter 3: Effect of alkali hydroxide on calcium silicate hydrate (C-S-H)

between 20 to 25 °C [24,41,42,48,110–112], which all show comparable trends in dissolved Si, Ca and pH values with respect to the bulk alkali content and Ca/Si ratio.

In the presence of KOH and NaOH, the dissolved Si and Ca concentrations show similar trends as in their absences: a rise of Ca and a decline of Si concentrations with increasing Ca/Si (Figure 8). This suggests that C-(N, K-)S-H solubility does not vary greatly as a function of the alkali cation (Na or K) present, but that the concentrations are just shifted to higher pH values, due to the common ion effect with C-S-H between pH, Ca and Si. The measured pH values, alkali (data in Table 9), Ca and Si concentrations can be well reproduced by thermodynamic modelling using the recent CASH+ solid solution model [61,62]. In agreement with the experimental data, no significant differences are observed in the modelled results, independent of whether NaOH or KOH are used.

The thermodynamic model predicts higher pH values in the presence of alkali hydroxides and increased Si concentrations due to the preference of Si to form negatively charged complexes such as $\text{SiO}(\text{OH})_3^-$ and $\text{SiO}_2(\text{OH})_2^{2-}$ at higher pH values. This tendency of silicon to remain in solution at high pH values leads to a complete dissolution of SiO_2 at 0.5 M NaOH and above and to a decrease of the calculated $\text{Ca}/\text{Si}_{\text{C-S-H}}$ from 0.75 (no alkali) to ~ 0.7 at 0.1, 0.5, and 1 M NaOH, due to the limited availability of SiO_2 in the experimental system studied.

In the presence of portlandite, the opposite effect can be observed: a decrease of Ca/Si in C-S-H at higher NaOH concentrations. Higher pH values and thus higher OH⁻ concentrations decrease the Ca concentrations in equilibrium with portlandite which lowers Ca-uptake in C-S-H. In the presence of portlandite, Ca concentration decrease from 21 mM to 5 mM (0.1 NaOH), 0.8 (0.5 M NaOH) and 0.3 mM Ca in 1 M NaOH leading to a decrease of the maximum calculated $\text{Ca}/\text{Si}_{\text{C-S-H}}$ from 1.44 at 0 and 0.1 M NaOH to 1.35 at 0.5 M NaOH and to 1.07 at 1 M NaOH as detailed also in Table 14.

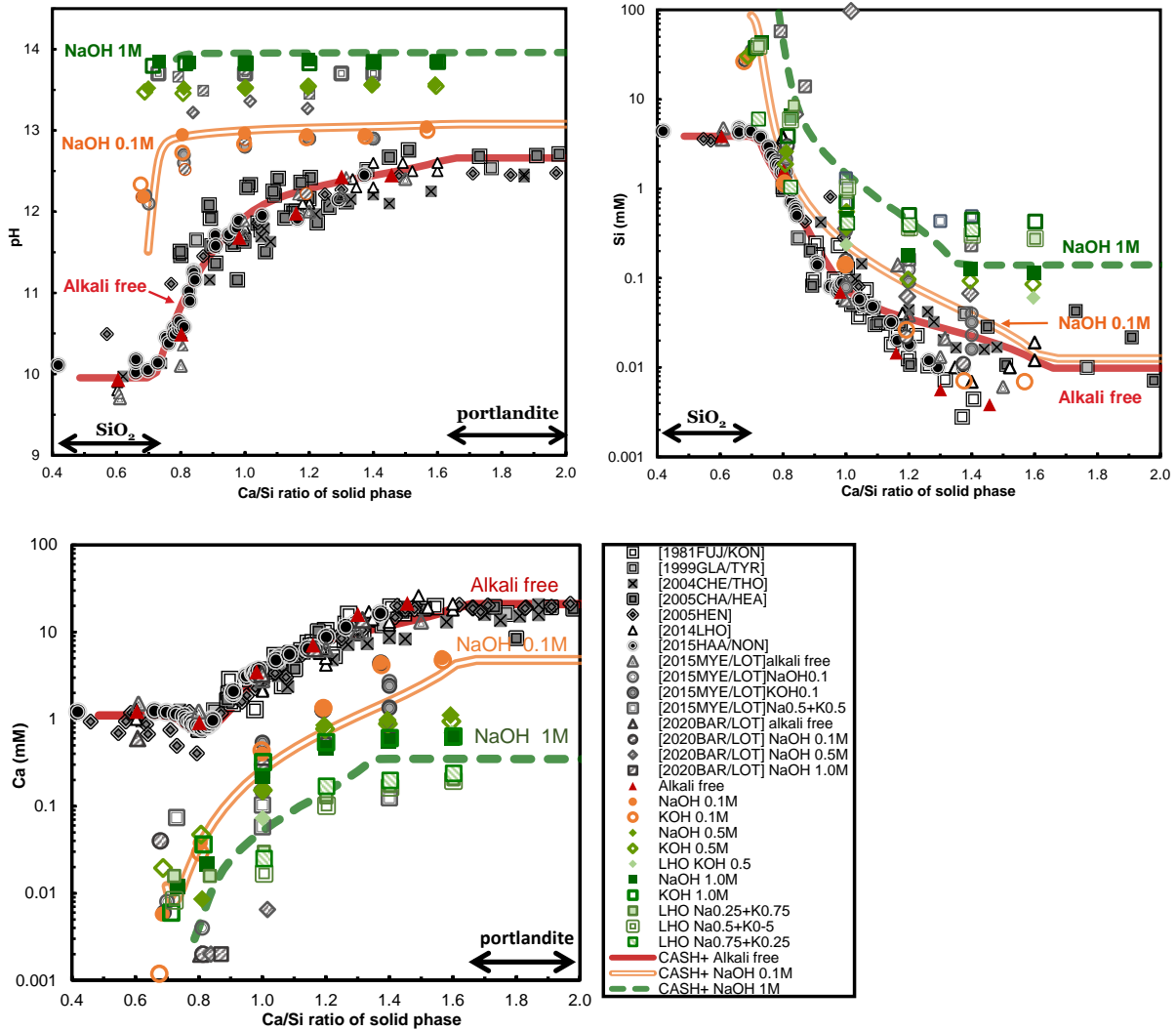


Figure 8. pH values, Si and Ca concentrations in the solutions of the C-(N,K)-S-H samples as a function of Ca/Si ratios in C-(N,K)-S-H. The estimated absolute errors are $\leq \pm 0.05$ units in the Ca/Si ratios and ± 0.2 in pH. The estimated relative uncertainty of the IC measurements is $\pm 10\%$. Grey symbols: synthetic C-S-H data from [18,40,42,98]; colored symbols: C-(N,K)-S-H from this study; red triangles: C-S-H in water; orange circles: C-(N,K)-S-H with 0.1 M alkali hydroxide solution, light green diamonds: C-(N,K)-S-H with 0.5 M alkali hydroxide solution, dark green squares: C-(N,K)-S-H with 1 M alkali hydroxide solution; filled symbol: C-(N,K)-S-H with NaOH solution; empty symbol: C-(N,K)-S-H with KOH solution. Lines: simulated using the thermodynamic CASH+ model[61,62].

3.2.3. Effect of NaOH / KOH on C-S-H

3.2.3.1. Alkali uptake in C-S-H

The alkali uptake by C-S-H measured using the direct and indirect methods is plotted in Figure 9. Determination using the indirect mass balance approach does not give meaningful results at 0.5 M alkali hydroxide and above due to large increase of the absolute error in the amount taken up at higher alkali concentrations as discussed in

detail in [41]. At 0.1 M NaOH or KOH, no systematic difference was observed between the direct and indirect method.

The amount of Na and K incorporated in the C-(N,K-)S-H is higher at low Ca/Si_{C-S-H} than at high Ca/Si_{C-S-H} ratio. For C-(N,K-)S-H at 0.1 M alkali hydroxide, bound alkalis decrease from alkali/Si $\approx 0.20 \pm 0.05$ for Ca/Si_{C-S-H} = 0.7 to alkali/Si < 0.05 for Ca/Si_{C-S-H} = 1.35 - 1.5. For C-(N,K-)S-H with 0.5 M alkali hydroxide, bound alkalis also decline from alkali/Si $\approx 0.6 \pm 0.1$ in C-(N,K-)S-H with low Ca/Si_{C-S-H} to around 0.3 ± 0.1 at C-(N,K-)S-H with high Ca/Si_{C-S-H}. This trend and the measured alkali/Si ratios are consistent with those reported in earlier studies of alkali uptake in laboratory synthesized C-(N,K-)S-H at room temperature [39,41,43,44,113]. No significant difference between K and Na uptake was observed in agreement with the data reported by Hong and Glasser and L'Hôpital et al. [41,113]. The experimental data is satisfactorily reproduced by the model at alkali concentrations of 0.1 M and 0.5 M and for Ca/Si_{C-S-H} ratios larger than 0.9. At alkali concentrations of 0.5 and low Ca/Si ratios, the model underestimates the experimental data (Figure 9). Compared to the experimental data that shows a monotonous decrease of alkali uptake with increasing Ca/Si ratio, the CASH+ model predicts a maximum uptake around Ca/Si_{C-S-H} = 0.77 (0.1 M alkali), which could be a model artifact. At these conditions the model simulates that the alkalis enter the C-S-H interlayer and have little competition from Ca. The uptake is further enhanced in the model by the presence of less Si bridging tetrahedra compared to conditions at lower Ca/Si (i.e., 0.73) and higher MCL values. Above the Ca/Si = 0.77 ratio, the decrease in alkali uptake is due to the increasing competition with Ca for the C-S-H interlayer. At high alkali concentration, e.g., 0.5 M and low Ca/Si ratio, the increase in pH results in that the model predicts that Si bridging tetrahedra are replaced by vacancies (silica becomes more soluble with increasing pH). In fact, this leads to a higher model calculated Ca/Si ratio in C-S-H (around 0.77) for conditions with the lowest target Ca/Si. The model is not compared to the experimental data carried out at 1 M alkali hydroxide due to the very large uncertainty for the experimental data at such a high concentration.

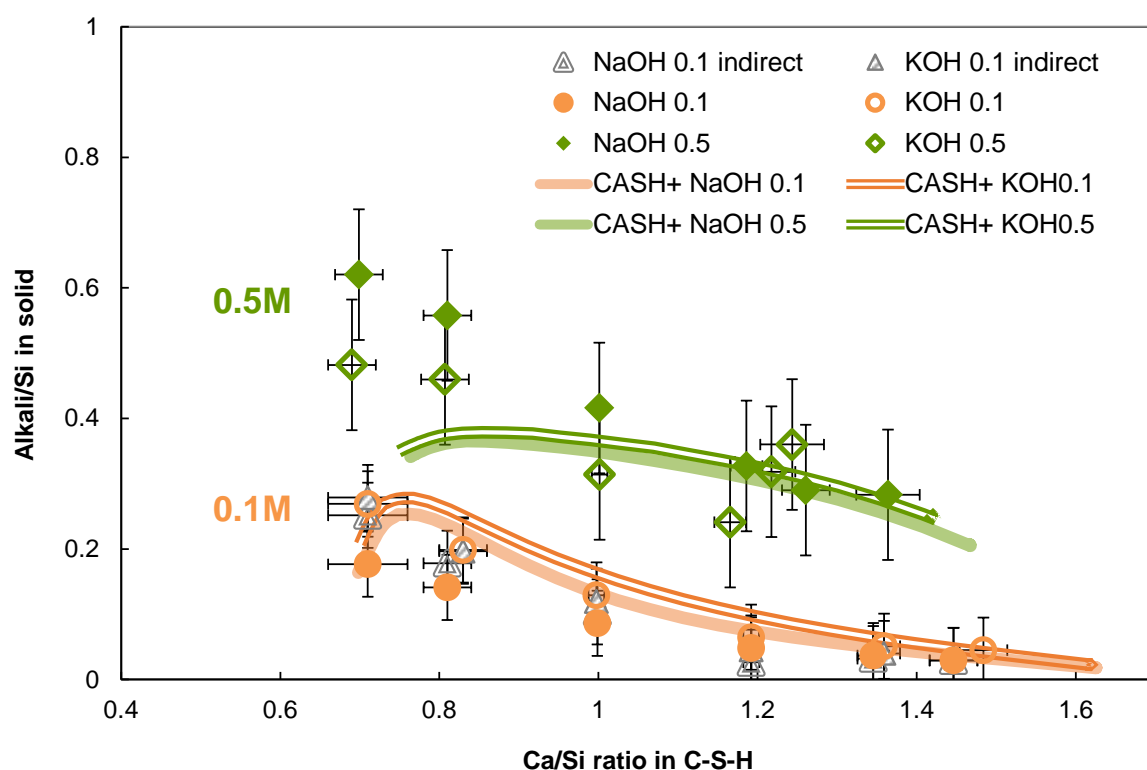


Figure 9. Alkali uptake in C-(N,K)-S-H as a function of the Ca/Si ratio, for samples synthesized with NaOH (filled symbols) and KOH (empty symbols) equilibrated for 3 months determined by the direct method. Orange circles: C-(N,K)-S-H synthesized with 0.1 M alkali hydroxide; green diamonds: C-(N,K)-S-H synthesized with 0.5 M alkali hydroxide. Lines: simulated using the thermodynamic CASH+ model [61,62]. The estimated absolute errors were ± 0.08 units in the (Na, K)/Si ratios of the C-(N,K)-S-H products synthesized with 0.5 M alkali hydroxide and ± 0.04 units of the C-(N,K)-S-H products synthesized with 0.1 M alkali hydroxide. The estimate errors of $\text{Ca/Si}_{\text{C-S-H}}$ were smaller than ± 0.05 . The values determined indirectly by mass balance at 0.1 M (grey triangles) are given for comparison.

3.2.3.2. Water content in C-S-H

Figure 10 shows the effect of KOH concentration on TGA of C-(K)-S-H with $\text{Ca/Si}_{\text{target}}$ of 1.2. The presence of alkali hydroxide increases moderately the amount of water present. The weight losses observed by TGA for the alkali free sample can be subdivided into a main weight loss at around 120 °C, which continues to reduce up to 600 °C associated with interlayer and surface water of C-S-H and a weaker weight loss in the range 600 – 980 °C, which has been assigned to the destabilization of C-S-H to wollastonite (CaSiO_3) and rankinite ($\text{Ca}_3\text{Si}_2\text{O}_7$) [47,114] as well as to the presence of carbonates. The TGA data confirm that in all cases C-S-H is the main solid precipitated. In 0.5 and 1 M KOH solution, in addition some portlandite is observed, in agreement

with other observations on synthetic C-S-H in the presence of KOH or NaOH [40,41,48]. At 1 M KOH concentration, the TGA data indicate an additional weight loss at around 380 °C, in agreement with the observations reported for C-N/K-A-S-H in [42], which has been double checked with the XRD Rietveld quantification and is tentatively assigned to finely dispersed portlandite.

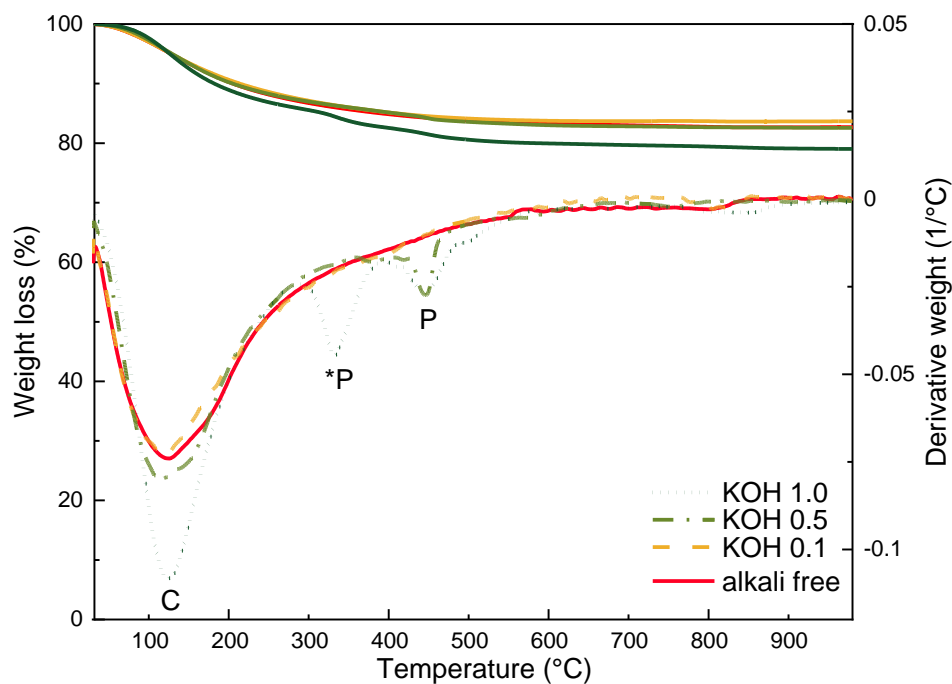


Figure 10. TGA of C-(K-)S-H with target Ca/Si=1.2 after an equilibration time of 3 months at different KOH concentrations. C: C-(K-)S-H ; P: portlandite. *P: The weight loss between 300 and 400 °C in 1 M KOH is tentatively assigned to finely dispersed portlandite. Similar weight losses have also been observed for C-N-S-H.

The TGA data were used to quantify the H₂O content in C-(N,K-)S-H based on the mass loss between 30 °C and 600 °C, after correction for the presence of portlandite. The H₂O/Si ratio has been measured on C-(N/K-)S-H samples equilibrated for more than 2 weeks at ~30% RH, where mainly interlayer water plus a layer of surface water is present, but no gel water [115]. In the absence of alkalis, C-S-H products typically contain 1.2 to 1.5 H₂O per Si (Figure 11), which agrees well with other observations of the H₂O content of C-S-H at ambient temperatures [18,23,41,42]. The H₂O/Si increases with the Ca/Si ratio, while it remains rather constant if expressed as H₂O per gram of C-S-H and decreases if expressed as H₂O/Ca as discussed in L'Hôpital et al. [26]. The presence of 0.1 M alkali hydroxide had little effect on the measured H₂O/Si, while higher alkali concentrations increased the amount of bound water, indicating that

the Na^+ and K^+ present in the interlayer or surfaces of C-S-H are associated with additional water [18,23,41,42]. No significant difference could be observed between Na and K.

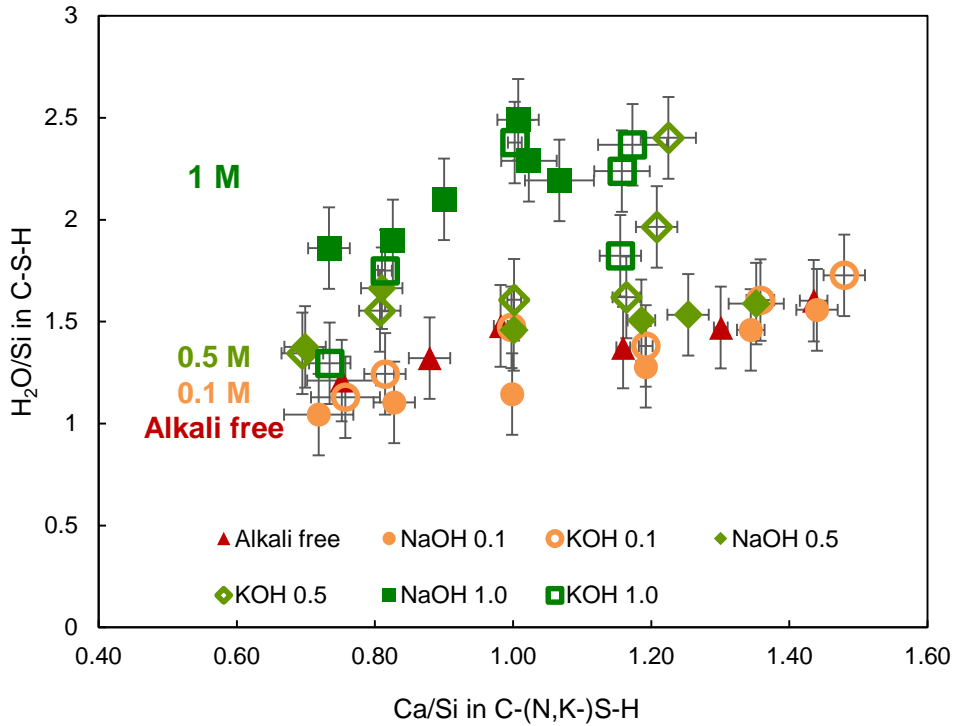


Figure 11. $\text{H}_2\text{O}/\text{Si}$ ratios of the C-(N,K)-S-H as functions of the Ca/Si ratio, for samples synthesized with water, 0.1 M, 0.5 M and 1 M NaOH (filled symbols) or KOH (empty symbols) solutions equilibrated for three months. The estimated absolute errors are ± 0.05 units in the Ca/Si ratios and ± 0.2 in the $\text{H}_2\text{O}/\text{Si}$ ratios of the C-(N,K)-S-H products. The estimate error of $\text{Ca}/\text{Si}_{\text{C-S-H}}$ is smaller than 0.05.

3.2.3.3. Basal spacing and crystallite size

In parallel to the water content, also the basal spacing of the dried C-S-H increases with the KOH concentration. The XRD data in Figure 12 indicate decrease of the (001) reflection [39,68] from 8.9 to 6.9° 2θ in the presence of KOH corresponding to an increase from 9.9 Å to 12.8 Å of the basal spacing. Such an increase of basal spacing has been reported previously [41] for samples where a comparable drying method has been used. In contrast, a decrease of basal spacing in the presence of NaOH has been observed [39] for only shortly (overnight) dried samples, which could indicate a faster drying at high NaOH concentrations. The presence of KOH also leads to a decrease

of the intensity of the (101) reflection at $\approx 5 \text{ \AA}$ ($16^\circ 2\theta$). The absence of the (101) reflection at 0.5 and 1 M KOH suggests a decreased occupancy of the Si bridging sites at higher alkali concentrations and thus the presence of more Si dimers, as further confirmed by ^{29}Si NMR, FTIR, and Raman data and in good agreement with the decrease of the amount of Q^2 species observed by ^{29}Si NMR for the sample with $\text{Ca/Si} = 1.0$ synthesized in the presence of NaOH [42,48,92].

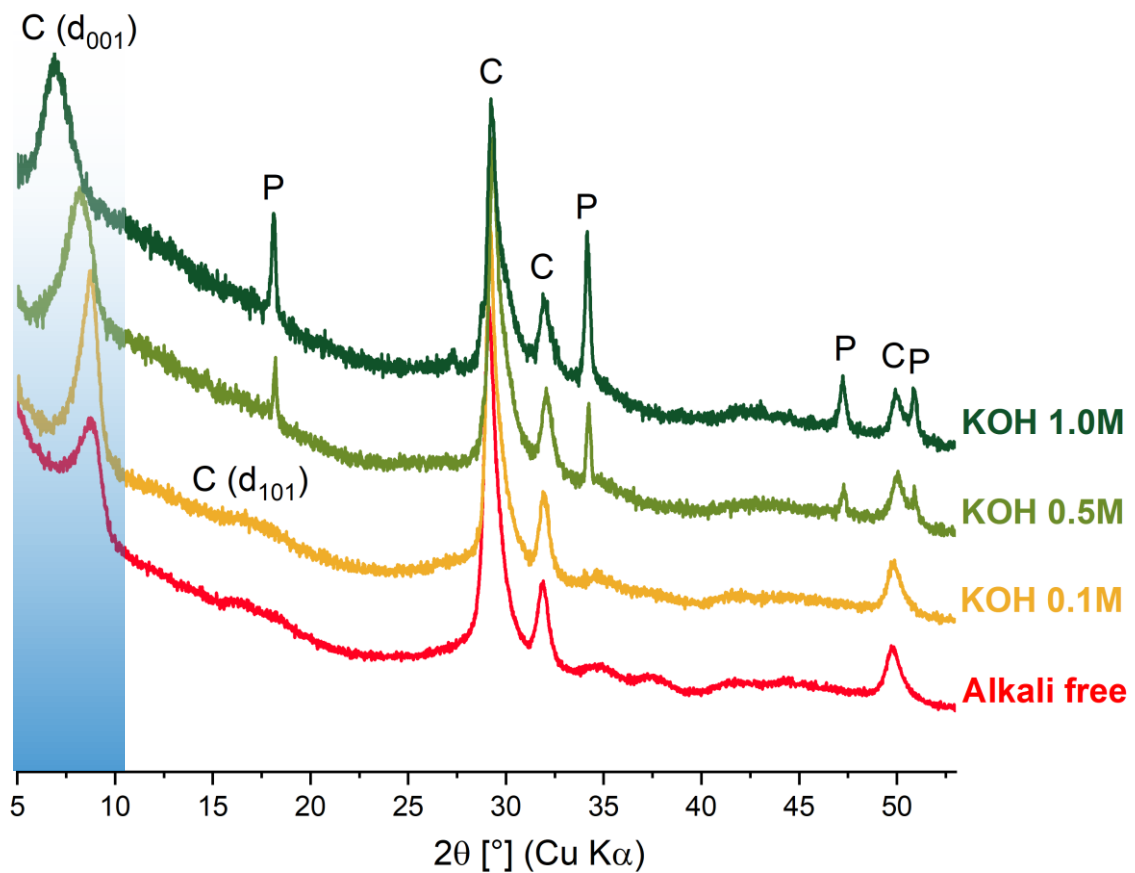


Figure 12. XRD diffractograms of C-(K-)S-H with target $\text{Ca/Si}=1.2$ after an equilibration time of 3 months at different KOH concentrations. C: C-(K-)S-H, P: portlandite

The positions of the (001) reflections in Figure 12 correspond to average basal spacings of 9.6 to 15.4 \AA for the C-(N, K-)S-H products as summarized in Figure 13. The variations in the basal spacing are related to drying and the amount of alkali and calcium in the interlayer, with lower interlayer distances at high Ca/Si and an increase at higher alkali contents. The variation in basal spacing could also be due to the presence of different C-(N,K-)S-H products, i.e. poorly-ordered 14 \AA , 11 \AA and 9 \AA tobermorite [23]. It needs to be emphasized that some samples synthesized in 1 M

alkali hydroxide contain two separate basal peaks, which indicates the presence of different analogues. The profile fitting and the crystallite size refinement for these samples give larger uncertainties.

For alkali-free and low-alkali C-S-H materials, basal space decreases with increasing Ca/Si. The reason of this reduction of interlayer distance could be the charge balance or the attraction effect of the Ca^{2+} in the interlayer [18,26,116]. XRD indicates that the presence of KOH and NaOH increases the mean basal spacing of the C-(N,K)-S-H as shown in Figure 13 and in fact, density function theory (DFT) calculations indicate a decrease of attractive forces between the layers upon replacement of Ca^{2+} in the interlayer of C-S-H by Na^+ [92].

Although at Ca/Si ratios ≥ 1.0 , only a small amount of alkali uptake occurs, the small quantity of KOH or NaOH affects strongly the basal spacing of C-(N, K)-S-H, which underlines that this increase is mainly caused by the removal of Ca^{2+} at high alkali hydroxide and thus low calcium concentrations.

Bach et al. [39] and L'Hôpital et al. [41] reported the decrease of the mean basal spacing in the presence of increasing amounts of NaOH, while the opposite was observed in Figure 14 (a). The main reason for this inconsistency is that [39] and [41] focused on alkali hydroxide concentrations lower than 0.1 M, where we also observe a slight decrease. However, from 0.1 to 1 M KOH or NaOH concentration, the basal spacing increased from ≈ 10 to ≈ 13 Å, as shown in Figure 14 (a). At equal concentrations, K and Na have a similar effect of changing the mean basal spacing. This is consistent with L'Hôpital et al. [41], but in contrast to the study of Bach et al. [39], who observed a stronger decrease of the mean basal spacing in the presence of NaOH than of KOH. The reasons for these contradictory observations are unclear, although they might be related to different washing and drying procedures of the solids, and the shorter equilibration times used in [39].

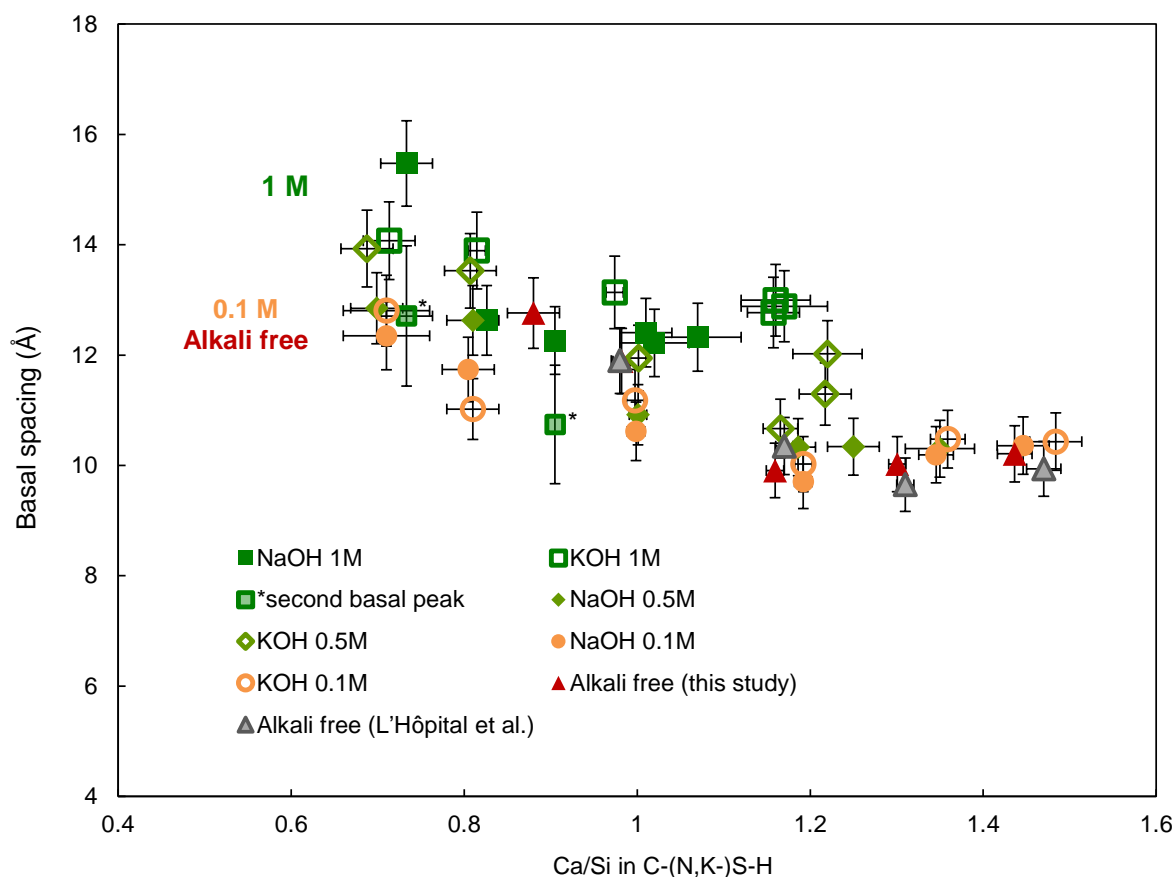


Figure 13. Variation of the mean basal spacing as a function of the total Ca/Si ratio in C-(N,K)-S-H solid after an equilibration time of 3 months. Grey symbol: C-S-H from L'Hôpital [26]; colored symbol: C-(N,K)-S-H from this study; triangles: C-S-H with water; circles: C-(N,K)-S-H with 0.1 M alkali hydroxide solution, squares: C-(N,K)-S-H with 1 M alkali hydroxide solution; filled symbols: C-(N,K)-S-H with NaOH solution; empty symbols: C-(N,K)-S-H with KOH solution.

Table 2 Unit cell parameters and domain sizes along the a -, and b -axes (l_a) and the c -axis (l_c) obtained from the Pawley fits in Figure 50 for the different alkali concentrations of C-(N,K)-S-H powder patterns with $Ca/Si_{target} = 1.0$. For the 1.0 M NaOH concentration, two tobermorite unit-cells were used, which differ only in the c -axis length and domain size.

Alkali concentration (M)	a (Å)	b (Å)	c (Å)	γ (°)	V (Å ³)	l_a (nm)	l_c (nm)	
0	6.405(2)	7.667(3)	24.10(3)	122.76(4)	995.2(13)	15(3)	2.10(10)	
KOH	0.1	6.454(5)	7.799(13)	22.282(17)	123.72(7)	933(2)	10.5(12)	2.01(5)
	0.6	6.441(2)	7.760(6)	23.546(18)	123.41(5)	982.4(13)	9.9(5)	1.81(4)
	1.1	6.464(5)	7.642(6)	26.071(16)	123.18(7)	1077.8(16)	9.0(14)	3.14(9)
NaOH	0.1	6.404(5)	7.871(9)	21.417(14)	123.52(8)	900.0(16)	8.5(6)	1.57(3)
	0.5	6.417(2)	7.817(5)	21.838(13)	123.45(3)	914.0(9)	13.5(8)	1.67(2)
	1.0	6.442(4)	7.589(7)	23.958(19)	124.27(8)	967.8(16)	11(3)	2.32(6)
	1.0	6.442(4)	7.589(7)	21.01(3)	124.27(8)	848.7(17)	11(3)	2.87(12)

The crystallite size was estimated from the X-ray diffraction data using a Pawley fit from the unit cells of tobermorite 11 Å [68] and tobermorite 14 Å (for 1.1 M KOH) [70]. An anisotropic crystallite size refinement with two domain lengths (one for the a - and

b-directions, and one for the *c*-axis direction) is conducted. The fits are given in Figure 50. The refinement results, presented in Table 2, show that the C-S-H has a much larger crystallite size along the *ab*-axes than along the *c*-axis, which verifies the poorly ordered nature of C-S-H along the *c*-axis, in agreement with earlier studies [117,118]. A crystallite size in the *c* direction of $l_c \approx 15 \text{ \AA}$ to 32 \AA is observed, denoting 1.5 to 3 layers of C-S-H stacking in the *c*-axis. In C-S-H with NaOH 1 M, a shoulder is observed at $\sim 10.7 \text{ \AA}$, other than the major basal peak at $\sim 12.3 \text{ \AA}$, indicating two major nanocrystalline structures in this sample that share similar structures in *ab*-plane but have different basal spacings.

The relative intensity and width of the (001) reflections are highly sensitive to the crystallite size along the *c*-axis (l_c). A correlation between increasing alkali hydroxide concentration and larger crystallite size in the *c*-direction with smaller crystallite size in the *ab*-plane can be observed for C-S-H with KOH. The trend of smaller crystallite size in *ab*-direction for C-S-H with NaOH is less clear, which may be due to the larger uncertainty from the mixture of tobermorite analogues present. The crystallite size in the *c*-direction and basal spacing follow the same trend along the higher amount alkali hydroxide.

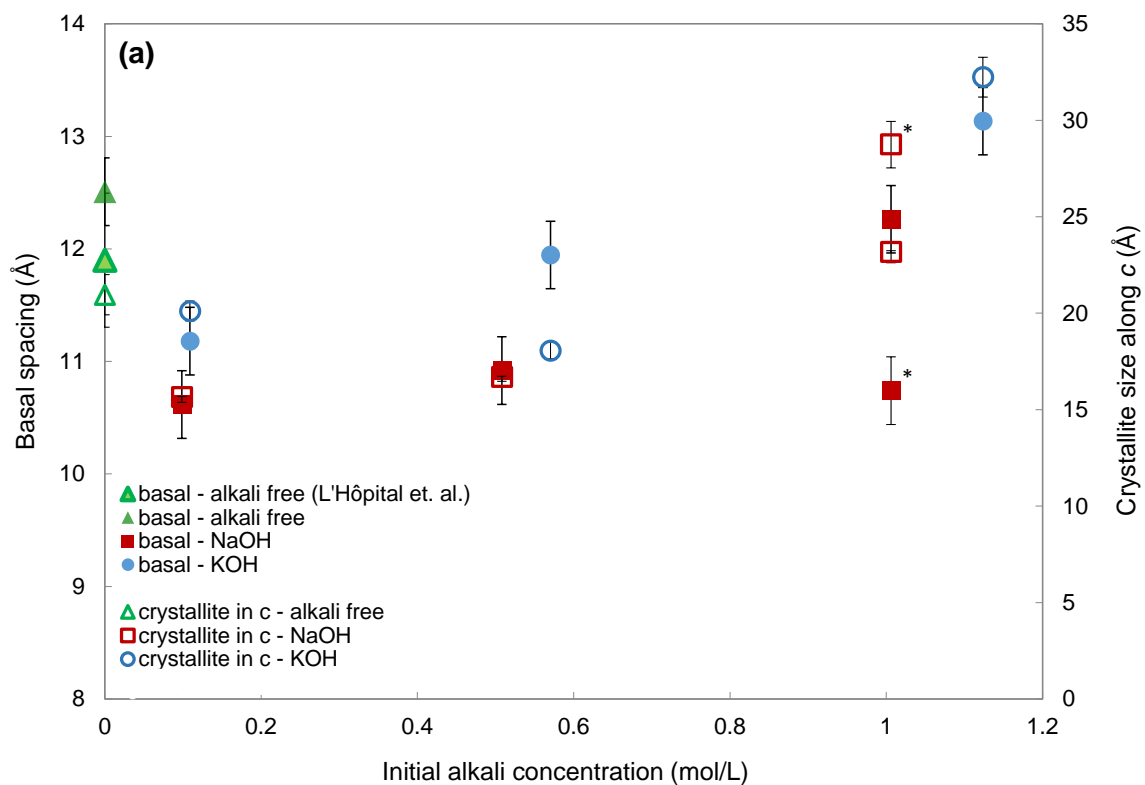
As discussed in previous studies [41,42,62,92], higher alkali hydroxide concentration shortens the silicate chains of C-S-H. So the increased crystallite size can be assumed to stem from an increase along the *c*-axis. Pair distribution function (PDF) calculations of synthetic C-S-H indicated a crystallite size of $\approx 4 \text{ nm}$ and no significant variations with the NaOH concentrations up to 5 M [92], but the C-S-H are pre-assumed as identical along *a*-, *b*- and *c*- axes.

Grangeon et al. [100] suggested that a shift of the basal reflection in XRD towards low angles and an increase in its FWHM could indicate fewer stacking layers in the *c* direction. In this study, the basal reflection shifts towards lower angles while the domain size increases (i.e. FWHM decreases) as a function of alkali concentration in C-(Na,K-)S-H, as shown in Figure 14 (b). The FWHM might include several analogues of tobermorite, giving the larger values for the 0.5 M concentration. The lower angle shifting of basal reflection and decreasing FWHM indicate:

i) an expansion of the interlayer distance, probably related to the replacement of Ca^{2+} by alkali ions in the interlayer [18,41,92,119], which either lowers the attractive forces

between the separate layers [92] or brings more water molecules into the interlayer [119]. The latter hypothesis can be explained as more water is associated with two Na^+ and K^+ cations than with one Ca^{2+} cation. The Na^+ or K^+ attracts the water molecule along the direction that is parallel to the silicate chain in C-(N,K)-S-H. The force resulting from this attraction decreases the lateral area (i.e., along the ab direction), while simultaneously increasing the length along the c -direction (i.e., expanding the interlayer).

ii) an increase in the crystallite size along c -axis. One possible interpretation of these phenomena is that alkali hydroxide lowers the degree of silicate polymerization in C-S-H and as a result the C-S-H grows rather in c -direction (rather than in the ab -direction) resulting in higher number of layers stacked along the c -axis.



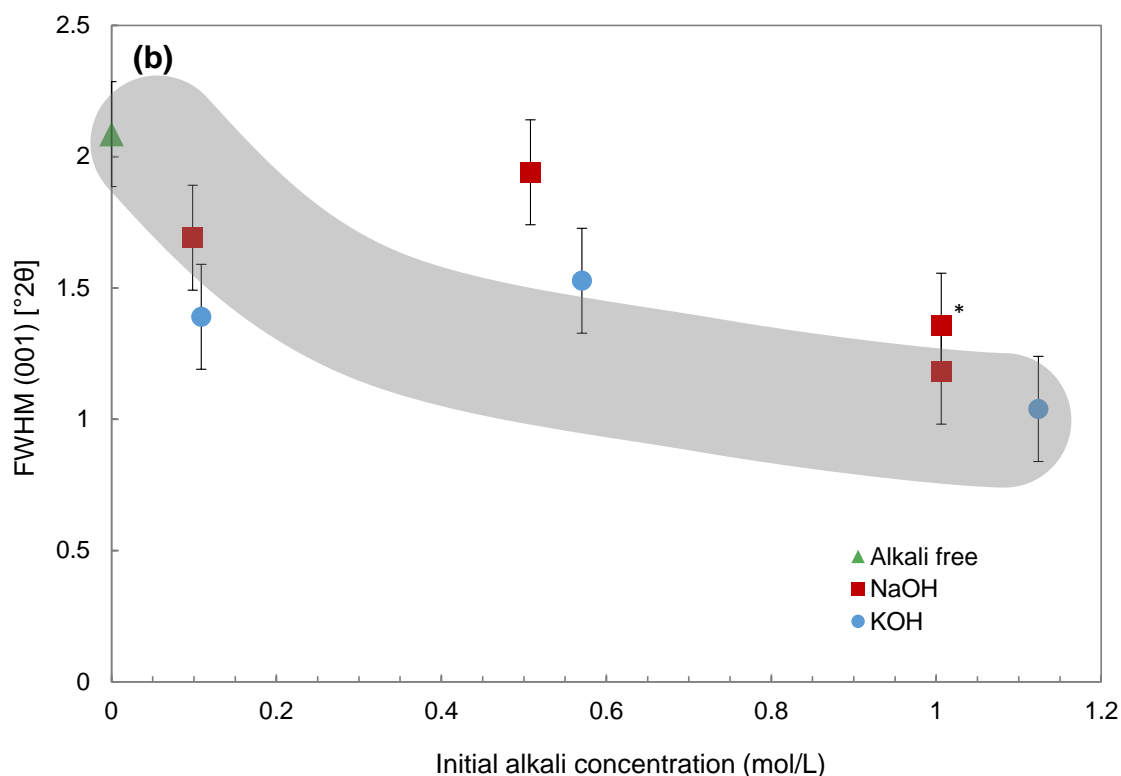


Figure 14 (a) Variation of mean basal spacing and crystallite size along the c -axis as a function of the initial alkali concentration for C-S-H with $\text{Ca/Si} = 1.0$ after an equilibration time of 3 months, solid symbols: mean basal spacing, empty symbol: crystallite size calculated based on the tobermorite model. Grey symbols: C-S-H from L'Hôpital et al. [26]; colored symbol: C-S-H from this study; triangle. (b) FWHM of the d_{001} reflection of C-(N,K)-S-H with target $\text{Ca/Si} = 1.0$ as a function of initial alkali concentration after an equilibration time of 3 months. Triangles: C-S-H synthesized with water, squares: C-(N, K)-S-H synthesized with NaOH solutions, circles: C-(N, K)-S-H synthesized with KOH solutions. The symbol marked with * stands for the second basal peak. The grey region is shown only as an eye-guide.

3.2.3.4. Composition of C-(N,K)-S-H

The chemical compositions of the C-(N,K)-S-H products formed at different $\text{Ca/Si}_{\text{target}}$ ratios was calculated by mass balance calculation considering the amount of Ca and Si in the aqueous phase and secondary phases present, only the amount of NaOH and KOH was obtained from direct measurements as detailed above. The variations in the composition of C-S-H are summarized in Figure 15. The C-(N,K)-S-H products formed in water and 0.1 M NaOH and KOH have Ca/Si ratios between 0.78 to 1.44. In general, the $\text{Ca/Si}_{\text{C-S-H}}$ ratios are similar to the $\text{Ca/Si}_{\text{target}}$, due to the relatively low levels of secondary phases formed in these specimen. The samples synthesized with $\text{Ca/Si}_{\text{target}} = 1.6$ contained portlandite, which lowered the $\text{Ca/Si}_{\text{C-S-H}}$ to slightly below 1.5. The presence of 1 M alkali hydroxide solutions lowered the maximum $\text{Ca/Si}_{\text{C-S-H}}$ of C-(N,K-

)S-H to 1.2, as more portlandite is formed at higher pH values (Figure 12), indicating a strong effect of pH on C-S-H composition under equilibrium conditions. The lowest Ca/Si_{C-S-H} is also affected by the presence of alkali hydroxide; the higher pH values increase the Si concentrations, which led to the dissolution of amorphous silica at 0.1 M alkali hydroxide and above, as well as to more Si in solution. The preference of Si to be in solution instead of solid phase results in an decrease of the observed minimum Ca/Si_{C-S-H} from 0.75 at alkali free C-S-H to ~ 0.7 at C-S-H with alkali hydroxide.

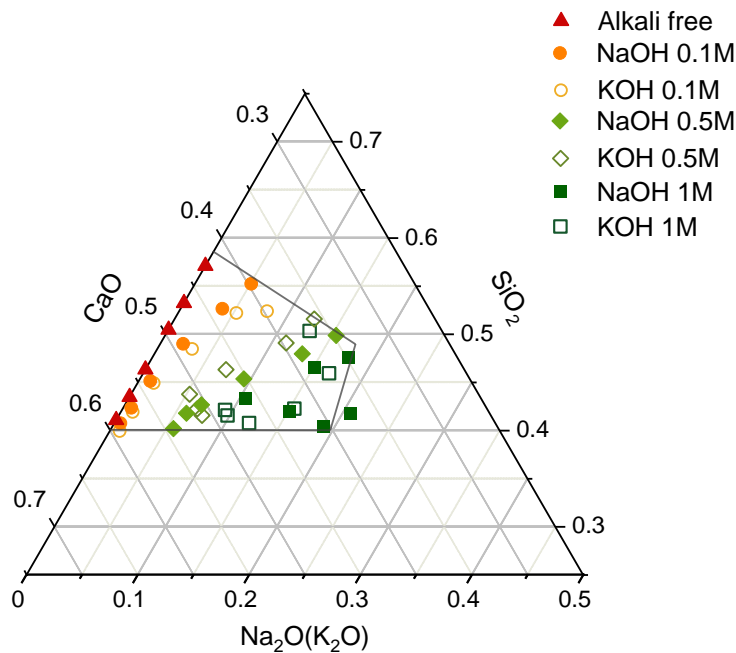


Figure 15. Chemical compositions (units in molar fraction) of the C-(N, K-) S-H products of different target Ca/Si and with different NaOH or KOH concentration projected in ternary diagram.

3.3. Effect of pH on silica sites in C-S-H

The ²⁹Si MAS NMR spectra of the C-S-H samples with Ca/Si = 1.2 and cured in different KOH concentrations are shown in Figure 16. Three resonances at approx. -79 ppm (Q^1), -83 ppm (Q_b^2) and -85 ppm (Q_{pa}^2) are identified for the alkali-free sample, as discussed above.

The presence of KOH shifts the Q¹ and Q² peaks to lower frequency as a result of the replacement of Ca²⁺ by K⁺ in the interlayer, which contribute to a weaker shielding of the Si atoms as compared to Ca²⁺ [92]. The observed shifts are consistent with earlier observations for C-S-H gels exposed to NaOH and KOH [42,48,92,120] and with the shifts to lower wavenumbers observed in both Raman and FTIR signals at around 1000 cm⁻¹ as discussed below.

With increasing KOH or NaOH concentrations, the intensity of the Q¹ signal increases indicating a shortening of the MCL, as also observed in previous studies [42,92]. For the C-S-H samples with Ca/Si_{target} of 1.0 and below, the changes in mean chain length are much more distinct than at 1.2, while at Ca/Si_{target} > 1.2, the mean chain length and silica connectivity is not strongly affected at higher KOH concentrations [18,45,92] since silicate dimers dominate at high Ca/Si.

In addition, small amounts (< 3 %) of Q⁰ peaks (-70 ppm) were observed for the C-S-H samples synthesized in 1M NaOH at (Ca/Si)_i values of 0.6 to 1.6 and in 1M KOH at Ca/Si 0.8 (see Figure 48). The Q⁰ peaks are assigned to hydrated monomeric silicate species in the solid following the assignment of Garg et al. [92]. For C-S-H synthesized in 1 M alkali hydroxide, these Q⁰ units are possibly charge-balanced by the high levels of alkalis. It should be noted that from a thermodynamic stability point of view, an excess of depolymerized Q⁰ silicate units are preferable dissolved [92].

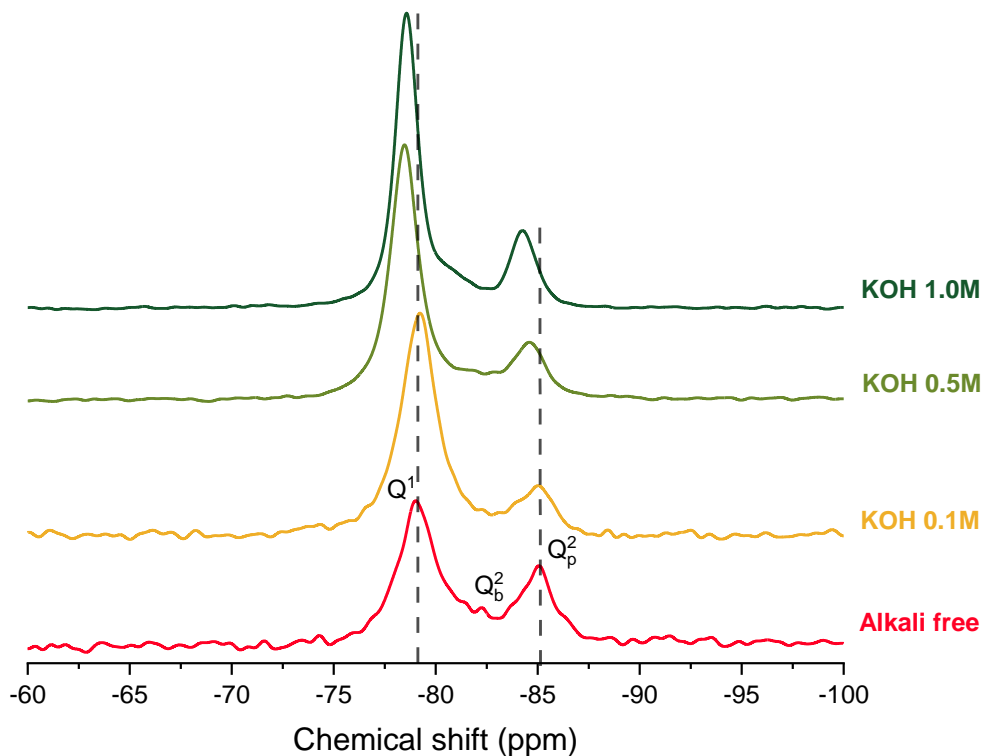


Figure 16 ^{29}Si NMR spectra of C-(N,K-)S-H a) with $\text{Ca}/\text{Si}_{\text{target}} = 1.2$ after an equilibration time of 3 months at different KOH concentrations.

Figure 17 shows the effect of KOH on the FTIR and Raman spectra of C-(K-)S-H with $\text{Ca}/\text{Si}_{\text{target}} = 1.2$. The main FTIR peak at 960 cm^{-1} is shifted to lower wavenumbers (redshift) confirming the depolymerisation of the silica chains [33]. This peak splits into two peaks at higher KOH concentrations indicating a lowering of the symmetry resulting from the transformation of structural sites into groups of non-equivalents sites [34]. The peak splitting has also been observed to a limited extent at higher $\text{Ca}/\text{Si}_{\text{target}}$ and much more distinct at low $\text{Ca}/\text{Si}_{\text{target}}$ (see Figure 45). This lower symmetry indicated peak split could be due to the substitution of Ca^{2+} by K^{+} in the interlayer, i.e. by the changes in the second coordination sphere. The shift to lower wavenumber indicates a structural rearrangement of C-S-H in the presence of KOH, for example a change in Si-O bond distances and/or the Si-O-Si angles [101]. In the Raman spectra a similar shift of the main peak related to Si-O-Si symmetric bending from 671.5 to 673

cm^{-1} occurs, which indicates the value of the angle $\langle\text{Si-O-Si}\rangle$ decreases in the presence of KOH [107]. Also the appearance of small peak at $\sim 1120 \text{ cm}^{-1}$ Raman spectra indicates increasing bond deformation of Si-O-Si linkages [61].

The Q^1 signal is located at $\sim 815 \text{ cm}^{-1}$ in FTIR and $\sim 882 \text{ cm}^{-1}$ in Raman. The intensity of the Q^1 signal in FTIR increases indicating the presence of more Q^1 silica and thus a shortening of the silica chain length, in agreement with the observations by Si-NMR. Also in Raman, the intensity of the SS Q^1 increases from alkali free to 0.5 M KOH indicating a shorter MCL. The SS Q^1 peak at 1 M KOH, however, does not follow the expected trend. During sample preparation and measurement a slight carbonation of the surface occurred, which led to a C-S-H decalcification and silica polymerization and diminishment of the SS Q^1 intensity [60] at the surface of the samples, although the bulk C-S-H show very little weight loss from 600-900°C in Figure 10. The carbonation is in particularly well visible in the Raman peaks at 1080 cm^{-1} , which are attributed to the C-O SS vibration of carbonation [28,106,107,109] and strongly affect the intensity of the Si-O SS of C-S-H at $\sim 1020 \text{ cm}^{-1}$. The carbonate peak at $\sim 1077 \text{ cm}^{-1}$ increasingly dominates the spectra of C-S-H with KOH, which is attributed to the symmetric stretching mode of vaterite [60]. The fast carbonation of the samples surface at high pH values and high $\text{Ca}/\text{Si}_{\text{C-S-H}}$ makes the interpretation of the Raman signals very challenging.

The addition of KOH increases the intensity of the FTIR band at 670 cm^{-1} , which has been related to Si-O-Si (O-Si-O) bending [33,102] and water liberations [102]. This increase has been observed at all Ca/Si ratios (see Figure 45) and could thus be related to the presence of additional water. The FTIR spectral range 2500-4000 cm^{-1} in Figure 44 shows that the intensity of the water signal is significantly higher at 1 M KOH

Chapter 3: Effect of alkali hydroxide on calcium silicate hydrate (C-S-H)

than for the other samples indicating the presence of more loosely bound water in agreement with the TGA results.

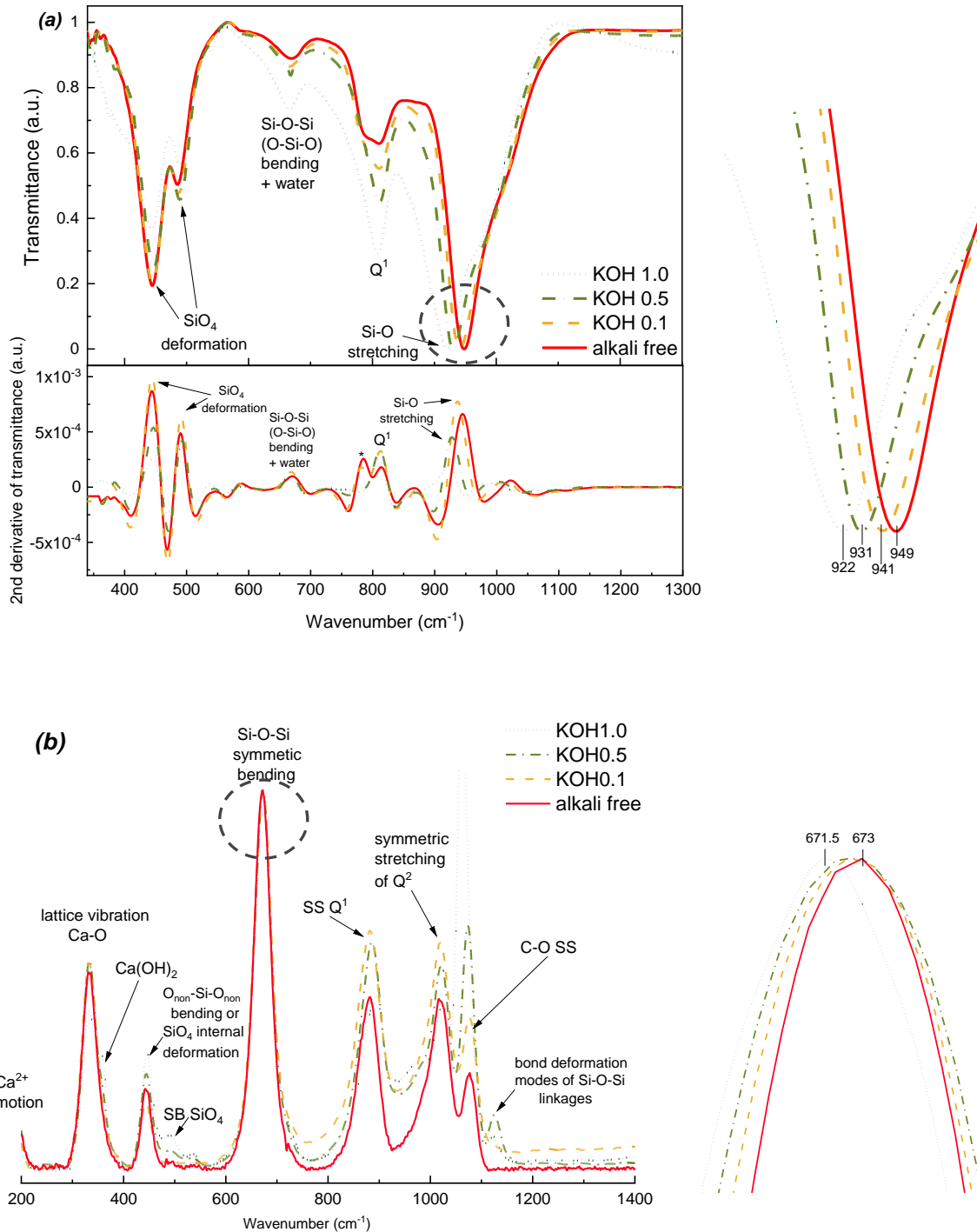


Figure 17 (a) FTIR and (b) Raman spectra of C-(N,K)-S-H with target Ca/Si=1.2 after an equilibration time of 3 months at different KOH concentrations.

In addition, in FTIR the peak at 450 cm^{-1} and a peak at 490 cm^{-1} are increasing, which has been assigned to internal deformation of the Si-tetrahedra [106] or O-Si-O bending [107] and symmetric bending vibrations of SiO_4 [28,106,107]. As discussed in Figure 6(c) the peak at 780 cm^{-1} is also observed and disappears at higher alkali concentrations. In Raman, the addition of KOH did not change the peak intensity of the Ca-O lattice vibrations at 325 cm^{-1} did not change except for 1 M KOH, which could be related to the formation of more portlandite.

The XRD, NMR, FTIR and Raman data all indicate the formation of shorter silica chains in the presence of more KOH and NaOH, which agrees with the decrease of MCL predicted based on thermodynamic modelling using the CASH+ model in Figure 18. In agreement with the experiments (the MCL calculated from NMR and secondary phases are presented in Figure 43), the presence of alkali hydroxide decreases the MCL in C-S-H due to the removal of Si from the bridging sites at higher pH values. The reason of the less bridging Si in C-S-H is because of the increasing tendency of negatively charged Si species (SiH_3O_4^- and $\text{SiH}_2\text{O}_4^{2-}$) to be present in solution at higher pH values. In addition, higher pH values increase the deprotonation of $\equiv\text{SiO}^-$ surface groups in C-S-H [40,41,87–89,112], which increases the negative surface and interlayer charge of C-S-H and thus lowers the tendency of silicon to bind on bridging sites.

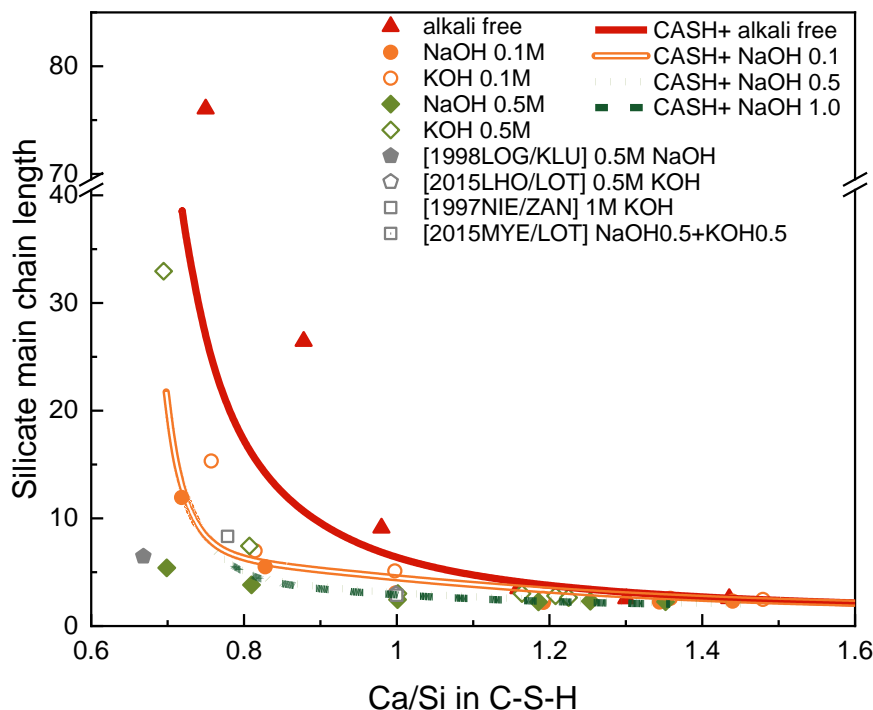


Figure 18. Calculated main chain length (MCL) of C-(N,K-)S-H from Gems compared with MCL values reported from ^{29}Si NMR. The estimated absolute errors are less than 30%. The error limits for the MCL from NMR is ± 0.05 . Solid and empty symbols: MCL from NMR; red triangles: C-S-H with MilliQ water; orange circles: C-(N,K-)S-H with 0.1 M alkali hydroxide solution, light green diamonds: C-(N,K-)S-H with 0.5 M alkali hydroxide solution, grey symbols: C-(N,K-)S-H with 0.5 M – 1M alkali hydroxide solution adapted from [42,48,120,121]. Lines: simulated using the thermodynamic CASH+ model.

3.4. Conclusion

The effect of Ca/Si and the influence of KOH and NaOH on the structure and solubility of C-S-H has been studied. An increase of $\text{Ca/Si}_{\text{target}}$ led to lower Si concentrations, to higher Ca concentrations and higher pH values in the surrounding solutions. In parallel to the solution composition, the composition and structure of the C-S-H varied from $\text{Ca/Si}_{\text{C-S-H}} = 0.75$ in the presence of amorphous SiO_2 to $\text{Ca/Si}_{\text{C-S-H}} = 1.44$ in the presence of portlandite, while the chain length of the silica chains decreased from > 70 to mainly dimers at $\text{Ca/Si}_{\text{C-S-H}} = 1.3$ and above. The MCLs quantified from the FTIR and Raman spectra agrees well with the results from ^{29}Si NMR, indicating that a reliable qualitative analysis is also possible based on FTIR and Raman. However, the Raman results were very sensitive to any surface carbonation occurring during the measurement, which would make them unsuitable for quantification. The disappearance of the bridging silica tetrahedra could also be observed by the

disappearance of the XRD d_{101} peak. A shift of the main Si-O stretching signal in FTIR to lower wavenumbers confirmed the depolymerisation of the silicate chains. XRD indicates a decrease of the interlayer distances at higher Ca/Si_{C-S-H} ratios, where more Ca²⁺ is in the interlayer, which increases the cohesion between the negatively charged main layers.

The presence of KOH and NaOH had a similar effect on both the aqueous phase and solid phase. The addition of KOH or NaOH increased the pH values and the Si concentrations and lowered the Ca concentrations in solution. The precipitation of additional portlandite at high pH values as well as the increased Si concentrations due to the preference of Si to form negatively charged complexes lead to a decrease of Ca/Si_{C-S-H} from 1.44 in the absence of NaOH to Ca/Si_{C-S-H} \approx 1.1 in the presence of 1 M NaOH or KOH. The uptake of alkali in C-S-H was higher at low Ca/Si as well as at higher pH values, as both the lower Ca-concentration and increased deprotonation of the silanol group $\equiv\text{SiO}^-$ surface at higher pH contribute to an increased alkali binding by C-S-H in agreement with the prediction of the thermodynamic model. Higher concentration of alkali hydroxide also prevented the polymerisation of C-(N,K)-S-H silicate as indicated by NMR, FTIR and Raman spectroscopy and increased the crystallite size along the *c*-axis from \approx 16 Å in 0.1 M KOH to 31 Å in 1.1 M KOH after 3 months of curing at 20°C degree.

This study for the first time combined a series of spectroscopy methods including NMR, FTIR and Raman to study the effect of alkali hydroxide on the structure of C-S-H. With the help of the Si NMR data, we assigned clearly the vibration bands of C-S-H in FTIR and Raman. The data showed that it is possible to use FTIR and Raman as heuristic tools to quantify the MCL, and it showed good qualitative agreements with the MCL from NMR. In addition, we observed the C-S-H composition change as a function of alkali hydroxide concentration, where the upper limit decreases of the Ca/Si_{C-S-H} from \sim 1.44 (no alkali) to 1.1 (1M KOH/NaOH), and the lower limit from 0.75(no alkali) to \sim 0.7 in the presence of alkali hydroxide. The comparison with the independently developed CASH+ thermodynamic model showed that the model reproduced the observed changes, including the shortening of the MCL in the presence of NaOH and KOH. This study adds important data to improve the thermodynamic modelling and the insights into the composition and structure relationship of C-(N,K)-S-H, which are expected to contribute our understanding on the effect of alkali hydroxides on C-S-H.

CHAPTER 4: Al uptake in calcium silicate hydrate (C-S-H) and the effect of pH²

4.1. Introduction

²⁷Al MAS NMR studies indicated that the major part of Al in C-S-H is present either tetrahedrally coordinated (mainly at low Ca/Si C-S-H) and octahedrally coordinated (at high Ca/Si), while less than 10% of Al is pentahedrally coordinated [15,17,28,122], as well as the different chemical environments of tetrahedral Al [45]. ²⁷Al MAS NMR indicated that tetrahedral Al can have different neighbors, while little difference was observed for octahedrally coordinated Al in C-A-S-H, while no Al K-edge XANES studies, which could add further insights on the kind and quantity of nearest neighbors of Al in C-A-S-H are available.

Different studies have shown that higher pH values increase Al and Si concentrations but lower Ca concentration and shorten the main chain length (MCL) in C-A-S-H [40–42,48,113]. Despite many studies on the chemistry and structure of C(-A)-S-H [17,23,116,118,123–126,26,40–42,47,48,112,113], the interplay between aluminium, alkali hydroxides in solution, the structure of C-A-S-H and aluminium uptake by C-A-S-H is still not fully understood, as most studies focus either on the study of aqueous concentrations [113] or on the characterization of the solid phases [118,124,127]. In particular it remains unclear whether Al or Si is preferentially taken up, and whether pH or Ca/Si would affect the uptake preferences or the coordination environment.

This chapter focusses on the interplay between aqueous concentrations and C-A-S-H composition and structure and the effect of pH on Al uptake. The influence of aluminium is studied in the first part and the effect of alkali hydroxide on C-A-S-H is studied in the second part. The solubility, the structure and the chemical composition of the resulting C-(A-)S-H are investigated after equilibration time of 3 months and 1 year. The experimental results are compared with data predicted by the CASH+ model [61–63]. The results and comparisons presented are particularly pertinent for the

² This chapter has been submitted as a manuscript to Cement and Concrete Research: Al uptake in calcium silicate hydrate and the effect of alkali hydroxide, Y. Yan, B. Ma, G.D. Miron, D.A. Kulik, K. Scrivener, B. Lothenbach.

further development of this and other thermodynamic models to predict of aqueous concentrations in hydrating blended cements.

4.2. Results and discussion

4.2.1. Influence of aluminium

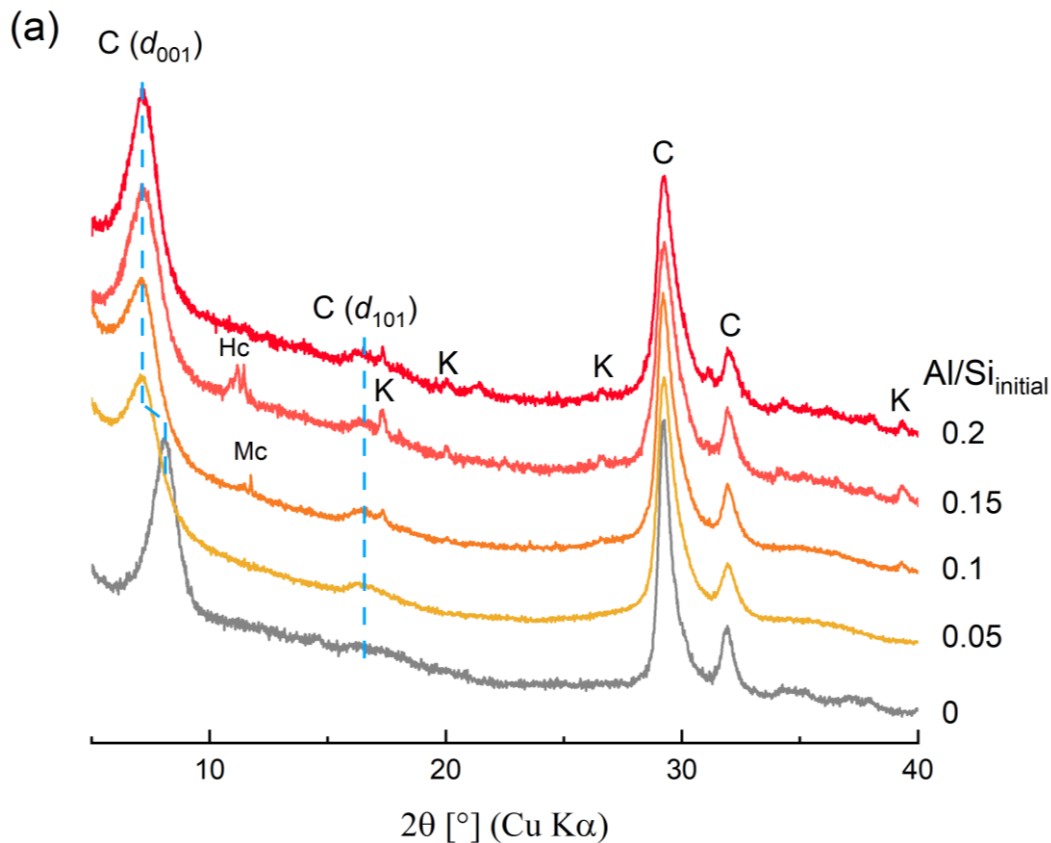
Figure 19 shows the effect of Al on C-S-H with $\text{Ca}/\text{Si}_{\text{target}}$ of 1.0 in 0.5 M NaOH solution; additional data for 0.1 and 1.0 M NaOH and for 0.5 M KOH are given in Figure 51 in Appendix J. The XRD and TGA data show that C-N,K-(A-)S-H is the main phase in all cases, and indicate the formation of secondary phases at higher Al content. In 0.5 M NaOH, katoite is observed at $\text{Al}/\text{Si}_{\text{target}} \geq 0.1$, in 0.1 M NaOH already at $\text{Al}/\text{Si}_{\text{target}} \geq 0.05$ (see Figure 51), while strätlingite is observed only at 0.1 M NaOH, due to the destabilization of strätlingite with increasing pH values as illustrated in Figure 20. Hemicarbonates and monocarbonates are identified in some samples and their presence is attributed to minor carbonation during sample preparation, drying and measurement. Hemicarbonates can contain different amounts of carbonate [128] so the peaks can be relatively broad. A small amount of portlandite is observed only in 1 M NaOH at $\text{Al}/\text{Si}_{\text{target}} = 0.15$.

The TGA shows a main water loss between 30 - 300 °C from interlayer and structurally bound water in C-N,K-(A-)S-H. A hump at 400-500 °C, marked with *, is observed at high sodium and aluminium concentrations ($\text{Al}/\text{Si}_{\text{target}} \geq 0.15$ in 0.5 M NaOH, $\text{Al}/\text{Si}_{\text{target}} = 0.05$ and 0.1 in 1 M NaOH) but not in the presence of KOH. This weight loss is tentatively assigned to thermal decomposition of more ordered water in C-N-A-S-H because none of the other phases identified by TGA, XRD presented here or by Al and Si NMR [45] can explain the weight loss associated with these bands. Similar weight losses have also been observed for C-N-A-S-H in the presence of high concentrations of NaOH [42,50] or for samples equilibrated at 50 and 80°C [47]. TGA indicates also minor carbonation (weight loss < 0.5%) in some samples during sample preparation, storage and/or analysis as visible in the region from 600-800 °C. The peaks above 800°C are assigned to the water loss due to the decomposition of C-K-(A-)S-H to wollastonite (CaSiO_3) [47,129].

The position of the main C-N,K-(A-)S-H peak observed by XRD and total weight loss did not vary systematically with the Al content, indicating that the Al is not the primary factor controlling the interlayer and structural water content of C-N,K-(A-)S-H products.

Chapter 4: Al uptake in calcium silicate hydrate (C-S-H) and the effect of pH

However, a broadening of the maximum diffraction at $\sim 3.1 \text{ \AA}$ ($\sim 29^\circ 2\theta$ Cu $K\alpha$) is observed in the presence of Al, as shown in Appendix Figure 53. The XRD data confirm that the addition of Al leads to more secondary phases and thus to a higher total weight loss in particular at lower NaOH and KOH concentrations. The basal spacings, d_{001} , in Figure 19 move to lower 2θ values in the presence of Al, indicating that the presence of aluminium increases the interlayer size within C-N,K-(A-)S-H. The same effect was also observed for 0.1 and 1 M NaOH and 0.5 M KOH (see Figure 51). The broad reflection at $\sim 17^\circ 2\theta$ (d-spacing $\sim 5 \text{ \AA}$), which has been assigned to a d_{101} reflection, indicates occupation of bridging sites in the silica chain and is more visible at higher Al/Si, which points out a prolongation of the mean silica chain length due to the incorporation of Al into the bridging sites.



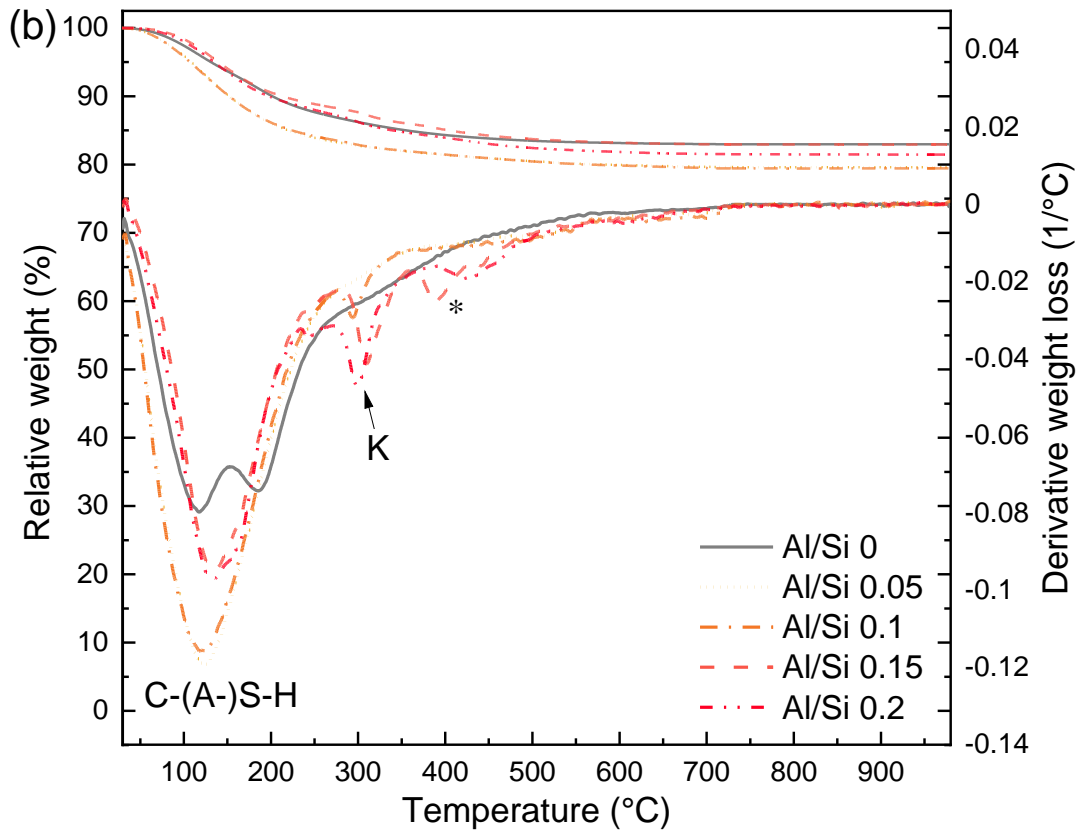


Figure 19 XRD and TGA of C-N,K-(A-)S-H with target Ca/Si=1.0 synthesized in NaOH 0.5 M with different initial Al/Si, equilibrated for 1 year. C: C-N,K-(A-)S-H, K: katoite ($\text{Ca}_3\text{Al}_2(\text{OH})_6$, PDF# 00-024-0217), Hc: Hemicarbonate ($\text{Ca}_4\text{Al}_2(\text{OH})_{12}(\text{OH})(\text{CO}_3)_{0.5}(\text{H}_2\text{O})_5$, PDF# 00-029-0285), Mc: monocarbonate ($\text{Ca}_4\text{Al}_2(\text{OH})_{12}(\text{OH})(\text{CO}_3)(\text{H}_2\text{O})_5$, PDF# 00-029-0285). *: The weight loss between 300 and 400 °C in (b) is tentatively assigned to C-N-A-S-H.

The simulated Al solubility of amorphous $\text{Al}(\text{OH})_3$, stätlingite, katoite and C-A-S-H with Ca/Si = 1, Al/Si = 0.1 are plotted against pH in Figure 20. Al solubilities of microcrystalline $\text{Al}(\text{OH})_3$, stätlingite and katoite decrease with increasing pH, pass minimum at pH \approx 6.5, 12.2 and 13.6 separately, and increase again with increasing pH, due to the formation of anionic aluminate species.

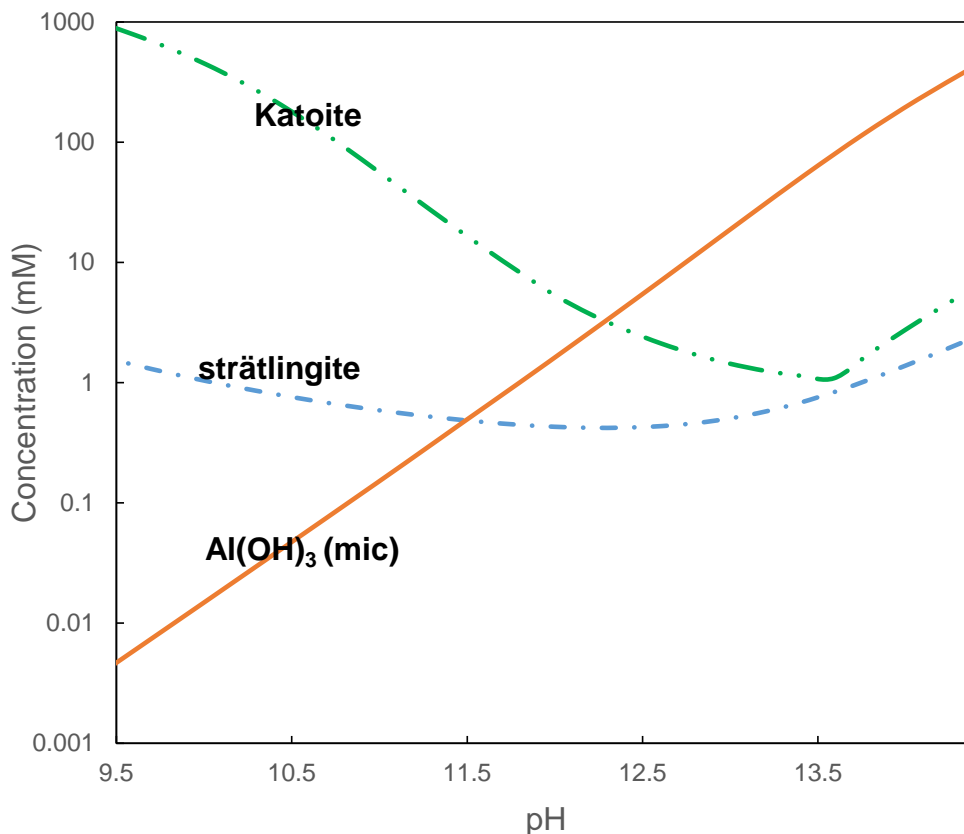


Figure 20. Effect of pH on Al solubility of microcrystalline $\text{Al}(\text{OH})_3$, strätlingite and katoite (all solids 1 mol/L) at equilibrium conditions. Above pH 13.7, the formation of portlandite is calculated in the presence of katoite.

The measurements of interlayer distance in C(-A)-S-H by XRD is associated with considerable variations as it also depends strongly on the relative humidity [130,131] and thus on the drying procedure and duration. In the present study as well as in the study of L'Hôpital et al. [48], all samples were equilibrated at least two weeks in a desiccator with a relative humidity of ~ 30 %, thus the water content in the C-A-S-H phases are comparable. In fact, a systematic increase of the basal spacing with Al/Si in C-S-H is observed as shown in Figure 21. In contrast, no clear trend was found between the basal spacing and water content ($\text{H}_2\text{O}/\text{Si}$ obtained from TGA, see Figure 52), which confirms that the Al substitution in C-S-H is a dominant factor for the observed increase of the basal spacing.

In 0.5 M NaOH, for C-S-H without Al, a basal spacing of ~10.8 Å is observed, and it increases strongly to 12.3-12.5 Å at $\text{Al}/\text{Si}_{\text{C-S-H}} = 0.05$ and levels off at ~ 12.5 Å at higher Al contents. This widening of the interlayer with Al can be explained i) based on the increase of negative charge due to the uptake of AlO_4 in the bridging tetrahedra increasing the repulsive force between the negatively charged main layers [26] and ii)

based on the about 8 - 10% longer Al-O than Si-O bonds [132,133], which is also visible in the, although more limited, increase of the interlayer distance observed for cross-linked 11 Å Al-tobermorite [65,134] in the presence of Al as shown in Figure 21.

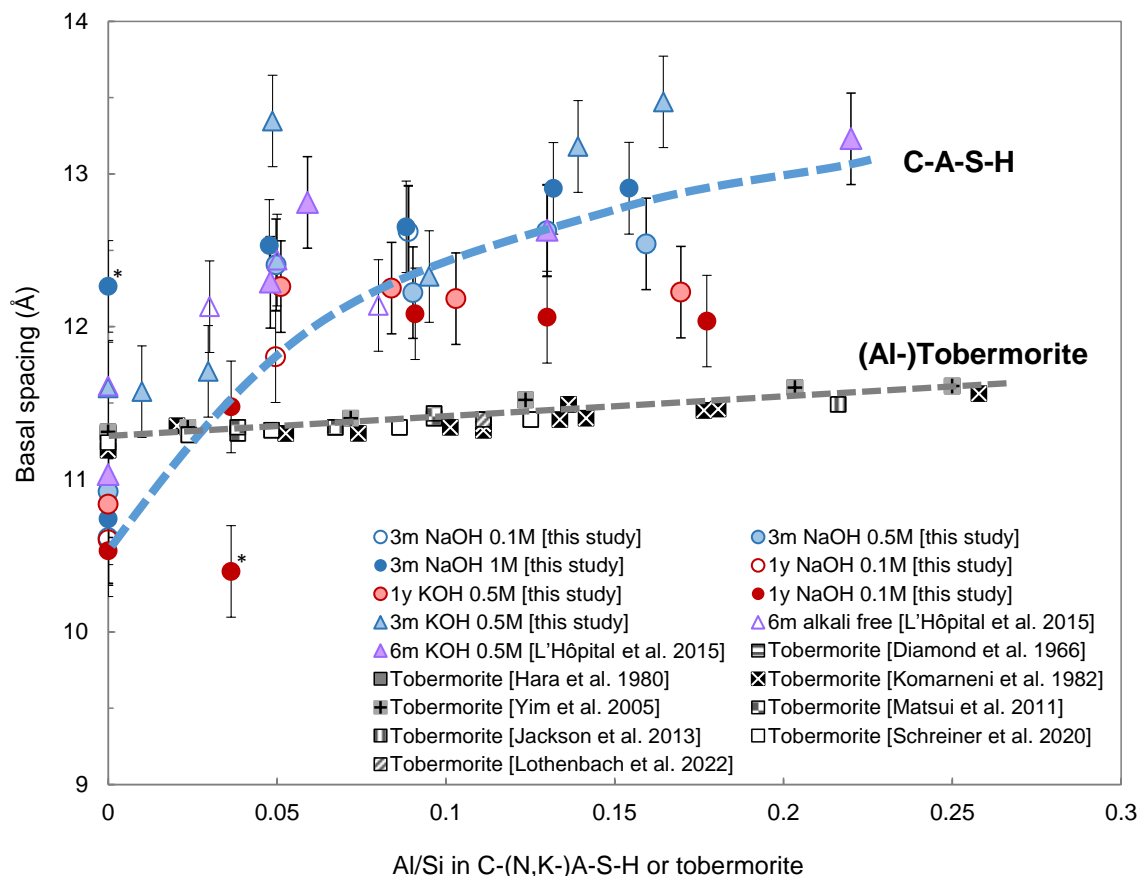


Figure 21 Variation of the mean basal spacing as a function of Al/Si in C-(N,K)-A-S-H and (Al-)tobermorite [65,135–140] . C-A-S-H with Ca/Si_{target} at 1.0. * indicates two reflections. The dash lines are shown only as an eye-guide

The changes in the structure upon the addition of Al have been investigated by Si and Al-solid state NMR, by FTIR and Raman as well as by XANES. Detailed Si and Al-solid state NMR investigations of these samples have recently been published by Yang et al. [45] and showed that at $Ca/Si = 1.0$, Al in C-S-H was mainly bound as Al(IV) in the bridging sites, with only minor amounts (< 10%) of Al(VI) present at all pH values and Al contents investigated. In addition, minor amounts of secondary phases were observed at low NaOH and/or high Al concentrations, in agreements with the XRD and TGA results reported here. The presence of Al increased the total chain length considering both Si and Al but did not increase the length of the silica chain only [45].

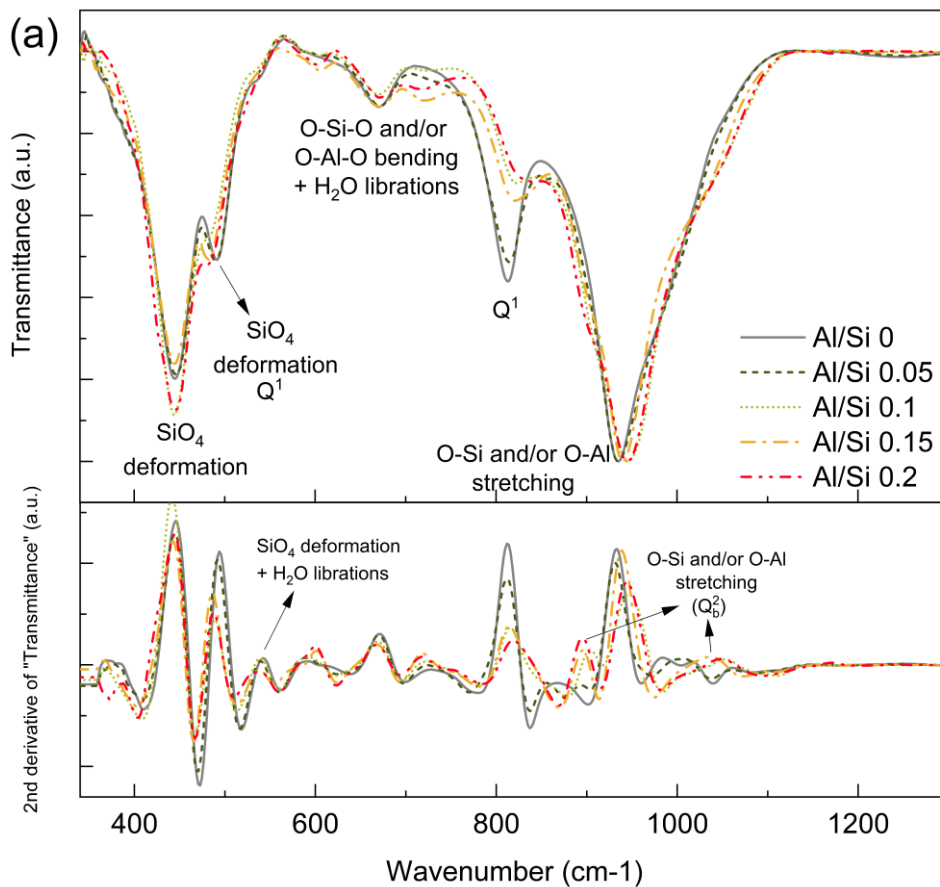
Figure 22 (a) illustrates the effect of Al on C-N-(A-)S-H based on FTIR spectroscopy. The vibrations from secondary phases were not discussed here since the maximum

secondary phase is lower than 8 wt %, such that they are hidden by the bands from C-A-S-H (see Table 3). The vibrational spectra can be divided into two regions: the bands in the region 800-1200 cm^{-1} are due to stretching vibration of O-Si and/or O-Al, while from 400 cm^{-1} to 800 cm^{-1} , the spectra have contributions from SiO_4 and/or AlO_4 deformation, bending vibrations of the O-Si-O and/or O-Al-O groups in the dreierketten chains and from water liberations [34,102,141], as detailed in Table 3. The most intensive band is moving from 933 cm^{-1} to 947 cm^{-1} in the presence of additional Al in 0.5 M NaOH. This movement to higher wavenumbers is also observed in 0.1 M and 1 M NaOH (see Figure 47). Similarly, the shoulder at $\sim 1050 \text{ cm}^{-1}$, indicating the stretching vibration of O-Si and/or O-Al in Q^2 position, is moving to a higher wavenumber as well the bridging Q^2_{b} band which shifts from 920 cm^{-1} (in the absence of any Al [141]) to 880 cm^{-1} at $\text{Al}/\text{Si}_{\text{initial}} = 0.2$. This shows a higher polymerization degree of the silicate chains [33,142] due to the addition of Al, which increases the total $(\text{Al}+\text{Si})/\text{Ca}$ ratio. In fact, the intensity of the Q^1 signal (band at $\sim 810 \text{ cm}^{-1}$ and at 490 cm^{-1}) is decreasing as more Al is present, while the Q^2_{b} signal at $\sim 920 \text{ cm}^{-1}$ increases confirming the increase of the connectivity also observed by NMR [45] and the Al-uptake in the bridging sites of C-S-H.

The Raman spectra in Figure 22 (b) show that the intensity of the peak at 316-333 cm^{-1} from vibrations of Ca-O [106][107] decreases and broadens with increasing $\text{Al}/\text{Si}_{\text{initial}}$. A peak assigned to internal deformation of the Si-tetrahedra [106] or to O-Si-O bending [107] is visible at 445 cm^{-1} , while a main Si-O-Si symmetrical bending peak is present at 670 cm^{-1} . The presence of Al had only a very weak effect on the positions of these peaks, but had clear effect on the intensity of the signals assigned to Q^1 and Q^2 sites. The Si-O symmetrical stretching (SS) band at $\sim 840 - 940 \text{ cm}^{-1}$, assigned to SS Q^1 [22,106,107], decrease in intensity with $\text{Al}/\text{Si}_{\text{initial}}$ indicating less Q^1 . In contrast, the peak area of the signal at $\sim 950 - 1040 \text{ cm}^{-1}$, assigned to SS Q^2 [22,106,107], increases with $\text{Al}/\text{Si}_{\text{initial}}$ confirming the FTIR data presented above and the solid state NMR [45]. The peak width of these Si-O silicate Q^1 and Q^2 signals broadens, which indicates a higher degree of disordering in the silicate chains [109,143], due to the presence of more different Q^2 species (Q^2_{p} , Q^2_{b} , and $\text{Q}^2_{\text{p}}(1\text{Al})$) with additional Al in C-A-S-H. The peaks located at 1065 cm^{-1} are attributed to the C-O SS vibrations from hemicarboaluminate [22].

Chapter 4: Al uptake in calcium silicate hydrate (C-S-H) and the effect of pH

A small peak located at 602 cm^{-1} appeared at $\text{Al}/\text{Si}_{\text{initial}} = 0.1$ and increased systematically with additional Al. A peak at similar Raman shift has been reported for tobermorite [106] and Al-tobermorite [12,127], where it has been assigned to Q^3 or $\text{Q}^3(1\text{Al})$. However, in the C-A-S-H phases analyzed here, no Q^3 signal has been observed from ^{29}Si NMR [45], such that this signal is tentatively assigned to Al-O-Si symmetrical bending. A sharp peak at 477 cm^{-1} present at $\text{Al}/\text{Si}_{\text{initial}} = 0.05$ and signals 437 cm^{-1} , 1114 cm^{-1} and 2410 cm^{-1} and 810 cm^{-1} are tentatively assigned to signals from secondary phases.



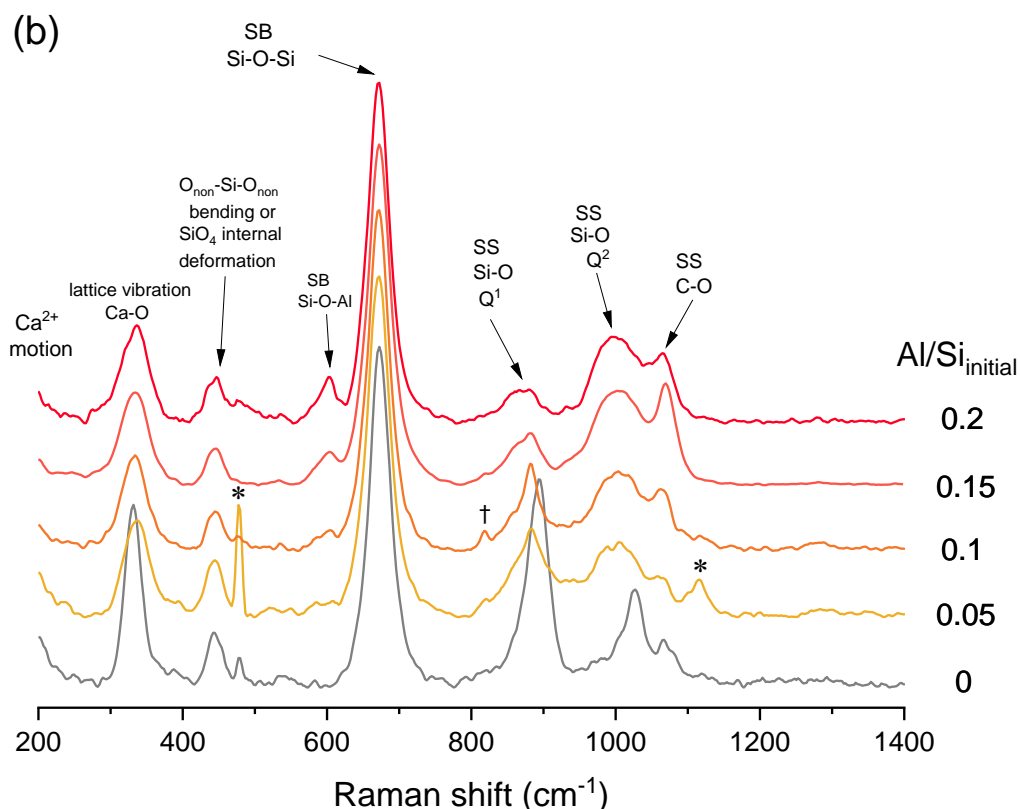


Figure 22 (a) FTIR and second derivative and (b) Raman spectra of C-N-(A-)S-H with target Ca/Si=1.0 after an equilibration time of 1 year with different initial Al/Si, synthesized in 0.5 M NaOH. Normalized to the most intensive band at ~ 970 cm⁻¹ of FTIR and ~ 670 of Raman. *, †: unidentified peaks from secondary phases.

Table 3. Assignments of FTIR spectra for C-A-S-H.

FTIR		
Absorption band (cm ⁻¹)	Assignment of vibration	References
400-550	Deformation of Si and/or Al tetrahedra	[33,102]
~ 480 ^a	Deformation of Si and/or Al tetrahedral (Q ¹)	[141]
~ 480 ^a	O-Si-O and/or O-Al-O bending	[144]
~ 525	Si-O-Si and/or Al-O-Si bending	[144]
~ 525	Deformation of Si(Al) tetrahedral and water	[102]
670	Si-O-Si and/or Al-O-Si (O-Si-O) bending and water librations	[33,102]
810 ^a	Si-O and/or Al-O stretching of Q ¹ tetrahedra	[33]
920 ^a	Si-O and/or Al-O stretching of Q ² tetrahedra	[102,141]
960	Si-O and/or Al-O stretching modes	[102]
1050 ^a	Si-O and/or Al-O stretching of Q ² tetrahedra	[141]
~810, ~537	Al-O vibration from katoite	[145,146]

Chapter 4: Al uptake in calcium silicate hydrate (C-S-H) and the effect of pH

~536,~	Al-O vibration from Hc and Mc	[145]
~ 1360	C-O vibration from Hc and Mc	[145]
~ 3660	H-O vibration from katoite	[145,146]

^a: bands visible as a shoulder.

. Table 4. Assignment of Raman spectra for C-A-S-H.

Raman shift (cm ⁻¹)	Assignment of vibration	References
316 - 333	Ca-O lattice vibration	[107]
445	internal deformation of the Si-tetrahedra	[106]
445	O-Si-O bending	[107]
477	'breathing' vibrations of the 4-membered	[147,148]
~ 600	Si-O-Al symmetrical bending	[22,106,107]
~ 670	Si-O-Si symmetrical bending	[22,106,107]
~ 840	Si-O Q ¹ symmetrical stretching	[22,106,107]
~ 950	Si-O Q ² symmetrical stretching	[22,106,107]
1065	C-O symmetrical stretching from hemicarboaluminate	[22]
2881, 2933, 2976	$\nu_s(\text{CH}_2)$, $\nu_s(\text{CH}_3)$, $\nu'_s(\text{CH}_3)$ from ethanol	[149]

The local structure and coordination geometry of Al sites in C-A-S-H samples were further investigated by Al K-edge XANES spectra. Katoite (C₃AH₆), AFm-CO₃ (as a structural analogue to strätlingite) and CaO·Al₂O₃ (CA) were characterized for comparison. The Al sites in both C₃AH₆ and AFm-CO₃ are octahedrally coordinated Al(VI) with a main signal C at 1572 eV in the XANES spectra, while the main signal C of tetrahedrally coordinated Al(IV) of CA appeared at a lower energy of 1565 eV (see Figure 23 (a)). The peaks A, C and E in Figure 23 (a) correspond to the transitions of 1s to 3s-like, 3p-like and 3d-like states, respectively, while peak D corresponds to the multiscattering within adjacent neighbor shells [150,151]. The 1s to 3s-like transition is forbidden for the tetrahedral geometry of Al and thus results in weak peak A intensity, while it is permitted in the case of octahedral geometry due to the hybridization of s and p orbitals [150,151]. Thus, peak A is quite weak in Al(IV) predominated environments (e.g., CA and C-A-S-H), whereas it is more visible in C₃AH₆ and AFm-CO₃ where Al(VI) is predominant. The position of peak C for Al(IV) in CA is a few eV lower than the position for octahedral Al(VI) in C₃AH₆ and AFm-CO₃, in good agreement with previous studies [150–155].

Iterative-target transformation factor analysis (ITFA) of the Al K-edge XANES dataset was performed to quantify the proportions of Al-containing components. XRD results suggest that the solid products mainly consist of C-A-S-H, katoite, and AFm phases. In combination with the assessments on the indicators of theoretical error functions (Table 20) and the principal component analysis (PCA), the number of abstract spectra (Figure 55) to reproduce the Al K-edge XANES spectra of C-A-S-H samples is determined to be three. Via iterative target test (ITT), the three components were identified as C-A-S-H, katoite, and AFm-CO₃, in good agreement with the XRD results. C-A-S-H with Al/Si_{initial} 0.05, having no visible impurity in XRD and TGA analysis, was used as reference of pure C-A-S-H in ITFA analysis. The quantitative fitting results of ITFA are shown in Table 20; the fitting curves together with the experimental spectra of C-A-S-H with Al/Si_{initial} 0.1, 0.15, and 0.2 are illustrated in Figure 5a. In accordance with XRD Rietveld analysis, ITFA analysis shows that majority of the solid phase is C-A-S-H and maximum amount of Al in secondary phases is about 15%. With increasing Al/Si ratios, the intensity of peak C of C-A-S-H samples becomes stronger, partially related to the growing proportion of secondary phases such as katoite and AFm phases. A directly proportional relation can be found in the amount of secondary phases from quantification by ITFA and Rietveld analysis (see Figure 24).

With increasing Al/Si ratios, the C-A-S-H sample spectra were reproduced less satisfactorily (Figure 23 (a)), characterized by more differences compared to the fitting curves in the peak C region. It indicates some contributions from other coordination environments of Al sites not included in the ITFA fitting. The local structures of Al sites in C₃AH₆ and AFm-CO₃ are well known and not expected to change with the Al/Si ratios, which is, however, not the case for C-A-S-H samples. Thus, the fitting difference could result from changes of the Al coordination environment and/or Al content in C-A-S-H samples.

To further investigate the relationship between the XANES spectrum features and the local structures of Al sites in C-A-S-Hs, the theoretical Al K-edge XANES spectra were calculated based on the atomic structures of different possible Al-centered C-A-S-H structures, including Al(IV) in bridging site without neighboring cations, Al(IV) in bridging site with a neighboring Ca, and with a neighboring Na, loosely bound Al(VI) without neighboring cations, Al(VI) with neighboring Ca, with neighboring Na and Al(VI) at end-of-chain, Q¹, position. As shown in Figure 23 (b), the theoretical spectra differ

clearly between the coordination geometries, i.e., Al(IV) and Al(VI), in both shape and peak position. The Al(VI) spectra are characterized by a strong peak at ~1571 eV, distinct from the main peak of Al(IV) spectra at ~1566 eV. However, different second neighboring atomic shells near Al(IV) or Al(VI) have no obvious effect on the calculated spectra, which might be explained by not good enough resolution of spectrum calculation or not large enough influence of the second neighboring shell on Al K-edge XANES spectra of C-A-S-H, in particular considering that the second neighbors are light elements with little difference in mass number. The comparison between the calculated spectra and the fitted experimental spectra indicates prevailing Al(IV), which is in agreement with the Al-NMR data of these samples [45]. Note that the fitting difference is located at the same energy range as the white-line peak of Al(VI) coordination environments. Thus, the missing contribution of Al sites in ITFA should be Al(VI) sites in C-A-S-H, which would indicate that with increasing Al/Si ratios, the amount of Al(VI) sites in C-A-S-H increases or that chemical environments of Al(VI) changes with the initial Al/Si.

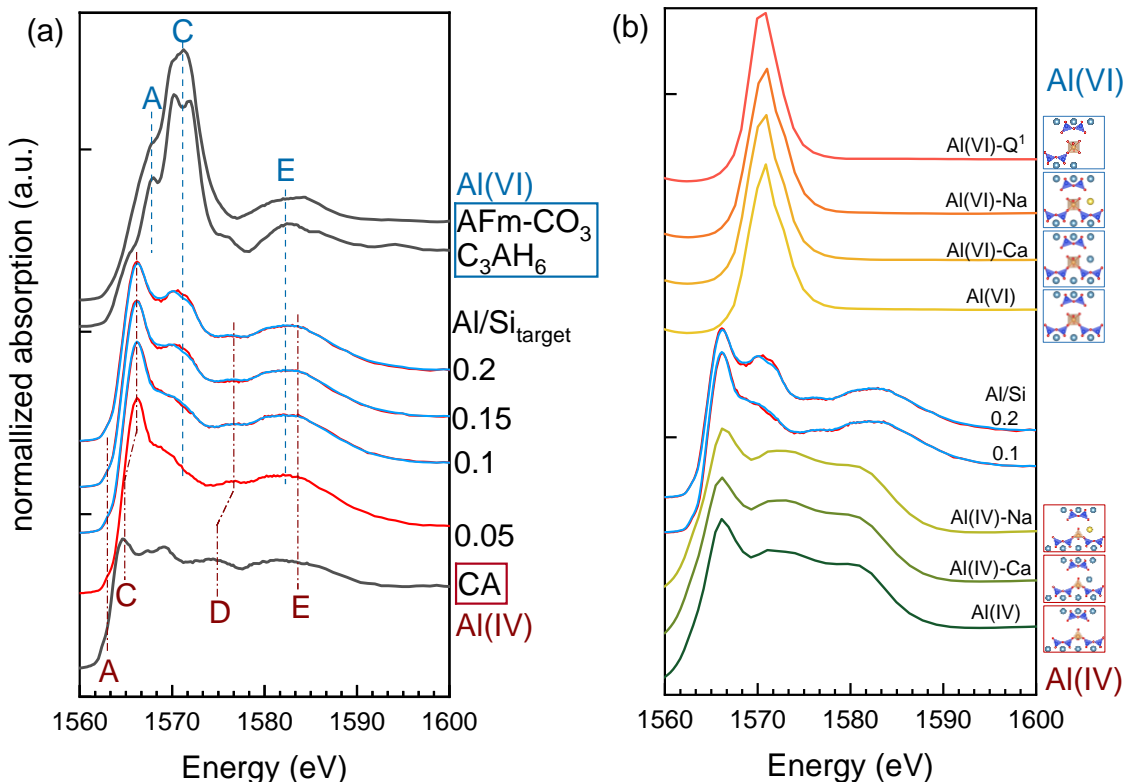


Figure 23 (a) Al K-edge XANES spectra for C-A-S-H synthesized in NaOH 0.1 M and reference spectra for CA, C₃AH₆ and CO₃-AFm. Black and red lines: experimental spectra; blue lines: ITFA fits. (b) Comparison between selected experimental Al K-edge XANES spectra (with

fitting curves in blue) and calculated spectra for tetrahedral and octahedral Al with different chemical environments.

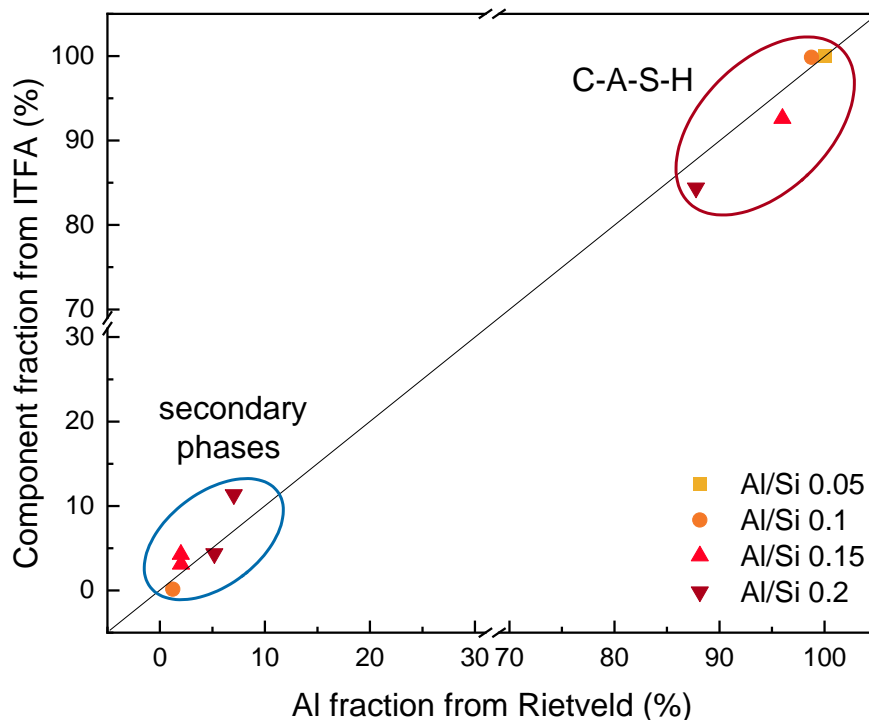


Figure 24. Comparison between component fraction from ITFA analysis and Al fraction from Rietveld quantification.

The Al/Si ratio affects also the composition of the solutions as shown in Figure 25, where changes of Ca, Si and Al concentrations are plotted as a function of the Al/Si in the solid. An increase of the Al/Si_{target} ratio leads to higher dissolved aluminium concentrations, while the silicon concentrations are only moderately increased indicating a lower tendency of Al than of Si to be taken up in C-A-S-H. The presence of additional aluminium also decreases the calcium concentrations. The measured dissolved concentrations are compared to the results of thermodynamic modelling using the CASH+ model [61–63] and a good agreement is observed as shown in Figure 25(a).

As at $Ca/Si_{target} = 1.0$ aluminium is taken up mainly as tetrahedral Al(IV) in the “dreierketten” chains [45] (Figure 23), an uptake of aluminium is expected to have a similar effect as the presence of more silica (Figure 25b): a higher silicon concentration

Chapter 4: Al uptake in calcium silicate hydrate (C-S-H) and the effect of pH

and lower calcium concentration corresponding to longer silica chains due to an increase of the fraction of bridging tetrahedra. Figure 25(b) shows that the measured trends are much better reproduced accounting for the effect of Al and Si separately (C-A-S-H), than if the effect of Al is considered to be the same as the effect of Si (C-S-H). While little difference is predicted at low Al contents ($\text{Ca}/(\text{Al}+\text{Si}) \geq 0.95$), a higher (Al+Si) concentration is predicted for C-A-S-H than for C-S-H, which confirms a lower tendency of Al than of Si to be in C-A-S-H at $0.81 < \text{Ca}/(\text{Al}+\text{Si}) < 0.95$.

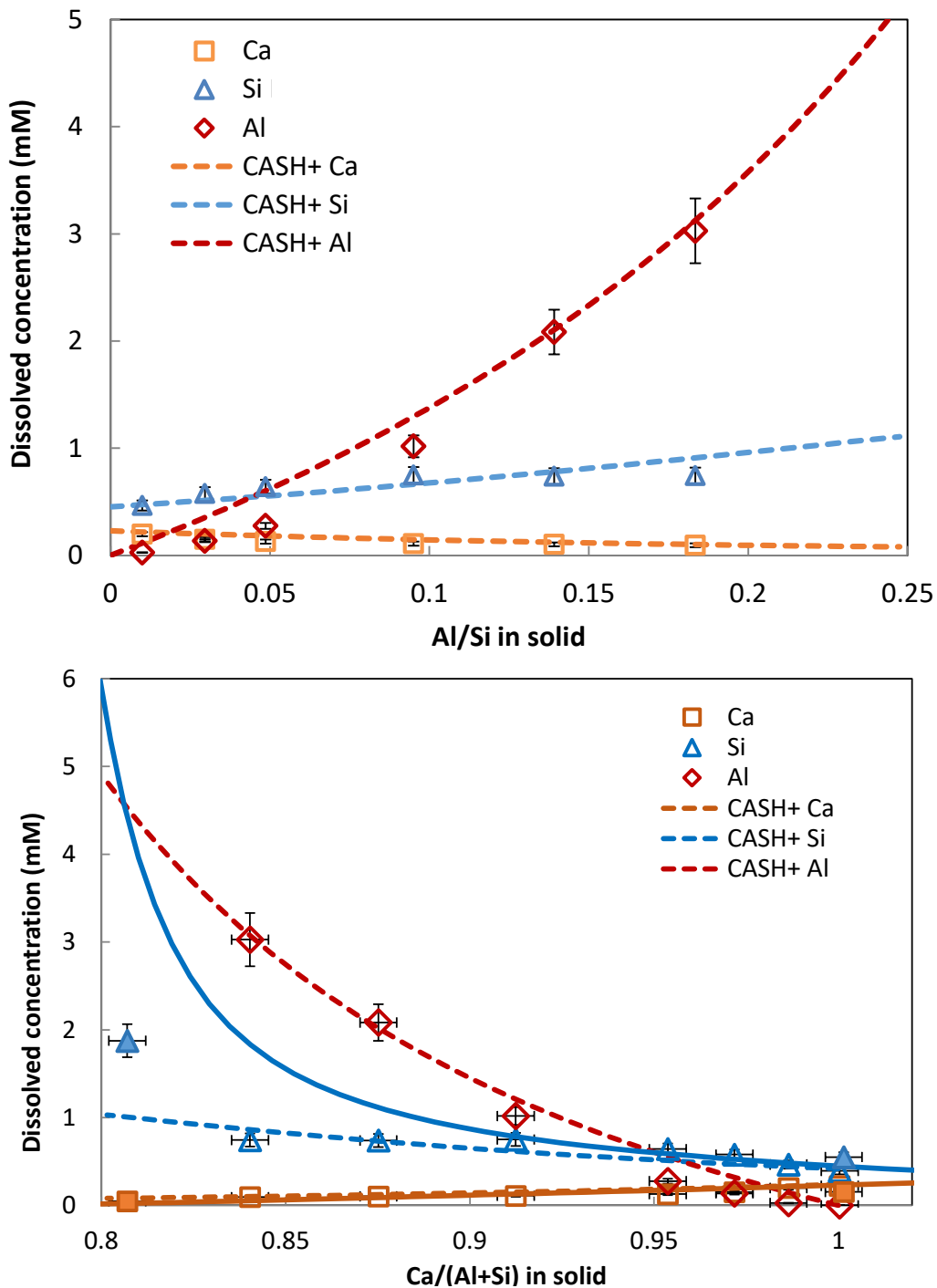


Figure 25 Measured (symbols) and calculated (lines) concentrations of Ca, Si and Al in solutions equilibrated with target Ca/Si=1.0 in KOH 0.5 M as a function of (a) Al/Si ratios and (b) Ca/(Al+Si). The equilibration time is 3 months. Orange squares: Ca, blue triangles: Si and red diamonds: Al, empty ones are C-A-S-H samples and the filled ones are C-S-H samples from [141]. The estimated relative uncertainty of the IC measurements is $\pm 10\%$. Lines: simulated using the thermodynamic CASH+ model [61–63], dashed lines: simulated C-A-S-H and solid lines: simulated C-S-H without Al.

Figure 26 illustrates the distribution of Al between C-A-S-H, aqueous phase and different secondary phases as a function of the initial Al content. At lower Al nearly all aluminum (> 99.9 %) is present in C-A-S-H. The fraction of Al bound in C-A-S-H decreases at higher Al concentrations as secondary phases precipitate for both solutions containing NaOH and KOH.

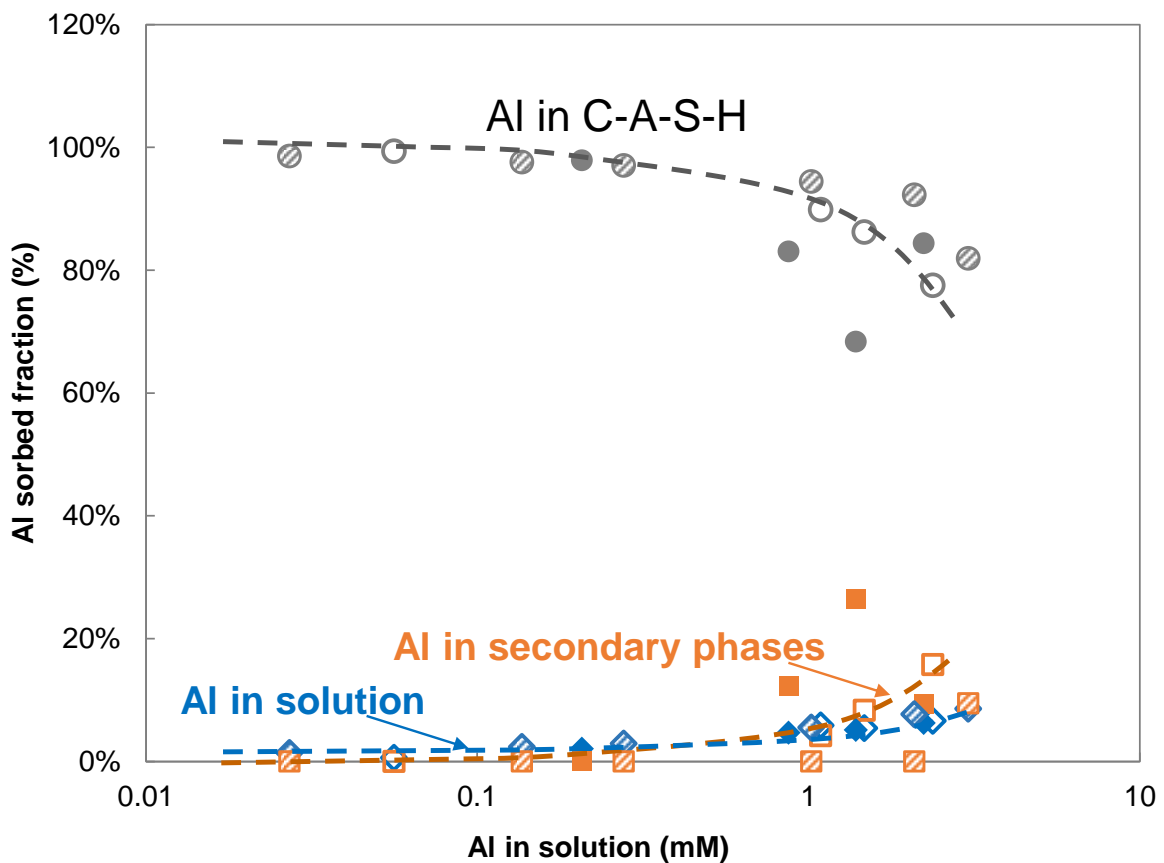


Figure 26 Al fraction in C-A-S-H, aqueous phase and different secondary phases for target Ca/Si = 1.0 after 3 months and 1 year equilibration in the presence of 0.5 M alkali hydroxide. Empty symbols: sample synthesized for 3 months and equilibrated in 0.5 M Na OH, solid symbols: sample synthesized for 1 year and equilibrated in 0.5 M NaOH, patterned symbols: sample synthesized for 3 months and equilibrated in 0.5 M KOH. The dash lines are shown only as an eye-guide

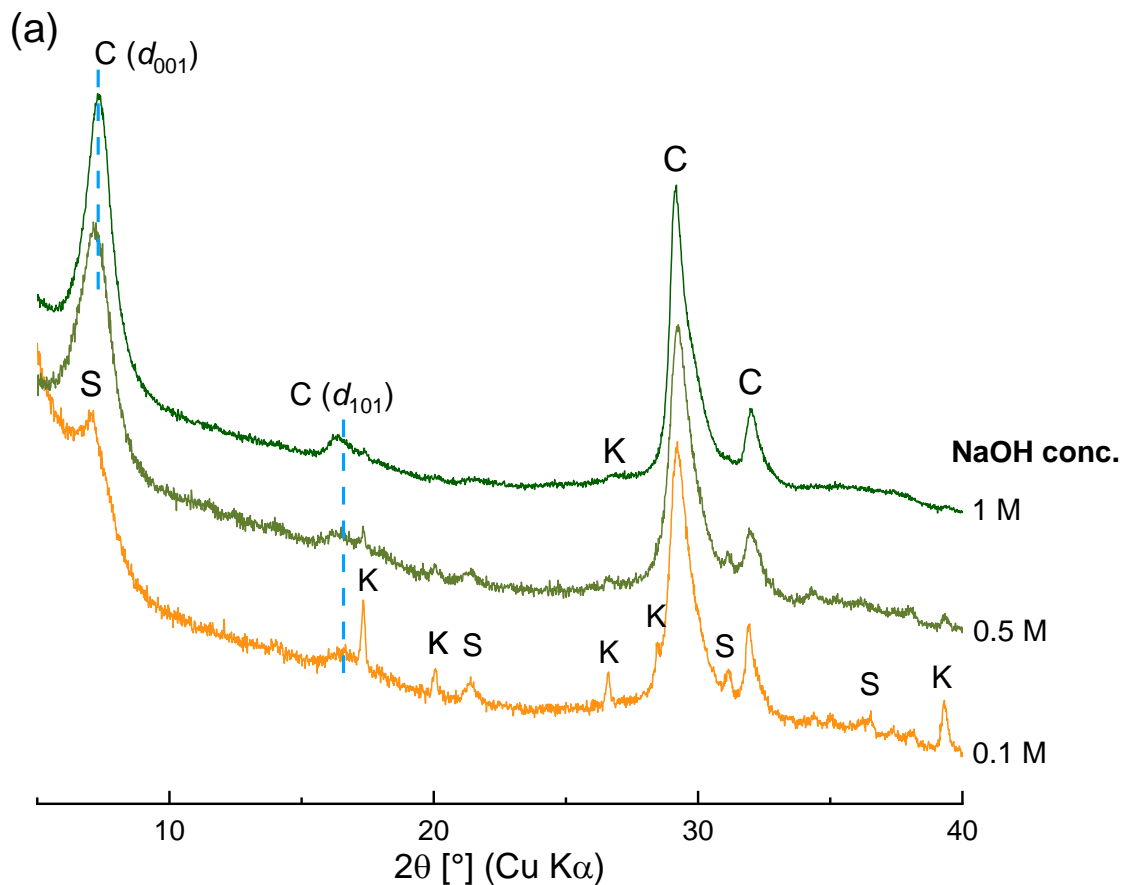
4.2.2. Influence of NaOH and KOH

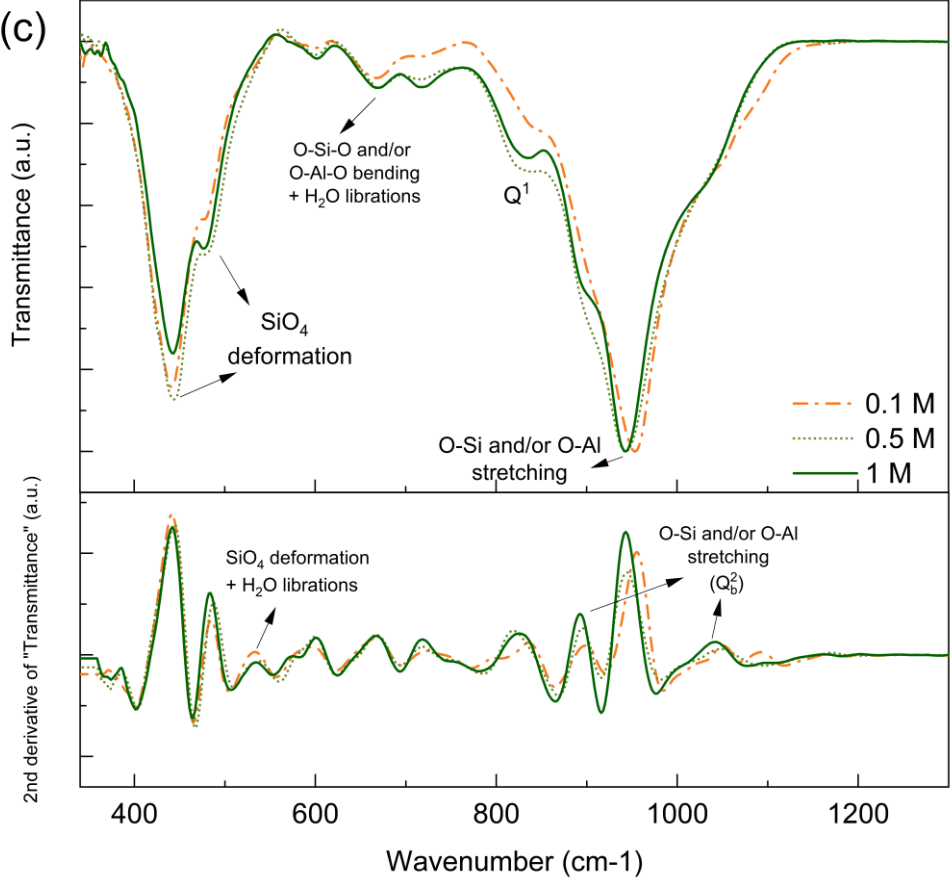
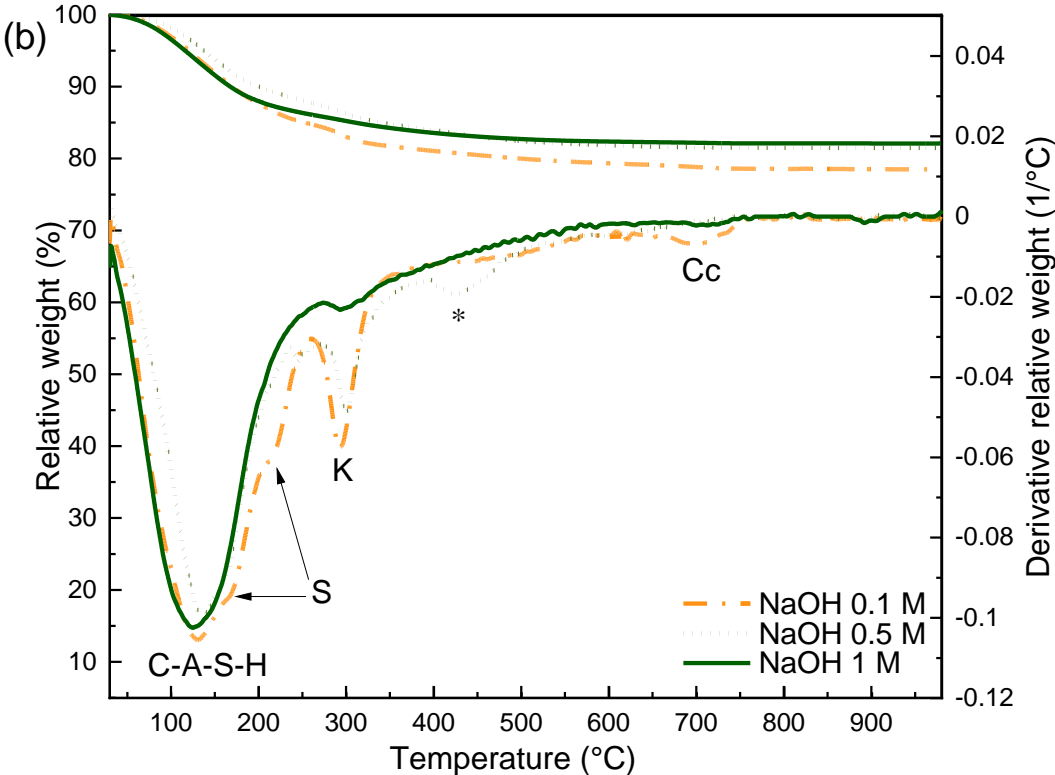
Increasing concentrations of NaOH lower the amount of secondary phases as shown in Figure 27 (a) and (b). While in 0.1 M NaOH strätlingite and katoite are present, in 1 M NaOH only katoite was present. Rietveld analysis indicates that the amount of secondary phases reduces from 7.0% katoite plus 5.2% strätlingite in 0.1 M NaOH to 1.9% katoite in 0.5 M NaOH and 1.0% katoite in 1 M NaOH. This is due to the destabilization of strätlingite with increasing pH values as illustrated in Figure 20. Figure 27 indicates also that the presence of alkali hydroxide shows no significant influence neither on the amount of water in C-A-S-H (see main water loss up to 300 °C in TGA) nor on the basal spacing observed by XRD for C-A-S-H, see also Figure 21. However, a somewhat more narrow d_{001} reflection is observed in 1 M NaOH compared with 0.5 M, which could indicate a more ordered structure of C-A-S-H along the *c*-axis and/or more stacking layers in *c*-axis direction [100,141]. Such a narrower d_{001} reflection has been observed previously for C-S-H without Al at higher NaOH concentrations [141], which has been assigned to an increased stacking in *c*-direction at higher pH values.

Figure 27 (c) shows that increased NaOH concentrations shift the most pronounced FTIR band at 950 cm^{-1} to lower wavenumbers (redshift from 957 cm^{-1} to 943 cm^{-1}), indicating that additional NaOH depolymerizes the silicate chains [33,142], in agreement with the effect observed by Si-NMR [45] and the observations for C-S-H without Al [141]. Also the intensity of the stretching vibration of O-Si and/or O-Al from Q^1 signal located at $\sim 810 \text{ cm}^{-1}$ and the bending vibration of O-Si-O and/or O-Al-O [144] or the deformation of Si and/or Al tetrahedral [33,102] of Q^1 signal located at $\sim 480 \text{ cm}^{-1}$ increase, indicating the presence of more Q^1 silica and thus a shortening of the silica chain length. At higher NaOH concentration the shoulders located at $\sim 900 \text{ cm}^{-1}$ and 1020 cm^{-1} are more visible, which indicates peak splitting due to lowering of the symmetry resulting from the transformation of structural equivalent sites into groups of non-equivalent sites [34]. This lowering of the symmetry seems to be caused by the presence of increasing amounts of Na^+ in the interlayer, i.e. by the changes in the second coordination sphere [34].

Chapter 4: Al uptake in calcium silicate hydrate (C-S-H) and the effect of pH

Similar conclusions can be drawn from the Raman spectra Figure 27 (d). The area of the SS Si-O Q¹ signal increases and SS Si-O Q² signal decreases at higher NaOH concentrations. The C-A-S-H synthesized at 1 M and 0.5 M NaOH are more prone to be carbonated than the C-A-S-H at 0.1 M NaOH. The peak at ~ 600 cm⁻¹, assigned to SB Si-O-Al, is more visible in C-A-S-H with 0.5 and 1 M, which indicates that increased substitution of Si by Al occurs in the presence of more alkali hydroxide, in agreement with the higher uptake observed by mass balance calculations (as detailed below), with density function calculations which predict a slight stabilization of Al-uptake in the presence of Na⁺ [156] as well as with recent NMR observations, which indicates a positive correlation between Na and Al uptake at Ca/Si ≥ 1.0 [45].





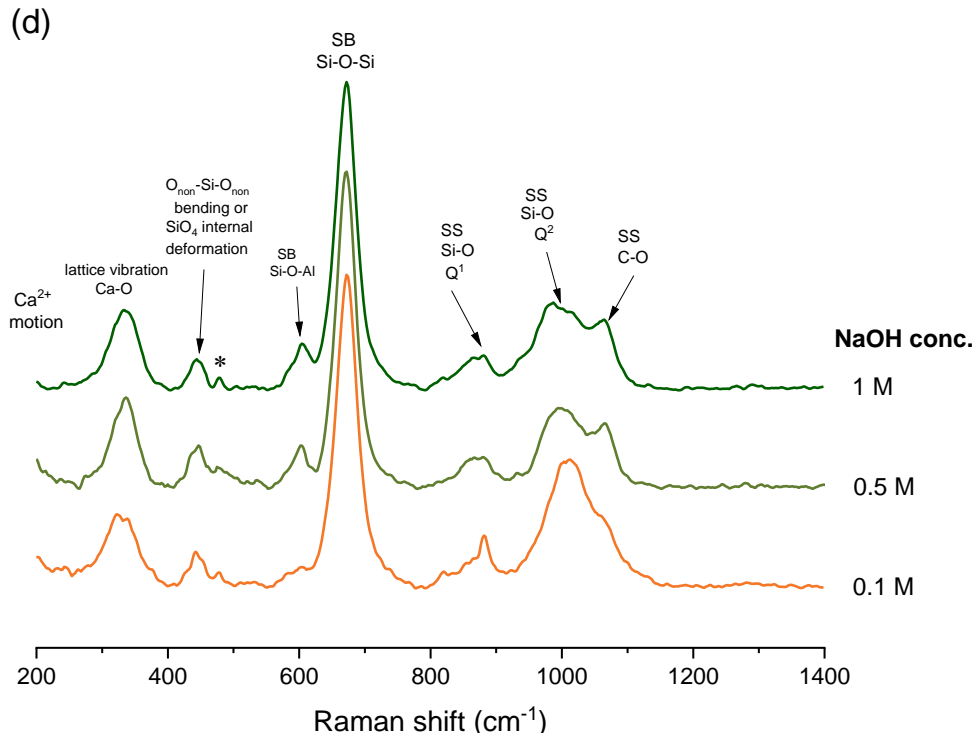


Figure 27 (a) XRD, (b) TGA, (c) FTIR and second derivative of FTIR and (d) Raman of C-A-S-H with a target Ca/Si of 1.0 and target Al/Si of 0.2 synthesized in NaOH from 0.1 M to 1 M after an equilibration time of 1 year. C: C-(K-)A-S-H; K: katoite, S: straelingite, Cc: carbonates *: unidentified peak from secondary phase.

Figure 28 shows the Al K-edge XANES spectra of C-A-S-H with initial Al/Si 0.05 synthesized in 0.1 M NaOH for 1 year and 1 M NaOH for 3 months. These two samples were chosen to minimize the disturbance from secondary phases, since no secondary phases are visible in both samples from XRD. The energy positions of the Al(IV) peak in C-A-S-H remains the same independent of the NaOH concentration, although the peak in 0.1 M NaOH is slightly narrower. This may indicate different chemical environments of Al(IV) in C-A-S-H formed under different alkaline conditions, in agreement with recent ^{27}Al NMR data [45]. In contrast, the shape, position and intensity of the Al(VI) peaks in C-A-S-H varies and an additional signal at 1568 eV is observed, which could suggest that the content and chemical environment of octahedral Al in the interlayer of C-A-S-H also changes with NaOH concentrations. The content of Al(VI) sites in C-A-S-H with initial Al/Si 0.05 is likely to increase or the chemical environments are different with increasing NaOH addition.

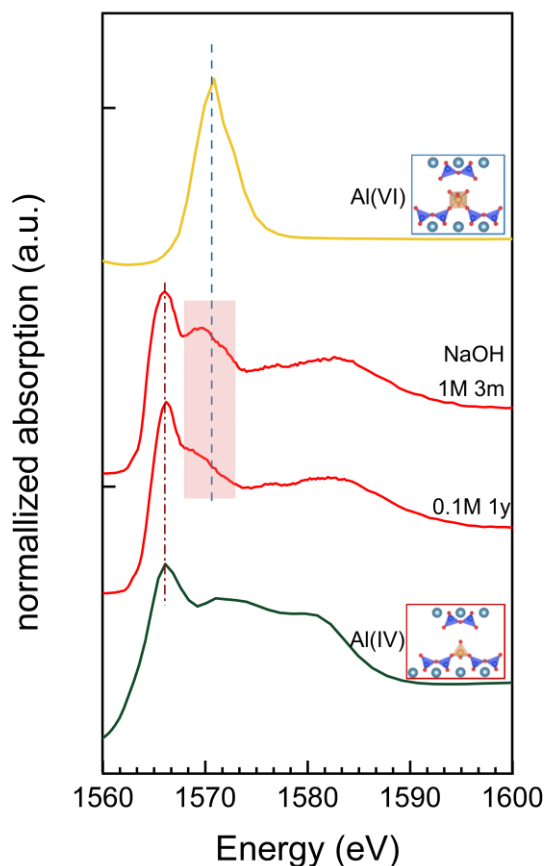


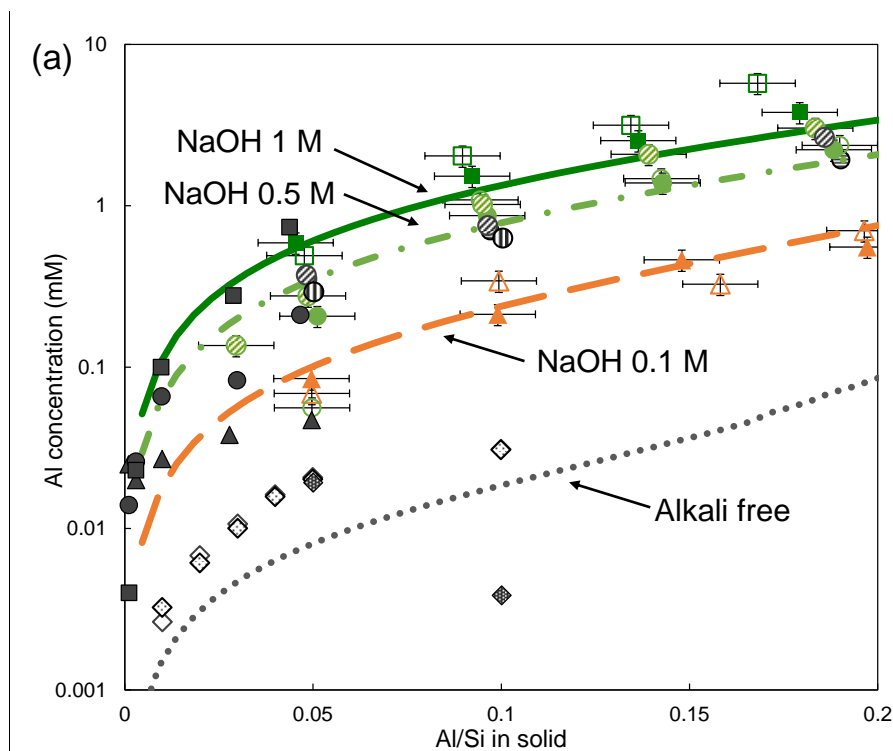
Figure 28 K-edge XANES spectra for C-A-S-H equilibrated for 1 year in NaOH 0.1 M, C-A-S-H equilibrated for 3 months in NaOH 1 M and calculated Al(IV) and Al(VI) spectra.

Figure 25 showed that at constant alkali hydroxide concentration, the measured aqueous Al and Si concentrations increase with rising Al/Si_{solid} , while the Ca concentrations decrease, while Figure 29 illustrates the strong effect of NaOH or KOH, which further elevates aluminium and silica concentrations and lowers the calcium concentrations. The concentrations measured in this study are consistent with previous solubility data of C-A-S-H in NaOH or KOH solutions at 20 °C [40,48], although there is some scatter in the measured data points. The dissolved Al, Si and Ca concentrations show in the absence of NaOH and KOH as well as in their presence similar trends: a rise of Al and Si and a decline of Ca with increasing Al/Si_{solid} . This suggests that C-(N, K-)A-S-H solubility does not vary greatly as a function of the alkali cation (Na or K) present, but that the concentrations are just shifted at higher pH values, due to the common ion effect with C-S-H between hydroxide, Al, Si and Ca. The measured Al, Si and Ca concentrations (data in Table 9) and their trends are in general well reproduced by thermodynamic modelling using the recent CASH+ solid

Chapter 4: Al uptake in calcium silicate hydrate (C-S-H) and the effect of pH

solution model [61–63]. In agreement with the experimental data, the use of NaOH or KOH did not significantly affect the modelled concentrations.

The thermodynamic model predicts higher Al and Si concentrations in the presence of alkali hydroxides due to the preference of Al to form negatively charged $\text{Al}(\text{OH})_4^-$ aqueous complexes and of Si to form $\text{SiO}(\text{OH})_3^-$ and $\text{SiO}_2(\text{OH})_2^{2-}$ complexes at higher pH values. The opposite effect can be observed for Ca concentration: in presence of higher concentration of alkali hydroxide, Ca concentrations decreased.



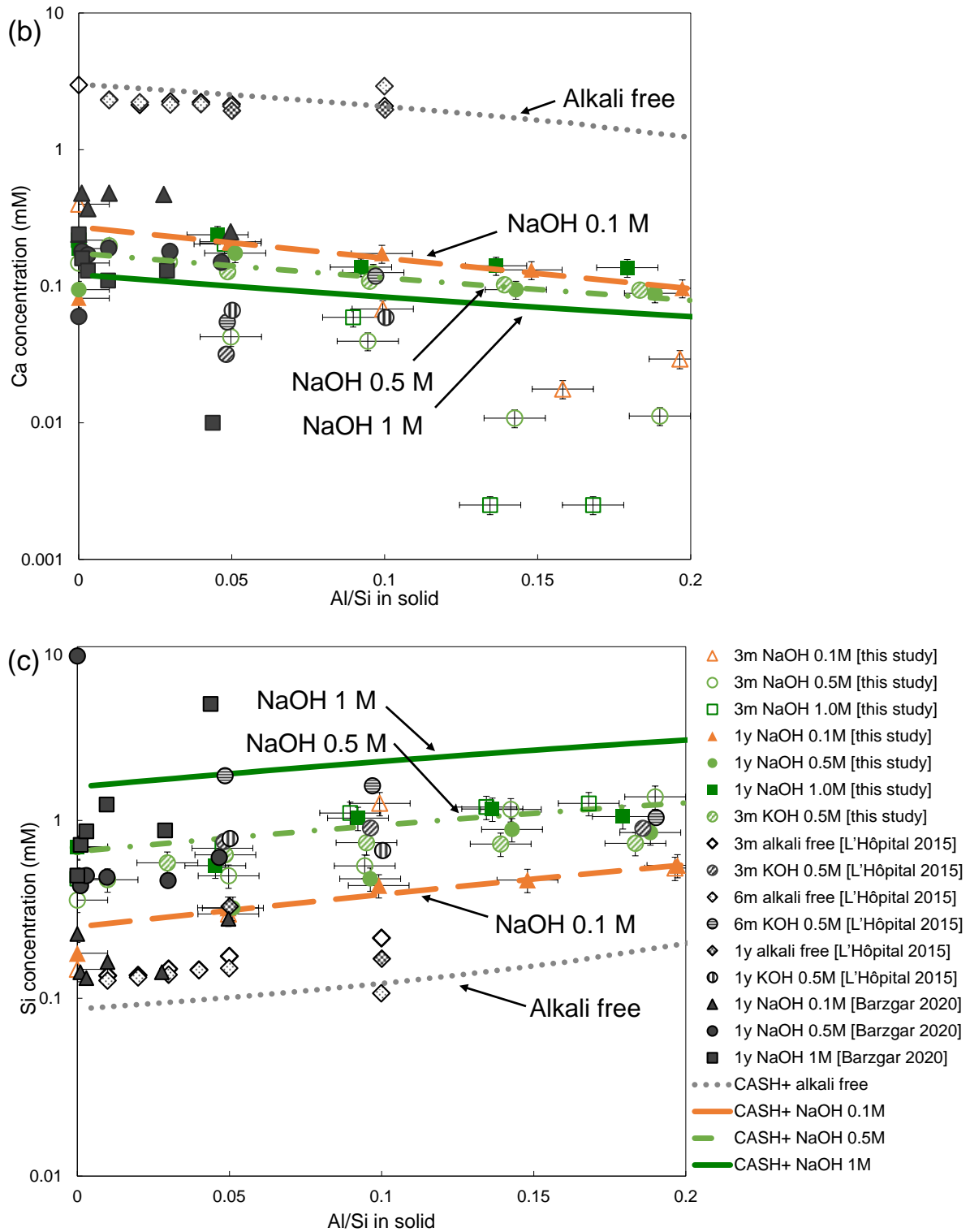


Figure 29 Al, Si and Ca concentrations in the solutions of the C-(A)-S-H samples as a function of Al/Si ratios in solid phase. The estimated absolute errors are $\leq \pm 0.01$ units in the Al/Si ratios and the estimated relative uncertainty of the IC measurements is $\pm 10\%$. Grey symbols: C-(A)-S-H data from [40,48]; colored symbols: C-(A)-S-H from this study; diamonds: C-A-S-H in water; triangles: C-(N,K)-A-S-H with 0.1 M alkali hydroxide solution; circles: C-(N,K)-A-S-H with 0.5 M alkali hydroxide solution, squares: C-(N,K)-A-S-H with 1 M alkali hydroxide solution. Lines: simulated using the thermodynamic CASH+ model [61–63].

The aluminium uptake in C-S-H as a function of dissolved aluminium concentration and pH is shown in Figure 30. The presence of alkali hydroxide increases the fraction of Al in solution and decreases the fraction in C-S-H in agreement with previous experimental studies [26,40,41,48,49], due to the increased tendency of Al to remain as $\text{Al}(\text{OH})_4^-$ in solution at higher pH values. The maximum $\text{Al}/\text{Si}_{\text{C-S-H}}$ of C-(N,K)-A-S-H is also affected by the alkali hydroxide concentration since at $\text{pH} > 13$ the Al concentrations in equilibrium with secondary phases such as katoite and strätlingite increase (see Figure 20). The higher Al concentrations at higher pH values allow a higher Al uptake in C-S-H: the maximum $\text{Al}/\text{Si}_{\text{C-S-H}}$ increases from 0.09 in alkali free solution [48] to 0.13 in 0.1 M NaOH, and to 0.17 in 1 M NaOH for C-N-A-S-H with $\text{Al}/\text{Si}_{\text{target}} = 0.2$ equilibrated for 15 months. The linear relation between aluminium in solution and Al/Si in C-A-S-H at different alkali hydroxide concentrations in Figure 30 indicate an Al uptake on similar sorption sites in C-S-H, independent of the Al concentration and pH value.

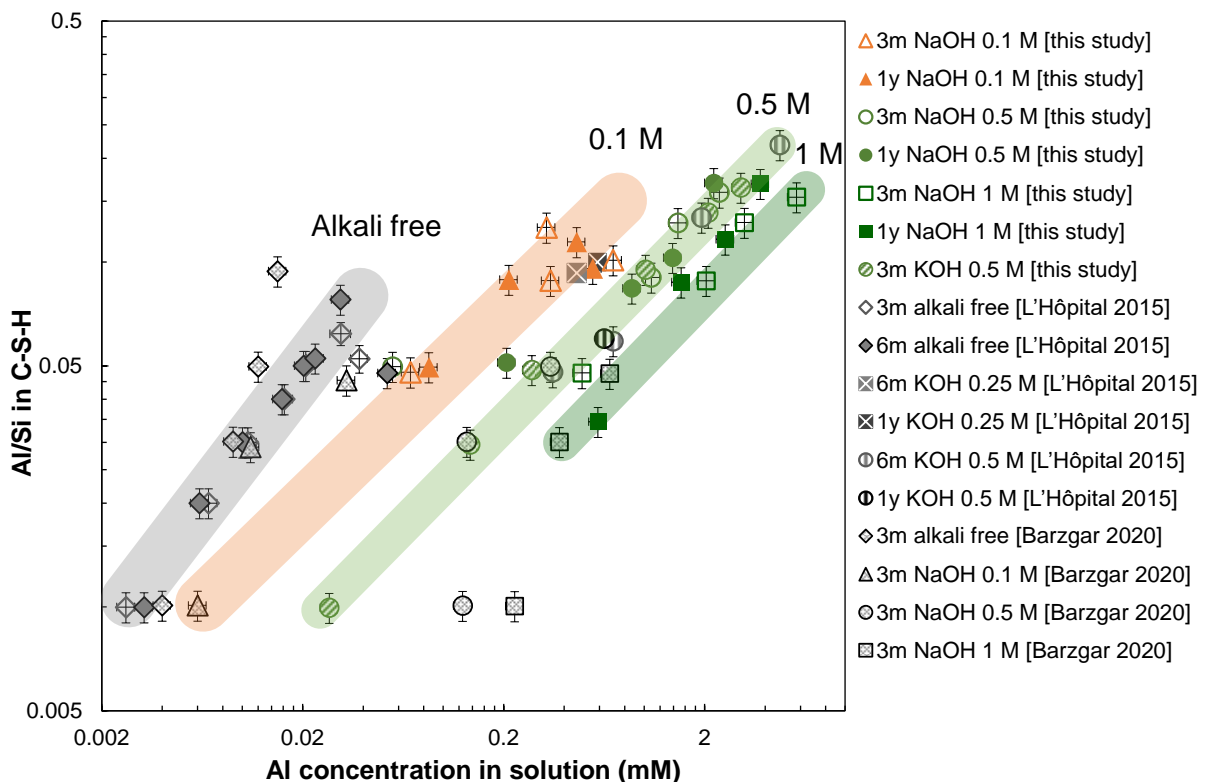


Figure 30 Al sorption isotherm on C-A-S-H for target $\text{Ca}/\text{Si} = 1.0$ synthesized in different alkali hydroxide and recorded after different equilibration times. Colorful symbols: C-A-S-H from this study, grey symbols: C-A-S-H data adapted from [40,48]

The Al uptake in C-S-H is also described by distribution coefficients, K_d values, which depict the relative affinity of Al to sorb on C-S-H as shown in Figure 31. While in the absence of alkali hydroxides, K_d values of $55 \pm 40 \text{ m}^3/\text{kg}$ are observed, they decrease strongly to approximately 2 in 0.1 M NaOH, to 0.6 in 0.5 M NaOH and to 0.3 in 1 M NaOH. The decrease of Al uptake at higher pH values is in accordance with [40], and can be explained mainly by the fact that prefers to be dissolved as $\text{Al}(\text{OH})_4^-$ species in solution at higher pH values, which lowers the tendency of Al to be sorbed by C-S-H. The mean K_d value of $\approx 600 \text{ m}^3/\text{kg}$ reported for similar C-A-S-H samples with $\text{Ca}/\text{Si} = 0.8$ [157] is significantly higher, which could indicate a strong effect of Ca/Si on the K_d values of Al on C-S-H.

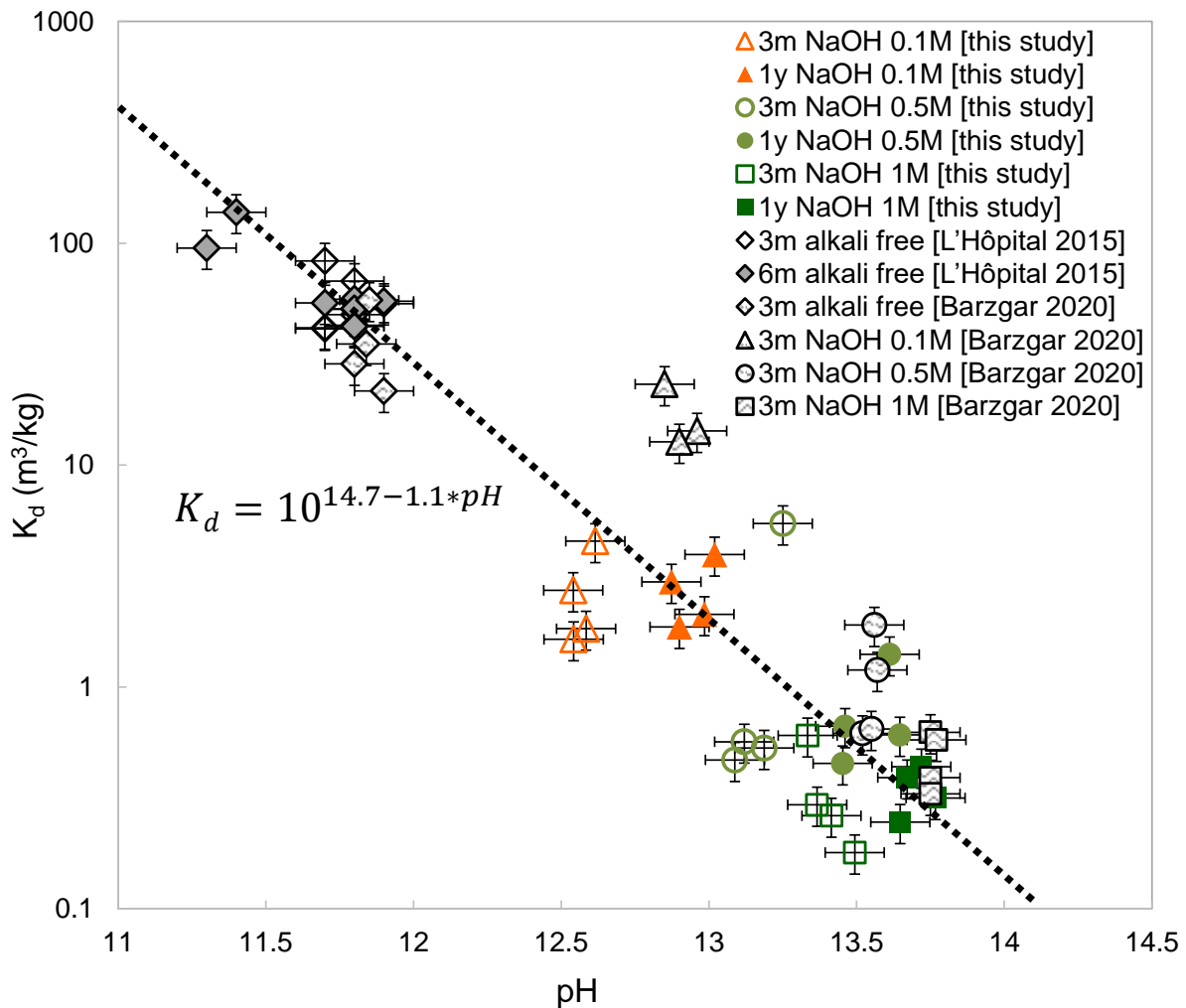


Figure 31. Effect of pH on the K_d values of Al on C-S-H with $\text{Ca}/\text{Si} = 1$.

4.3. Conclusions

In this chapter we studied the effect of Al and of KOH and NaOH concentration on the structure and solubility of C-S-H with Ca/Si = 1.0. XRD, TGA and ITFA analysis of XANES show the presence of more secondary phases at higher Al contents and at lower pH values. The uptake of Al increases the interlayer distance of C-A-S-H, much stronger than observed in Al-tobermorite [65], indicating that the increase of the negative charge due to the uptake of AlO_4 in the bridging tetrahedra increases the basal spacing. The uptake of Al in the bridging tetrahedral of the silica chain results in more Q^2 and less Q^1 sites as observed by FTIR and Raman spectroscopy, indicating longer dreierketten chains in C-A-S-H. In agreement with Al NMR studies [45], XANES data show that Al in C-S-H with Ca/Si = 1 is present as tetrahedral Al independent of the Al concentration or pH values.

More initial Al increases both the dissolved Al and Si concentrations due to their competition for uptake in the bridging sites in the silica chain and lowers the Ca concentrations in the aqueous phase. The aqueous data show a slight preference of Si over Al for uptake in the bridging sites of C-A-S-H, although under all conditions studied, Al is predominantly bound in C-A-S-H in 0.5 M NaOH: $\text{Al}/\text{Si}_{\text{initial}} \leq 0.05$ Al in C-A-S-H > 99% , which decreases to > 70% at $\text{Al}/\text{Si}_{\text{initial}} = 0.2$ due to the formation of secondary phases.

Higher NaOH or KOH concentrations progressively destabilize stratlingite to katoite and reduce the amount of secondary phases. In the C-A-S-H phase less Q^2 and more Q^1 silicate are observed at higher pH indicating a shortening of the silica chain length. XANES spectra show the presence of predominantly Al(IV) in the absence of alkali hydroxide, but more Al(VI) at higher pH values. High pH values also change the spectra of octahedrally bound Al(VI) but less of tetrahedral Al(IV).

Higher pH values increase the aqueous Al and Si concentrations and lower the Ca concentrations. The higher Al concentration lead to a higher fraction of Al bound in C-A-S-H. The linear correlations between the aluminium concentration in solution and Al/Si in C-A-S-H indicate that Al is taken up at similar sorption sites in C-S-H independent of Al concentration or pH values. The distribution coefficients of Al on C-S-H strongly decrease with increasing pH values.

Chapter 4: Al uptake in calcium silicate hydrate (C-S-H) and the effect of pH

The comparison of the measured concentrations with those predicted by thermodynamic modelling using the CASH+ model, showed in general a good agreement, thus providing an independent validation of this only very recently developed thermodynamic model for aluminium and alkali uptake in C-S-H.

CHAPTER 5: Effect of time on Al uptake in calcium silicate hydrate³

5.1. Introduction

The equilibration time [151,158] as well as the preparation method [159–161] can influence the kind of hydrates formed and also the composition of the hydrates. In the experimental setup chosen, precipitation from CaO, CaO·Al₂O₃ (CA) and silica fume (SiO₂), it can be expected that in all cases the system is dominated initially by a high availability of CaO, while SiO₂ will be released much slower due to the slower reactivity of silica fume compared to CaO (or Ca(OH)₂). Thus in all cases the initial C-S-H formed is expected to be Ca-rich and to convert slowly to a Ca poorer C-S-H depending on the target Ca/Si of the individual experiments. This is similar to the changes observed in blended cements, where the relatively fast alite reaction leads to a high CaO availability at early times, while the silica rich SCMs react considerably slower. The reactivity of CaO·Al₂O₃ is higher than that of silica fume, such that the systems studied here are initially also rich in aluminum, leading to relatively high initial Al-concentration and thus to the formation of secondary phases which decompose only slowly.

The present chapter aims to study the composition of C-S-H formed under these conditions and the uptake of aluminum as a function of time.

5.2. Results and discussion

Different C-A-S-H phases with target Ca/Si_{target} from 0.6 to 1.6 were studied. The effect of time is in the following discussed mainly based on Ca/Si_{target} = 0.6, 1.0 and 1.4 as typical low, intermediate and high Ca/Si C-S-H phases.

5.2.1. Effect of time on solid phases

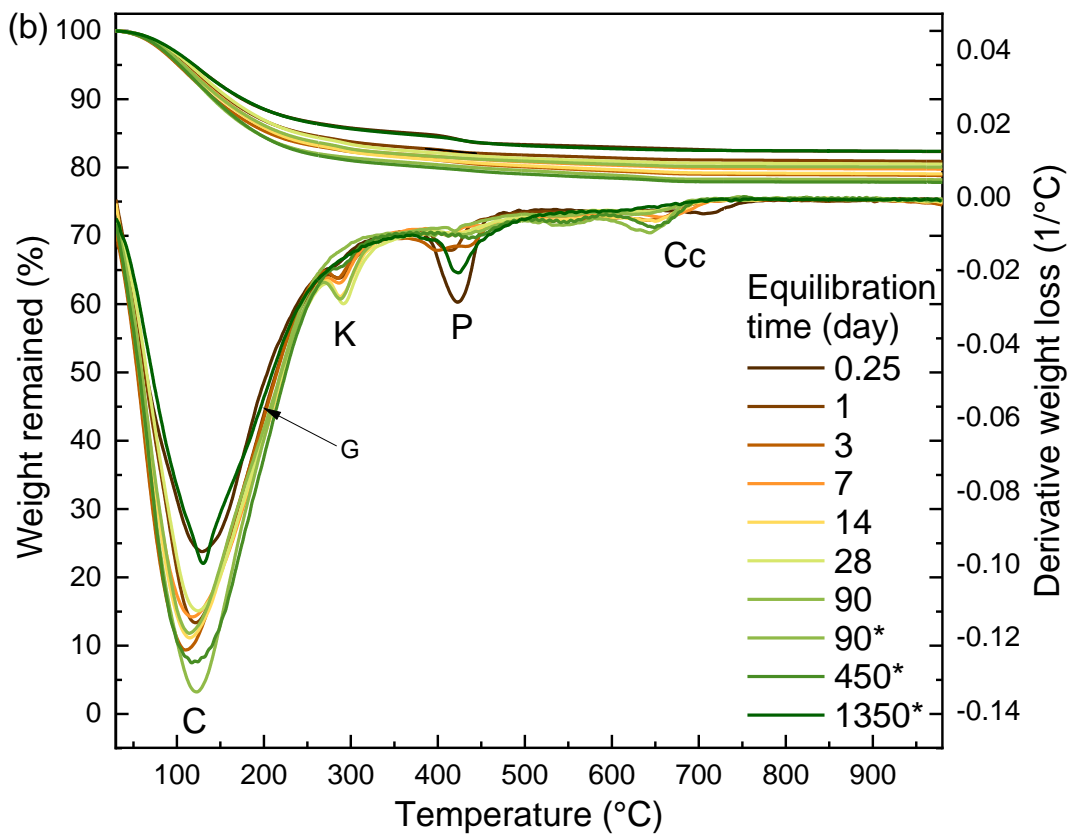
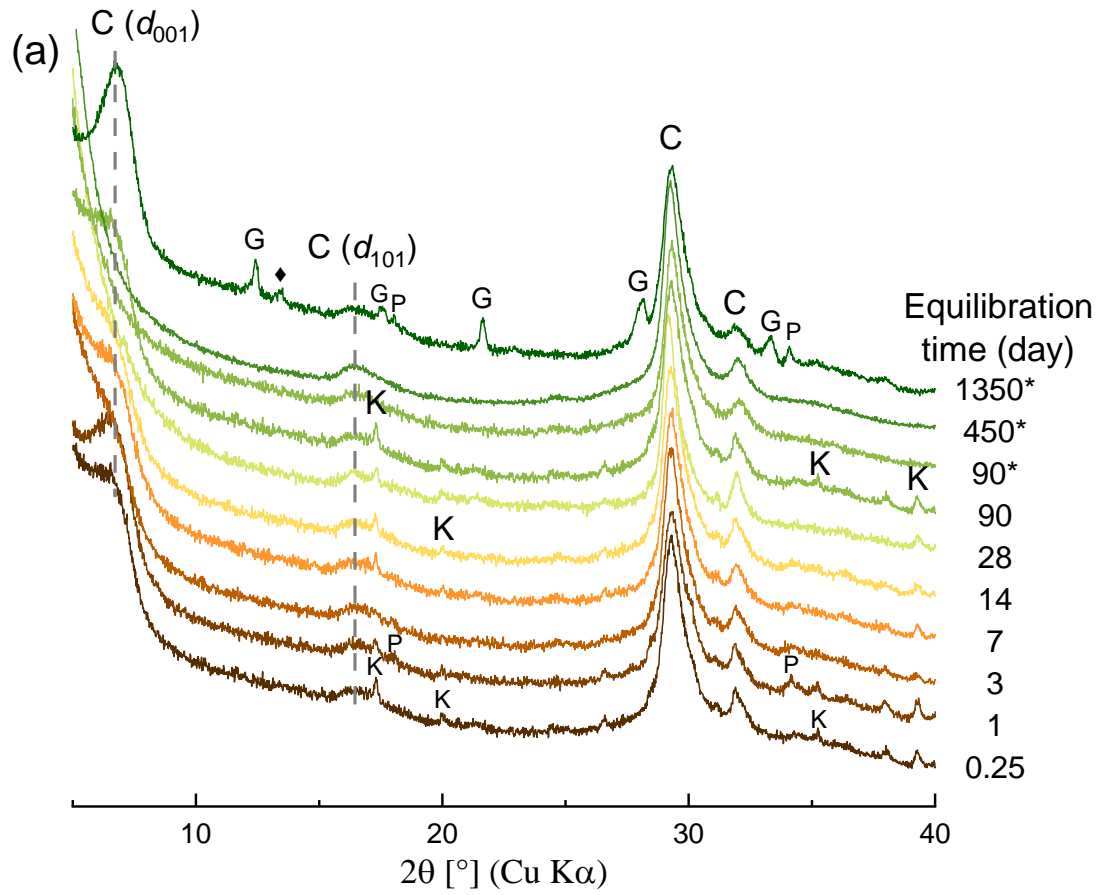
5.2.1.1. Solids present

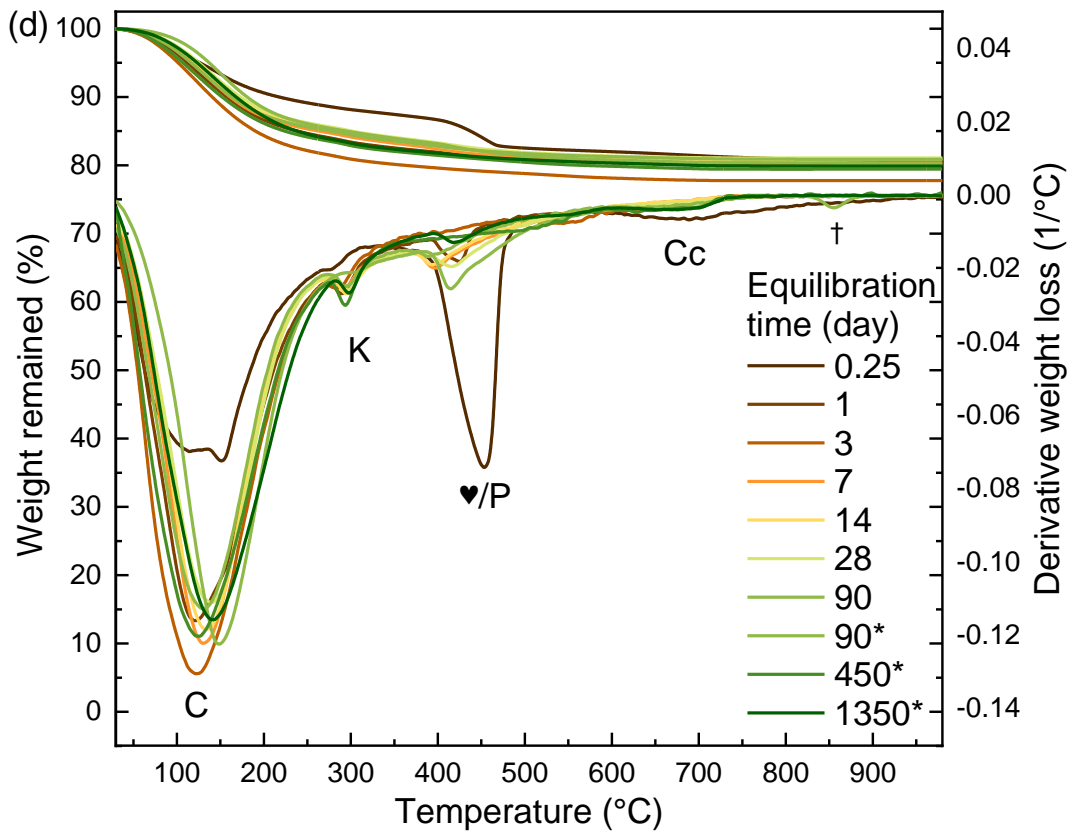
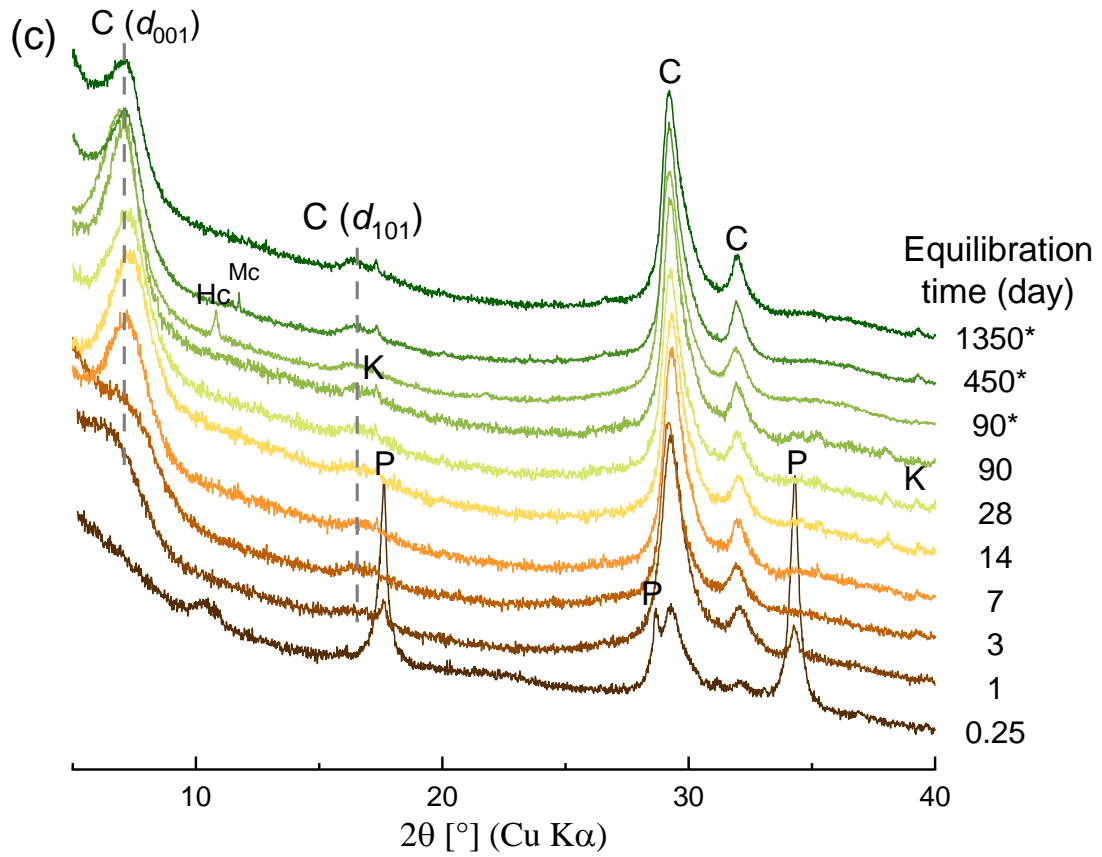
Figure 32 shows the solid phase evolution from XRD and TGA. C-A-S-H is the main phase in all cases, independent of the Ca/Si_{target} and equilibration time. At Ca/Si_{target} = 0.6, 1.0 and 1.4, initially portlandite precipitated and is observed after 6 hours. After 1 day, i.e. when more silica fume has reacted, less portlandite is observed and

³ This chapter will be submitted as a manuscript to Cement and Concrete Research: Effect of time on Al uptake in calcium silicate hydrate.

portlandite is completely consumed after 7 days at $\text{Ca/Si}_{\text{target}} = 0.6$ and 1.0, while at $\text{Ca/Si}_{\text{target}} = 1.4$ portlandite is present and its quantity remains constant up to 1350 days. The formation of some katoite is observed in most C-A-S-H samples after 1 (at $\text{Ca/Si}_{\text{target}} = 1.4$) or 3 days and longer, which indicates the formation of katoite is fast. Hemicarbonates and monocarbonates are identified in some samples and their presence is attributed to minor carbonation during sample preparation, drying and measurement. At $\text{Ca/Si}_{\text{target}} = 0.6$ after 3 years of equilibration, the formation of gismondine-P1 ($\text{Na}_6\text{Al}_6\text{Si}_{10}\text{O}_{32}\cdot 12\text{H}_2\text{O}$), a small amount of portlandite as well as another unidentified phase is observed (see \blacklozenge in Figure 32), indicating that at low Ca/Si content and high alkali concentrations in the long-term zeolitic phases can form, in agreement with other long-term experiments [84]. The presence of portlandite in addition to gismondine-P1 may indicate the heterogeneity of the C-A-S-H suspension.

The TGA shows a main water loss between 30 - 300 °C from interlayer and structurally bound water in C-A-S-H. The water loss of C-A-S-H increases from 6 hours to 1 day for all $\text{Ca/Si}_{\text{target}}$ while little change is observed afterwards up to 3 years (except for $\text{Ca/Si}_{\text{target}} = 0.6$ where gismondine-P1 had formed). A hump at 400-500 °C, marked with \heartsuit , is observed at $\text{Ca/Si}_{\text{target}} = 1.0$ at longer equilibration times and tentatively assigned to the thermal decomposition of more ordered water in C-N-A-S-H because none of the other phases identified by TGA, XRD presented here or by Al and Si NMR can explain the weight loss associated at this temperature. Similar weight losses have also been observed for C-N-A-S-H in the presence of high concentrations of NaOH [42,50] or for samples equilibrated at 50 and 80°C [47]. TGA indicates also minor carbonation (weight loss < 0.6%) in some samples during sample preparation, storage and/or analysis as visible in the region from 600-800 °C. The peak marked with \dagger above 800°C is assigned to the water loss due to the decomposition of C-K-(A-)S-H to wollastonite (CaSiO_3) [47,129].





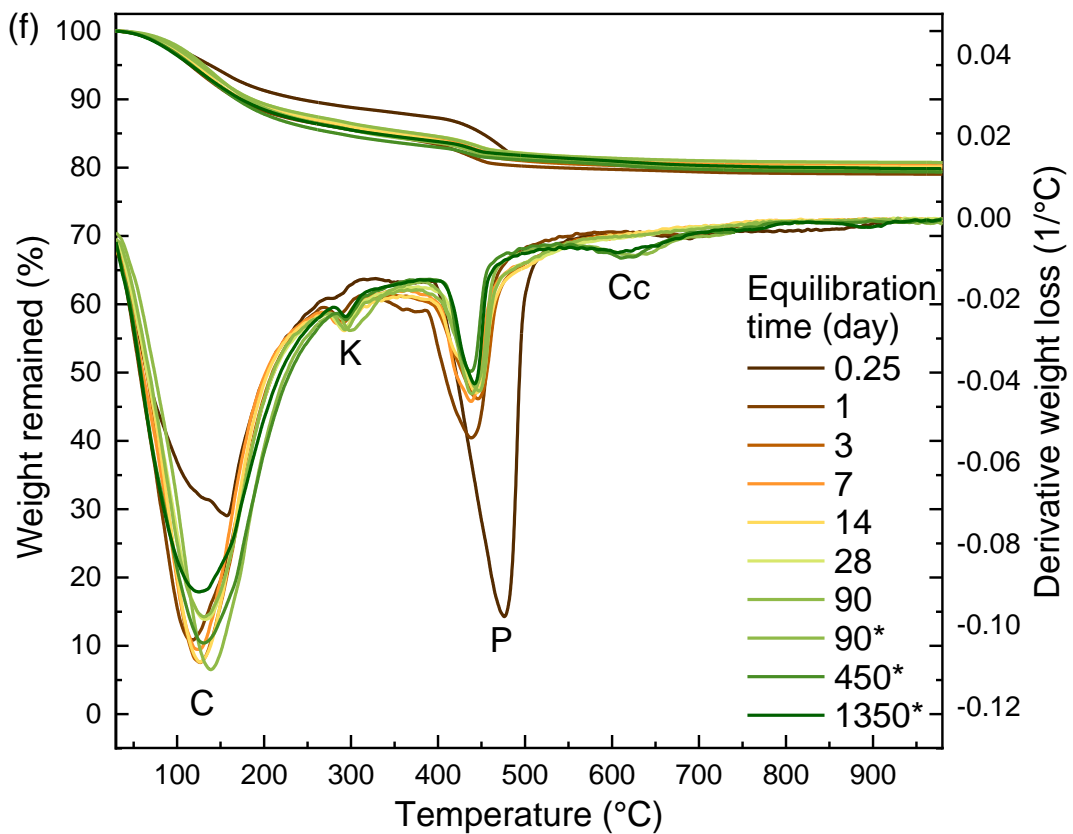
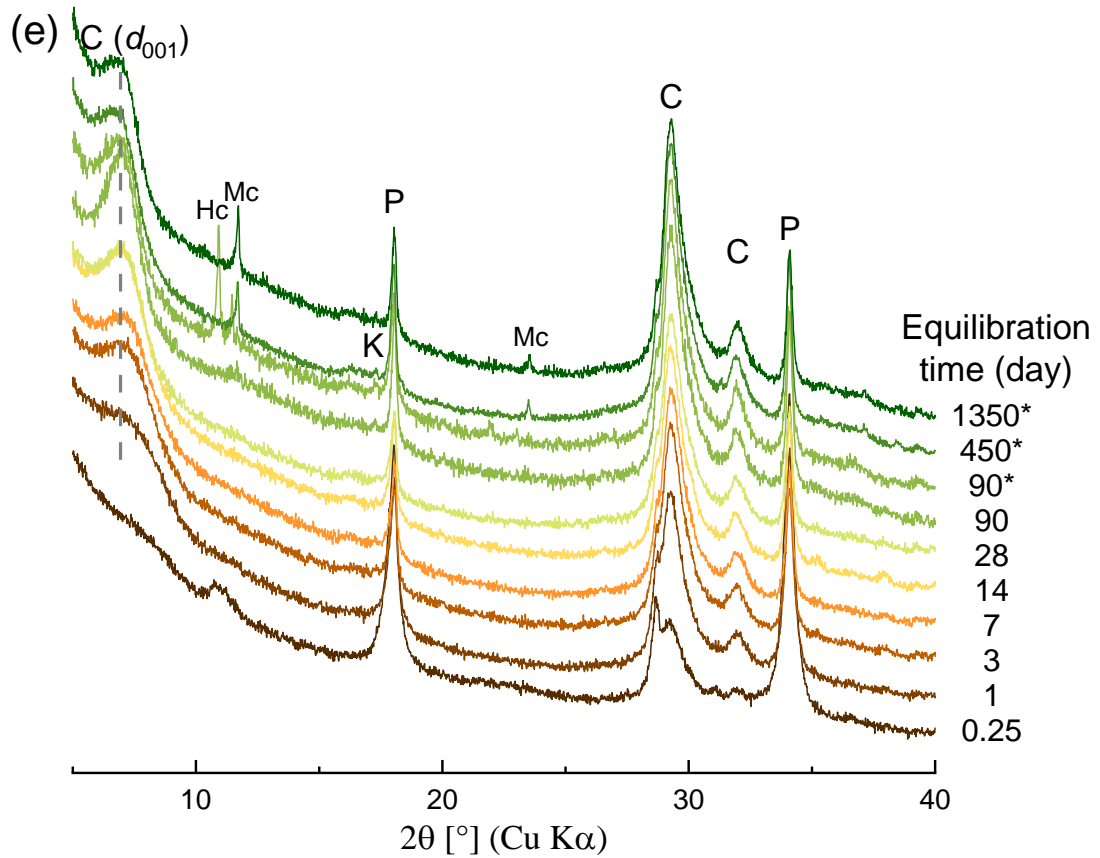


Figure 32. XRD and TGA of C-A-S-H with (a) and (b) target Ca/Si=0.6, (c) and (d) target Ca/Si=1.0, (e) and (f) target Ca/Si=1.4 synthesized in NaOH 0.5 M with initial Al/Si 0.1, equilibrated for different time from 0.25 day to 1350 day. C: C-N,K-(A-)S-H, K: katoite ($\text{Ca}_3\text{Al}_2(\text{OH})_6$, PDF# 00-024-0217), Hc: hemicarbonate ($\text{Ca}_4\text{Al}_2(\text{OH})_{12}(\text{OH})(\text{CO}_3)_{0.5}(\text{H}_2\text{O})_5$, PDF# 00-029-0285), Mc: monocarbonate ($\text{Ca}_4\text{Al}_2(\text{OH})_{12}(\text{OH})(\text{CO}_3)(\text{H}_2\text{O})_5$, PDF# 00-029-0285). G: gismondine-P1 ($\text{Na}_6\text{Al}_6\text{Si}_{10}\text{O}_{32} \cdot 12\text{H}_2\text{O}$), P: portlandite; ♦: unidentified phase. ♥: The weight loss from C-A-S-H Ca/Si = 0.6 and 1.0 at later ages is tentatively assigned to C-N-A-S-H, as portlandite is absent in XRD and FTIR, and the solutions are strongly undersaturated with respect to portlandite. †: The weight loss from C-A-S-H synthesized for 90 day* between 850 and 900 °C in (d) is assigned to phase transformation of C-N-A-S-H to wollastonite. C-A-S-H equilibrated for 0.25- 90 days: synthesized with water/solid = 45, C-A-S-H equilibrated for 90*, 450* and 1350* days: synthesized with water/solid = 40.

Figure 33 summarizes the effect of time on the portlandite content in solid phase and as expected more portlandite is formed at higher Ca/Si. After 6 hours of hydration, portlandite is observed at every target Ca/Si, which indicates the initial precipitation of portlandite at all target Ca/Si. Due to the reaction of SiO_2 most of the portlandite is consumed during the first day, a limited further reduction is observed from 1 day to 14 days while after 14 days the portlandite content show little variations.

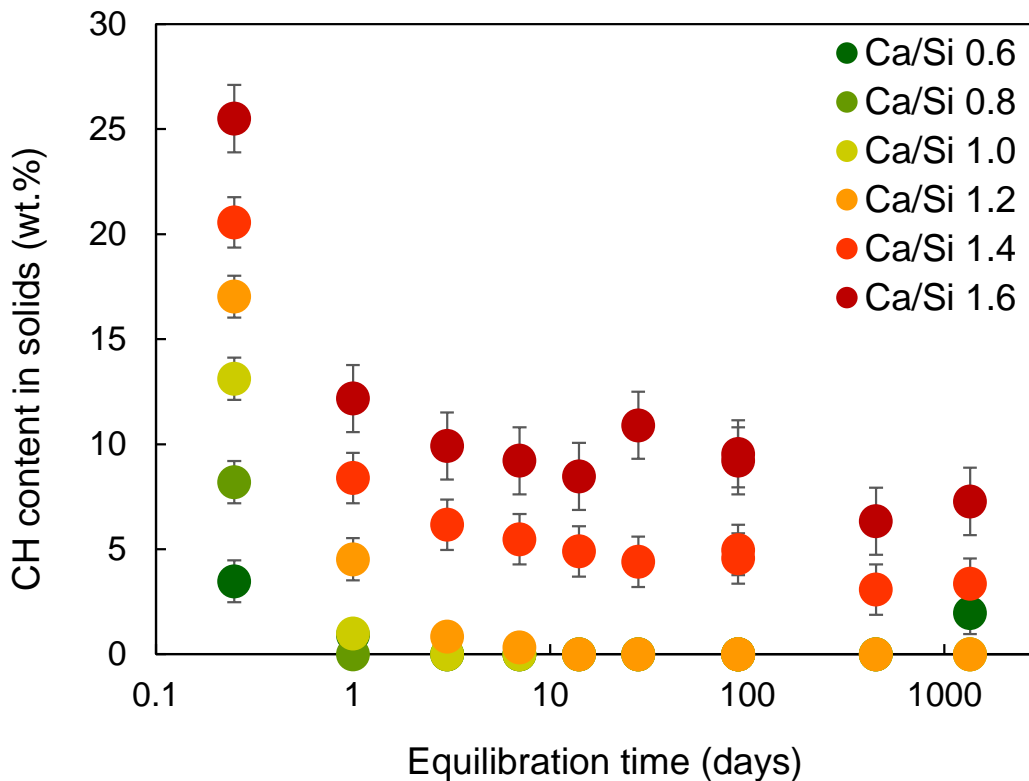


Figure 33. Portlandite content evolution in solid phases

5.2.1.2. C-A-S-H structure

The C-A-S-H structure evolves with time, as visible in the XRD, FTIR and NMR data. The positions of basal spacings, d_{001} , of C-A-S-H in the XRD spectra given in Figure

32 (a) (c) and (e) show no significant difference at different equilibration time, indicating that the equilibration time has little influence on the interlayer distance in C-A-S-H. However, at $\text{Ca/Si}_{\text{target}} = 0.6$ and 1.0 the broad reflection, d_{101} , at $\sim 17^\circ 2\theta$ (d-spacing $\sim 5 \text{ \AA}$), which indicates the occupation of the bridging sites in the silica chain, is better visible after 3 days and longer, indicating the rearrangement from the initial high Ca/Si C-S-H with mainly silica dimers to longer dreierketten chains with time.

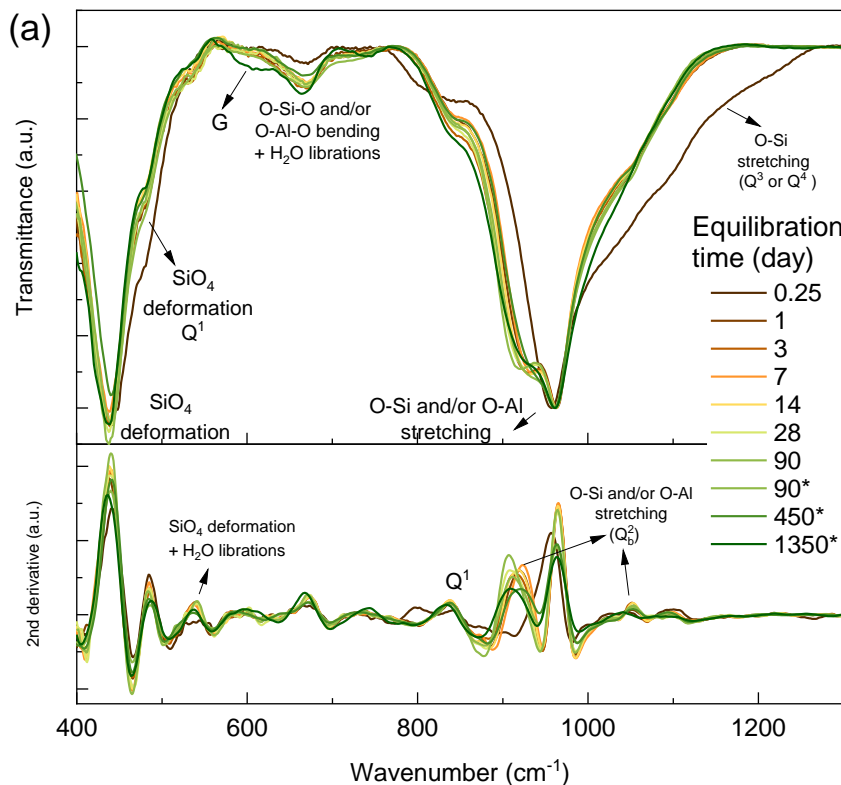
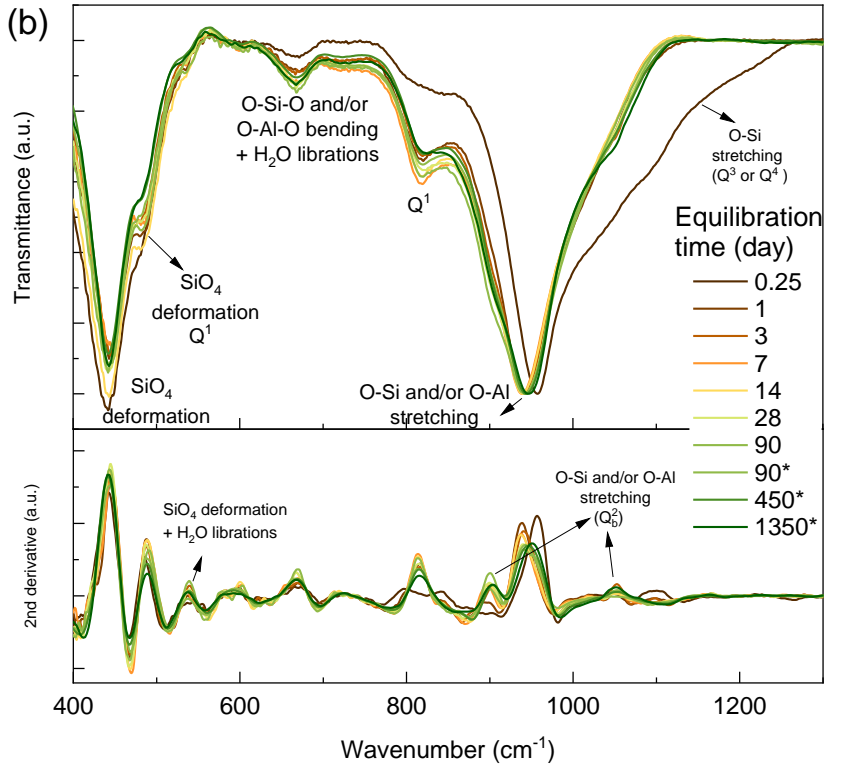
The FTIR spectra of all C-A-S-H with $\text{Ca/Si}_{\text{target}} = 0.6, 1.0$ and 1.4 in Figure 34 show the presence of some unreacted silica fume after 6 hours, which has largely reacted after 1 day, indicated by the disappearance of the very broad bands between 1050 to 1300 cm^{-1} related to the presence of Q^3 and Q^4 in silica fume. The band located at 670 cm^{-1} , related to O-Si-O and/or O-Al-O bending and water librations, increases from 6 hours to 3 days for all C-A-S-H phases and no significant changes are observed afterwards, indicating that C-A-S-H formed mainly during the first 3 days of hydration.

The formation of C-A-S-H is visible by the main bands with a maximum between 950 to 960 cm^{-1} . For C-A-S-H with $\text{Ca/Si}_{\text{target}} = 0.6$ the most intensive band is moving from 957 cm^{-1} at 6 hours to 963 cm^{-1} at 1 day, then moving back to 961 cm^{-1} after 3 months and longer, as shown in Figure 34 (a). In contrast, for C-A-S-H with $\text{Ca/Si}_{\text{target}} = 1.0$ the signal moves from 957 cm^{-1} at 6 hours to 940 cm^{-1} at 1 day and then back to 946 cm^{-1} after 3 years of hydration (Figure 34 (b)) and for C-A-S-H with $\text{Ca/Si}_{\text{target}} 1.4$ the signal moves from 952 cm^{-1} at 6 hours to 937 cm^{-1} at 1 day and then back to 952 cm^{-1} after 3 years of hydration (Figure 34 (c)).

At $\text{Ca/Si}_{\text{target}} = 1.0$ and 1.4 the dissolution of the silica fume after 1 day and longer leads to a higher polymerization degree as visible by the shift to higher wavenumbers [33,141]. The replacement of silica by alumina in C-S-H lowers the wavenumber of Si-O stretching [34]. For C-A-S-H with $\text{Ca/Si}_{\text{target}} = 0.6$ in Figure 34 (a), the shoulders located at about 915 cm^{-1} and 1050 cm^{-1} , assigned to the Si-O stretching of Q^2 silicate (and or aluminate) tetrahedra, start to be observed after an equilibration time of 1 day and increase until 90 days, confirming a higher polymerization degree with longer equilibration time and shows good agreements with the shift of the peak at $\sim 960 \text{ cm}^{-1}$. For C-A-S-H with $\text{Ca/Si}_{\text{target}} = 1.0$ and 1.4 in Figure 34 (b) and (c), the shoulders are less visible because of the low amount of Q^2 .

Chapter 5: Effect of time on Al uptake in calcium silicate hydrate

The intensity of the Q^1 signals located at 815 cm^{-1} and at 490 cm^{-1} increases rapidly between 6 hours to 1 day for C-A-S-H with $\text{Ca/Si}_{\text{target}} = 1.0$ and 1.4 , and more slowly up to 3 days due to the formation of more C-S-H. At longer reaction times, however, this Q^1 signal decreases in intensity, indicating a slow polymerization of the silicate chains with time.



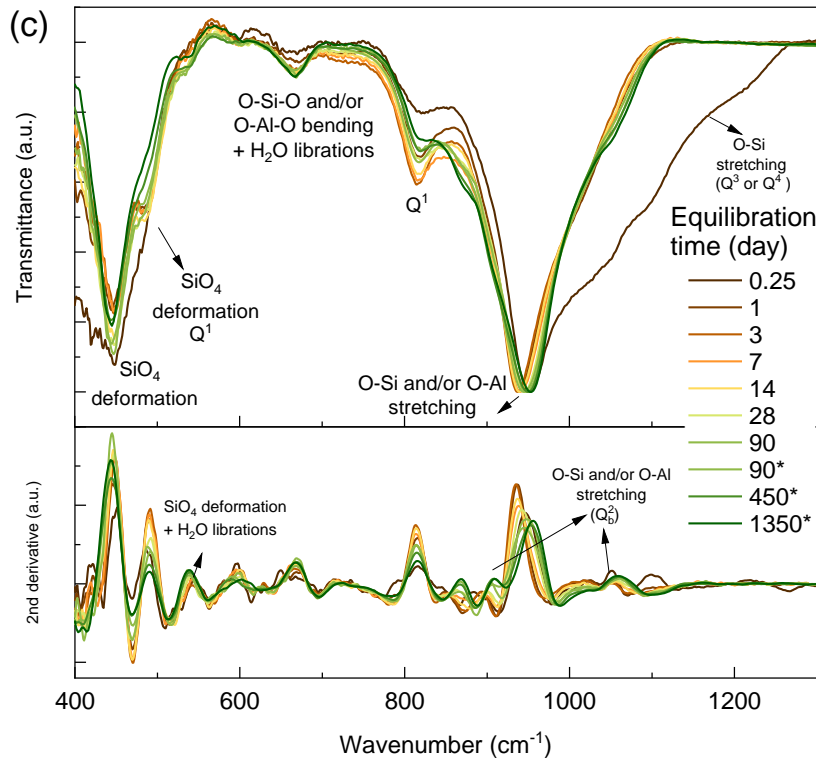


Figure 34. FTIR and second derivative spectra of C-A-S-H with $Ca/Si_{target} = (a) 0.6, (b) 1.0$ and $(c) 1.4$ after different equilibration time synthesized in 0.5 M NaOH. Normalized to the most intensive band at $\sim 970\text{ cm}^{-1}$ of FTIR. C-A-S-H equilibrated for 0.25- 90 days: synthesized with water/solid = 45, C-A-S-H equilibrated for 90*, 450* and 1350* days: synthesized with water/solid = 40.

Figure 35 shows the effect of time on the Al content in C-A-S-H with $Ca/Si = 1$ and in secondary phases. The ^{27}Al MAS NMR spectra shows resonances from Al in tetrahedral (50-80 ppm) and octahedral (0-20 ppm) coordination and a low amount of aluminum in pentahedral coordination. Two tetrahedral resonances at 74 and 65 ppm are observed and assigned to the Al(IV) in the bridging sites of silicate chains [45]. In the octahedral region, resonances at $\sim 11.5, 10,$ and 6.5 ppm are observed, which correspond to secondary phases of katoite, AFm phases and Al(VI) sites associated with C-A-S-H phase [45]. The deconvolution of the signals allowed to roughly quantify the amount bound in the different sites as shown in Table 5 (^{27}Al MAS NMR spectra and their deconvolutions are detailed in Appendix H. While initially approximately $1/3$ of the Al was present in secondary phases, its fraction decreased with hydration time, while the amount of Al(IV) incorporated in the bridging sites of C-S-H increased clearly up to 3 days as more C-A-S-H precipitates, in agreements with the FTIR results. The quantities of Al(V) and Al(VI) in C-S-H showed some variation, but were in tendency higher after 3 and 1 years.

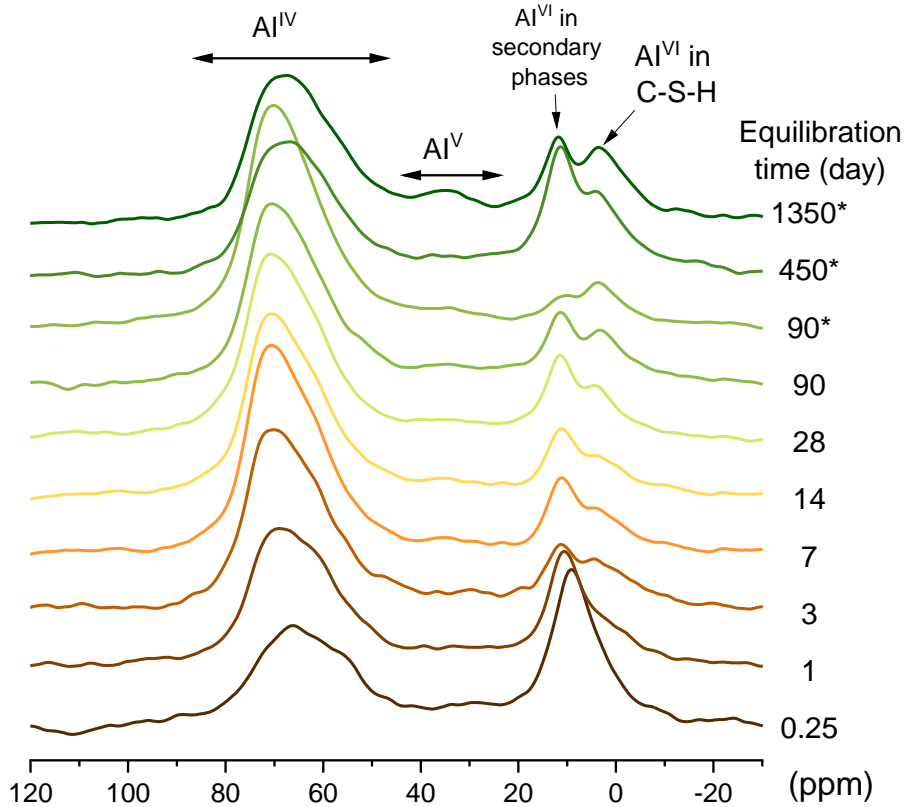


Figure 35. Effect of time on the ^{27}Al MAS NMR of the C-A-S-H with $\text{Ca}/\text{Si}_{\text{target}} = 1.0$ synthesized in 0.5 M NaOH. C-A-S-H equilibrated for 0.25- 90 days: synthesized with water/solid = 45, C-A-S-H equilibrated for 90*, 450* and 1350* days: synthesized with water/solid = 40.

Table 5. Fractions of Al(IV), Al(V), and Al(VI) obtained by deconvolution of the ^{27}Al NMR spectra in C-S-H with $\text{Ca}/\text{Si}_{\text{target}} = 1.0$. C-A-S-H equilibrated for 0.25- 90 days: synthesized with water/solid = 45, C-A-S-H equilibrated for 90*, 450* and 1350* days: synthesized with water/solid = 40.

hydration time (day)	C-A-S-H			Al(VI) in 2 nd phases (%)
	Al(IV) (%)	Al(V) (%)	Al(VI) (%)	
0.25	47±3	6±1	11±1	36±2
1	63±3	3±1	10±1	25±2
3	71±4	4±1	10±1	15±1
7	73±4	4±1	8±1	15±2
14	73±4	4±1	6±1	18±2
28	71±4	4±1	7±1	18±2
90	69±4	4±1	9±1	17±2
90*	80±4	4±1	7±1	9±1
450*	55±3	3±1	14±1	29±2
1350*	64±3	5±1	14±1	18±2

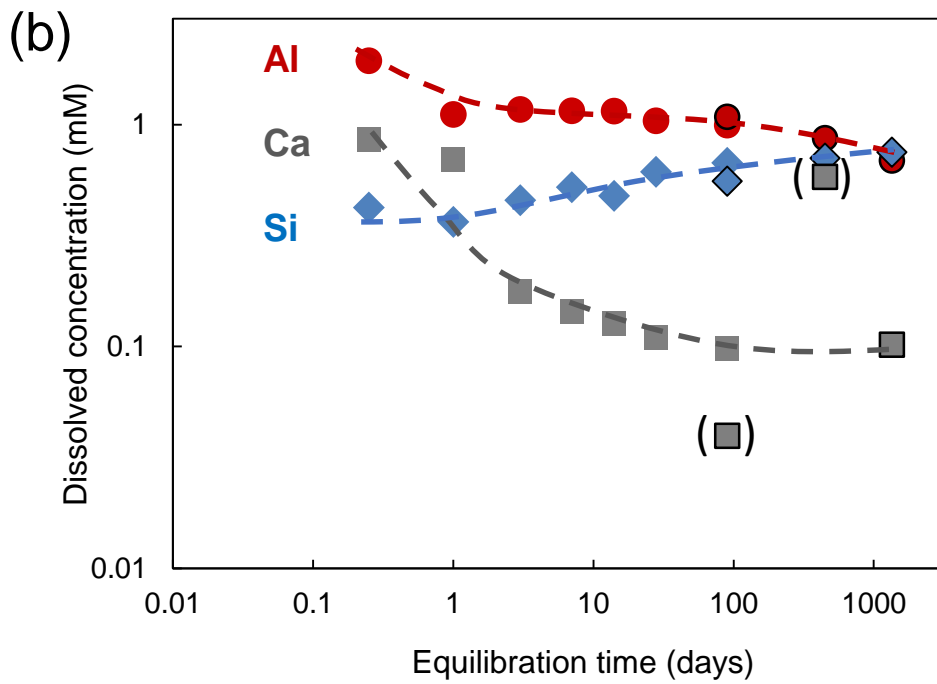
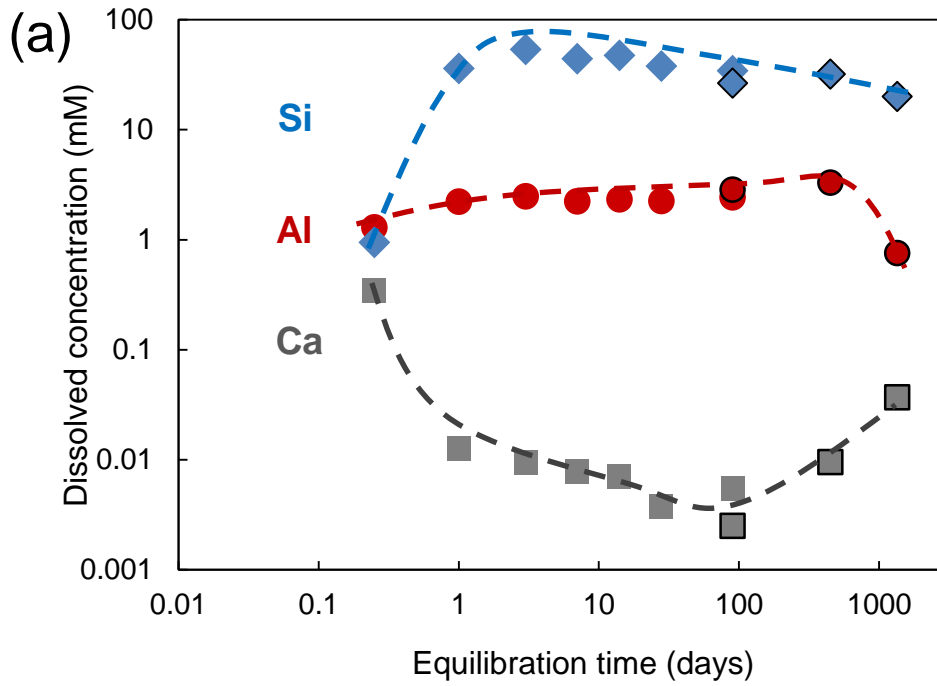
5.2.2. Effect of time on aqueous phases

Figure 36 shows the effect of equilibration time on the dissolved Al, Si and Ca concentrations in solution. At $\text{Ca}/\text{Si}_{\text{target}} = 0.6$, the Al concentration increases rapidly

from 1 mM at 6 hours to 2 mM at 1 day and then stays relatively constant up to 1 year. The Si concentration increases from 1 mM at 6 hours to 36 mM at 1 day and 54 mM at 3 days, and decreases slowly up to 3 years equilibration time. As expected the initial Ca concentration is with 0.4 mM at 6 hours relatively high and decreases rapidly to 0.01 mM after 1 day. The Ca concentrations continue to decrease slightly up to 3 months, but increase slowly again to 0.04 mM after 3 years, tentatively indicating the formation of an additional solid after 1 year and longer. The early decrease in Ca concentration underlines the fast CaO reaction, while the increase of Si up to 3 days mirrors the slower the dissolution progress of silica fume. The minor changes observed up to 3 months are then related to the slow restructuring of C-S-H as observed by NMR and FTIR.

In contrast, at $\text{Ca/Si}_{\text{target}} = 1.0$, where much less silica fume has been added, the silicon concentrations are lower and calcium concentrations higher. Relatively high Ca concentrations of ≈ 1 mM are measured after 6 and 24 hours, due to fast reaction of CaO and the initial formation of portlandite which dominates the Ca concentration up to 24 hours of hydration. At later times the Ca is consumed by C-S-H and the gradual changes in Ca and Si concentration point again towards a slow restructuring of C-S-H over months to years. The Al concentrations decrease slowly indicating a slow uptake of Al in the solids up to 3 years.

At $\text{Ca/Si}_{\text{target}} = 1.4$, the Ca concentration is constant from 6 hours to 3 years, since it is dominated by the solubility of portlandite. The Si concentration decreases from 6 hours to 7 days, demonstrating the formation of C-S-H. The Al concentration continuous to decrease, indicating a slow sorption progress up to 3 years. The different concentrations in the aqueous phase at different $\text{Ca/Si}_{\text{target}}$ ratio show that the Ca/Si ratio in C-S-H plays an important role in the kinetics of C-A-S-H formation.



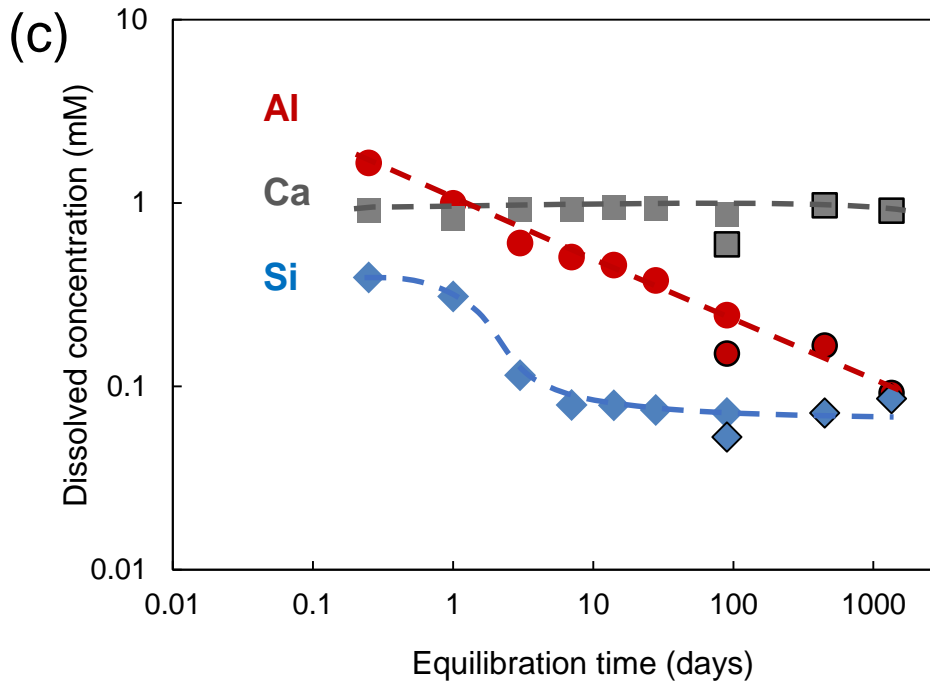


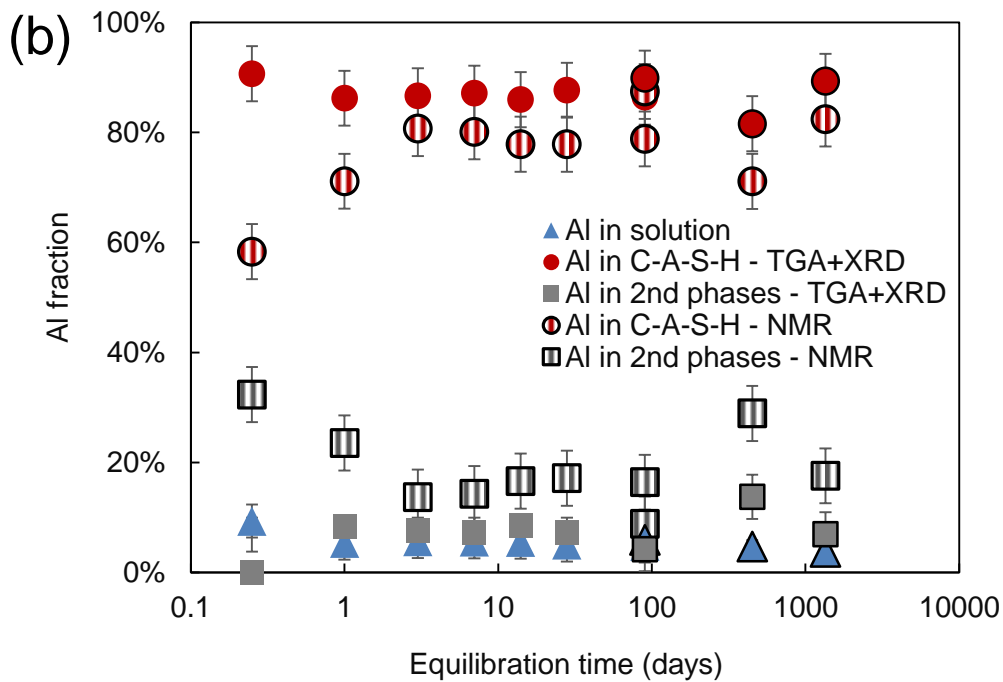
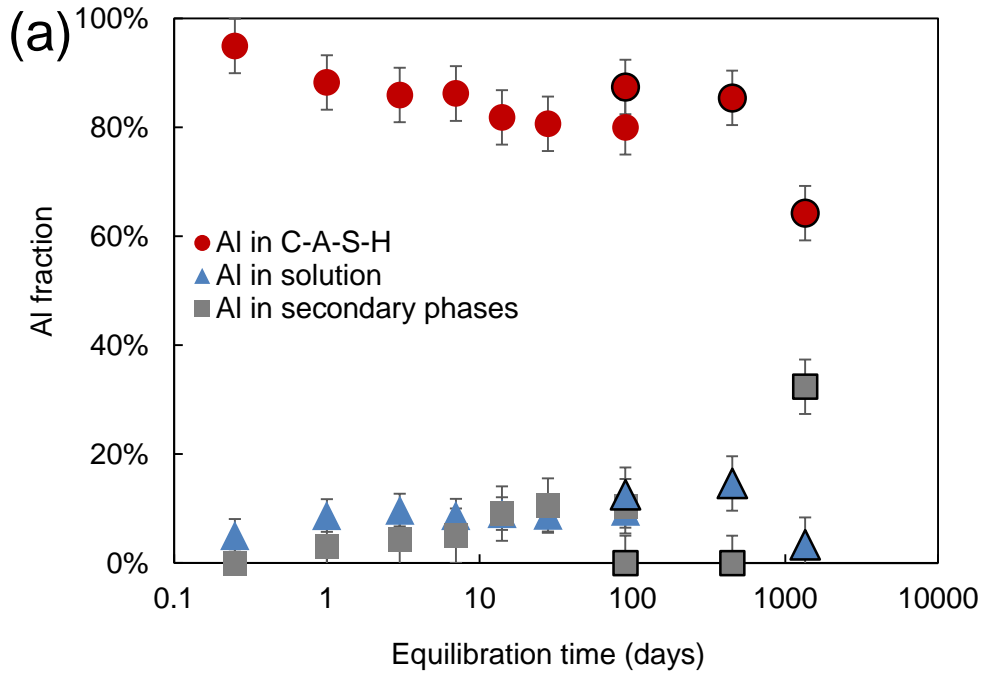
Figure 36. The evolution of dissolved Al, Si and Ca concentrations in solution for Ca/Si_{target} ratios of (a) 0.6, (b) 1.0 and (c) 1.4 synthesized in NaOH 0.5 M with initial Al/Si 0.1 equilibrated for different time. Two series were studied: Series A: filled symbols: in $w/s = 40$; Series B: symbols with black border: $w/s = 45$. The error of the dissolved concentrations are 10% and the error bars are smaller than the symbols. (.): outlier Ca concentration after 3 months and 1 year. Lines are only for eye-guides

5.2.3. Al uptake in C-S-H

Based on the aqueous concentrations, and the amount of secondary phases quantified by TGA and XRD, the distribution of Al between in C-A-S-H, in solution and secondary phases can be plotted as shown in Figure 37. The major part of Al is bound in C-A-S-H and less than 20% of Al stays in solution and secondary phases. For C-A-S-H with $Ca/Si_{target} = 0.6$, the Al fraction in solution increases from 6 hours to 1 year and drop down 64% after 3 years of hydration, while the Al in C-A-S-H decreases due to the formation of gismondine-P1. For C-A-S-H with $Ca/Si_{target} = 1.0$ and 1.4, the amount of Al in solution decreases during the first days while the amount in secondary phases observed by TGA and XRD seems to increase. Note that the XRD analysis underestimates the amount of secondary phases at early reaction times due to their poor crystallinity, as visible by the comparison with the Al-NMR data in Figure 37b), while at later ages the difference between NMR and TGA and XRD is smaller. The Al fraction in C-S-H shows little variation after 3 days hydration in C-A-S-H with $Ca/Si_{target} = 1.0$. For C-A-S-H with $Ca/Si_{target} = 1.4$ at longer ages, i.e. after 3 months and longer,

Chapter 5: Effect of time on Al uptake in calcium silicate hydrate

however, the fraction of Al in secondary phases observed by TGA and XRD increases resulting in less Al in C-A-S-H after 1 and 3 years.



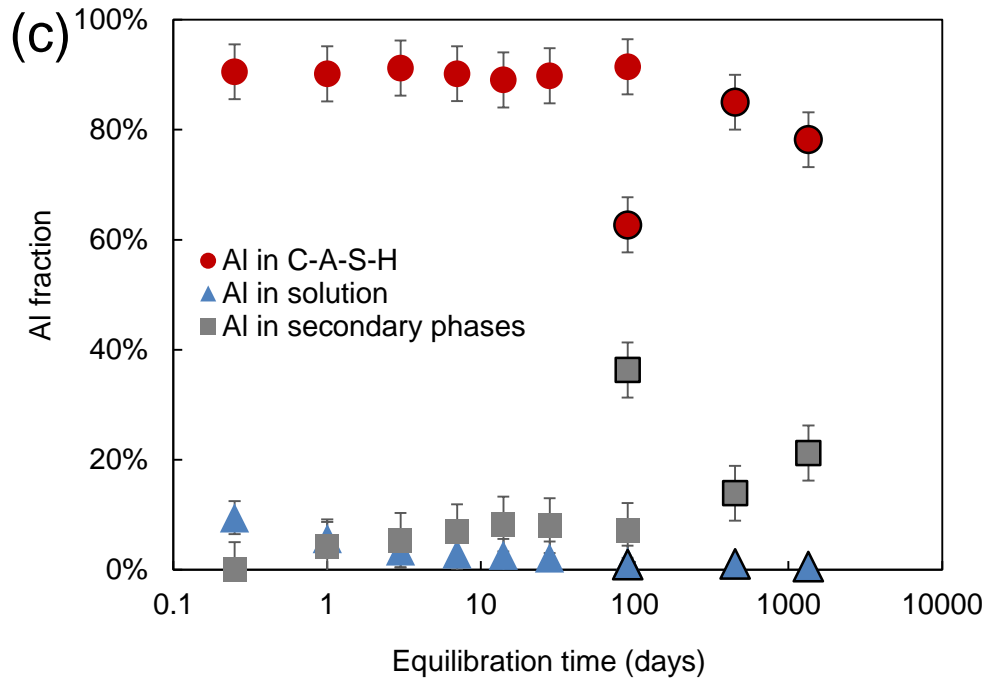


Figure 37. Al fraction in C-A-S-H, aqueous phase and different secondary phases for target Ca/Si = (a) 0.6, (b) 1.0 and (c) 1.4 after different equilibration time in the presence of 0.5 M NaOH. Symbols without border: C-A-S-H samples synthesized in a vessel and stopped hydration after certain equilibration time; symbols with border: C-A-S-H samples synthesized independently.

Figure 38 compares the amount of Al bound per g C-S-H and Al/Si in C-S-H for all Ca/Si studied. In general, the Al bound in C-A-S-H decreases with the increasing equilibration time from 6 hours to 7 days, although the very early results might be influenced by the underestimation of secondary phases by XRD and TGA (indicated by the shaded area). As shown in Figure 36, the Al, Si and Ca concentrations are changing considerably from 6 hours to 3 days hydration and as discussed in Figure 37, in most cases, more than 80% of Al is absorbed in C-S-H, so the decreasing Al sorption from 6 hours to 3 days mirrors also the continuing precipitation of C-S-H. C-A-S-H with low Ca/Si_{target} takes up more Al per g C-S-H than high Ca/Si C-S-H. C-A-S-H with Ca/Si_{target} = 0.6 is able to take up to 0.79 mmol Al in 1 gram of C-A-S-H, while the uptake of Al is about 0.46 mmol Al in 1 gram of C-A-S-H at 3 years, because of the precipitation of gismondine-P1. In C-A-S-H with Ca/Si_{target} = 0.8, a modest increase of Al uptake per g C-S-H with time is visible from 1 day up to 3 years, while in C-A-S-H with Ca/Si_{target} = 1.0 to 1.6, no clear trend is observed. For Ca/Si > 1.0 in addition, the decrease of the Al concentration with time lowers the Al uptake by C-S-H. The Al uptake between the different Ca/Si C-S-H is comparable if plotted as molar Al/Si in C-

S-H (Figure 38 (b)), but much higher at low Ca/Si if plotted as Al per g of C-S-H (Figure 38 (a)), due to lower C-S-H weight per mol Si at low Ca/Si C-S-H.

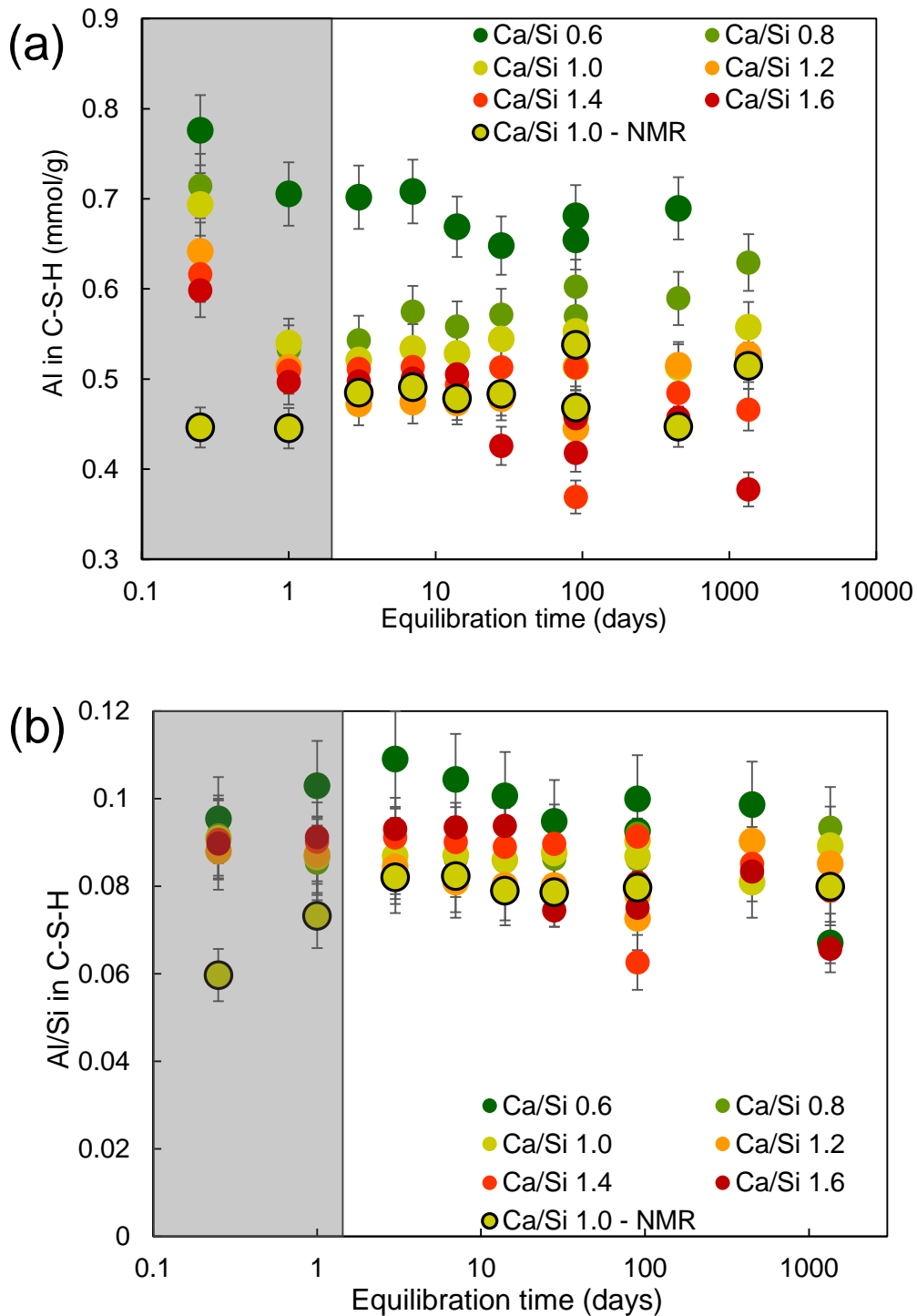


Figure 38. Effect of time on the Al sorption in C-A-S-H: (a) Al bound per g C-S-H, (b) Al/Si in C-S-H and (c) Al/Si in solid. The shade area after 6 hours and 1 days indicates the potential underestimation of Al in secondary phases.

The Al uptake in C-S-H can also be described by distribution coefficients, K_d values, which depict the relative affinity of Al to bind on C-S-H as shown in Figure 39. The K_d values show different trends compared with the Al uptake in per unit mass of C-S-H, mainly because K_d is defined as the ratio of the quantity of aluminum adsorbed per unit mass of C-S-H to the quantity of aluminum remaining in solution, and trend of decreasing Al concentration in most solutions reverses the trends. The distribution coefficient show a clear preference of Al uptake at high Ca/Si.

The long-term K_d values (3 months and 1 year) are with $\sim 0.3 \text{ m}^3/\text{kg}$ for Ca/Si = 0.8 and with $\sim 0.6 \text{ m}^3/\text{kg}$ for Ca/Si = 1.0 comparable to the few values reported in previous studies [157,162]. With longer equilibration time, the K_d values of C-A-S-H with Ca/Si ≥ 1.0 increase and those of C-A-S-H with Ca/Si ≤ 0.8 decrease slightly. The decrease of Al uptake at C-A-S-H with low Ca/Si can be explained by the competition of Si and Al to occupy bridging sites the preference of C-S-H for Si over Al [162]. The K_d values of C-A-S-H with Ca/Si at 1.4 and 1.6 are comparable after 3 days of reaction and longer although some scatter is observed.

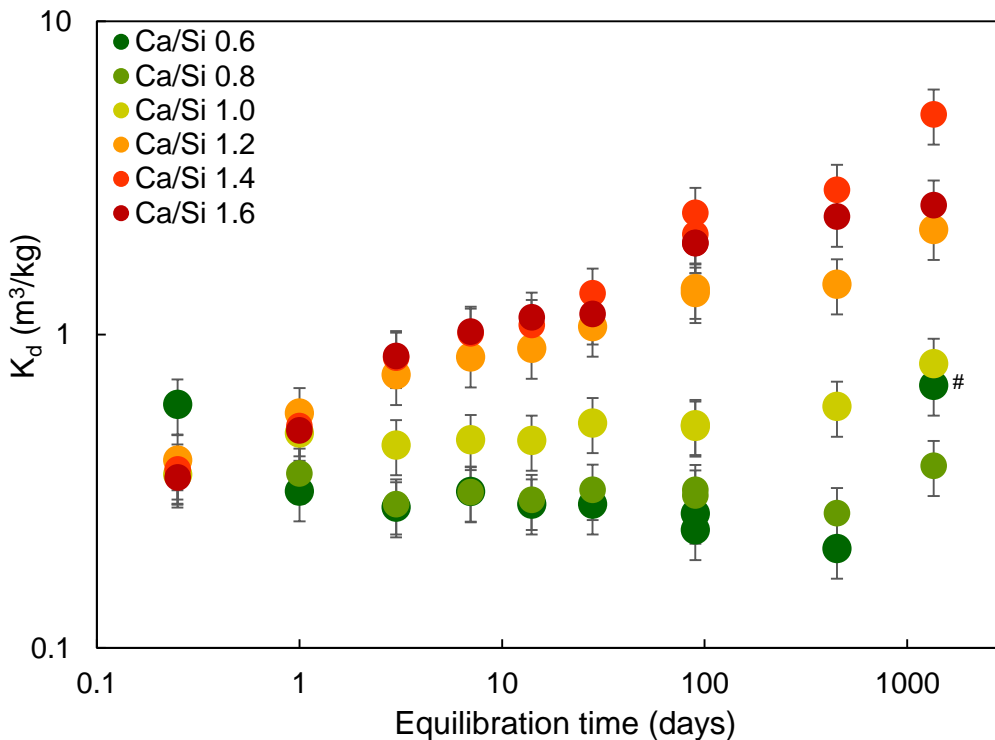


Figure 39 Effect of equilibration time on the K_d values of Al on C-S-H synthesized in NaOH 0.5 M. #: gismondine formation observed after 3 years at Ca/Si = 0.6.

5.2.4. Na uptake in C-S-H

Figure 40 shows the effect of equilibration time on the Na sorption in C-A-S-H. The undissolved silica was not quantified so the first points at 6 hours refer to Na/Si in (C-S-H + silica fume), while the later points refer to C-S-H only. In all cases a relatively low Na uptake was observed after 6 hours, which is related to the presence of less C-S-H at this early time as well as to initial precipitation of high Ca/Si C-S-H, which binds little alkali ions [162]. The increased uptake of Na in C-S-H from 6 hours to 1 day is due to the formation of more C-S-H during the first day leading also to the presence of C-S-H with different Ca/Si and thus to a higher alkali uptake in the samples with lower initial Ca/Si.

Interestingly in all cases, the highest Na binding is observed after one day, while it decreases with time. Since the aqueous phase Na concentrations are not changing significantly after 7 days hydration, the continuous decrease of Na sorption shows a rearrangement of C-A-S-H phases with time, and indicates a preference of Ca over Na in C-A-S-H in the long-term. The initial high binding could be related to a co-precipitation of a relatively high amount of Na due to the high Na concentrations during the fast initial formation of C-S-H leading to a high Na uptake. This co-precipitated Na is partially released again as the C-S-H structure is rearranged towards its thermodynamic equilibrium composition.

The sorption of Na in C-A-S-H with $\text{Ca/Si}_{\text{target}} = 0.6$ shows some scatter with a maximum big value of 3 mmol Na per g C-S-H. At this low Ca/Si the Ca concentrations in solution are very low and no or very little Ca is available to compensate the negative charge of C-S-H [64,87], leading to a strong uptake of Na^+ . At higher Ca/Si, the competition with Ca^{2+} leads to a much lower uptake of Na^+ , and C-A-S-H phases with $\text{Ca/Si}_{\text{target}}$ above 1.2 have all a similar capacity to absorb Na^+ in agreement with [141].

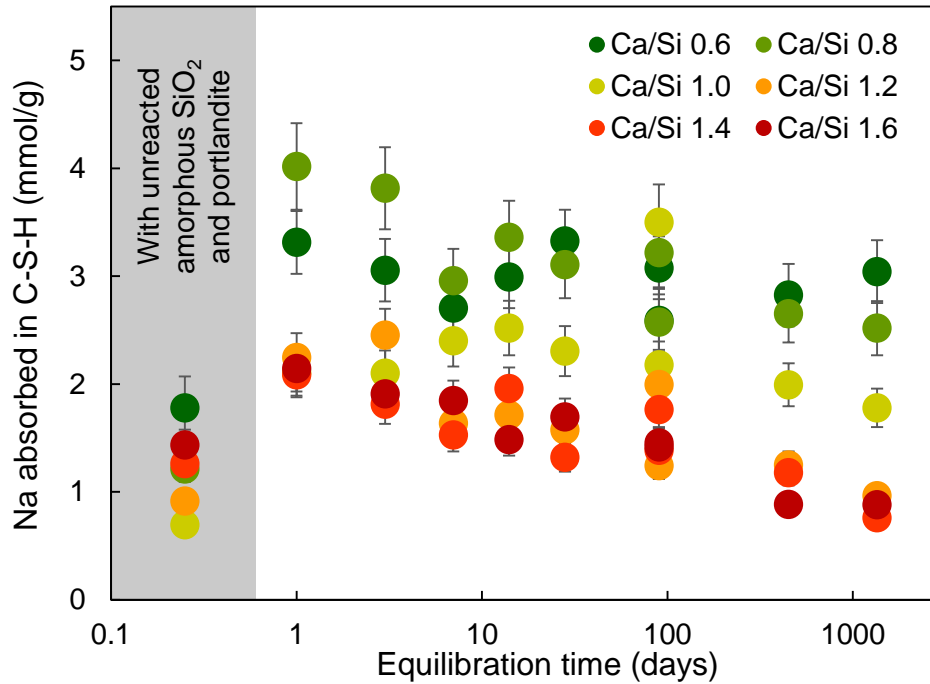
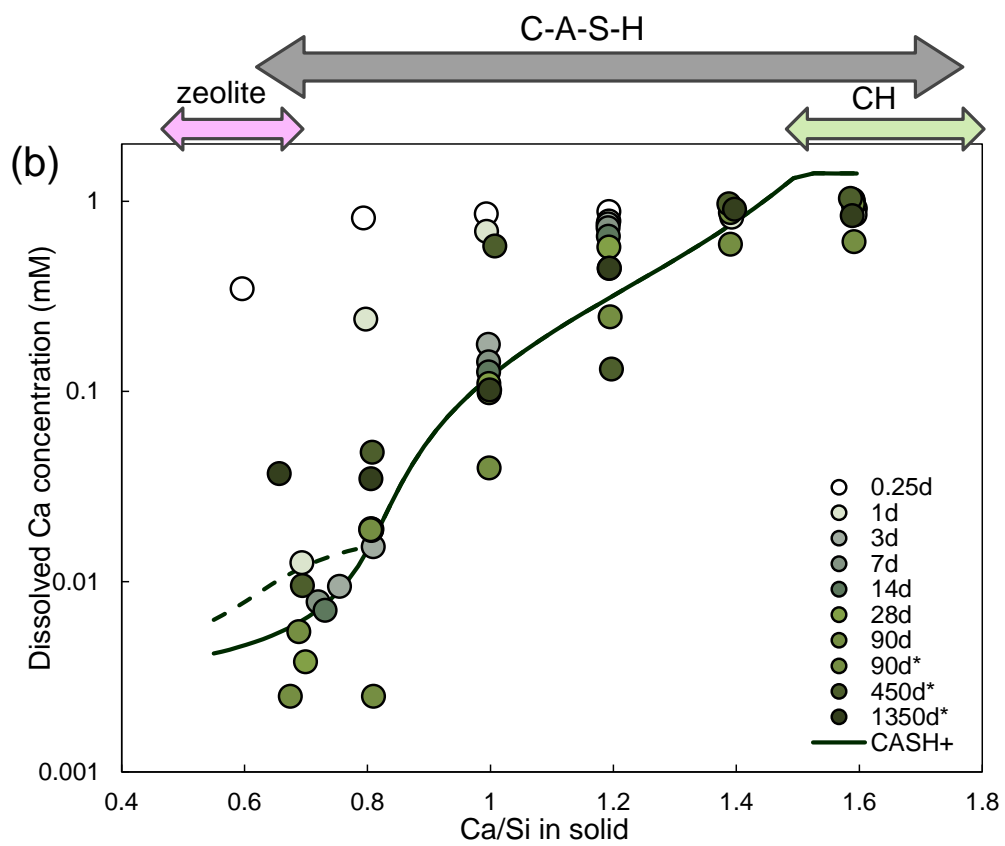
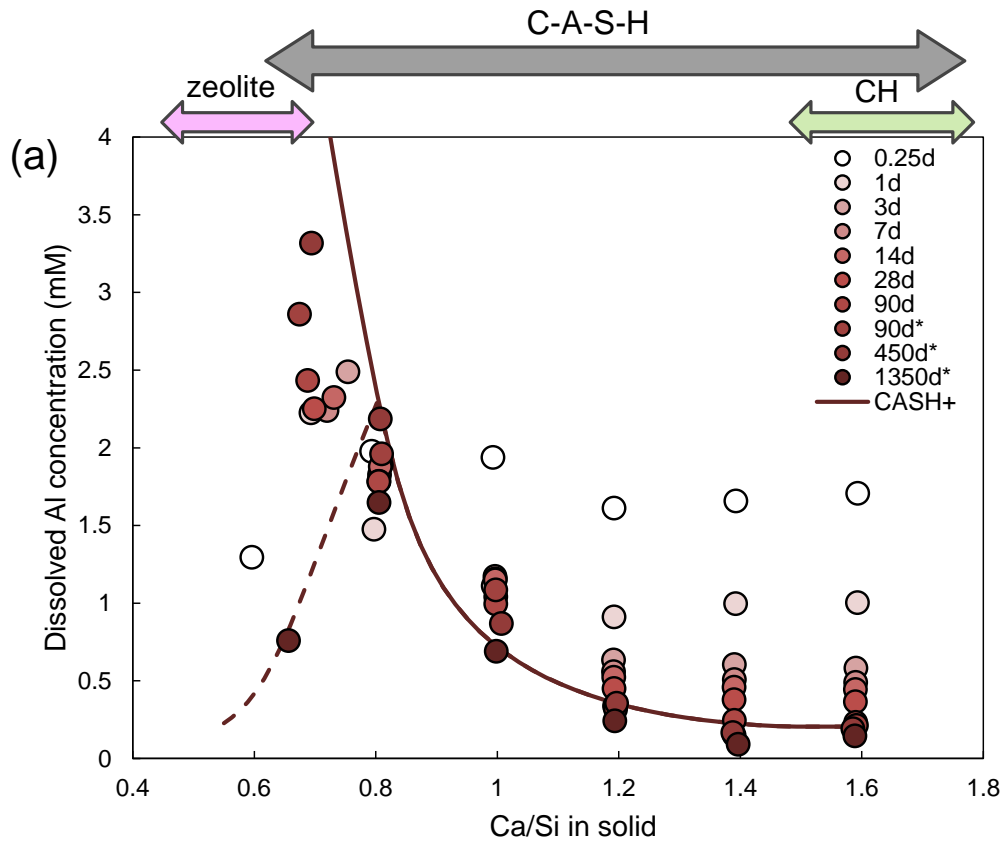


Figure 40. Effect of time on the Na absorption in C-A-S-H

5.2.5. Effect of Ca/Si on kinetics of C-A-S-H

The Ca/Si ratio affects the composition of the solutions as shown in Figure 41, where changes of Al, Ca and Si concentrations are plotted as a function of the Ca/Si in the solid. The simulated concentrations at equilibrium state are in good agreement with the experimental results of samples equilibrated for 90d, 450d and 1350d. The equilibrated Al concentration at the low Ca/Si solids is lowered in the long-term samples by the precipitation of gismondine-P1 below $\text{Ca/Si}_{\text{solid}} = 0.8$, which causes also the considerable scatter in Al concentration. Due to the gismondine-P1 formation, the Ca and Si concentrations also shift.

The Al concentration at $\text{Ca/Si}_{\text{solids}} \geq 1.0$ decreases up to 3 years of hydration, which indicates the long-term uptake of Al in C-S-H and secondary phases. Si and Ca concentration in samples with $\text{Ca/Si}_{\text{solids}} \leq 0.8$ also show some scatter, while for samples with $\text{Ca/Si}_{\text{solids}} \geq 1.2$ little variation is observed after 7 days.



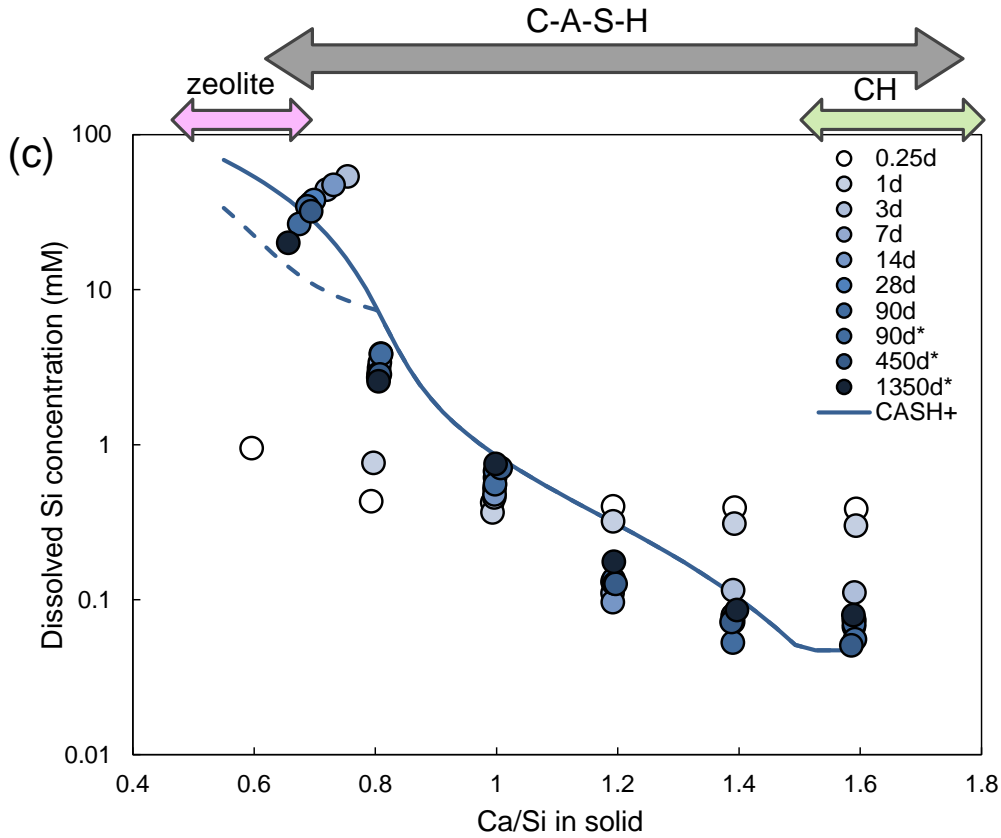
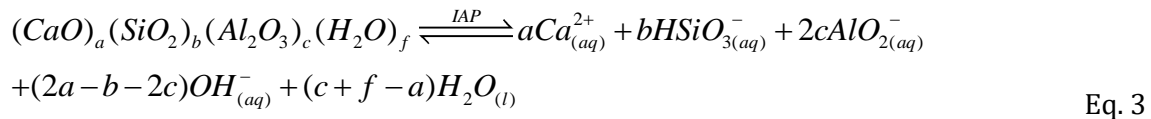


Figure 41. Al, Ca and Si concentrations in the solutions of the C-A-S-H samples in 0.5 M NaOH with different equilibration time as a function of Ca/Si ratios in solid. The estimated absolute errors are $\leq \pm 0.05$ units in the Ca/Si ratios. The estimated relative uncertainty of the IC measurements is $\pm 10\%$. Symbols with color filled from light to dark: synthetic C-A-S-H data with equilibration time from 0.25 day to 1350 days. Solid lines: calculated concentrations using the thermodynamic CASH+ model, suppressing the formation of zeolitic phases, which form only slowly. dashed lines: considering the possible formation of gismondine-P1 ($\text{Na}_6\text{Al}_6\text{Si}_{10}\text{O}_{32} \cdot 12\text{H}_2\text{O}$). C-A-S-H equilibrated for 0.25- 90 days: synthesized with water/solid = 45, C-A-S-H equilibrated for 90*, 450* and 1350* days: synthesized with water/solid = 40.

Ion activity products (IAP) were calculated for hypothetical C-A-S-H end-members with chemical compositions corresponding to the bulk chemistry of the systems studied (Ca/Si = 0.6-1.6) and normalized to (Al+Si) = 1, using the reaction represented by:



where a, b, c and f are the respective stoichiometric coefficients for CaO, SiO₂, Al₂O₃ and H₂O in the C-A-S-H end members. Thus the IAP of C-A-S-H is defined as:

$$IAP = \{Ca_{(aq)}^{2+}\}^a \cdot \{HSiO_{3(aq)}^{-}\}^b \cdot \{AlO_{2(aq)}^{-}\}^{2c} \cdot \{OH_{(aq)}^{-}\}^{(2a-b-2c)} \cdot \{H_2O_{(l)}\}^{(c+f-a)} \quad \text{Eq. 4}$$

In Figure 42, the IAP calculated for C-A-S-H with different equilibration times are compared to the IAP of C-(A-)S-H and Al-tobermorite reported in literature [47,50,65]. A moderate decrease in the IAP of C-A-S-H was observed between 6 hours and 7 days: by ≈ 0.3 log units for $Ca/Si_{\text{target}} = 0.8$ and by ≈ 0.6 log units for $Ca/Si_{\text{target}} = 1.0-1.6$, while at very low Ca/Si the IAP increased. Some scatter, but no significant differences were observed between 7 days to 3 years, underlining that the aqueous phase reached quasi-equilibrium already after the first 7 days.

The IAP of C-A-S-H after 3 months and longer are comparable to the solubility products reported by Myers et al. [47] and Barzgar et al. [50]. Those with Ca/Si targeted at 0.8 are only slightly higher than the solubility product reported for laboratory-synthesized Al-tobermorite with $Ca/(Al+Si) = 0.83$, as expected for these structurally and compositionally similar phases.

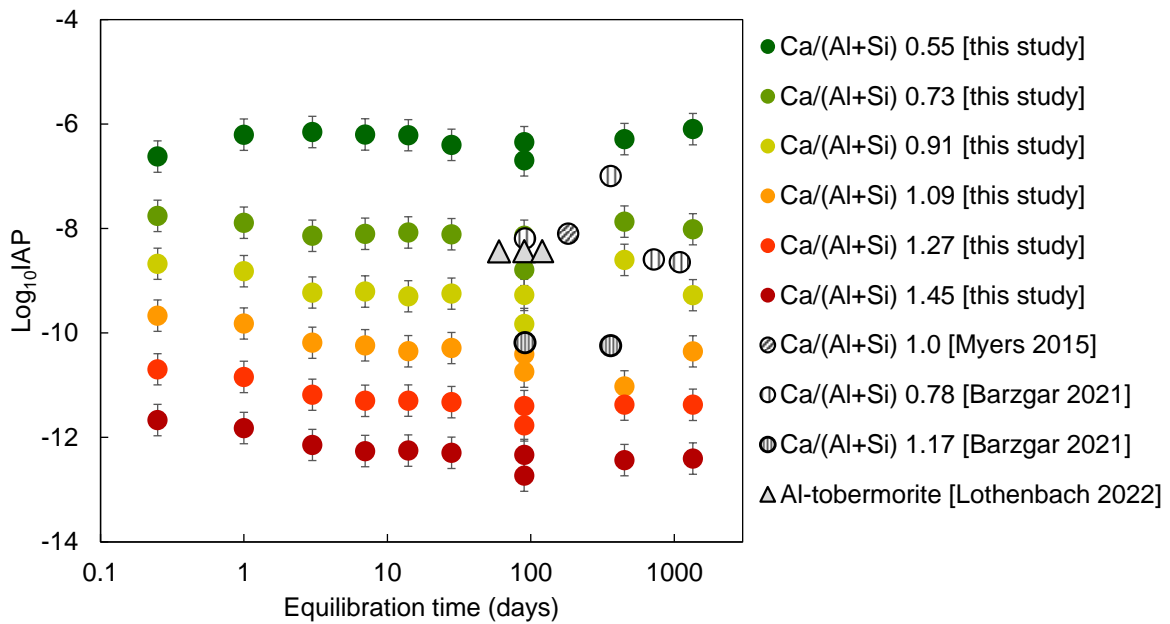


Figure 42. Calculated $\log_{10}IAP$ values for hypothetical C-(A-)S-H and Al-tobermorite with different equilibration time, normalised to $SiO_2+Al_2O_3=1$. The approximate uncertainty in the $\log_{10} (IAP)$ values are ± 0.3 . Colored circles: C-A-S-H from this study; patterned circles: C-A-S-H from Myers et al. and Barzgar et al. [47,50], and triangles: Al-tobermorite with $Ca/(Al+Si) = 0.83$ from Lothenbach et al. [65]. Data from this study and [47,50] are calculated from oversaturation condition and [65] is calculated from undersaturation condition.

5.3. Conclusion

This chapter studies the effect of time on C-A-S-H formation, its structure and solubility. C-A-S-H was precipitated from CaO, CaO·Al₂O₃ and silica fume (SiO₂) in 0.5 M NaOH solutions, such that the system is initially dominated by a high availability of Ca and Al, while Si is released slower due to the slower reactivity of silica fume compared to CaO (or Ca(OH)₂) and CaO·Al₂O₃. Thus, in all cases the initial C-S-H formed after a few hours is Ca-rich, but converts within a day to Ca poorer C-S-H depending on the target Ca/Si of the individual experiments. Initially portlandite formation was observed in all samples. Its amount decreased rapidly within the first day and remained stable after more than 7 days based on XRD and TGA data.

C-A-S-H was the main solid in all experiments, however, in some cases a small quantity of secondary phases, mainly katoite and in some cases monocarboaluminate were observed. At target Ca/Si = 0.6, initially C-A-S-H formed, which was later destabilized to a zeolitic phase (gismondine-P1) between 1 and 3 years.

XRD showed that the basal spacings, d_{001} , of C-A-S-H did not significantly change with equilibration time, indicating little influence of the equilibration time on the interlayer distance of C-A-S-H. However, the main layer structure of C-A-S-H evolved with time. XRD and FTIR spectroscopy indicated a higher occupation of bridging sites in the silica chains with longer equilibration time. ²⁷Al NMR showed the initial formation of secondary phases as well an increasing fraction of Al(V) and Al(VI) in C-S-H with longer equilibration times.

The dissolved concentrations of Al, Ca and Si changed rapidly from 6 hours to 1 day, i.e. at the time additional C-S-H formed. Slower variations were observed after 1 day, which become very small after 14 days. The Ca/Si ratio of C-S-H played an important role on the changes in aqueous concentration: an increasing of Al concentrations with time was observed in C-A-S-H with Ca/Si_{target} = 0.6, while a decrease was observed for C-A-S-H with Ca/Si_{target} ≥ 1.0

In most samples, more than 80% of the Al present was bound by C-A-S-H at all Ca/Si. The fraction of Al in C-A-S-H decreased in most cases after 4 days and longer as well as the uptake of Na, which was highest after 1 day and decreased thereafter. The continuous decrease of Na and Al shows a rearrangement of C-A-S-H phases with time. The initial high binding could be related to a co-precipitation binding relatively high amounts of Na and Al in C-S-H during the fast initial formation, which partially

Chapter 5: Effect of time on Al uptake in calcium silicate hydrate

released again as the C-S-H structure is rearranged towards its thermodynamic equilibrium composition.

CHAPTER 6: Conclusions and outlook

The understanding of the incorporation of aluminium, alkali and the effect of equilibration time in C-S-H is important, since it relates to the durability of construction materials. However, the mechanism of aluminium and alkalis uptake in the C-S-H structure is still under debate and there is little experimental data on the C-A-S-H formation kinetics available in the literature. The objective of this work is to investigate the effect of the uptake of alkali, hydroxide and aluminium and equilibration time on C-A-S-H in-depth by combining aqueous phase measurements and solid phase characterization. Systematic experiments were carried out to investigate the solubility, structure and composition of C(-A)-S-H gel as a function of different parameters such as Ca/Si ratio, aluminium contents, alkali concentration and equilibration time in order to obtain a better understanding of the uptake of aluminium and alkali in C-S-H as well as their kinetics.

6.1. Effect of alkali hydroxide on C-S-H

Both KOH and NaOH showed similar effects on the aqueous and solid phase. The Si concentrations in solution were enhanced and Ca concentrations were lowered in the presence of additional KOH or NaOH. Higher pH values led to the precipitation of additional portlandite and changed the C-S-H composition, the upper limit $\text{Ca/Si}_{\text{C-S-H}}$ decreased from 1.44 in the absence of NaOH to 1.1 in the presence of 1 M NaOH or KOH, and the lower limit from $\text{Ca/Si}_{\text{C-S-H}} = 0.75$ (no alkali) to ~ 0.7 in the presence of alkali hydroxide. Higher alkali uptake in C-S-H was observed at low Ca/Si as well as at higher pH values. Higher pH prevented the polymerisation of C-(N,K-)S-H silicate and increased the crystallite size along the *c*-axis.

A comparison with the independently developed CASH+ thermodynamic model showed that the model reproduced the observed changes, including the shortening of the main chain length (MCL) in the presence of NaOH and KOH.

6.2. Effect of alkali hydroxide on Al uptake in C-S-H with Ca/Si = 1

The increased amount of Al in the system led to the precipitation of additional secondary phases containing Al and raised both the dissolved Al and Si concentrations and lowered the Ca concentrations in the aqueous phase. A slight preference of C-S-

H for Si uptake over Al uptake was observed based on the observed difference in the aqueous concentrations. The uptake of Al increased the interlayer distance of C-A-S-H and led to longer dreierketten chains in C-A-S-H, indicating indirectly an uptake of Al in the silica chain.

Higher pH values progressively destabilized Al-containing secondary phases such as $\text{Al}(\text{OH})_3$ and strätlingite, shortened the silicate chains as visible in the reduction of the numbers of Q^2 and increase of Q^1 silicate species and resulted in a higher fraction of octahedrally bound Al(VI) in the C-A-S-H phase. Higher pH values also increased the aqueous Al and Si concentrations and lowered the Ca concentrations. The higher Al concentration lead to a higher fraction of Al bound in C-A-S-H. The linear correlation between the aluminium concentration in solution and Al/Si in C-A-S-H indicate that Al is taken up at similar sorption sites in C-S-H independent of Al concentration or pH values. The distribution coefficients of Al on C-S-H strongly decrease with increasing pH values, indicating a higher tendency of Al to remain in solution.

6.3. Effect of time on Al uptake in C-S-H

Equilibration time had a significant influence on C-A-S-H formation, its composition, structure and solubility, as well as on the kind and amount of secondary phases. Due to the high reactivity of CaO compared to silica fume, C-S-H formed during the first few hours is rich in calcium, but converts within one day to Ca-poorer C-S-H depending on the target Ca/Si of the individual experiments; the rearrangement of C-S-H continues more slowly for several months. Portlandite formation was observed in the first hours for all samples at all Ca/Si and its amount decreased rapidly within the first day and remained stable after more than 7 days. At target Ca/Si = 0.6, the initially precipitated C-A-S-H was later destabilized to a zeolitic phase (gismondine-P1) between 1 and 3 years.

The main layer structure of C-A-S-H was observed to evolve with time. Longer equilibration time led to a higher occupation of bridging sites in the dreierketten chains and an increasing fraction of Al(V) and Al(VI) in C-S-H.

The dissolved concentrations of Al, Ca and Si changed rapidly within the first day, i.e. at the time additional C-S-H formed and portlandite dissolved. Slower variations were

observed after 1 day, which become very small after 14 days. The Ca/Si ratio of C-S-H played an important role on the changes in aqueous concentration: an increasing of Al concentrations with time was observed in C-A-S-H with $\text{Ca/Si}_{\text{target}} = 0.6$, while a decrease was observed for C-A-S-H with $\text{Ca/Si}_{\text{target}} \geq 1.0$. The uptake of Al and Na in C-A-S-H was observed to decrease after 4 days and longer, which also indicates a rearrangement of C-A-S-H phases with time.

6.4. Outlook

Although many different aspects have been investigated, a number of open questions will need to be addressed in more details in the future:

The comprehensive experimental dataset collected within this thesis can serve as a basis for the further development of more sophisticated kinetic and thermodynamic models. It would be very interesting to extend the thermodynamic modelling of C-S-H to account for both short- and long-term properties of C-A-S-H.

More than 80% of Al added has been observed to be taken up into C-A-S-H in this study. However, to which extent this uptake is reversible if the Al concentrations or pH values change has not yet been investigated. Also the effect of temperature changes is further an important topic where systematic data missing as well as on the competitive effects of other ions such as e.g. Fe(III), which might be taken up in the bridging sites of C-S-H. The reversibility and the long-term binding of Al in C-S-H influences not only the C-S-H, but also the kind and amount of other phases and thus the stability of cement.

The destabilisation of C-A-S-H to gismondine-P1 was observed after more than 1 year at room temperature. It remains, however, unclear whether similar changes would also occur in KOH solutions or in solutions with both NaOH and KOH, as present in Portland cements. The potential formation of zeolitic phases such as gismondine-P1 have been predicted at the surface of cements exposed to chloride solutions [163] or at the interface between cement and clays present in the surrounding rock [164,165].

C-(A-)S-H with additional alkali hydroxide has been investigated in previous studies [40,41,162] as well as in this study. However, the effect of acids such as HCl or H₂SO₄, which lower the pH, on the composition, structure, alkali, calcium and aluminium

Chapter 6: Conclusions and outlook

uptake by C-S-H is not well investigated, and it is poorly known below which critical pH value C-S-H and C-A-S-H are destabilised.

The experimental data gained here and in other systematic studies of C-S-H and C-A-S-H have been used to establish the thermodynamic model CASH+. Another important task for future studies will be the critical verification of this thermodynamic model against independent data measured at different conditions, e.g. at low availability of water, in the presence of additional anions and cations, and lower and higher temperatures, to verify the accurateness of the predictions and its validity for hydrated cements.

Appendix

Appendix

Appendix A Mixing proportions used to prepared C-(A-)S-H

Table 6. Mixing proportions used to prepared C-(Na,K-)S-H with equilibrium time of 3 months (in g per 180 mL of solution)

Synthesis solution	CaO (g)	SiO ₂ (g)
Ca/Si* = 0.6		
Water	1.4364	2.5643
0.1 M NaOH	1.4364	2.5643
0.1 M KOH	1.4357	2.5647
0.5 M NaOH	1.4362	2.5646
0.5 M KOH	1.435	2.5645
1.0 M NaOH	1.4364	2.5643
1.0 M KOH	1.4366	2.564
Ca/Si* = 0.8		
Water	1.7102	2.2899
0.1 M NaOH	1.7102	2.2899
0.1 M KOH	1.7102	2.2895
0.5 M NaOH	1.7101	2.2902
0.5 M KOH	1.7102	2.2902
1.0 M NaOH	1.7102	2.2899
1.0 M KOH	1.71	2.2907
Ca/Si* = 1.0		
Water	1.9309	2.069
0.1 M NaOH	1.9309	2.069
0.1 M KOH	1.929	2.0687
0.5 M NaOH	1.9309	2.0691
0.5 M KOH	1.93	2.0692
1.0 M NaOH	1.9309	2.069
1.0 M KOH	1.932	2.0693
Ca/Si* = 1.2		
Water	2.1134	1.887
0.1 M NaOH	2.1134	1.887
0.1 M KOH	2.112	1.8866
0.5 M NaOH	2.1134	1.8874
0.5 M KOH	2.1151	1.8868
1.0 M NaOH	2.1134	1.887
1.0 M KOH	2.1144	1.8869
Ca/Si* = 1.4		
Water	2.266	1.734
0.1 M NaOH	2.266	1.734
0.1 M KOH	2.268	1.7343
0.5 M NaOH	2.2667	1.7342
0.5 M KOH	2.2668	1.7346
1.0 M NaOH	2.266	1.734
1.0 M KOH	2.267	1.7339
Ca/Si* = 1.6		
Water	2.396	1.6043
0.1 M NaOH	2.396	1.6043
0.1 M KOH	2.396	1.6042
0.5 M NaOH	2.3957	1.6041
0.5 M KOH	2.3959	1.604
1.0 M NaOH	2.3959	1.6043
1.0 M KOH	2.3973	1.604

Appendix

Table 7. Mixing proportions used to prepared C-(A-)S-H (in g per 180 mL of solution)

Synthesis solution	time (months)	target Al/Si	CaO (g)	SiO ₂ (g)	CaO.Al ₂ O ₃ (g)
0.1M NaOH	12	0	1.9309	2.069	0
	15	0.05	1.843	2.0251	0.1331
	15	0.1	1.757	1.9821	0.2622
	15	0.15	1.676	1.9414	0.383
	15	0.2	1.5981	1.9021	0.5
0.5M NaOH	12	0	1.9309	2.0691	0
	15	0.05	1.8422	2.0248	0.1329
	15	0.1	1.757	1.982	0.261
	15	0.15	1.6762	1.9412	0.3824
	15	0.2	1.5999	1.902	0.5051
1M NaOH	12	0	1.9309	2.069	0
	15	0.05	1.825	2.013	0.1328
	15	0.1	1.7584	1.983	0.2615
	15	0.15	1.6771	1.9421	0.386
	15	0.2	1.5983	1.906	0.49994
0.1M NaOH	3	0	1.9307	2.0695	0
	3	0.05	1.8443	2.0243	0.133
	3	0.1	1.7562	1.9825	0.2608
	3	0.15	1.6768	1.9406	0.3833
	3	0.2	1.5982	1.903	0.5001
0.5M NaOH	3	0	1.9318	2.0688	0
	3	0.05	1.842	2.026	0.139
	3	0.1	1.7773	1.9819	0.2627
	3	0.15	1.6765	1.9418	0.3828
	3	0.2	1.5982	1.9041	0.501
1M NaOH	3	0	1.9321	2.0689	0
	3	0.05	1.8343	2.0851	0.1325
	3	0.1	1.7572	1.9832	0.261
	3	0.15	1.6765	1.945	0.3827
	3	0.2	1.598	1.907	0.5008
0.5M KOH	3	0	1.9315	2.0699	0
	3	0.01	1.913	2.069	0.0274
	3	0.03	1.8772	2.0421	0.0812
	3	0.05	1.8429	2.0251	0.1331
	3	0.1	1.7584	1.9821	0.2613
	3	0.15	1.6772	1.9415	0.3835
	3	0.2	1.5982	1.9018	0.4999

Appendix

Table 8. Mixing proportions used to prepared C-A-S-H (in g per 260 mL of solution for samples with equilibration time from 0.25 day to 90 days and per 180mL for samples with 90, 450* and 1350* days)*

Equilibration time (days)	target Ca/Si ratio	CaO (g)	SiO ₂ (g)	CaO.Al ₂ O ₃ (g)
0.25-90	0.6	2.0289	3.9524	0.5205
	0.8	2.4852	3.549	0.4671
	1.0	2.8562	3.2215	0.4239
	1.2	3.1651	2.9501	0.3881
	1.4	3.4244	2.718	0.3569
	1.6	3.6478	2.521	0.3317
90*	0.6	1.248	2.4332	0.3228
	0.8	1.528	2.1846	0.287
	1.0	1.757	1.982	0.261
	1.2	1.948	1.8144	0.2387
	1.4	2.107	1.674	0.2198
	1.6	2.245	1.552	0.2047
450*	0.6	1.2492	2.433	0.3222
	0.8	1.5316	2.1841	0.2863
	1.0	1.7773	1.9819	0.2627
	1.2	1.949	1.8138	0.239
	1.4	2.1067	1.6738	0.2202
	1.6	2.2422	1.5534	0.208
1350*	0.6	1.255	2.4327	0.321
	0.8	1.5293	2.1843	0.2882
	1.0	1.7571	1.9823	0.2616
	1.2	1.947	1.8142	0.2386
	1.4	2.1198	1.6744	0.2223
	1.6	2.2434	1.5522	0.2046

Appendix

Appendix B Dissolved concentration

Table 9 Aqueous dissolved concentrations and pH results for the C-(N, K-)S-H samples

Synthesis solution	[Si] (mM)	[Ca] (mM)	[K] (mM)	[Na] (mM)	[OH-] (mM)	pH ^a
Ca/Si* = 0.6						
Water	3.84	1.23	0	0	0.19	9.9
0.1 M NaOH	29.2	0.01	0	46.2	16.6	12.2
0.1 M KOH	26.5	b.d.l	50.1	0	23.0	12.3
0.5 M NaOH	33.5	b.d.l	0	440	418	13.5
0.5 M KOH	30.3	0.02	462	0	404	13.5
1 M NaOH	43.1	0.01	0	944	868	13.9
1 M KOH	37.5	0.01	1082	0	871	13.8
Ca/Si* = 0.8						
Water	1.60	0.91	0	0	0.65	10.5
0.1 M NaOH	1.20	0.04	0	61.0	97.1	12.9
0.1 M KOH	1.13	0.03	67.5	0	59.0	12.7
0.5 M NaOH	2.59	0.01	0	437	418	13.5
0.5 M KOH	1.88	0.05	467	0	388	13.5
1 M NaOH	6.63	0.02	0	937	839	13.8
1 M KOH	3.87	0.04	1074	0	937	13.8
Ca/Si* = 1.0						
Water	0.07	3.50	0	0	9.2	11.7
0.1 M NaOH	0.15	0.40	0	78.7	101	13.0
0.1 M KOH	0.14	0.44	85.9	0	75.4	12.8
0.5 M NaOH	0.36	0.15	0	472	406	13.5
0.5 M KOH	0.55	0.15	501	0	457	13.5
1 M NaOH	0.47	0.22	0	978	839	13.8
1 M KOH	0.71	0.32	1081	0	937	13.8
Ca/Si* = 1.2						
Water	0.01	7.11	0	0	16.9	12.0
0.1 M NaOH	b.d.l	1.39	0	94.0	97.1	12.9
0.1 M KOH	0.03	1.34	101	0	88.8	12.9
0.5 M NaOH	b.d.l	0.85	0	495	422	13.5
0.5 M KOH	0.10	0.77	515	0	476	13.5
1 M NaOH	0.18	0.47	0	968	899	13.9
1 M KOH	0.51	0.54	1108	0	937	13.8
Ca/Si* = 1.4						
Water	0.01	16.0	0	0	51.4	12.4
0.1 M NaOH	b.d.l	4.45	0	93.3	97.1	12.9
0.1 M KOH	0.01	4.17	102	0	92.5	12.9
0.5 M NaOH	b.d.l	0.98	0	486	455	13.6
0.5 M KOH	0.09	0.88	516	0	496	13.6
1 M NaOH	0.13	0.56	0	980	839	13.8
1 M KOH	0.45	0.61	1104	0	972	13.8
Ca/Si* = 1.6						
Water	b.d.l	21.3	0	0	55.2	12.5
0.1 M NaOH	b.d.l	5.09	0	94.1	122	13.0
0.1 M KOH	0.01	4.72	1123	0	129	13.0
0.5 M NaOH	b.d.l	1.11	0	498	472	13.6
0.5 M KOH	0.09	0.94	514	0	476	13.5
1 M NaOH	0.11	0.61	0	990	868	13.9
1 M KOH	0.43	0.63	1102	0	972	13.8

^a pH measured at ~ 24°C

Appendix

Table 10. Aqueous dissolved concentrations and pH values for the C-(N, K-)A-S-H samples (target Ca/Si = 1.0)

Synthesis solution	time (months)	target Al/Si	[Si] (mM)	[Ca] (mM)	[Al] (mM)	[Na] (mM)	[K] (mM)	[OH ⁻] (mM)	pH ^a
0.1M NaOH	12	0	0.179	0.0818	0	82.9	0	92.7	13.0
	15	0.05	0.323	0.207	0.085	74.2	0	41.2	12.6
	15	0.1	0.431	0.173	0.212	71.0	0	38.4	12.6
	15	0.15	0.463	0.132	0.462	69.7	0	34.7	12.5
	15	0.2	0.559	0.0966	0.555	70.6	0	34.8	12.5
0.5M NaOH	12	0	0.705	0.0945	0	473	0	322	13.5
	15	0.05	0.322	0.175	0.207	485	0	178	13.3
	15	0.1	0.470	0.126	0.869	483	0	154	13.2
	15	0.15	0.891	0.0944	1.39	468	0	132	13.1
	15	0.2	0.856	0.0889	2.22	405	0	122	13.1
1M NaOH	12	0	0.713	0.189	0	940	0	689	13.8
	15	0.05	0.56	0.238	0.590	994	0	216	13.3
	15	0.1	1.03	0.138	1.53	974	0	232	13.4
	15	0.15	1.16	0.141	2.53	1200	0	260	13.4
	15	0.2	1.05	0.137	3.79	1027	0	312	13.5
0.1M NaOH	3	0	0.146	0.399	0	78.7	0	111	13.0
	3	0.05	0.298	0.212	0.069	80.4	0	105	13.0
	3	0.1	1.25	0.0681	0.342	80.1	0	74.7	12.9
	3	0.15	11.4	0.0177	0.327	69.3	0	79.5	12.9
	3	0.2	0.541	0.0293	0.701	63.6	0	96.6	13.0
0.5M NaOH	3	0	0.357	0.1476	0	472	0	341	13.5
	3	0.05	0.489	0.0426	0.056	580	0	409	13.6
	3	0.1	0.556	0.0396	1.09	493	0	289	13.5
	3	0.15	1.15	0.0108	1.47	512	0	443	13.6
	3	0.2	1.36	0.0112	2.37	511	0	284	13.5
1M NaOH	3	0	0.472	0.218	0.00	978	0	572	13.8
	3	0.05	0.699	0.204	0.490	1097	0	524	13.7
	3	0.1	1.10	0.0591	2.04	986	0	469	13.7
	3	0.15	1.19	<0.0025	3.16	1236	0	585	13.8
	3	0.2	1.25	<0.0025	5.74	1165	0	444	13.6
0.5M KOH	3	0	0.392	0.222	0	0	493	309	13.5
	3	0.01	0.465	0.197	0.027	0	496	309	13.5
	3	0.03	0.578	0.151	0.136	0	483	309	13.5
	3	0.05	0.641	0.128	0.276	0	503	309	13.5
	3	0.1	0.750	0.109	1.02	0	473	309	13.5
	3	0.15	0.738	0.103	2.08	0	475	297	13.5
	3	0.2	0.744	0.0936	3.03	0	478	309	13.5

^apH measured at ~ 24 °C

Appendix

Table 11 Aqueous dissolved concentrations and pH values for the C-(N-)A-S-H samples with different equilibration time (target Al/Si = 0.1). C-A-S-H equilibrated for 0.25- 90 days: synthesized with water/solid = 45, C-A-S-H equilibrated for 90, 450* and 1350* days: synthesized with water/solid = 40.*

Equilibration time (days)	target Ca/Si ratio	Si (mM)	Ca (mM)	Al (mM)	Na (mM)	OH- (mM)	pH ^a
0.25	0.6	0.95	0.35	1.3	520	319	13.5
	0.8	0.43	0.82	2.0	528	286	13.5
	1.0	0.42	0.86	1.9	528	302	13.5
	1.2	0.40	0.88	1.6	528	319	13.5
	1.4	0.39	0.91	1.7	536	319	13.5
	1.6	0.38	0.92	1.7	536	337	13.5
1	0.6	36.1	0.013	2.2	499	256	13.4
	0.8	0.76	0.24	1.5	504	302	13.5
	1.0	0.36	0.69	1.1	518	319	13.5
	1.2	0.32	0.79	0.91	521	319	13.5
	1.4	0.31	0.83	1.0	524	337	13.5
	1.6	0.30	0.85	1.0	531	337	13.5
3	0.6	53.9	0.009	2.5	472	217	13.3
	0.8	3.87	0.015	1.9	469	286	13.5
	1.0	0.46	0.18	1.2	491	256	13.4
	1.2	0.13	0.76	0.63	513	302	13.5
	1.4	0.11	0.92	0.61	518	302	13.5
	1.6	0.11	0.96	0.58	522	302	13.5
7	0.6	44.1	0.008	2.2	426	174	13.2
	0.8	3.12	0.019	1.8	427	206	13.3
	1.0	0.52	0.14	1.2	446	230	13.4
	1.2	0.11	0.72	0.56	467	230	13.4
	1.4	0.079	0.92	0.51	470	230	13.4
	1.6	0.074	0.99	0.49	474	230	13.4
14	0.6	47.4	0.007	2.3	433	219	13.3
	0.8	3.39	0.019	1.9	432	247	13.4
	1.0	0.48	0.13	1.1	454	267	13.4
	1.2	0.10	0.65	0.52	479	277	13.4
	1.4	0.079	0.95	0.46	481	277	13.4
	1.6	0.074	1.02	0.44	480	277	13.4
28	0.6	37.8	0.0038	2.3	418	228	13.4
	0.8	2.87	0.019	1.8	416	247	13.4
	1.0	0.61	0.11	1.0	441	256	13.4
	1.2	0.13	0.57	0.45	465	267	13.4
	1.4	0.074	0.93	0.38	471	267	13.4
	1.6	0.067	1.01	0.37	473	277	13.4
90	0.6	34.39	0.0055	2.4	432	195	13.3
	0.8	2.72	0.019	1.8	423	237	13.4
	1.0	0.67	0.10	1.0	453	256	13.4
	1.2	0.14	0.44	0.34	476	256	13.4
	1.4	0.072	0.87	0.25	482	256	13.4
	1.6	0.069	0.97	0.23	489	350	13.5
90*	0.6	26.6	b.d.l	2.9	545	147	13.2
	0.8	3.83	b.d.l	2.0	542	147	13.2
	1.0	0.56	0.040	1.1	580	154	13.2
	1.2	0.13	0.25	0.32	517	147	13.2
	1.4	0.053	0.59	0.15	522	168	13.2
	1.6	0.055	0.61	0.21	530	176	13.2
450*	0.6	32.00	0.010	3.3	503	425	13.6
	0.8	2.84	0.048	2.2	465	367	13.6

Appendix

	1.0	0.71	0.58	0.87	479	289	13.5
	1.2	0.13	0.13	0.36	500	336	13.5
	1.4	0.072	0.97	0.17	504	371	13.6
	1.6	0.051	1.04	0.19	505	353	13.5
	0.6	20.1	0.037	0.76	459	321	13.5
	0.8	2.56	0.035	1.6	467	334	13.5
1350*	1.0	0.75	0.10	0.69	496	362	13.6
	1.2	0.18	0.44	0.24	515	348	13.5
	1.4	0.086	0.91	0.09	526	362	13.6
	1.6	0.080	0.84	0.15	524	392	13.6

^apH measured at ~ 24°C

Appendix

Appendix C Saturation indices

Table 12. Saturation indices for the relevant reaction products in C-(A-)S-H synthesized in different alkali hydroxide solutions.

Synthesis solution	(months)	target Al/Si	C-(A-)S-H	portlandite	amorphous-SiO ₂	katoite	strätlingite	gibbsite-P1	natrolite	zeolite X	AH ₃ (mic)
0.1M NaOH	12	0	-2.5	-2.0	-4.4	-	-	-	-	-	-
	15	0.05	-0.9	-1.7	-4.1	-5.8	-2.2	-1.8	-1.4	-2.3	-2.3
	15	0.1	-0.6	-1.8	-3.9	-5.3	-1.4	-1.4	-1.0	-1.8	-1.8
	15	0.15	-0.7	-1.9	-3.9	-5.0	-1.0	-1.2	-0.8	-1.5	-1.5
	15	0.2	-0.8	-2.1	-3.8	-5.3	-1.0	-1.0	-0.6	-1.3	-1.4
0.5M NaOH	12	0	-1.2	-1.2	-5.1	-	-	-	-	-	-
	15	0.05	-1.2	-0.9	-5.5	-4.4	-2.9	-2.5	-2.1	-2.8	-2.7
	15	0.1	-1.0	-1.1	-5.3	-3.6	-1.8	-2.0	-1.5	-2.1	-2.0
	15	0.15	-0.6	-1.2	-5.0	-3.6	-1.4	-1.6	-1.1	-1.7	-1.8
	15	0.2	-0.4	-1.3	-4.9	-3.3	-0.9	-1.4	-0.9	-1.4	-1.6
1M NaOH	12	0	-0.7	-0.7	-5.7	-	-	-	-	-	-
	15	0.05	-0.6	-0.6	-5.9	-3.0	-2.3	-2.5	-2.0	-2.6	-2.5
	15	0.1	-0.5	-0.8	-5.6	-2.9	-1.7	-2.0	-1.5	-2.0	-2.1
	15	0.15	-0.4	-0.8	-5.7	-2.5	-1.5	-1.9	-1.4	-1.9	-2.0
	15	0.2	-0.4	-0.8	-5.6	-2.1	-1.0	-1.8	-1.3	-1.7	-1.7
0.1M NaOH	3	0	-1.2	-1.3	-4.5	-	-	-	-	-	-
	3	0.05	-0.9	-1.6	-4.2	-5.9	-2.4	-1.9	-1.6	-2.4	-2.4
	3	0.1	-0.6	-2.2	-3.5	-6.4	-1.6	-0.8	-0.5	-1.2	-1.7
	3	0.15	-0.6	-3.6	-2.3	-10.3	-3.0	0.3	0.7	-0.1	-1.6
	3	0.2	-1.9	-2.6	-3.7	-6.7	-1.8	-0.9	-0.5	-1.2	-1.3
0.5M NaOH	3	0	-1.3	-1.0	-5.4	-	-	-	-	-	-
	3	0.05	-2.3	-1.5	-5.4	-7.3	-5.3	-2.8	-2.4	-3.2	-3.3
	3	0.1	-1.8	-1.6	-5.2	-4.9	-2.6	-1.9	-1.4	-2.0	-2.0
	3	0.15	-2.3	-2.1	-5.0	-6.4	-3.2	-1.5	-1.0	-1.6	-1.8
	3	0.2	-2.0	-2.1	-4.9	-5.9	-2.7	-1.3	-0.8	-1.4	-1.6
1M NaOH	3	0	-1.0	-0.6	-5.9	-	-	-	-	-	-
	3	0.05	-0.7	-0.6	-5.8	-3.4	-2.6	-2.5	-2.0	-2.6	-2.6
	3	0.1	-1.2	-1.2	-5.6	-3.8	-2.2	-1.9	-1.4	-1.9	-2.0
	3	0.15	-16.8	-8.9	-5.8	-26.7	-17.6	-1.9	-1.4	-1.8	-1.9
	3	0.2	-16.5	-8.9	-5.7	-26.2	-17.0	-1.7	-1.2	-1.6	-1.6
0.5M KOH	3	0	-0.9	-0.8	-5.5	-	-	-	-	-	-
	3	0.01	-0.9	-0.8	-5.4	-6.0	-4.5	-8.2	-8.4	-10.4	-3.6
	3	0.03	-0.9	-1.0	-5.3	-4.9	-3.2	-7.7	-7.8	-9.7	-2.9
	3	0.05	-0.9	-1.0	-5.3	-4.5	-2.8	-7.5	-7.6	-9.4	-2.6
	3	0.1	-0.8	-1.1	-5.1	-3.6	-1.7	-7.0	-7.1	-8.9	-2.0
	3	0.15	-0.7	-1.1	-5.2	-3.1	-1.1	-6.8	-6.9	-8.6	-1.7
	3	0.2	-0.7	-1.2	-5.2	-2.9	-0.9	-6.7	-6.8	-8.5	-1.5

Appendix

Table 13. Saturation indices for the relevant reaction products in C-(A-)S-H system with $Al/Si_{target} = 0.1$ and different Ca/Si as a function of equilibration time. C-A-S-H equilibrated for 0.25- 90 days: synthesized with water/solid = 45, C-A-S-H equilibrated for 90, 450* and 1350* days: synthesized with water/solid = 40.*

Target Ca/Si	Equilibrium time (days)	C-A-S-H	AH ₃	C ₃ AH ₆	Charba-zite	Gismondine-P1	Strätlingite	CH	amor-Si
0.6	0.25	0.7	-1.9	-1.9	-1.6	-16.5	-0.4	-0.6	-5.1
	1	-0.1	-1.8	-8.1	0.1	0.8	-2.7	-2.7	-3.3
	3	-0.1	-1.8	-9.1	0.3	3.3	-3.1	-3.1	-3.1
	7	-0.4	-1.7	-9.2	0.3	3.0	-3.2	-3.2	-3.1
	14	-0.4	-1.7	-9.4	0.3	3.2	-3.3	-3.2	-3.1
	28	-1.1	-1.7	-10.0	0.2	2.4	-3.7	-3.4	-3.2
	90	-0.8	-1.7	-9.3	0.2	2.0	-3.3	-3.2	-3.2
	90*	-1.5	-1.7	-9.5	-0.1	-0.5	-3.8	-3.3	-3.6
	450*	-0.3	-1.6	-7.9	0.1	1.3	-2.6	-2.8	-3.4
	1350*	0.5	-2.2	-7.0	-0.4	-3.8	-2.4	-2.1	-3.6
0.8	0.25	1.0	-1.7	-0.4	-1.9	-19.1	0.4	-0.2	-5.5
	1	0.2	-1.8	-2.3	-1.7	-16.9	-0.6	-0.8	-5.1
	3	-1.0	-1.7	-6.0	-0.9	-8.7	-2.3	-2.1	-4.4
	7	-1.0	-1.7	-5.8	-0.9	-9.1	-2.1	-2.0	-4.4
	14	-0.9	-1.7	-5.8	-0.9	-8.7	-2.1	-2.0	-4.3
	28	-1.0	-1.7	-5.8	-0.9	-9.3	-2.1	-2.0	-4.4
	90	-1.1	-1.7	-5.8	-1.0	-9.7	-2.1	-2.0	-4.4
	90*	-2.7	-1.8	-8.3	-1.0	-9.6	-4.0	-2.8	-4.5
	450*	-0.2	-1.6	-4.3	-1.0	-9.6	-1.2	-1.6	-4.5
	1350*	-0.6	-1.8	-4.9	-1.1	-10.8	-1.8	-1.7	-4.5
1.0	0.25	1.0	-1.7	-0.3	-1.9	-19.3	0.4	-0.2	-5.5
	1	0.6	-2.0	-1.1	-2.1	-21.1	-0.3	-0.3	-5.5
	3	-0.6	-1.9	-2.8	-2.0	-19.5	-1.3	-0.9	-5.3
	7	-0.6	-1.9	-3.2	-1.8	-18.3	-1.3	-1.0	-5.2
	14	-0.8	-1.9	-3.3	-1.9	-18.8	-1.5	-1.1	-5.2
	28	-0.8	-1.9	-3.6	-1.8	-17.8	-1.6	-1.2	-5.1
	90	-0.8	-2.0	-3.8	-1.8	-17.7	-1.7	-1.2	-5.1
	90*	-1.9	-2.0	-4.9	-2.0	-19.8	-2.7	-1.5	-5.4
	450*	0.9	-2.0	-1.6	-1.8	-18.4	-0.3	-0.4	-5.1
	1350*	-0.8	-2.2	-4.1	-1.9	-18.7	-2.0	-1.2	-5.1
1.2	0.25	1.0	-1.8	-0.5	-2.0	-20.0	0.2	-0.2	-5.5
	1	0.5	-2.1	-1.1	-2.2	-22.3	-0.4	-0.2	-5.6
	3	-0.3	-2.2	-1.4	-2.7	-27.0	-1.1	-0.2	-5.9
	7	-0.5	-2.2	-1.6	-2.7	-27.5	-1.2	-0.3	-5.9
	14	-0.7	-2.3	-1.8	-2.8	-28.4	-1.5	-0.3	-6.0
	28	-0.6	-2.3	-2.1	-2.7	-27.3	-1.6	-0.4	-5.9
	90	-0.9	-2.4	-2.7	-2.8	-27.9	-2.0	-0.5	-5.8
	90*	-1.6	-2.5	-3.5	-2.9	-28.7	-2.7	-0.7	-5.9
	450*	-2.2	-2.4	-4.2	-2.8	-28.2	-3.1	-1.0	-5.9
	1350*	-0.8	-2.6	-3.0	-2.8	-28.1	-2.3	-0.5	-5.8
1.4	0.25	1.0	-1.8	-0.4	-2.0	-20.1	0.3	-0.2	-5.5
	1	0.6	-2.0	-1.0	-2.2	-22.2	-0.3	-0.2	-5.6
	3	-0.2	-2.2	-1.2	-2.8	-27.8	-1.1	-0.2	-6.0
	7	-0.5	-2.3	-1.4	-2.9	-29.3	-1.3	-0.2	-6.1
	14	-0.5	-2.3	-1.4	-3.0	-29.7	-1.4	-0.2	-6.1
	28	-0.6	-2.4	-1.6	-3.0	-30.3	-1.6	-0.2	-6.1
	90	-0.8	-2.6	-2.1	-3.2	-31.7	-2.0	-0.2	-6.1
	90*	-1.5	-2.8	-3.0	-3.5	-34.7	-3.0	-0.3	-6.3
	450*	-0.7	-2.8	-2.3	-3.3	-33.0	-2.3	-0.1	-6.2
	1350*	-0.7	-3.1	-2.9	-3.4	-34.0	-2.9	-0.2	-6.1

Appendix

	0.25	1.0	-1.8	-0.4	-2.0	-20.1	0.3	-0.2	-5.5
	1	0.6	-2.0	-0.9	-2.2	-22.4	-0.3	-0.2	-5.6
	3	-0.2	-2.2	-1.2	-2.8	-28.1	-1.1	-0.1	-6.0
	7	-0.5	-2.3	-1.3	-3.0	-29.7	-1.3	-0.2	-6.1
1.6	14	-0.5	-2.3	-1.4	-3.0	-30.1	-1.4	-0.1	-6.1
	28	-0.6	-2.4	-1.5	-3.1	-30.9	-1.6	-0.1	-6.2
	90	-0.7	-2.6	-2.0	-3.2	-32.1	-2.0	-0.2	-6.2
	90*	-1.4	-2.7	-2.7	-3.4	-33.7	-2.7	-0.3	-6.3
	450*	-0.9	-2.7	-2.1	-3.4	-34.2	-2.3	-0.1	-6.3
	1350*	-0.8	-2.8	-2.6	-3.3	-33.1	-2.5	-0.2	-6.2

Appendix

Appendix D C-(A-)S-H compositions

Table 14. Chemical compositions of the C-(N,K-)S-H products, determined from IC, TGA, XRD and pH measurements, The estimated absolute errors are less than ± 0.05 units in the Ca/Si ratios, ± 0.2 units in the H₂O/Si ratios, and ± 0.05 units for the 0.1 M alkali samples in the (Na/K)/Si ratios of the C-(N,K-)S-H products. Ca/Si = target Ca/Si*

Synthesis solution	C-(N,K-)S-H chemical formula	Ca/Si _{C-S-H}	Na/Si ^c	K/Si ^c	H ₂ O/Si
Ca/Si* = 0.6					
Water	(CaO) _{0.78} SiO ₂ (H ₂ O) _{1.2} ^a	0.78 ^a	-	-	1.21
0.1 M NaOH	(CaO) _{0.71} (Na ₂ O) _{0.13} SiO ₂ (H ₂ O) _{1.0}	0.71	0.21	-	1.04
0.1 M KOH	(CaO) _{0.71} (K ₂ O) _{0.14} SiO ₂ (H ₂ O) _{1.1}	0.71	-	0.27	1.13
0.5 M NaOH	(CaO) _{0.70} (Na ₂ O) _{0.65} SiO ₂ (H ₂ O) _{1.4}	0.70	0.65 ^c	-	1.38
0.5 M KOH	(CaO) _{0.69} (K ₂ O) _{0.48} SiO ₂ (H ₂ O) _{1.3}	0.69	-	0.48	1.35
1.0 M NaOH	(CaO) _{0.73} (Na ₂ O) _{0.76} SiO ₂ (H ₂ O) _{1.9}	0.73	0.76	-	1.86
1.0 M KOH	(CaO) _{0.73} (K ₂ O) _{0.49} SiO ₂ (H ₂ O) _{1.3}	0.73	-	0.49	1.30
Ca/Si* = 0.8					
Water	(CaO) _{0.88} SiO ₂ (H ₂ O) _{1.3}	0.88	-	-	1.32
0.1 M NaOH	(CaO) _{0.81} (Na ₂ O) _{0.17} SiO ₂ (H ₂ O) _{1.1}	0.81	0.17	-	1.10
0.1 M KOH	(CaO) _{0.83} (K ₂ O) _{0.20} SiO ₂ (H ₂ O) _{1.2}	0.83	-	0.20	1.24
0.5 M NaOH	(CaO) _{0.81} (Na ₂ O) _{0.56} SiO ₂ (H ₂ O) _{1.7}	0.81	0.56	-	1.66
0.5 M KOH	(CaO) _{0.81} (K ₂ O) _{0.46} SiO ₂ (H ₂ O) _{1.6}	0.81	-	0.46	1.55
1.0 M NaOH	(CaO) _{0.83} (Na ₂ O) _{0.67} SiO ₂ (H ₂ O) _{1.9}	0.83	0.67	-	1.90
1.0 M KOH	(CaO) _{0.81} (K ₂ O) _{0.73} SiO ₂ (H ₂ O) _{1.8}	0.81	-	0.73	1.75
Ca/Si* = 1.0					
Water	(CaO) _{0.98} SiO ₂ (H ₂ O) _{1.5}	0.98	-	-	1.48
0.1 M NaOH	(CaO) _{1.00} (Na ₂ O) _{0.10} SiO ₂ (H ₂ O) _{1.1}	1.00	0.10	-	1.14
0.1 M KOH	(CaO) _{1.00} (K ₂ O) _{0.13} SiO ₂ (H ₂ O) _{1.5}	1.00	-	0.13	1.47
0.5 M NaOH	(CaO) _{1.00} (Na ₂ O) _{0.43} SiO ₂ (H ₂ O) _{1.5}	1.00	0.43	-	1.46
0.5 M KOH	(CaO) _{1.00} (K ₂ O) _{0.31} SiO ₂ (H ₂ O) _{1.6}	1.00	-	0.31	1.61
1.0 M NaOH	(CaO) _{0.90} (Na ₂ O) _{1.12} SiO ₂ (H ₂ O) _{2.1}	0.90 ^b	1.12	-	2.10
1.0 M KOH	(CaO) _{1.00} (K ₂ O) _{0.73} SiO ₂ (H ₂ O) _{2.4}	0.97	-	0.73	2.38
Ca/Si* = 1.2					
Water	(CaO) _{1.16} SiO ₂ (H ₂ O) _{1.4}	1.16	-	-	1.37
0.1 M NaOH	(CaO) _{1.19} (Na ₂ O) _{0.06} SiO ₂ (H ₂ O) _{1.3}	1.19	0.06	-	1.28
0.1 M KOH	(CaO) _{1.19} (K ₂ O) _{0.06} SiO ₂ (H ₂ O) _{1.4}	1.19	-	0.06	1.38
0.5 M NaOH	(CaO) _{1.19} (Na ₂ O) _{0.34} SiO ₂ (H ₂ O) _{1.5}	1.19 ^b	0.34	-	1.51
0.5 M KOH	(CaO) _{1.16} (K ₂ O) _{0.24} SiO ₂ (H ₂ O) _{1.6}	1.16 ^b	-	0.24	1.62
1.0 M NaOH	(CaO) _{1.01} (Na ₂ O) _{1.02} SiO ₂ (H ₂ O) _{2.5}	1.01 ^b	1.02	-	2.49
1.0 M KOH	(CaO) _{1.16} (K ₂ O) _{0.44} SiO ₂ (H ₂ O) _{1.8}	1.16 ^b	-	0.44	1.82
Ca/Si* = 1.4					
Water	(CaO) _{1.30} SiO ₂ (H ₂ O) _{1.5}	1.30	-	-	1.47
0.1 M NaOH	(CaO) _{1.34} (Na ₂ O) _{0.04} SiO ₂ (H ₂ O) _{1.5}	1.34 ^b	0.04	-	1.46
0.1 M KOH	(CaO) _{1.36} SiO ₂ (H ₂ O) _{1.6}	1.36 ^b	-	-	1.61
0.5 M NaOH	(CaO) _{1.25} (Na ₂ O) _{0.32} SiO ₂ (H ₂ O) _{1.5}	1.25 ^b	0.32	-	1.53
0.5 M KOH	(CaO) _{1.21} (K ₂ O) _{0.32} SiO ₂ (H ₂ O) _{2.0}	1.21 ^b	-	0.32	1.96
1.0 M NaOH	(CaO) _{1.02} (Na ₂ O) _{0.85} SiO ₂ (H ₂ O) _{2.3}	1.02 ^b	0.85	-	2.29
1.0 M KOH	(CaO) _{1.16} (K ₂ O) _{0.60} SiO ₂ (H ₂ O) _{2.2}	1.16 ^b	-	0.60	2.24
Ca/Si* = 1.6					
Water	(CaO) _{1.44} SiO ₂ (H ₂ O) _{1.6}	1.44 ^b	-	-	1.60
0.1 M NaOH	(CaO) _{1.44} (Na ₂ O) _{0.03} SiO ₂ (H ₂ O) _{1.6}	1.44 ^b	0.03	-	1.56
0.1 M KOH	(CaO) _{1.48} SiO ₂ (H ₂ O) _{1.7}	1.48 ^b	-	-	1.73
0.5 M NaOH	(CaO) _{1.35} (Na ₂ O) _{0.31} SiO ₂ (H ₂ O) _{1.6}	1.35 ^b	0.31	-	1.59
0.5 M KOH	(CaO) _{1.22} (K ₂ O) _{0.36} SiO ₂ (H ₂ O) _{2.4}	1.22 ^b	-	0.36	2.40
1.0 M NaOH	(CaO) _{1.07} (Na ₂ O) _{0.54} SiO ₂ (H ₂ O) _{2.2}	1.07 ^b	0.54	-	2.19
1.0 M KOH	(CaO) _{1.17} (K ₂ O) _{0.47} SiO ₂ (H ₂ O) _{2.4}	1.17 ^b	-	0.47	2.37

- = not applicable: as no Na or K was added during synthesis (<0.6 mM Na is present as an impurity in the 0.1 M KOH synthesis solution).

Appendix

^a lowered due to the presence of SiO₂ as indicated by NMR and saturation indices with respect to SiO₂; ^b portlandite present in addition to C-S-H; ^c Alkali/Si ratios based on direct methods [41] are associated with an error of ±0.2 units for the 0.5 M alkali samples and ±0.7 for the 1 M alkali samples.

Table 15 Chemical compositions of the C-(N,K-)A-S-H products, determined from Rietveld analysis, mass balance and dissolution experiments. The estimated absolute errors are less than ±0.02 units in the Ca/Si ratios, ±0.2 units in the H₂O/Si ratios, and ±0.05 units for the 0.1 M alkali samples in the Na/Si ratios of the C-(N,K-)A-S-H products.

synth esis soluti on	time		Ca/ Si	Na/Si ^a	K/Si ^b	Al/Si	H ₂ O/ Si	chemical formula
	(mo nths)	targ et Al/Si						
0.1M NaO H	12	0	1.00	0.15	0	0	1.30	(CaO) _{1.00} (Na ₂ O) _{0.15} SiO ₂ (H ₂ O) _{1.3}
	15	0.05	1.00	0.12	0	0.05	1.27	(CaO) _{1.00} (Na ₂ O) _{0.12} (Al ₂ O ₃) _{0.05} SiO ₂ (H ₂ O) _{1.3}
	15	0.1	0.98	0.12	0	0.09	1.54	(CaO) _{0.98} (Na ₂ O) _{0.12} (Al ₂ O ₃) _{0.09} SiO ₂ (H ₂ O) _{1.5}
	15	0.15	0.96	0.16	0	0.11	2.00	(CaO) _{0.96} (Na ₂ O) _{0.16} (Al ₂ O ₃) _{0.11} SiO ₂ (H ₂ O) _{2.0}
	15	0.2	0.88	0.18	0	0.10	1.57	(CaO) _{0.88} (Na ₂ O) _{0.18} (Al ₂ O ₃) _{0.10} SiO ₂ (H ₂ O) _{1.6}
0.5M NaO H	12	0	1.00	0.45	0	0	1.37	(CaO) _{1.00} (Na ₂ O) _{0.45} SiO ₂ (H ₂ O) _{1.4}
	15	0.05	1.00	0.34	0	0.05	1.94	(CaO) _{1.00} (Na ₂ O) _{0.34} (Al ₂ O ₃) _{0.05} SiO ₂ (H ₂ O) _{1.9}
	15	0.1	0.99	0.33	0	0.08	1.80	(CaO) _{0.99} (Na ₂ O) _{0.33} (Al ₂ O ₃) _{0.08} SiO ₂ (H ₂ O) _{1.8}
	15	0.15	0.93	0.39	0	0.10	1.39	(CaO) _{0.93} (Na ₂ O) _{0.39} (Al ₂ O ₃) _{0.10} SiO ₂ (H ₂ O) _{1.4}
	15	0.2	0.97	0.39	0	0.17	1.81	(CaO) _{0.97} (Na ₂ O) _{0.39} (Al ₂ O ₃) _{0.17} SiO ₂ (H ₂ O) _{1.8}
1M NaO H	12	0	1.00	0.73	0	0	1.53	(CaO) _{1.00} (Na ₂ O) _{0.73} SiO ₂ (H ₂ O) _{1.5}
	15	0.05	0.95	0.36	0	0.03	1.59	(CaO) _{0.95} (Na ₂ O) _{0.36} (Al ₂ O ₃) _{0.03} SiO ₂ (H ₂ O) _{1.6}
	15	0.1	0.99	0.27	0	0.09	1.60	(CaO) _{0.99} (Na ₂ O) _{0.27} (Al ₂ O ₃) _{0.09} SiO ₂ (H ₂ O) _{1.6}
	15	0.15	0.95	0.36	0	0.12	1.53	(CaO) _{0.95} (Na ₂ O) _{0.36} (Al ₂ O ₃) _{0.12} SiO ₂ (H ₂ O) _{1.5}
	15	0.2	0.98	0.34	0	0.17	1.84	(CaO) _{0.98} (Na ₂ O) _{0.34} (Al ₂ O ₃) _{0.17} SiO ₂ (H ₂ O) _{1.8}
0.1M NaO H	3	0	1.00	0.09	0	0	1.14	(CaO) _{1.00} (Na ₂ O) _{0.09} SiO ₂ (H ₂ O) _{1.1}
	3	0.05	1.00	0.12	0	0.05	1.95	(CaO) _{1.00} (Na ₂ O) _{0.12} (Al ₂ O ₃) _{0.05} SiO ₂ (H ₂ O) _{1.9}
	3	0.1	0.99	0.20	0	0.09	1.73	(CaO) _{0.99} (Na ₂ O) _{0.20} (Al ₂ O ₃) _{0.09} SiO ₂ (H ₂ O) _{1.7}
	3	0.15	1.02	0.16	0	0.14	2.08	(CaO) _{1.02} (Na ₂ O) _{0.16} (Al ₂ O ₃) _{0.14} SiO ₂ (H ₂ O) _{2.1}
	3	0.2	0.91	0.24	0	0.10	1.74	(CaO) _{0.91} (Na ₂ O) _{0.24} (Al ₂ O ₃) _{0.10} SiO ₂ (H ₂ O) _{1.7}
0.5M NaO H	3	0	1.00	0.42	0	0	1.44	(CaO) _{1.00} (Na ₂ O) _{0.42} SiO ₂ (H ₂ O) _{1.4}
	3	0.05	1.00	0.32	0	0.05	2.06	(CaO) _{1.00} (Na ₂ O) _{0.32} (Al ₂ O ₃) _{0.05} SiO ₂ (H ₂ O) _{2.1}
	3	0.1	0.99	0.37	0	0.09	1.81	(CaO) _{0.99} (Na ₂ O) _{0.37} (Al ₂ O ₃) _{0.09} SiO ₂ (H ₂ O) _{1.8}
	3	0.15	0.98	0.36	0	0.13	1.99	(CaO) _{0.98} (Na ₂ O) _{0.36} (Al ₂ O ₃) _{0.13} SiO ₂ (H ₂ O) _{2.0}
	3	0.2	0.97	0.46	0	0.16	1.86	(CaO) _{0.97} (Na ₂ O) _{0.46} (Al ₂ O ₃) _{0.16} SiO ₂ (H ₂ O) _{1.9}
1M NaO H	3	0	1.00	0.99	0	0	2.08	(CaO) _{1.00} (Na ₂ O) _{0.99} SiO ₂ (H ₂ O) _{2.1}
	3	0.05	1.00	0.45	0	0.05	1.57	(CaO) _{1.00} (Na ₂ O) _{0.45} (Al ₂ O ₃) _{0.05} SiO ₂ (H ₂ O) _{1.6}
	3	0.1	0.99	0.34	0	0.09	1.42	(CaO) _{0.99} (Na ₂ O) _{0.34} (Al ₂ O ₃) _{0.09} SiO ₂ (H ₂ O) _{1.4}
	3	0.15	0.97	0.38	0	0.13	1.48	(CaO) _{0.97} (Na ₂ O) _{0.38} (Al ₂ O ₃) _{0.13} SiO ₂ (H ₂ O) _{1.5}
	3	0.2	0.95	0.52	0	0.15	1.55	(CaO) _{0.95} (Na ₂ O) _{0.52} (Al ₂ O ₃) _{0.15} SiO ₂ (H ₂ O) _{1.6}
0.5M KOH	3	0	1.00	0	0.11	0	1.52	(CaO) _{1.00} (K ₂ O) _{0.11} SiO ₂ (H ₂ O) _{1.5}
	3	0.01	1.00	0	0.09	0.01	1.43	(CaO) _{1.00} (K ₂ O) _{0.09} (Al ₂ O ₃) _{0.01} SiO ₂ (H ₂ O) _{1.4}
	3	0.03	1.00	0	0.16	0.03	1.44	(CaO) _{1.00} (K ₂ O) _{0.16} (Al ₂ O ₃) _{0.03} SiO ₂ (H ₂ O) _{1.4}

Appendix

3	0.05	1.00	0	0.06	0.05	1.57	(CaO) _{1.00} (K ₂ O) _{0.06} (Al ₂ O ₃) _{0.05} SiO ₂ (H ₂ O) _{1.6}
3	0.1	1.00	0	0.22	0.10	1.50	(CaO) _{1.00} (K ₂ O) _{0.22} (Al ₂ O ₃) _{0.10} SiO ₂ (H ₂ O) _{1.5}
3	0.15	1.00	0	0.21	0.14	1.56	(CaO) _{1.00} (K ₂ O) _{0.21} (Al ₂ O ₃) _{0.14} SiO ₂ (H ₂ O) _{1.6}
3	0.2	0.96	0	0.20	0.16	1.62	(CaO) _{0.96} (K ₂ O) _{0.20} (Al ₂ O ₃) _{0.16} SiO ₂ (H ₂ O) _{1.6}

a: Na/Si ratios based on direct methods [41] are associated with an error of ± 0.2 units for the 0.5 M alkali samples and ± 0.4 for the 1 M alkali samples.

b: K/Si ratios based on indirect methods [41] are associated with an error of ± 0.3 units

Table 16. Chemical compositions of the C-N-A-S-H products, determined from Rietveld analysis, TGA, mass balance and dissolution experiments. The estimated absolute errors are less than ± 0.05 units in the Ca/Si ratios, ± 0.2 units in the H₂O/Si ratios, and ± 0.05 units for the 0.1 M alkali samples in the Na/Si ratios of the C-N-A-S-H products. C-A-S-H equilibrated for 0.25- 90 days: synthesized with water/solid = 45, C-A-S-H equilibrated for 90, 450* and 1350* days: synthesized with water/solid = 40.*

target Ca/Si ratio	hydration time (days)	Ca/Si	Na/Si	Al/Si	H ₂ O/Si	chemical formula
0.6	0.25	0.54	0.23	0.10	1.1	(CaO) _{0.54} (Na ₂ O) _{0.11} (Al ₂ O ₃) _{0.048} (SiO ₂) ₁ (H ₂ O) _{1.1}
	1	0.67	0.50	0.10	1.4	(CaO) _{0.67} (Na ₂ O) _{0.25} (Al ₂ O ₃) _{0.051} (SiO ₂) ₁ (H ₂ O) _{1.4}
	3	0.75	0.51	0.11	1.7	(CaO) _{0.75} (Na ₂ O) _{0.26} (Al ₂ O ₃) _{0.055} (SiO ₂) ₁ (H ₂ O) _{1.7}
	7	0.71	0.43	0.10	1.7	(CaO) _{0.71} (Na ₂ O) _{0.22} (Al ₂ O ₃) _{0.052} (SiO ₂) ₁ (H ₂ O) _{1.7}
	14	0.71	0.49	0.10	1.7	(CaO) _{0.71} (Na ₂ O) _{0.25} (Al ₂ O ₃) _{0.05} (SiO ₂) ₁ (H ₂ O) _{1.7}
	28	0.68	0.58	0.09	1.6	(CaO) _{0.68} (Na ₂ O) _{0.29} (Al ₂ O ₃) _{0.047} (SiO ₂) ₁ (H ₂ O) _{1.6}
	90	0.67	0.51	0.09	1.6	(CaO) _{0.67} (Na ₂ O) _{0.26} (Al ₂ O ₃) _{0.046} (SiO ₂) ₁ (H ₂ O) _{1.6}
	90*	0.67	0.45	0.10	1.6	(CaO) _{0.67} (Na ₂ O) _{0.23} (Al ₂ O ₃) _{0.050} (SiO ₂) ₁ (H ₂ O) _{1.6}
	450*	0.69	0.39	0.10	1.5	(CaO) _{0.69} (Na ₂ O) _{0.20} (Al ₂ O ₃) _{0.049} (SiO ₂) ₁ (H ₂ O) _{1.5}
	1350*	0.64	0.42	0.07	1.4	(CaO) _{0.64} (Na ₂ O) _{0.21} (Al ₂ O ₃) _{0.034} (SiO ₂) ₁ (H ₂ O) _{1.4}
0.8	0.25	0.64	0.17	0.09	1.1	(CaO) _{0.64} (Na ₂ O) _{0.09} (Al ₂ O ₃) _{0.046} (SiO ₂) ₁ (H ₂ O) _{1.1}
	1	0.78	0.75	0.09	1.6	(CaO) _{0.78} (Na ₂ O) _{0.37} (Al ₂ O ₃) _{0.043} (SiO ₂) ₁ (H ₂ O) _{1.6}
	3	0.80	0.70	0.09	1.6	(CaO) _{0.80} (Na ₂ O) _{0.35} (Al ₂ O ₃) _{0.043} (SiO ₂) ₁ (H ₂ O) _{1.6}
	7	0.80	0.50	0.09	1.6	(CaO) _{0.80} (Na ₂ O) _{0.25} (Al ₂ O ₃) _{0.043} (SiO ₂) ₁ (H ₂ O) _{1.6}
	14	0.80	0.61	0.09	1.6	(CaO) _{0.80} (Na ₂ O) _{0.30} (Al ₂ O ₃) _{0.043} (SiO ₂) ₁ (H ₂ O) _{1.6}
	28	0.79	0.56	0.09	1.6	(CaO) _{0.79} (Na ₂ O) _{0.28} (Al ₂ O ₃) _{0.043} (SiO ₂) ₁ (H ₂ O) _{1.6}
	90	0.79	0.57	0.09	1.6	(CaO) _{0.79} (Na ₂ O) _{0.29} (Al ₂ O ₃) _{0.043} (SiO ₂) ₁ (H ₂ O) _{1.6}
	90*	0.81	0.40	0.09	1.7	(CaO) _{0.81} (Na ₂ O) _{0.20} (Al ₂ O ₃) _{0.046} (SiO ₂) ₁ (H ₂ O) _{1.7}
	450*	0.81	0.41	0.09	1.9	(CaO) _{0.81} (Na ₂ O) _{0.21} (Al ₂ O ₃) _{0.045} (SiO ₂) ₁ (H ₂ O) _{1.9}
	1350*	0.81	0.37	0.09	1.7	(CaO) _{0.81} (Na ₂ O) _{0.18} (Al ₂ O ₃) _{0.047} (SiO ₂) ₁ (H ₂ O) _{1.7}
1.0	0.25	0.72	0.10	0.09	1.1	(CaO) _{0.72} (Na ₂ O) _{0.05} (Al ₂ O ₃) _{0.045} (SiO ₂) ₁ (H ₂ O) _{1.1}
	1	0.96	0.39	0.09	1.7	(CaO) _{0.96} (Na ₂ O) _{0.19} (Al ₂ O ₃) _{0.043} (SiO ₂) ₁ (H ₂ O) _{1.7}
	3	0.98	0.42	0.09	2.0	(CaO) _{0.98} (Na ₂ O) _{0.21} (Al ₂ O ₃) _{0.043} (SiO ₂) ₁ (H ₂ O) _{2.0}
	7	0.99	0.44	0.09	1.8	(CaO) _{0.99} (Na ₂ O) _{0.22} (Al ₂ O ₃) _{0.044} (SiO ₂) ₁ (H ₂ O) _{1.8}
	14	0.98	0.49	0.09	1.7	(CaO) _{0.98} (Na ₂ O) _{0.24} (Al ₂ O ₃) _{0.043} (SiO ₂) ₁ (H ₂ O) _{1.7}
	28	0.99	0.44	0.09	1.7	(CaO) _{0.99} (Na ₂ O) _{0.22} (Al ₂ O ₃) _{0.044} (SiO ₂) ₁ (H ₂ O) _{1.7}
	90	0.98	0.57	0.09	1.7	(CaO) _{0.98} (Na ₂ O) _{0.29} (Al ₂ O ₃) _{0.043} (SiO ₂) ₁ (H ₂ O) _{1.7}
	90*	0.99	0.37	0.09	1.8	(CaO) _{0.99} (Na ₂ O) _{0.18} (Al ₂ O ₃) _{0.045} (SiO ₂) ₁ (H ₂ O) _{1.8}
	450*	0.98	0.33	0.08	2.0	(CaO) _{0.98} (Na ₂ O) _{0.16} (Al ₂ O ₃) _{0.040} (SiO ₂) ₁ (H ₂ O) _{2.0}
	1350*	0.99	0.29	0.09	2.0	(CaO) _{0.99} (Na ₂ O) _{0.15} (Al ₂ O ₃) _{0.045} (SiO ₂) ₁ (H ₂ O) _{2.0}
1.2	0.25	0.80	0.15	0.09	1.1	(CaO) _{0.80} (Na ₂ O) _{0.073} (Al ₂ O ₃) _{0.044} (SiO ₂) ₁ (H ₂ O) _{1.1}

Appendix

	1	1.07	0.47	0.09	1.5	(CaO) _{1.07} (Na ₂ O) _{0.23} (Al ₂ O ₃) _{0.044} (SiO ₂) ₁ (H ₂ O) _{1.5}
	3	1.15	0.55	0.08	1.8	(CaO) _{1.15} (Na ₂ O) _{0.27} (Al ₂ O ₃) _{0.042} (SiO ₂) ₁ (H ₂ O) _{1.8}
	7	1.16	0.33	0.08	2.0	(CaO) _{1.16} (Na ₂ O) _{0.17} (Al ₂ O ₃) _{0.040} (SiO ₂) ₁ (H ₂ O) _{2.0}
	14	1.17	0.37	0.08	1.8	(CaO) _{1.17} (Na ₂ O) _{0.18} (Al ₂ O ₃) _{0.040} (SiO ₂) ₁ (H ₂ O) _{1.8}
	28	1.17	0.34	0.08	1.8	(CaO) _{1.17} (Na ₂ O) _{0.17} (Al ₂ O ₃) _{0.040} (SiO ₂) ₁ (H ₂ O) _{1.8}
	90	1.16	0.43	0.08	1.7	(CaO) _{1.16} (Na ₂ O) _{0.21} (Al ₂ O ₃) _{0.039} (SiO ₂) ₁ (H ₂ O) _{1.7}
	90*	1.15	0.21	0.07	2.0	(CaO) _{1.15} (Na ₂ O) _{0.11} (Al ₂ O ₃) _{0.036} (SiO ₂) ₁ (H ₂ O) _{2.0}
	450*	1.18	0.24	0.09	2.4	(CaO) _{1.18} (Na ₂ O) _{0.12} (Al ₂ O ₃) _{0.045} (SiO ₂) ₁ (H ₂ O) _{2.4}
	1350*	1.17	0.15	0.09	1.8	(CaO) _{1.17} (Na ₂ O) _{0.073} (Al ₂ O ₃) _{0.043} (SiO ₂) ₁ (H ₂ O) _{1.8}
	0.25	0.89	0.22	0.09	1.2	(CaO) _{0.89} (Na ₂ O) _{0.11} (Al ₂ O ₃) _{0.045} (SiO ₂) ₁ (H ₂ O) _{1.2}
1.4	1	1.17	0.45	0.09	1.6	(CaO) _{1.17} (Na ₂ O) _{0.23} (Al ₂ O ₃) _{0.045} (SiO ₂) ₁ (H ₂ O) _{1.6}
	3	1.23	0.41	0.09	1.7	(CaO) _{1.23} (Na ₂ O) _{0.21} (Al ₂ O ₃) _{0.046} (SiO ₂) ₁ (H ₂ O) _{1.7}
	7	1.23	0.35	0.09	1.8	(CaO) _{1.23} (Na ₂ O) _{0.18} (Al ₂ O ₃) _{0.045} (SiO ₂) ₁ (H ₂ O) _{1.8}
	14	1.25	0.47	0.09	1.8	(CaO) _{1.25} (Na ₂ O) _{0.23} (Al ₂ O ₃) _{0.044} (SiO ₂) ₁ (H ₂ O) _{1.8}
	28	1.26	0.30	0.09	1.8	(CaO) _{1.26} (Na ₂ O) _{0.15} (Al ₂ O ₃) _{0.045} (SiO ₂) ₁ (H ₂ O) _{1.8}
	90	1.26	0.41	0.09	1.7	(CaO) _{1.26} (Na ₂ O) _{0.21} (Al ₂ O ₃) _{0.046} (SiO ₂) ₁ (H ₂ O) _{1.7}
	90*	1.20	0.25	0.06	1.7	(CaO) _{1.20} (Na ₂ O) _{0.12} (Al ₂ O ₃) _{0.031} (SiO ₂) ₁ (H ₂ O) _{1.7}
	450*	1.28	0.21	0.09	1.8	(CaO) _{1.28} (Na ₂ O) _{0.11} (Al ₂ O ₃) _{0.043} (SiO ₂) ₁ (H ₂ O) _{1.8}
	1350*	1.27	0.13	0.08	1.6	(CaO) _{1.27} (Na ₂ O) _{0.065} (Al ₂ O ₃) _{0.039} (SiO ₂) ₁ (H ₂ O) _{1.6}
		0.25	0.91	0.27	0.09	1.2
1.6	1	1.26	0.51	0.09	1.5	(CaO) _{1.26} (Na ₂ O) _{0.26} (Al ₂ O ₃) _{0.046} (SiO ₂) ₁ (H ₂ O) _{1.5}
	3	1.31	0.46	0.09	1.7	(CaO) _{1.31} (Na ₂ O) _{0.23} (Al ₂ O ₃) _{0.047} (SiO ₂) ₁ (H ₂ O) _{1.7}
	7	1.32	0.47	0.09	1.8	(CaO) _{1.32} (Na ₂ O) _{0.23} (Al ₂ O ₃) _{0.047} (SiO ₂) ₁ (H ₂ O) _{1.8}
	14	1.34	0.37	0.09	1.9	(CaO) _{1.34} (Na ₂ O) _{0.19} (Al ₂ O ₃) _{0.047} (SiO ₂) ₁ (H ₂ O) _{1.9}
	28	1.23	0.39	0.07	2.0	(CaO) _{1.23} (Na ₂ O) _{0.19} (Al ₂ O ₃) _{0.037} (SiO ₂) ₁ (H ₂ O) _{2.0}
	90	1.28	0.35	0.08	1.6	(CaO) _{1.28} (Na ₂ O) _{0.17} (Al ₂ O ₃) _{0.040} (SiO ₂) ₁ (H ₂ O) _{1.6}
	90*	1.29	0.28	0.08	1.7	(CaO) _{1.29} (Na ₂ O) _{0.14} (Al ₂ O ₃) _{0.038} (SiO ₂) ₁ (H ₂ O) _{1.7}
	450*	1.37	0.17	0.08	2.0	(CaO) _{1.37} (Na ₂ O) _{0.084} (Al ₂ O ₃) _{0.042} (SiO ₂) ₁ (H ₂ O) _{2.0}
	1350*	1.34	0.17	0.07	1.8	(CaO) _{1.34} (Na ₂ O) _{0.083} (Al ₂ O ₃) _{0.033} (SiO ₂) ₁ (H ₂ O) _{1.8}

Appendix

Appendix E Secondary phase quantification

Table 17 Secondary phase quantification and mean silica chain length (MCL) of C-S-H samples without and with alkali hydroxide.

Synthesis solution	Ca/Si _{C-S-H}	SiO ₂ amorphous (wt. %)	Portlandite (wt. %)	K ₂ CO ₃ ·1.5H ₂ O (wt. %)	MCL
Ca/Si* = 0.6					
Water	0.75 ^a	10.1			76.1
0.1 M NaOH	0.71	2.22			11.9
0.1 M KOH	0.71	4.84			15.3
0.5 M NaOH	0.70				5.41
0.5 M KOH	0.69	0.42			33.0
1 M NaOH	0.73				
1 M KOH	0.73	1.28			
Ca/Si* = 0.8					
Water	0.88	4.05			26.5
0.1 M NaOH	0.81	1.27			5.50
0.1 M KOH	0.83	0.53			6.99
0.5 M NaOH	0.81				3.82
0.5 M KOH	0.81				7.44
1 M NaOH	0.83				
1 M KOH	0.81				
Ca/Si* = 1.0					
Water	0.98				9.12
0.1 M NaOH	1.00				3.06
0.1 M KOH	1.00				5.11
0.5 M NaOH	1.00				2.46
0.5 M KOH	1.00				3.01
1 M NaOH	0.90 ^b		4.69		
1 M KOH	0.97		0.85	4.65	
Ca/Si* = 1.2					
Water	1.16				3.48
0.1 M NaOH	1.19				2.20
0.1 M KOH	1.19				2.56
0.5 M NaOH	1.19 ^b		0.44		2.24
0.5 M KOH	1.16 ^b		1.42		3.01
1 M NaOH	1.01 ^b		7.83		
1 M KOH	1.16 ^b		2.05		
Ca/Si* = 1.4					
Water	1.30				2.55
0.1 M NaOH	1.34 ^b		1.27		2.22
0.1 M KOH	1.36 ^b		0.75		2.56
0.5 M NaOH	1.25 ^b		6.09		2.31
0.5 M KOH	1.21 ^b		7.21		2.80
1 M NaOH	1.02 ^b		14.9		
1 M KOH	1.16 ^b		9.70		
Ca/Si* = 1.6					
Water	1.44 ^b				2.56
0.1 M NaOH	1.44 ^b		5.27		2.30
0.1 M KOH	1.48 ^b		3.72		2.47
0.5 M NaOH	1.35 ^b		9.87		2.26
0.5 M KOH	1.22 ^b		12.8		2.64
1 M NaOH	1.07 ^b		20.3		
1 M KOH	1.17 ^b		15.8		

* Amorphous SiO₂ and MCL quantified from ²⁹Si NMR. Portlandite quantified by TGA.

Appendix

Table 18 Solid phase assemblages of the C-(N,K)-A-S-H samples, as determined by XRD / Rietveld analysis. The estimated absolute error is ± 2 wt.%.

synthesis solution	time (months)	target Al/Si	C-(N,K)-A-S-H (wt.%)	CH (wt.%)	C ₃ AH ₆ (wt.%)	C ₂ ASH ₈ (wt.%)	Hc (wt.%)	Mc (wt.%)
0.1M NaOH	12	0	100					
	15	0.05	100					
	15	0.1	98.8		1.2			
	15	0.15	96.0		2.0	2.0		
	15	0.2	87.8		7.0	5.2		
0.5M NaOH	12	0	100					
	15	0.05	100					
	15	0.1	98.4		1.1			0.4
	15	0.15	94.6		2.5		0.5	2.3
	15	0.2	98.1		1.9			
1M NaOH	12	0	100					
	15	0.05	98.8		1.2			
	15	0.1	99.4		0.6			
	15	0.15	96.4	0.3			1.6	1.7
	15	0.2	99.0		1.0			
0.1M NaOH	3	0	100					
	3	0.05	100					
	3	0.1	98.7		1.3			
	3	0.15	97.5	0.6	1.9			
	3	0.2	88.3		3.9	7.9		
0.5M NaOH	3	0	100					
	3	0.05	100					
	3	0.1	99.3				0.7	
	3	0.15	98.5		1.1		0.4	
	3	0.2	96.2		1.4	2.4		
1M NaOH	3	0	100					
	3	0.05	100					
	3	0.1	99.3	0.5			0.3	
	3	0.15	98.4	0.9			0.2	0.5
	3	0.2	97.0	0.8	0.3		0.6	1.4
0.5M KOH	3	0	100					
	3	0.01	100					
	3	0.03	100					
	3	0.05	100					
	3	0.1	100					
	3	0.15	100					
	3	0.2	97.2		0.9			1.9

Appendix

Table 19. Solid phase assemblages of the C-(N,K)-A-S-H samples, as determined by TGA and XRD Rietveld analysis. The estimated absolute error is ± 2 wt.%. C-A-S-H equilibrated for 0.25-90 days: synthesized with water/solid = 45, C-A-S-H equilibrated for 90, 450* and 1350* days: synthesized with water/solid = 40.*

Equilibration time (days)	target Ca/Si ratio	C-A-S-H (wt.%)	CH (wt.%)	C ₃ AH ₆ (wt.%)	Hc (wt.%)	Mc (wt.%)	Gismondine-P1 (wt.%)
0.25	0.6	96.5	3.5				
	0.8	91.8	8.2				
	1.0	86.9	13.1				
	1.2	82.6	17.0	0.4			
	1.4	79.4	20.6				
	1.6	74.5	25.5				
1	0.6	98.6	0.9	0.5			
	0.8	98.9		1.1			
	1.0	98.0	1.0	1.0			
	1.2	94.6	4.5	0.9			
	1.4	91.2	8.4	0.4			
	1.6	87.6	12.2	0.3			
3	0.6	99.3		0.7			
	0.8	99.0		1.0			
	1.0	99.1		0.9			
	1.2	97.8	0.8	1.3			
	1.4	93.3	6.2	0.5			
	1.6	89.8	9.9	0.3			
7	0.6	99.3		0.7			
	0.8	99.1		0.9			
	1.0	99.2		0.8			
	1.2	98.0	0.3	1.7			
	1.4	93.9	5.5	0.7			
	1.6	90.5	9.2	0.3			
14	0.6	98.7		1.3			
	0.8	99.1		0.9			
	1.0	99.0		1.0			
	1.2	98.2		1.8			
	1.4	94.3	4.9	0.8			
	1.6	91.2	8.5	0.3			
28	0.6	98.5		1.5			
	0.8	99.1		0.9			
	1.0	99.1		0.9			
	1.2	98.2		1.8			
	1.4	94.8	4.4	0.8			
	1.6	86.0	11.1	0.4	0.3	2.2	
90	0.6	98.5		1.5			
	0.8	99.1		0.9			
	1.0	99.0		1.0			
	1.2	97.8		2.2			
	1.4	94.7	4.6	0.7			
	1.6	87.9	9.9	0.3	0.1	1.8	
90*	0.6	100.0					
	0.8	100.0					
	1.0	99.3			0.7		
	1.2	97.2	0.0	2.1	0.7		
	1.4	90.2	5.0	1.3	1.7	1.9	
	1.6	87.4	9.3	0.0		3.3	
450*	0.6	99.8		0.2			
	0.8	100.0					

Appendix

	1.0	98.3		1.3	0.4	
	1.2	99.0		0.3	0.7	
	1.4	95.0	3.1	0.4	1.5	
	1.6	91.5	6.4	0.5	1.6	
	0.6	92.0	2.0	1.0		5.1
	0.8	100.0	0.0			
	1.0	99.2		0.8		
	1.2	98.0			2.0	
	1.4	93.6	3.4	0.4	2.6	
1350*	1.6	88.7	7.1	1.0	3.3	

Appendix

Appendix F Silicate main chain length and Q¹ species determined by FTIR, Raman and ²⁹Si NMR

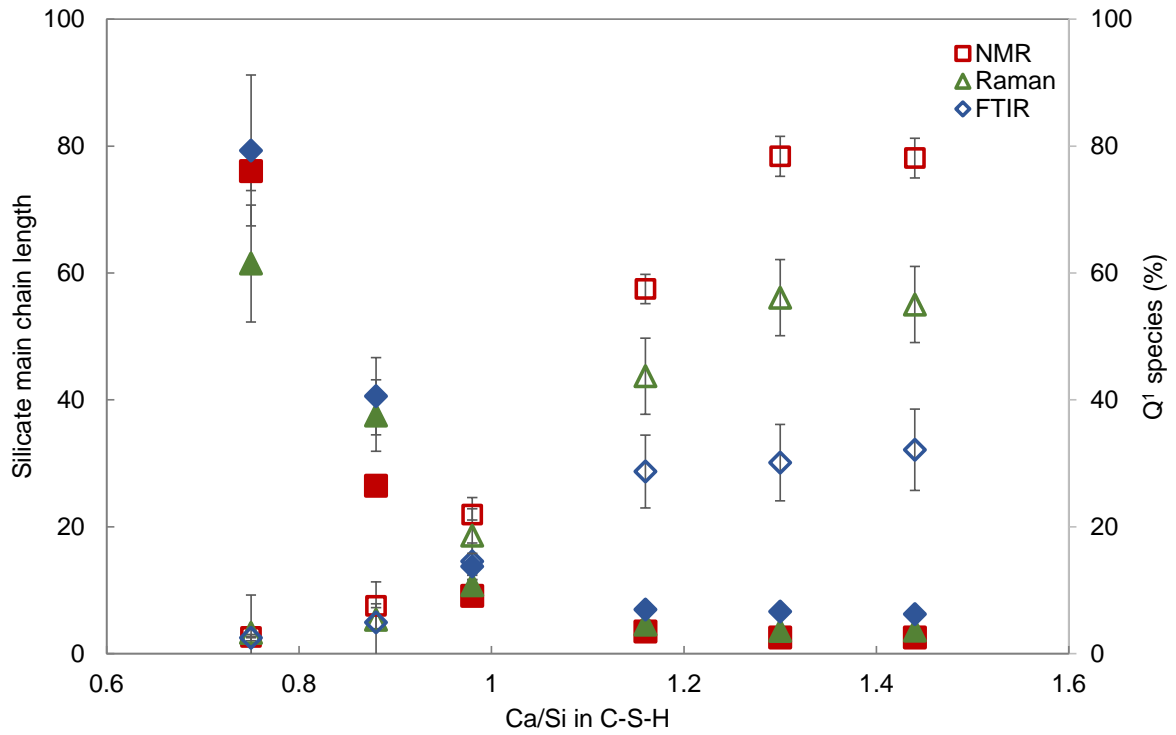


Figure 43. Silicate main chain length and Q¹ species determined by FTIR, Raman and ²⁹Si NMR. Filled symbols: silicate main chain length, empty symbols: Q¹ species

Appendix

Appendix G FTIR and Raman spectra of C-(N,K-)S-H and C-N-(A-)S-H

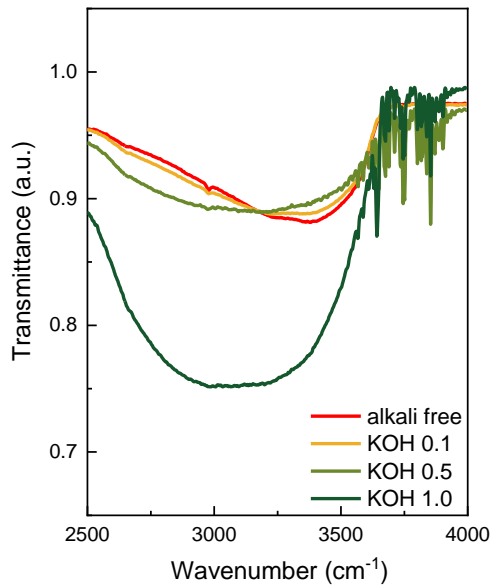


Figure 44. FTIR spectra water region of C-(N,K-)S-H with target $Ca/Si=1.2$ after an equilibration time of 3 months at different KOH concentrations

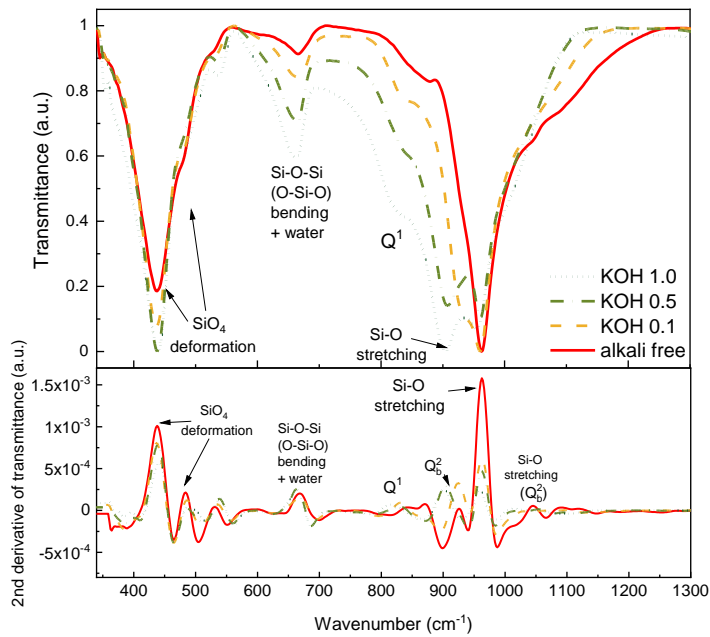


Figure 45. FTIR spectra of C-(N,K-)S-H with $Ca/Si_{target} = 0.6$ after an equilibration time of 3 months at different KOH concentrations

Appendix

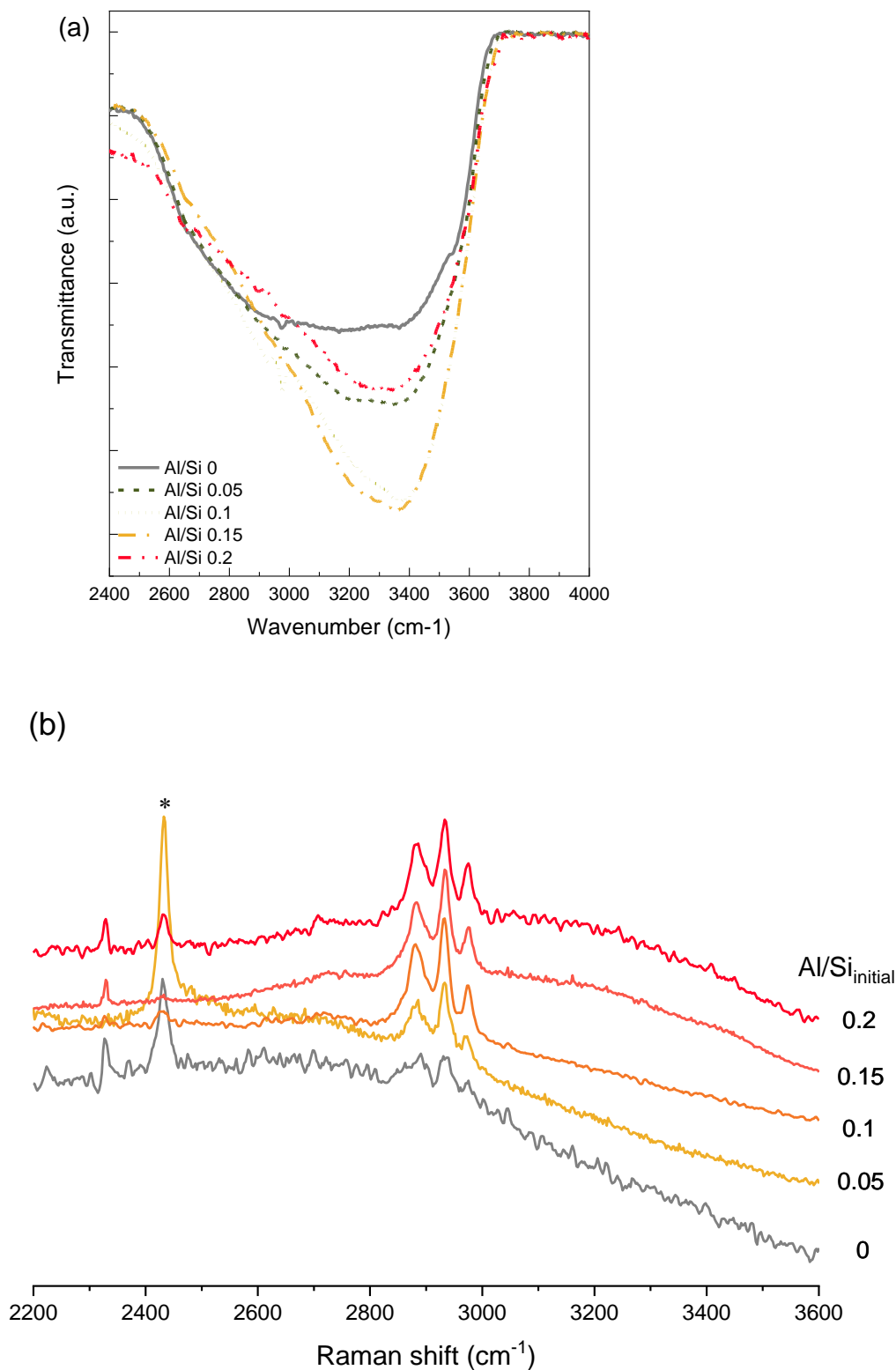


Figure 46. (a) FTIR -OH region and (b) Raman -OH region of C-N-(A-)S-H with target Ca/Si=1.0 after an equilibration time of 1 year with different initial Al/Si, synthesized in 0.5 M NaOH. Three FTIR peaks are observed at 2881, 2933 and 2975 cm⁻¹ corresponding to symmetric C-H stretching modes, $\nu_s(\text{CH}_2)$, $\nu_s(\text{CH}_3)$, and $\nu'_s(\text{CH}_3)$ of ethanol molecules [149] on the surface which were not removed during freeze-drying. A Raman peak at 2432 cm⁻¹ increasing with the intensity of peak at 477 cm⁻¹, which could indicate the presence of ethanol or water molecules captured in a 4-membered ring.

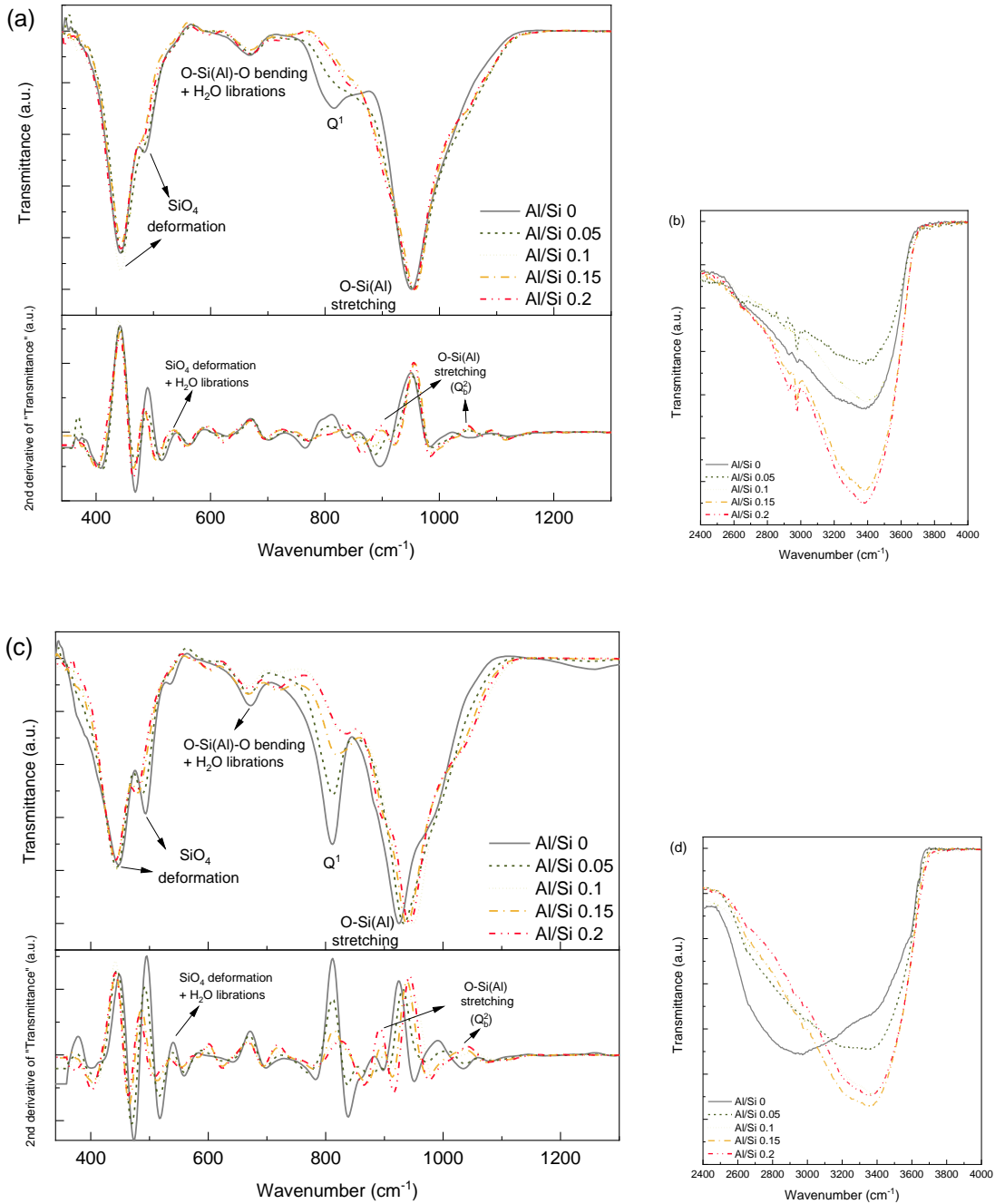
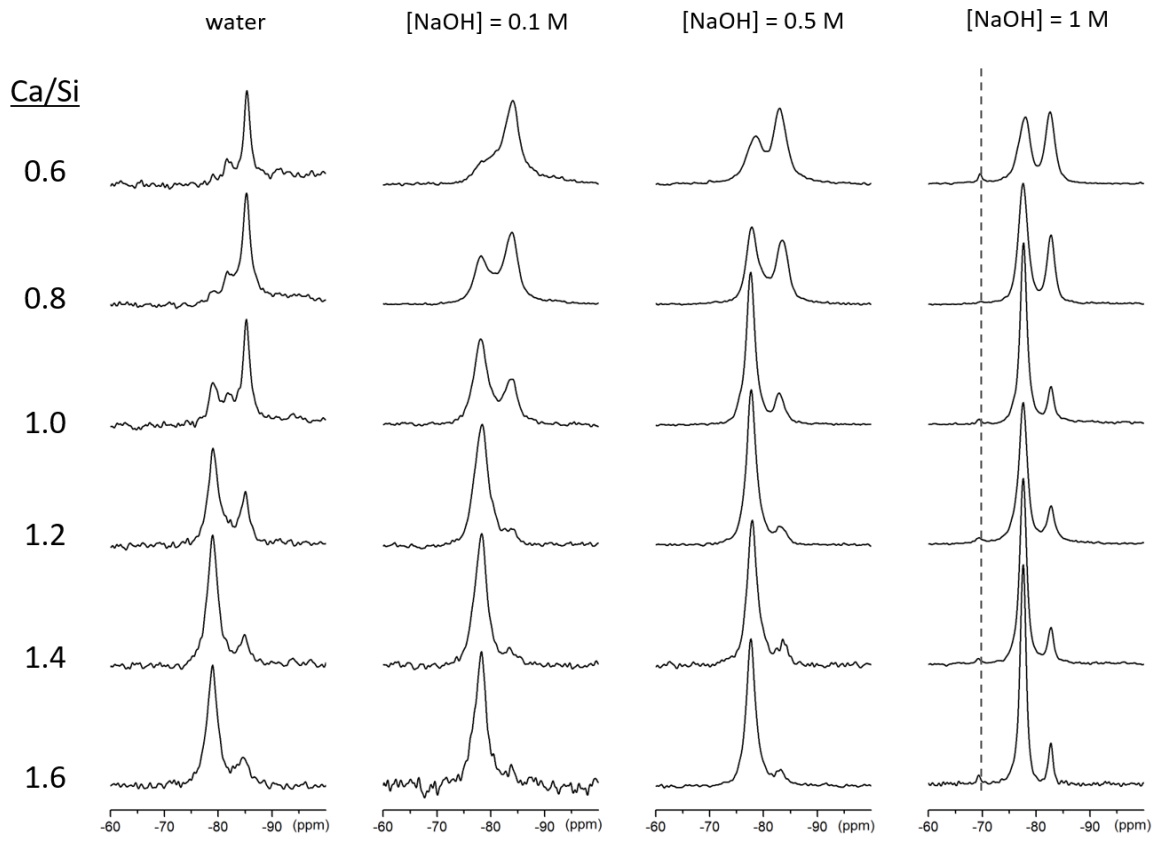


Figure 47. FTIR and second derivative of C-N-(A-)S-H with target Ca/Si=1.0 after an equilibration time of 1 year with different initial Al/Si, synthesized in (a), (b) 0.1 M NaOH, and (c), (d) 1 M NaOH. Normalized to the most intensive band at $\sim 970\text{ cm}^{-1}$.

Appendix

Appendix H NMR spectra



Appendix

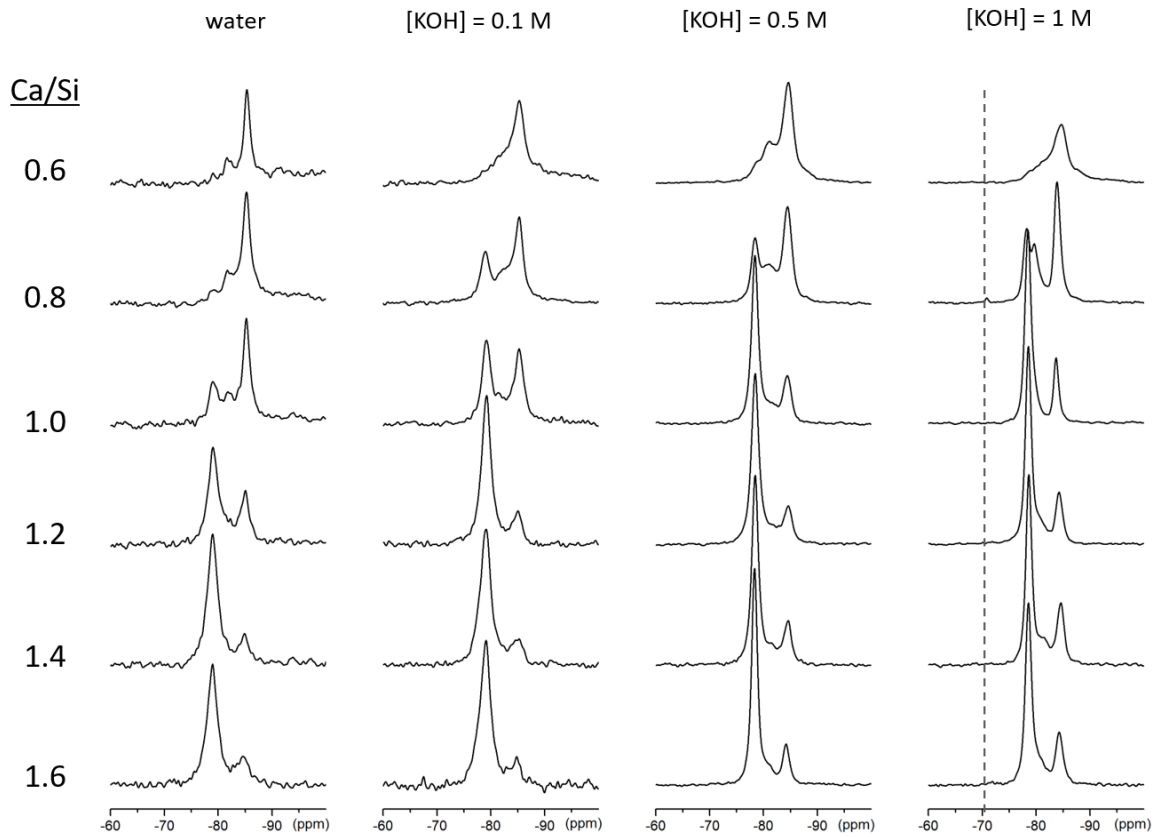
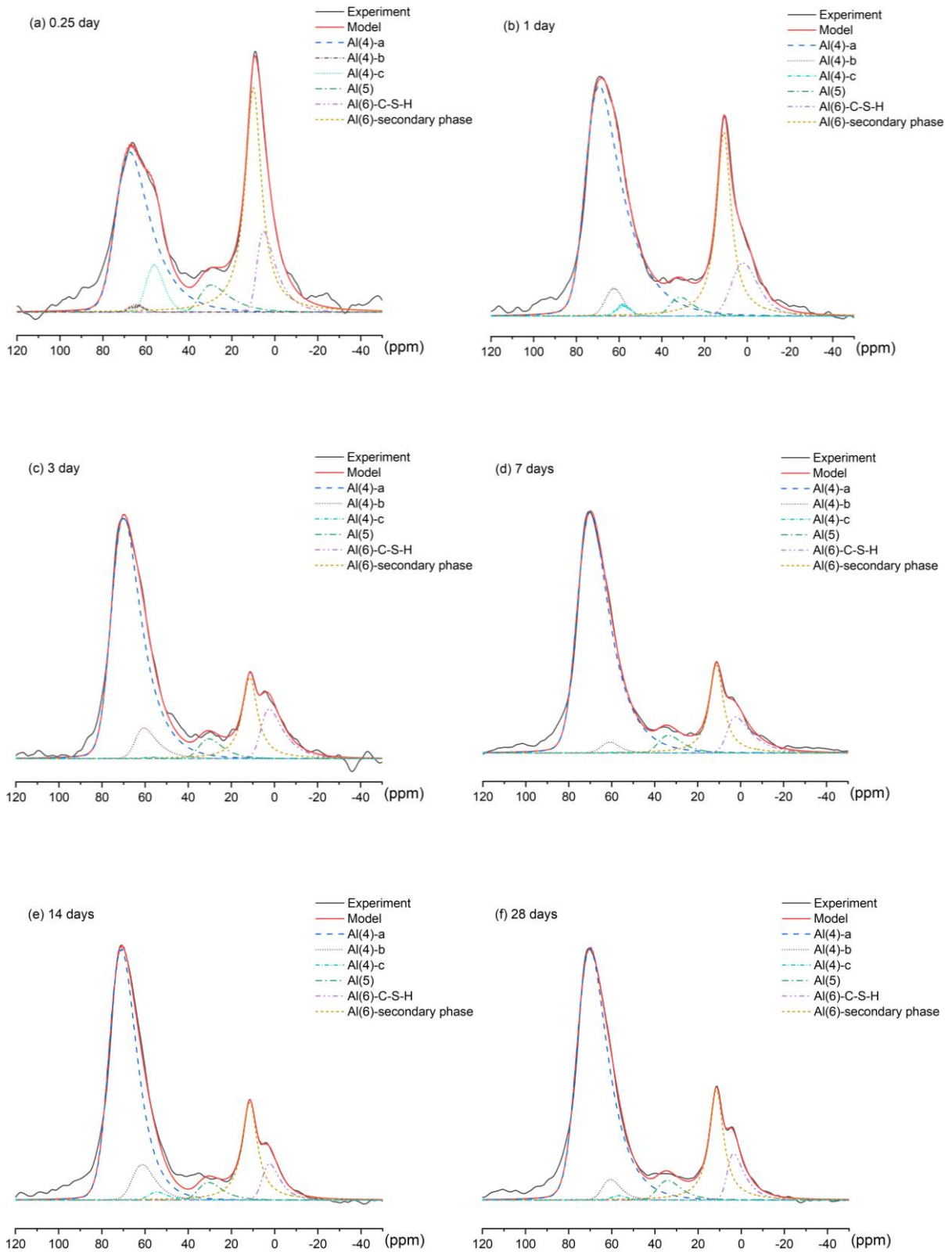


Figure 48. ^{29}Si NMR spectra of C-(N,K)-S-H synthesized in different NaOH and concentrations after an equilibration time of 3 months. The dashed line located at ~ -70 ppm indicates the Q^0 signal.

Appendix



Appendix

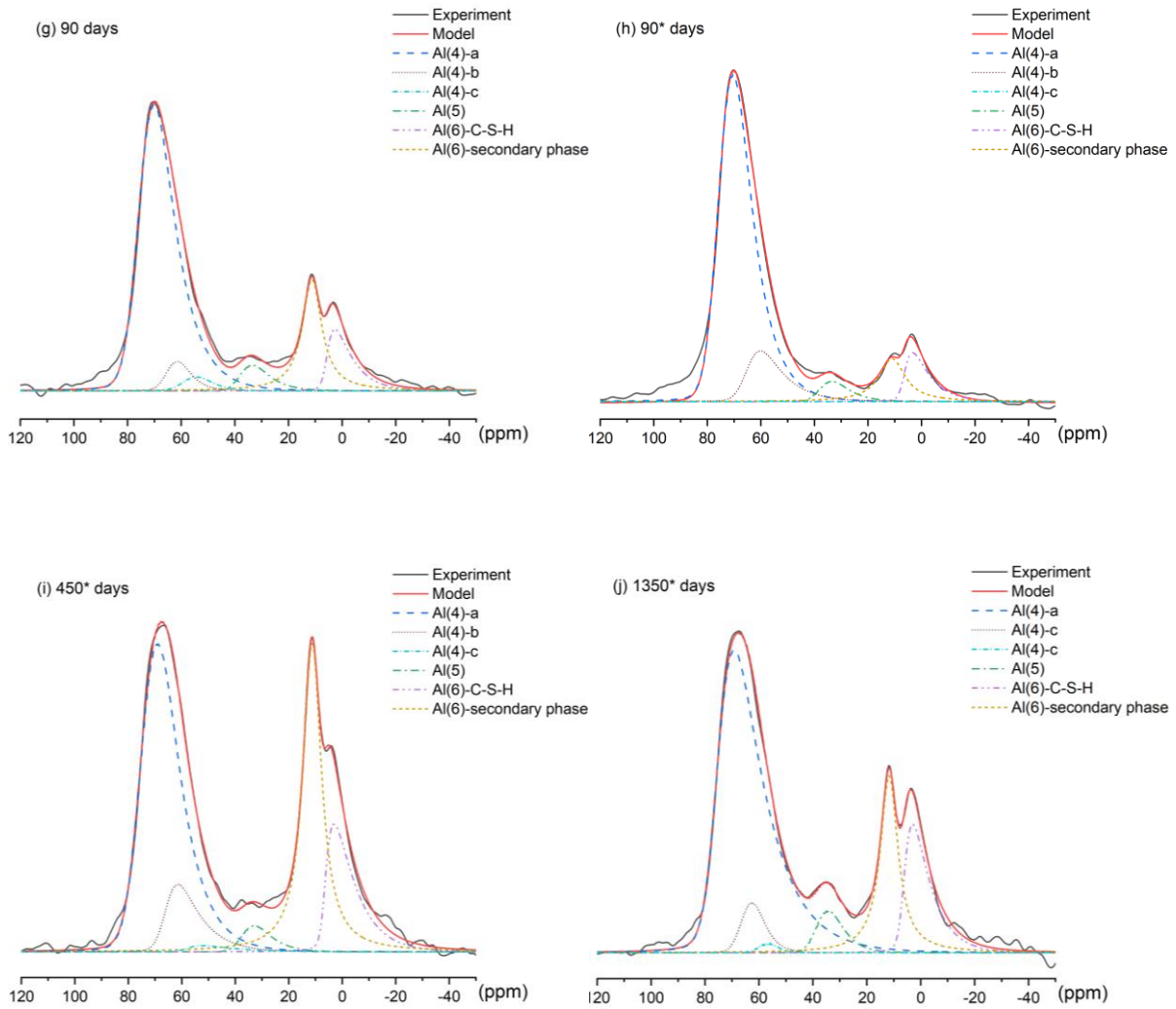


Figure 49. Detailed ^{27}Al NMR deconvolution result in C-A-S-H with Ca/Si 1.0 equilibrated from 0.25 day to 1350 days (target Al/Si = 0.1). C-A-S-H equilibrated for 0.25- 90 days: synthesized with water/solid = 45, C-A-S-H equilibrated for 90*, 450* and 1350* days: synthesized with water/solid = 40.

Appendix

Appendix I Pawley fits of the tobermorite 11 Å and 14 Å (for 1.0 M KOH) model to the C-(N,K-)S-H

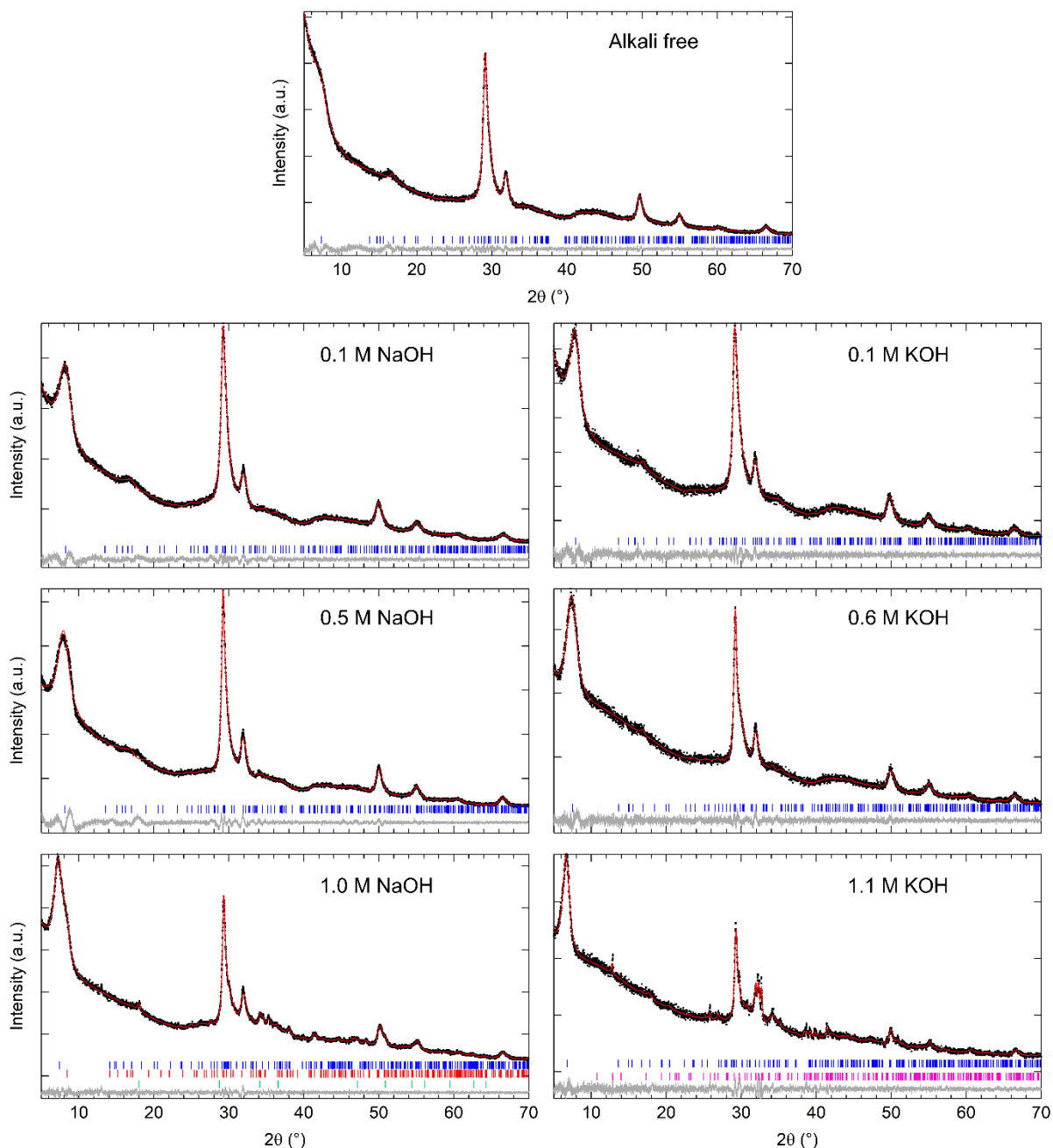


Figure 50. Pawley fits of the tobermorite 11 Å and 14 Å (for 1.0 M KOH) model to the C-(N,K-)S-H powder patterns with $\text{Ca}/\text{Si}_{\text{target}} = 1.0$. Experimental data are shown as black points, red line as the fit, grey line the data-fit curve, and the blue hkl tick marks for tobermorite reflections. In the case of 1.1 M KOH, an additional impurity phase of $\text{K}_2\text{CO}_3 \cdot 1.5\text{H}_2\text{O}$ (PDF# 00-011-0655) was present, which was Rietveld refined with the pink hkl tick marks indicating the reflections. For the 1.0 M NaOH synthesis condition, two reflections are visible for the first diffraction peak, therefore two tobermorite 11 Å models were used to fit the data (shown by the blue and red hkl tick marks). These have different c-axis and crystallite size along the c-direction parameters, but all other parameters are kept equal between the two phases. In addition, the portlandite impurity phase was present and was Rietveld refined with the green hkl tick marks indicating the reflection positions.

Appendix J XRD and TGA

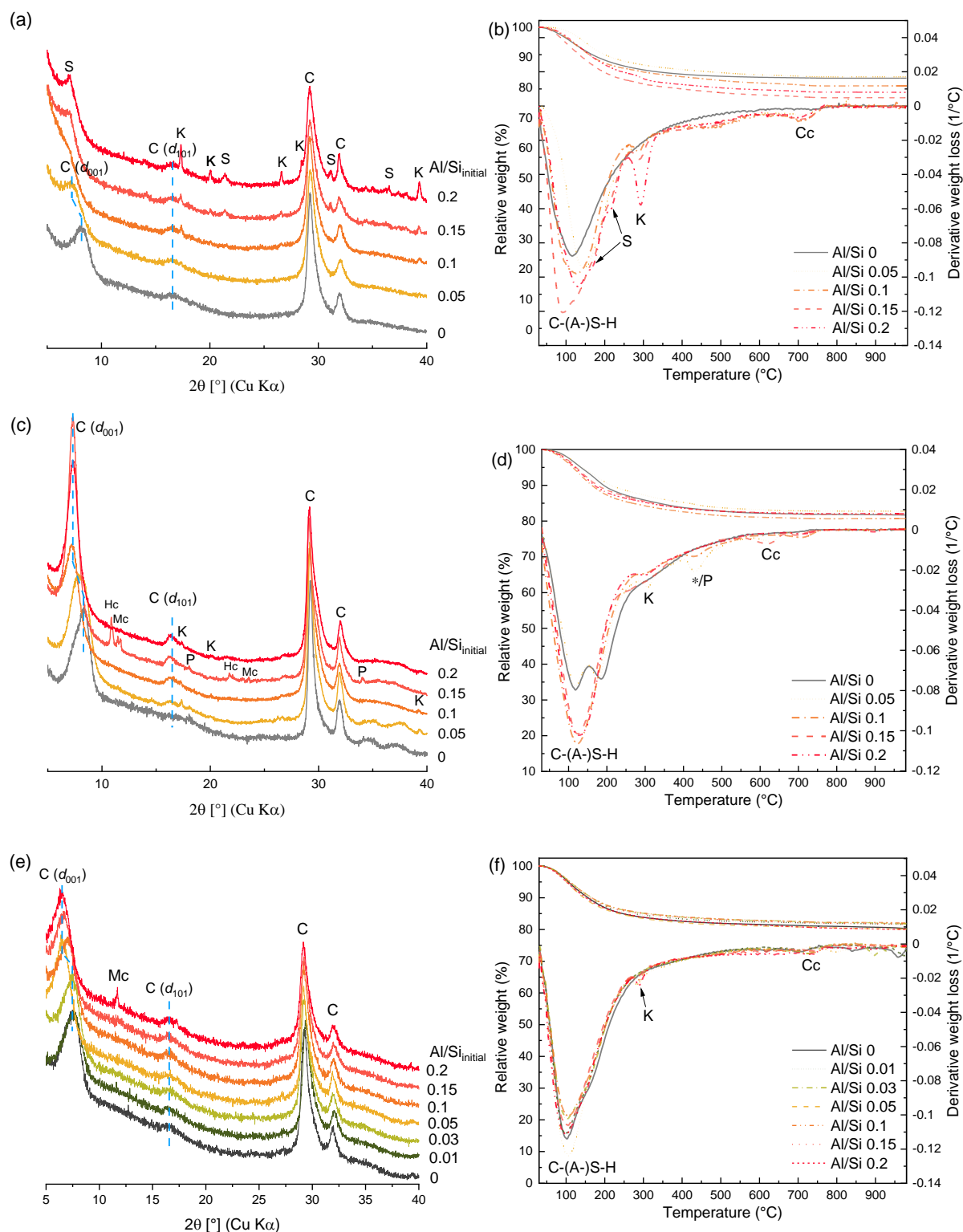


Figure 51 XRD and TGA of C-N,K-(A-)S-H with target Ca/Si=1.0 and different initial Al/Si, synthesized in (a), (b) NaOH 0.1 M; (c), (d) NaOH 1 M, equilibrated for 1 year; (e), (f) KOH 0.5 M, equilibrated for 3 months. S: strätlingite ($\text{Ca}_2\text{Al}((\text{AlSi})_{1.1}\text{O}_2)(\text{OH})_{12}(\text{H}_2\text{O})_8$, PDF# 00-041-0221), K: katoite ($\text{Ca}_3\text{Al}_2(\text{OH})_6$, PDF# 00-024-0217), P: portlandite ($\text{Ca}(\text{OH})_2$, PDF# 00-004-733), Hc: Hemicarbonate ($\text{Ca}_4\text{Al}_2(\text{OH})_{12}(\text{OH})(\text{CO}_3)_{0.5}(\text{H}_2\text{O})_5$, PDF# 00-029-0285), Mc: monocarbonate ($\text{Ca}_4\text{Al}_2(\text{OH})_{12}(\text{OH})(\text{CO}_3)(\text{H}_2\text{O})_5$, PDF# 00-029-0285), Cc: Carbonates. */P: The weight loss at around 450 °C in (d) is tentatively assigned to C-N-A-S-H and/or portlandite. The d_{001} reflections of Al/Si_{target} = 0.15 and 0.2, NaOH 0.1 M are hidden because of the overlap with strätlingite.

Appendix

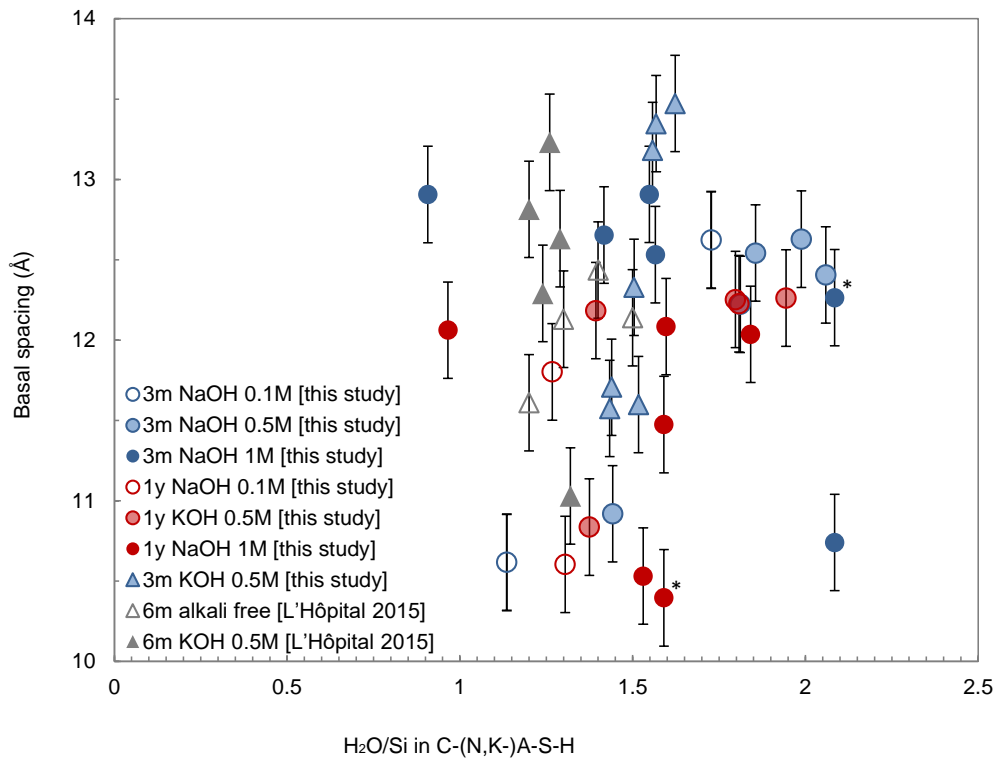


Figure 52. Variation of the mean basal spacing as a function of the H₂O/Si in C-(N,K-)A-S-H with Ca/Si_{target} at 1.0.

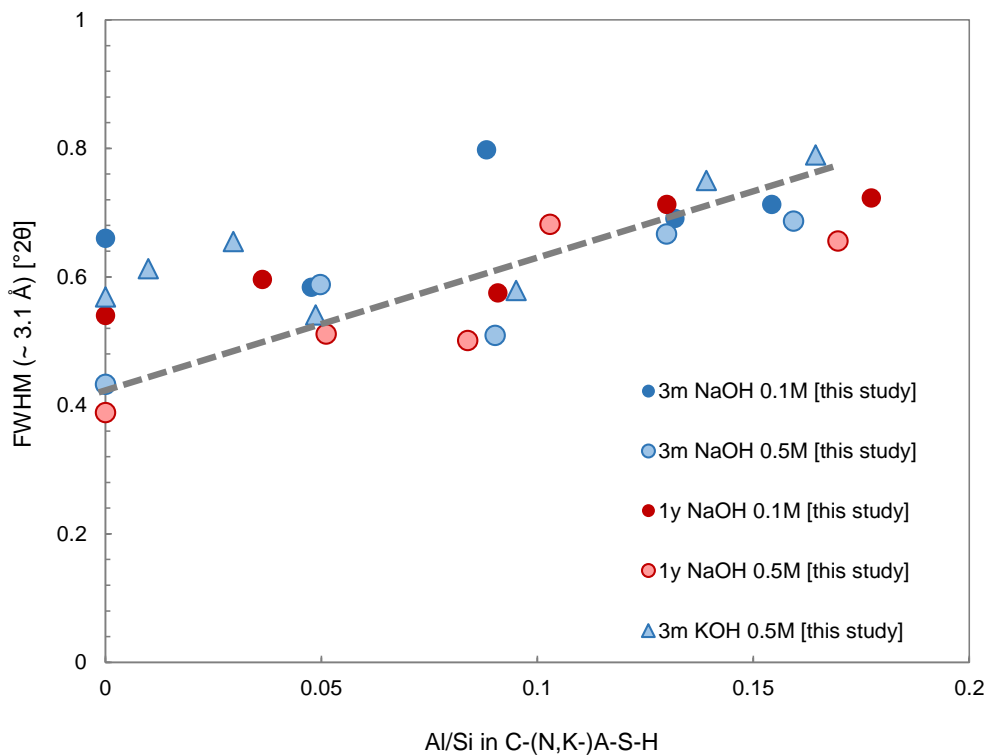


Figure 53. FWHM (~ 3.1 Å) vs Al/Si in C-A-S-H. A weak increase of the FWHM (full width at half maximum) of the main peak at ~ 3.1 Å (~ 29° 2θ Cu Kα) is observed with the Al/Si in C-S-H. Several different signals contribute to the peak at ~ 3.1 Å: 020, -220, 2-22, 022[100]. The broadening of this peak could indicate a growth of the silicate layer and/or a more disordered structure in the presence of more Al.

Appendix

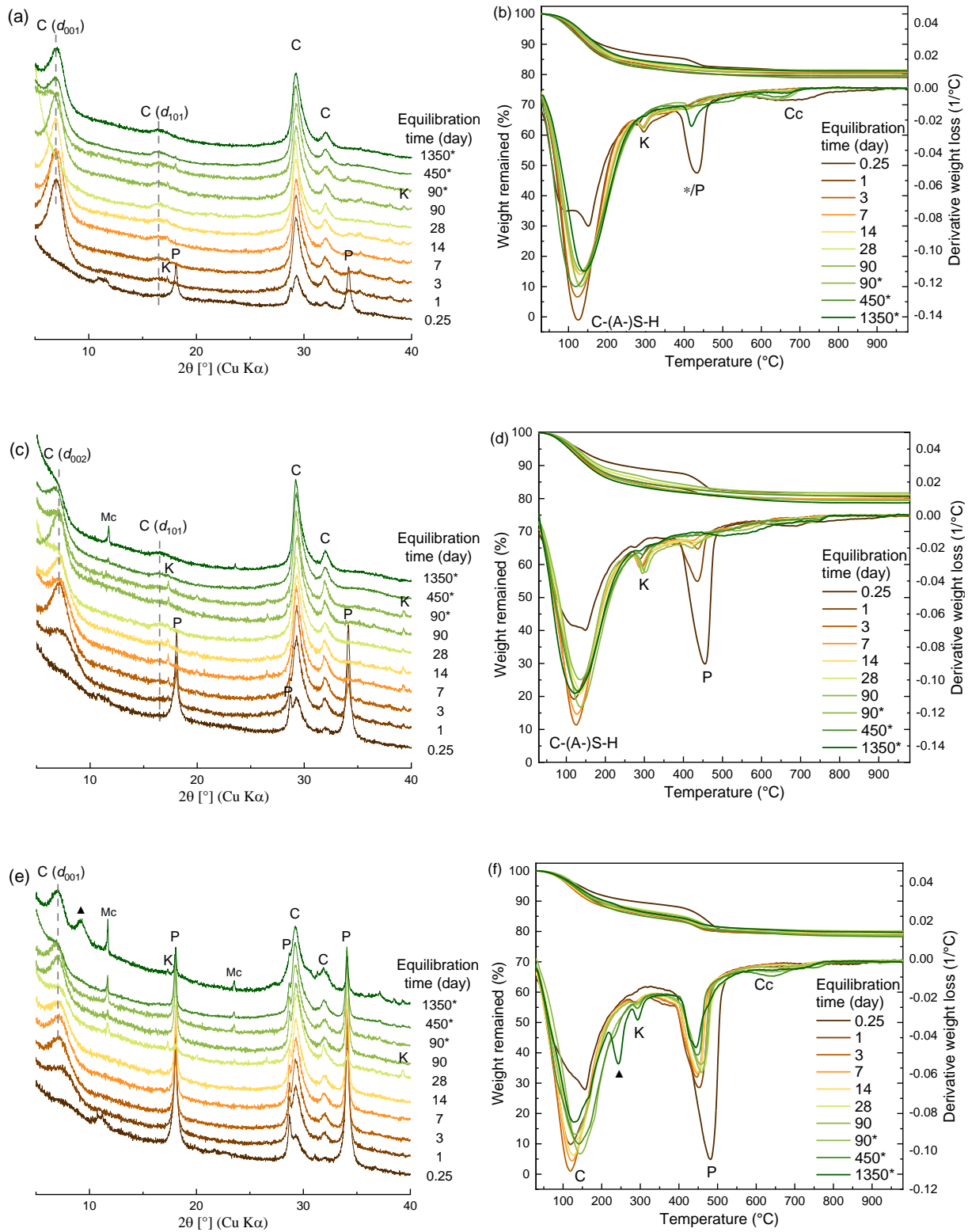


Figure 54 XRD and TGA of C-A-S-H with (a) and (b) target Ca/Si=0.8, (c) and (d) target Ca/Si=1.2, (e) and (f) target Ca/Si=1.6 synthesized in NaOH 0.5 M with initial Al/Si 0.1, equilibrated for different time from 0.25 day to 1350 day. C: C-N,K-(A-)S-H, K: katoite ($\text{Ca}_3\text{Al}_2(\text{OH})_6$, PDF# 00-024-0217), Hc: Hemicarbonate ($\text{Ca}_4\text{Al}_2(\text{OH})_{12}(\text{OH})(\text{CO}_3)_{0.5}(\text{H}_2\text{O})_5$, PDF# 00-029-0285), Mc: monocarbonate ($\text{Ca}_4\text{Al}_2(\text{OH})_{12}(\text{OH})(\text{CO}_3)(\text{H}_2\text{O})_5$, PDF# 00-029-0285), Cc: carbonates. ▲: unidentified phase.

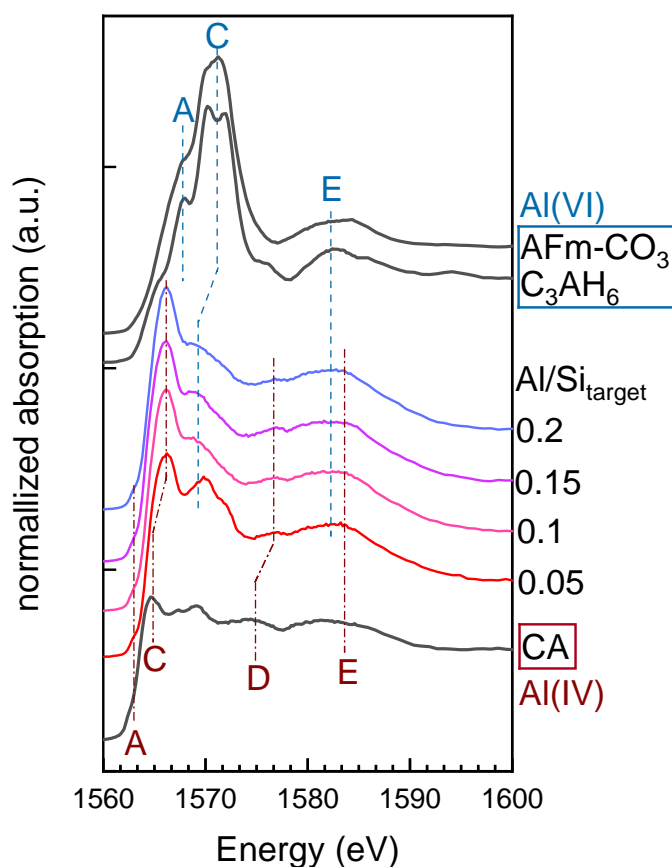


Figure 55. Al K-edge XANES spectra for C-A-S-H with different initial Al/Si synthesized in NaOH 1 M and reference spectra for CA, C_3AH_6 and CO_3 -AFm.

Table 20 Indicators of theoretical error functions. IND_n shows at $n = 2$ a minimum, indicating that only 2 components are responsible for the variation of the spectra; RPV_n and RE_n drop down rapidly and level off above at $n = 3$, and thus the system contains 3 components; IE_n fails to show a inflection point for a minimum and thus to indicate the number of components.

n	RE_n	IE_n	XE_n	IND_n	RPV_n
1	0.01055	0.00431	0.00963	0.00042	2.37323
2	0.00150	0.00086	0.00122	0.00009	0.03831
3	0.00098	0.00069	0.00069	0.00011	0.01230
4	0.00044	0.00036	0.00015	0.00011	0.00166
5	0.00027	0.00025	0.00011	0.00027	0.00032

Note: n – number of components, RE_n – real error in data, IE_n – imbedded error, XE_n – extracted error, IND – indicator function, RPV_n – residual percent variance.

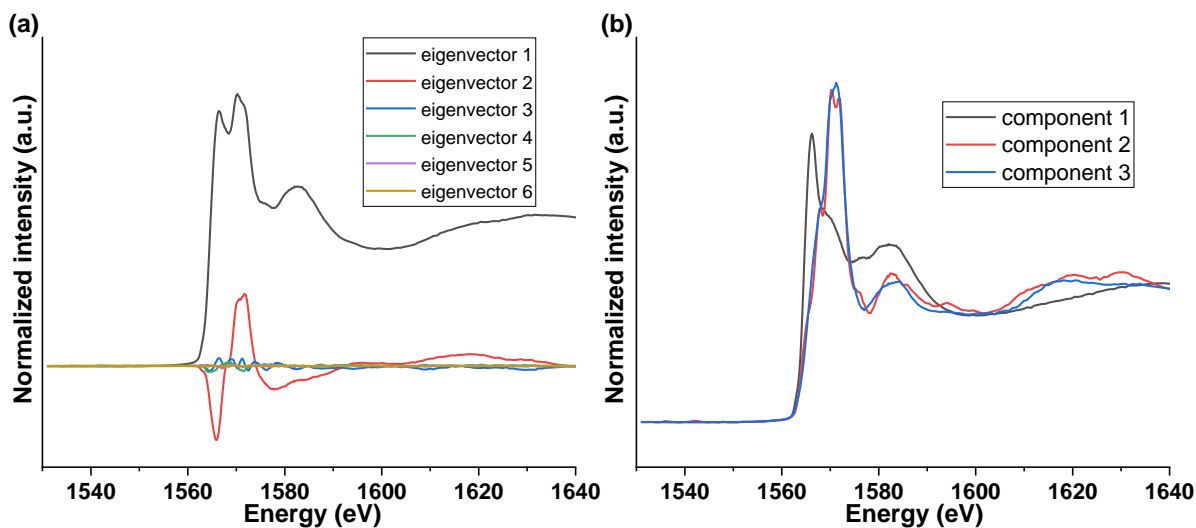


Figure 56. Iterative-target transformation factor analysis (ITFA) of Al K-edge XANES spectra. (a) Abstract spectra of the components from the principal component analysis (PCA), with the first three components displaying “spectrum” features more obviously. It indicates that all spectra can be well reproduced with only three components. (b) The three component spectra calculated with the ITFA code, which are identified as CASH, katoite, and AFm-CO₃ in sequence.

Appendix L Concentrations of Ca, Si and Al in solutions

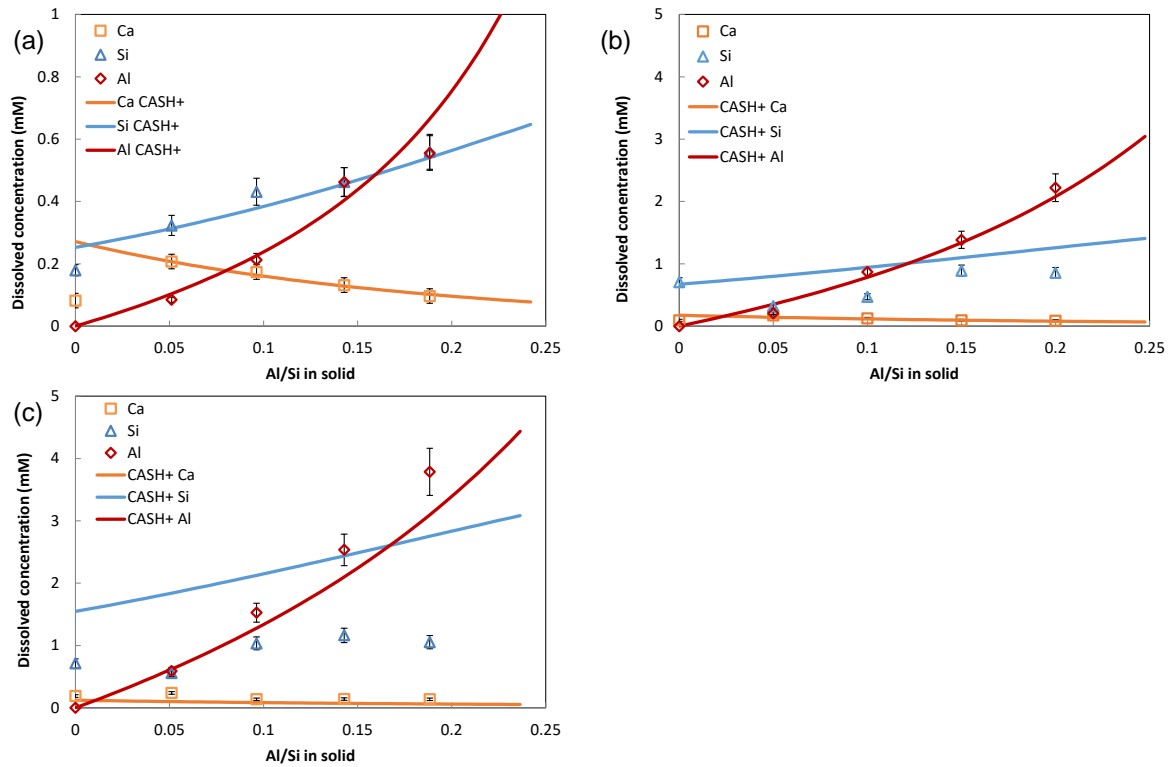


Figure 57. Concentrations of Ca, Si and Al in solutions equilibrated with C-N,K-(A-)S-H samples as a function of Al/Si ratios. C-N,K-(A-)S-H with target Ca/Si=1.0 synthesized in (a) 0.1 M NaOH, (b) 0.5 M NaOH and (c) 1 M NaOH. The equilibration time is 1 year. Orange squares: Ca, blue triangles: Si and red diamonds: Al. The estimated relative uncertainty of the IC measurements is $\pm 10\%$. Lines: simulated using the thermodynamic CASH+ model [61–63]. The thermodynamic model overestimated the Si concentration at 0.5 M and 1 M NaOH.

Appendix

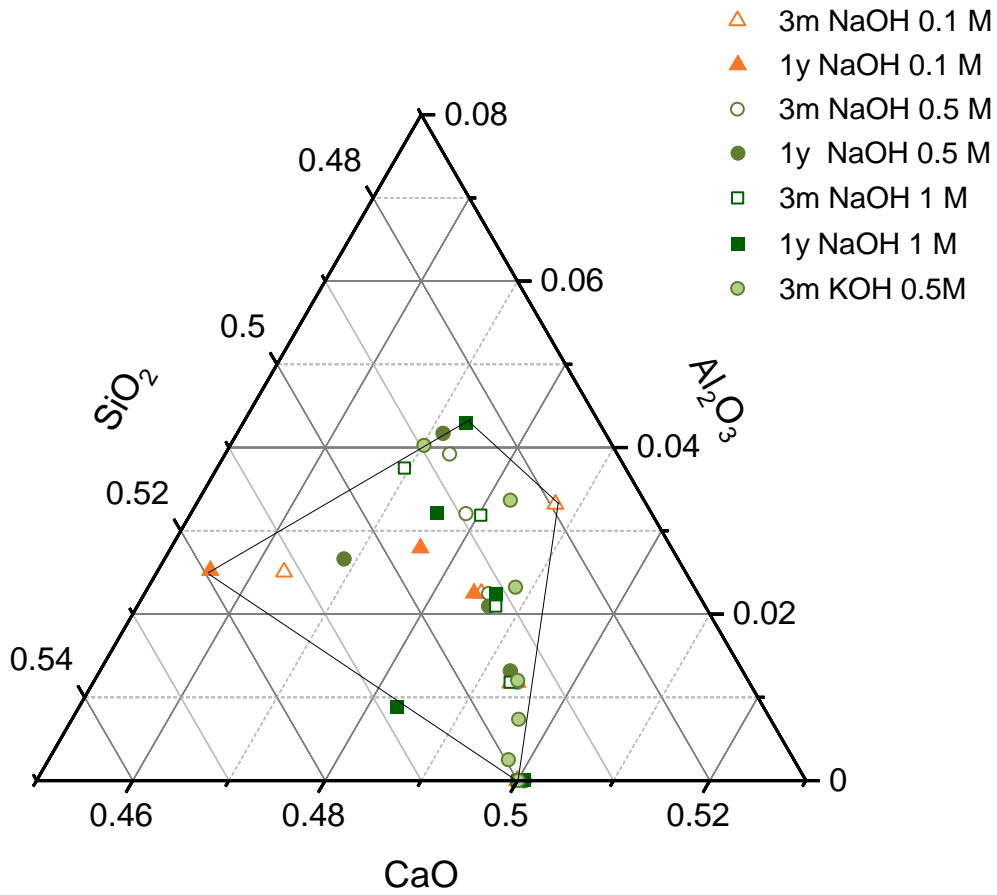


Figure 58. Chemical compositions (units in molar fraction) of the C-N,K-A-S-H products of target Ca/Si at 1.0 and different target Al/Si and with different NaOH or KOH concentration projected in a ternary diagram.

References

- [1] M. Schneider, The cement industry on the way to a low-carbon future, *Cem. Concr. Res.* 124 (2019) 105792.
- [2] The Global Cement Report, 13th ed., Tradeship Publications Ltd, Dorking, 2019.
- [3] IEA, CSI-WBCSD, Technology Roadmap - Low-Carbon Transition in the Cement Industry, Paris, 2018.
- [4] <https://www.mckinsey.com/industries/chemicals/our-insights/laying-the-foundation-for-zero-carbon-cement#>, (2019).
- [5] B. Lothenbach, K. Scrivener, R.D. Hooton, Supplementary cementitious materials, *Cem. Concr. Res.* 41 (2011) 1244–1256.
- [6] M. Ahmaruzzaman, A review on the utilization of fly ash, *Prog. Energy Combust. Sci.* 36 (2010) 327–363.
- [7] I.G. Richardson, Nature of C-S-H in hardened cements, *Cem. Concr. Res.* 29 (1999) 1131–1147.
- [8] A.J. Allen, J.J. Thomas, H.M. Jennings, Composition and density of nanoscale calcium-silicate-hydrate in cement, *Nat. Mater.* 6 (2007) 311–316.
- [9] L.B. Skinner, S.R. Chae, C.J. Benmore, H.R. Wenk, P.J.M. Monteiro, Nanostructure of calcium silicate hydrates in cements, *Phys. Rev. Lett.* 104 (2010) 1–4.
- [10] B. Sabir, S. Wild, J. Bai, Metakaolin and calcined clays as pozzolans for concrete: A review, *Cem. Concr. Compos.* 23 (2001) 441–454.
- [11] M.D. Jackson, S.R. Mulcahy, H. Chen, Y. Li, Q. Li, P. Cappelletti, H.R. Wenk, Phillipsite and Al-tobermorite mineral cements produced through low-temperature water-rock reactions in Roman marine concrete, *Am. Mineral.* 102 (2017) 1435–1450.
- [12] M.D. Jackson, S.R. Chae, S.R. Mulcahy, C. Meral, R. Taylor, P. Li, A.H. Emwas, J. Moon, S. Yoon, G. Vola, H.R. Wenk, P.J.M. Monteiro, Unlocking the secrets of Al-tobermorite in Roman seawater concrete, *Am. Mineral.* 98 (2013) 1669–1687.
- [13] Z. Shi, B. Ma, B. Lothenbach, Effect of Al on the formation and structure of alkali-silica reaction products, *Cem. Concr. Res.* 140 (2021) 106311.
- [14] F. Deschner, F. Winnefeld, B. Lothenbach, S. Seufert, P. Schwesig, S. Dittrich, F. Goetz-Neunhoeffer, J. Neubauer, Hydration of Portland cement with high replacement by siliceous fly ash, *Cem. Concr. Res.* 42 (2012) 1389–1400.
- [15] X. Pardal, F. Brunet, T. Charpentier, I. Pochard, A. Nonat, ²⁷Al and ²⁹Si solid-state NMR characterization of calcium-aluminosilicate-hydrate, *Inorg. Chem.* 51 (2012) 1827–1836.
- [16] J. Skibsted, M.D. Andersen, The effect of alkali ions on the incorporation of aluminum in the calcium silicate hydrate (C-S-H) phase resulting from portland cement hydration studied by ²⁹Si MAS NMR, *J. Am. Ceram. Soc.* 96 (2013) 651–656.
- [17] G.K. Sun, J.F. Young, R.J. Kirkpatrick, The role of Al in C-S-H: NMR, XRD, and compositional results for precipitated samples, *Cem. Concr. Res.* 36 (2006) 18–29.
- [18] B. Lothenbach, A. Nonat, Calcium silicate hydrates: Solid and liquid phase composition, *Cem. Concr. Res.* 78 (2015) 57–70.
- [19] J.J. Chen, J.J. Thomas, H.F.W. Taylor, H.M. Jennings, Solubility and structure of calcium silicate hydrate, 34 (2004) 1499–1519.
- [20] X. Cong, R.J. Kirkpatrick, R. James Kirkpatrick, ²⁹Si MAS NMR study of the structure of calcium

References

- silicate hydrate, *Adv. Cem. Based Mater.* 3 (1996) 144–156.
- [21] I.G. Richardson, The calcium silicate hydrates, *Cem. Concr. Res.* 38 (2008) 137–158.
- [22] I.G. Richardson, J. Skibsted, L. Black, R.J. Kirkpatrick, Characterisation of cement hydrate phases by TEM, NMR and Raman spectroscopy, *Adv. Cem. Res.* 22 (2010) 233–248.
- [23] I.G. Richardson, Model structures for C-(A)-S-H(I), *Acta Crystallogr. Sect. B Struct. Sci. Cryst. Eng. Mater.* 70 (2014) 903–923.
- [24] J. Haas, A. Nonat, From C-S-H to C-A-S-H: Experimental study and thermodynamic modelling, *Cem. Concr. Res.* 68 (2015) 124–138.
- [25] T.F. Sevelsted, J. Skibsted, Carbonation of C-S-H and C-A-S-H samples studied by ^{13}C , ^{27}Al and ^{29}Si MAS NMR spectroscopy, *Cem. Concr. Res.* 71 (2015) 56–65.
- [26] E. L'Hôpital, B. Lothenbach, D.A. Kulik, K. Scrivener, Influence of calcium to silica ratio on aluminium uptake in calcium silicate hydrate, *Cem. Concr. Res.* 85 (2016) 111–121.
- [27] X. Cong, R.J. Kirkpatrick, ^{29}Si and ^{17}O NMR investigation of the structure of some crystalline calcium silica hydrates, *Adv. Cem. Based Mater.* 3 (1996) 133–143.
- [28] G. Renaudin, J. Russias, F. Leroux, C. Cau-dit-Coumes, F. Frizon, Structural characterization of C-S-H and C-A-S-H samples-Part II: Local environment investigated by spectroscopic analyses, *J. Solid State Chem.* 182 (2009) 3320–3329.
- [29] I.G. Richardson, A.R. Brough, R. Brydson, G.W. Groves, C.M. Dobsont, Location of aluminum in substituted calcium silicate hydrate (C-S-H) gels as determined by ^{29}Si and ^{27}Al NMR and EELS, *J. Am. Ceram. Soc.* 9 (1993) 2285–2288.
- [30] K. Garbev, B. Gasharova, P. Stemmermann, A modular concept of crystal structure applied to the thermal transformation of α -C2 SH, *J. Am. Ceram. Soc.* 97 (2014) 2286–2297.
- [31] I. García Lodeiro, A. Fernández-Jimenez, A. Palomo, D.E. Macphee, Effect on fresh C-S-H gels of the simultaneous addition of alkali and aluminium, *Cem. Concr. Res.* 40 (2010) 27–32.
- [32] E. Kapeluszna, Ł. Kotwica, A. Różycka, Ł. Gołek, Incorporation of Al in C-A-S-H gels with various Ca/Si and Al/Si ratio: Microstructural and structural characteristics with DTA/TG, XRD, FTIR and TEM analysis, *Constr. Build. Mater.* 155 (2017) 643–653.
- [33] P. Yu, R.J. Kirkpatrick, B. Poe, P.F. McMillan, X. Cong, Structure of calcium silicate hydrate (C-S-H): near-, mid-, and far-infrared spectroscopy, *J. Am. Ceram. Soc.* 48 (1999) 742–748.
- [34] N.V.N. V. Chukanov, *Infrared Spectra of Mineral Species*, Springer, 2014.
- [35] A. Gruskovnjak, B. Lothenbach, L. Holzer, R. Figi, F. Winnefeld, Hydration of alkali-activated slag: Comparison with ordinary Portland cement, *Advances Cem. Res.* 18 (2006) 119–128.
- [36] R.J. Myers, S.A. Bernal, J.L. Provis, A thermodynamic model for C-(N-)A-S-H gel: CNASH_{ss}. Derivation and validation, *Cem. Concr. Res.* 66 (2014) 27–47.
- [37] Z. Shi, B. Lothenbach, The combined effect of potassium, sodium and calcium on the formation of alkali-silica reaction products, *Cem. Concr. Res.* 127 (2020) 105914.
- [38] J. Lindgård, Ö. Andiç-Çakir, I. Fernandes, T.F. Rønning, M.D.A. Thomas, Alkali-silica reactions (ASR): Literature review on parameters influencing laboratory performance testing, *Cem. Concr. Res.* 42 (2012) 223–243.
- [39] T.T.H. Bach, E. Chabas, I. Pochard, C. Cau Dit Coumes, J. Haas, F. Frizon, A. Nonat, Retention of alkali ions by hydrated low-pH cements: Mechanism and Na^+/K^+ selectivity, *Cem. Concr. Res.* 51 (2013) 14–21.
- [40] S. Barzgar, B. Lothenbach, M. Tarik, A. Di Giacomo, C. Ludwig, The effect of sodium hydroxide

References

- on Al uptake by calcium silicate hydrates (C-S-H), *J. Colloid Interface Sci.* 572 (2020) 246–256.
- [41] E. L'Hôpital, B. Lothenbach, K. Scrivener, D.A.A. Kulik, Alkali uptake in calcium alumina silicate hydrate (C-A-S-H), *Cem. Concr. Res.* 85 (2016) 122–136.
- [42] R.J. Myers, E. L'Hôpital, L. Provis, B. Lothenbach, Composition-solubility-structure relationships in calcium (alkali) aluminosilicate hydrate (C-(N,K)-A-S-H), *Dalt. Trans.* 44 (2015) 13530–13544.
- [43] S. Hong, F.P. Glasser, Alkali binding in cement pastes: Part I. The C-S-H phase, *Cem. Concr. Res.* 29 (1999) 1893–1903.
- [44] H. Stade, On the reaction of C-S-H(di, poly) with alkali hydroxides, *Cem. Concr. Res.* 19 (1989) 802–810.
- [45] S.-Y. Yang, Y. Yan, B. Lothenbach, J. Skibsted, Sodium and tetrahedral aluminium in cementitious calcium-aluminate-silicate hydrate phases (C-A-S-H), *J. Phys. Chem. C.* 125 (2021) 27975–27995.
- [46] A. Kunhi Mohamed, P. Moutzouri, P. Berruyer, B.J. Walder, J. Siramanont, J. Siramanont, M. Harris, M. Negroni, S.C. Galmarini, S.C. Parker, S.C. Parker, K.L. Scrivener, L. Emsley, P. Bowen, The Atomic-Level Structure of Cementitious Calcium Aluminate Silicate Hydrate, *J. Am. Chem. Soc.* 142 (2020) 11060–11071.
- [47] R.J. Myers, E. L'Hôpital, J.L. Provis, B. Lothenbach, Effect of temperature and aluminium on calcium (alumino)silicate hydrate chemistry under equilibrium conditions, *Cem. Concr. Res.* 68 (2015) 83–93.
- [48] E. L'Hôpital, B. Lothenbach, G. Le Saout, D. Kulik, K. Scrivener, E. L'Hôpital, B. Lothenbach, G. Le Saout, D. Kulik, K. Scrivener, Incorporation of aluminium in calcium-silicate-hydrates, *Cem. Concr. Res.* 75 (2015) 91–103.
- [49] X. Pardal, I. Pochard, A. Nonat, Experimental study of Si-Al substitution in calcium-silicate-hydrate (C-S-H) prepared under equilibrium conditions, *Cem. Concr. Res.* 39 (2009) 637–643.
- [50] S. Barzgar, M. Tarik, C. Ludwig, B. Lothenbach, The effect of equilibration time on Al uptake in C-S-H, *Cem. Concr. Res.* 144 (2021) 106438.
- [51] H.F.W. Taylor, *Cement chemistry*, London, 1997.
- [52] T.G. Jappy, F.P. Glasser, Synthesis and stability of silica-substituted hydro garnet $\text{Ca}_3\text{Al}_2\text{Si}_3\text{xO}_{12-4\text{x}}(\text{OH})_{4\text{x}}$, *Adv. Cem. Res.* 4 (1991) 1–8.
- [53] B.Z. Dilnesa, B. Lothenbach, G. Renaudin, A. Wichser, D. Kulik, Synthesis and characterization of hydrogarnet $\text{Ca}_3(\text{Al xFe}_{1-x})_2(\text{SiO}_4)_y(\text{OH})_{4(3-y)}$, *Cem. Concr. Res.* 59 (2014) 96–111.
- [54] B. Lothenbach, G. Le Saout, E. Gallucci, K. Scrivener, Influence of limestone on the hydration of Portland cements, *Cem. Concr. Res.* 38 (2008) 848–860.
- [55] G.A. Lager, T. Armbruster, F.J. Rotella, G.R. Rossman, OH substitution in garnets: X-ray and neutron diffraction, infrared, and geometric-modeling studies, *Am. Mineral.* 74 (1989) 840–851.
- [56] F. Bonk, J. Schneider, M.A. Cincotto, H. Panepucci, Characterization by Multinuclear High-Resolution NMR of Hydration Products in Activated Blast-Furnace Slag Pastes, *J. Am. Ceram. Soc.* 86 (2003) 1712–1719.
- [57] M. Frías, S. Martínez-Ramírez, R. Vigil de la Villa, R. García-Giménez, M.I. Sánchez de Rojas, New scientific evidence of the effect of high temperatures and long curing times on MK-blended cement paste mineralogy, *Cem. Concr. Res.* 152 (2022).
- [58] C.E. Tilley, Hydrocalumite ($4\text{CaO} \cdot \text{Al}_2\text{O}_3 \cdot 12\text{H}_2\text{O}$), a new mineral from Scawt Hill, Co. Antrim, *Mineral. Mag. J. Mineral. Soc.* 23 (1934) 607–615.
- [59] S.A. Bernal, J.L. Provis, V. Rose, R. Mejía De Gutierrez, Evolution of binder structure in sodium

References

- silicate-activated slag-metakaolin blends, *Cem. Concr. Compos.* 33 (2011) 46–54.
- [60] J.L. Provis, G.C. Lukey, J.S.J. van Deventer, Do Geopolymers Actually Contain Nanocrystalline Zeolites? A Reexamination of Existing Results, *Chem. Mater.* 17 (2005) 3075–3085.
- [61] D.A. Kulik, G.D. Miron, B. Lothenbach, A structurally-consistent CASH+ sublattice solid solution model for fully hydrated C-S-H phases: Thermodynamic basis, methods, and Ca-Si-H₂O core sub-model, *Cem. Concr. Res.* 151 (2022) 106585.
- [62] G.D. Miron, D.A. Kulik, Y. Yan, J. Tits, B. Lothenbach, Extensions of CASH+ thermodynamic solid solution model for the uptake of alkali metals and alkaline earth metals in C-S-H, *Cem. Concr. Res.* 152 (2022) 106667.
- [63] G.D. Miron, D.A. Kulik, B. Lothenbach, S. Barzgar, E. Wieland, B. Lothenbach, Extensions of CASH+ thermodynamic solid solution model for the uptake of aluminium and iron in C-S-H. in preparation, 2022.
- [64] E. Bernard, Y. Yan, B. Lothenbach, Effective cation exchange capacity of calcium silicate hydrates (C-S-H), *Cem. Concr. Res.* 143 (2021) 106393.
- [65] B. Lothenbach, D. Jansen, Y. Yan, J. Schreiner, Solubility and characterization of synthesized Al-tobermorite, *Cem. Concr. Res.* in review (2022).
- [66] B. Traynor, H. Uvegi, E. Olivetti, B. Lothenbach, R.J. Myers, Methodology for pH measurement in high alkali cementitious systems, *Cem. Concr. Res.* 135 (2020) 106122.
- [67] B. Lothenbach, P. Durdzinski, K. De Weerd, Thermogravimetric analysis, in: K.L. Scrivener, R. Snellings, B. Lothenbach (Eds.), *A Pract. Guid. to Microstruct. Anal. Cem. Mater.*, CRC Press, Oxford, UK, 2016: pp. 177–212.
- [68] S.T. Merlino, E.L. Bonaccorsi, T.H. Armbruster, The real structure of tobermorite 11 Å : normal and anomalous forms , OD character and polytypic modifications, *Eur. J. Mineral.* 13 (2001) 577–590.
- [69] A.A. Coelho, TOPAS and TOPAS-Academic: An optimization program integrating computer algebra and crystallographic objects written in C++: *An, J. Appl. Crystallogr.* 51 (2018) 210–218.
- [70] E. Bonaccorsi, S. Merlino, A.R. Kampf, The crystal structure of tobermorite 14 Å (plombierite), a C-S-H phase, *J. Am. Ceram. Soc.* 88 (2005) 505–512.
- [71] D. Ectors, F. Goetz-Neunhoffer, J. Neubauer, A generalized geometric approach to anisotropic peak broadening due to domain morphology, *J. Appl. Crystallogr.* 48 (2015) 189–194.
- [72] J. Skibsted, J. Hjorth, H.J. Jakobsen, Correlation between ²⁹Si NMR chemical shifts and mean SiO bond lengths for calcium silicates, *Chem. Phys. Lett.* 172 (1990) 279–283.
- [73] D. Massiot, F. Fayon, M. Capron, I. King, L. Calv, B. Alonso, J. Durand, B. Bujoli, Z. Gan, G. Hoatson, Modelling one- and two-dimensional solid-state NMR, *Magn. Reson. Chem.* 40 (2002) 70–76.
- [74] J.B. d’Espinose de Lacaillerie, C. Fretigny, D. Massiot, MAS NMR spectra of quadrupolar nuclei in disordered solids: The Czjzek model, *J. Magn. Reson.* 192 (2008) 244–251.
- [75] F. Menges, Spectragryph - optical spectroscopy software, Version 1.2.15. (2020) <http://www.effemm2.de/spectr>.
- [76] B. Ma, A. Fernandez-Martinez, A. Mancini, B. Lothenbach, Spectroscopic investigations on structural incorporation pathways of Fe^{III} into zeolite frameworks in cement-relevant environments, *Cem. Concr. Res.* 140 (2021) 106304.
- [77] B. Ravel, M. Newville, ATHENA, ARTEMIS, HEPHAESTUS: Data analysis for X-ray absorption spectroscopy using IFEFFIT, *J. Synchrotron Radiat.* 12 (2005) 537–541.

References

- [78] A. Roßberg, T. Reich, G. Bernhard, Complexation of uranium(VI) with protocatechuic acid-application of iterative transformation factor analysis to EXAFS spectroscopy, *Anal. Bioanal. Chem.* 376 (2003) 631–638.
- [79] A.L. Ankudinov, A.I. Nesvizhskii, J.J. Rehr, Dynamic screening effects in x-ray absorption spectra, *Phys. Rev. B - Condens. Matter Mater. Phys.* 67 (2003) 6.
- [80] D.W. Oscarson, H.B. Hume, Effect of the solid: Liquid ratio on the sorption of Sr²⁺ and Cs⁺ on bentonite, Woodhead Publishing Limited, 1998.
- [81] T. Wagner, D.A. Kulik, F.F. Hingerl, S. V. Dmytrievava, Gem-selektor geochemical modeling package: TSolMod library and data interface for multicomponent phase models, *Can. Mineral.* 50 (2012) 1173–1195.
- [82] T. Thoenen, W. Hummel, U. Berner, E. Curti, The PSI/Nagra Chemical Thermodynamic Database 12/07, 5232 Villigen PSI, 2014.
- [83] B. Lothenbach, D.A. Kulik, T. Matschei, M. Balonis, L. Baquerizo, B. Dilnesa, G.D. Miron, R.J. Myers, Cemdata18: A chemical thermodynamic database for hydrated Portland cements and alkali-activated materials, *Cem. Concr. Res.* 115 (2019) 472–506.
- [84] B. Lothenbach, E. Bernard, U. Mäder, Zeolite formation in the presence of cement hydrates and albite, *Phys. Chem. Earth.* 99 (2017) 77–94.
- [85] B. Ma, B. Lothenbach, Tetrahedral Atom Ordering and Si/Al Ratio on Thermodynamic Properties of Selected Zeolites, 2022.
- [86] H.C. Helgeson, D.H. Kirkham, G.G. Flowers, Theoretical prediction of the thermodynamic behavior of aqueous electrolytes at high pressure and temperature: IV. Calculation of activity coefficients, osmotic coefficients, and apparent molal and standard and relative partial molal properties to 600°C a, *Am. J. Sci.* 281 (1981) 1249–1516.
- [87] C. Labbez, I. Pochard, B. Jönsson, A. Nonat, C-S-H/solution interface: Experimental and Monte Carlo studies, *Cem. Concr. Res.* 41 (2011) 161–168.
- [88] C. Labbez, A. Nonat, I. Pochard, B. Jönsson, Experimental and theoretical evidence of overcharging of calcium silicate hydrate, *J. Colloid Interface Sci.* 309 (2007) 303–307.
- [89] S. V. Churakov, C. Labbez, L. Pegado, M. Sulpizi, Intrinsic acidity of surface sites in calcium silicate hydrates and its implication to their electrokinetic properties, *J. Phys. Chem. C.* 118 (2014) 11752–11762.
- [90] N. Krattiger, B. Lothenbach, S. V. Churakov, Sorption and electrokinetic properties of ASR product and C-S-H: A comparative modelling study, *Cem. Concr. Res.* 146 (2021) 106491.
- [91] G. Zhu, H. Li, X. Wang, S. Li, X. Hou, W. Wu, Q. Tang, G. Scherer, Synthesis of Calcium Silicate Hydrate in highly alkaline system, *J. Am. Ceram. Soc.* 99 (2016) 2778–2785.
- [92] N. Garg, V.O. Özçelik, J. Skibsted, C.E. White, Nanoscale ordering and depolymerization of calcium silicate hydrates in the presence of alkalis, *J. Phys. Chem. C.* 123 (2019) 24873–24883.
- [93] J. Tits, E. Wieland, C.J. Müller, C. Landesman, M.H. Bradbury, Strontium binding by calcium silicate hydrates, *J. Colloid Interface Sci.* 300 (2006) 78–87.
- [94] M. Tsuji, S. Komarneni, Alkali metal ion exchange selectivity of Al-substituted tobermorite, *J. Mater. Res.* 4 (1989) 698–703.
- [95] A. Leemann, L. Lörtscher, L. Bernard, G. Le, B. Lothenbach, R.M. Espinosa-marzal, Mitigation of ASR by the use of LiNO₃ — Characterization of the reaction products, *Cem. Concr. Res.* 59 (2014) 73–86.
- [96] T. H F W, A method for predicting alkali ion concentrations in cement pore solutions, *Advances Cem. Res.* 1 (1987) 5–17.

References

- [97] H. Viallis-Terrisse, A. Nonat, J.C. Petit, Zeta-potential study of calcium silicate hydrates interacting with alkaline cations, *J. Colloid Interface Sci.* 244 (2001) 58–65.
- [98] C.S. Walker, S. Sutou, C. Oda, M. Mihara, A. Honda, Calcium silicate hydrate (C-S-H) gel solubility data and a discrete solid phase model at 25 °C based on two binary non-ideal solid solutions, *Cem. Concr. Res.* 79 (2016) 1–30.
- [99] S. Masoumi, S. Zare, H. Valipour, M.J. Abdolhosseini Qomi, Effective Interactions between Calcium-Silicate-Hydrate Nanolayers, *J. Phys. Chem. C.* 123 (2019) 4755–4766.
- [100] S. Grangeon, F. Claret, Y. Linard, C. Chiaberge, X-ray diffraction: a powerful tool to probe and understand the structure of nanocrystalline calcium silicate hydrates, *Acta Crystallogr. Sect. B Struct. Sci. Cryst. Eng. Mater.* 69 (2013) 465–473.
- [101] V. Stubičan, R. Roy, Infrared spectra of layer-structure silicates, *J. Am. Ceram. Soc.* 44 (1961) 625–627.
- [102] A. Vidmer, G. Sclauzero, A. Pasquarello, Infrared spectra of jennite and tobermorite from first-principles, *Cem. Concr. Res.* 60 (2014) 11–23.
- [103] I.F. Sáez Del Bosque, S. Martínez-Ramírez, M.T. Blanco-Varela, FTIR study of the effect of temperature and nanosilica on the nano structure of C-S-H gel formed by hydrating tricalcium silicate, *Constr. Build. Mater.* 52 (2014) 314–323.
- [104] I. García Lodeiro, D.E. Macphee, A. Palomo, A. Fernández-Jiménez, Effect of alkalis on fresh C-S-H gels. FTIR analysis, *Cem. Concr. Res.* 39 (2009) 147–153.
- [105] J. Higl, D. Hinder, C. Rathgeber, B. Ramming, M. Lindén, Detailed in situ ATR-FTIR spectroscopy study of the early stages of C-S-H formation during hydration of monoclinic C3S, *Cem. Concr. Res.* 142 (2021).
- [106] R.J. Kirkpartick, J.L. Yarger, P.F. McMillan, P. Yu, X. Cong, Raman spectroscopy of C-S-H, tobermorite, and jennite, *Adv. Cem. Based Mater.* 5 (1997) 93–99.
- [107] K. Garbev, P. Stemmermann, L. Black, C. Breen, J. Yarwood, B. Gasharova, Structural features of C-S-H(I) and its carbonation in air-A Raman spectroscopic study. Part I: Fresh phases, *J. Am. Ceram. Soc.* 90 (2007) 900–907.
- [108] Z. Shi, G. Geng, A. Leemann, B. Lothenbach, Synthesis, characterization, and water uptake property of alkali-silica reaction products, *Cem. Concr. Res.* 121 (2019) 58–71.
- [109] S. Ortaboy, J. Li, G. Geng, R.J. Myers, P.J.M.M. Monteiro, R. Maboudian, C. Carraro, Effects of CO₂ and temperature on the structure and chemistry of C-(A)-S-H investigated by Raman spectroscopy, *RSC Adv.* 7 (2017) 48925–48933.
- [110] R. Dupuis, J.S. Dolado, J. Sarga, A. Ayuela, Doping as a way to protect silicate chains in calcium silicate hydrates, *ACS Sustain. Chem. Eng.* 6 (2018) 15015–15021.
- [111] C. Famy, K.L. Scrivener, A.K. Crumbie, What causes differences of C-S-H gel grey levels in backscattered electron images?, *Cem. Concr. Res.* 32 (2002) 1465–1471.
- [112] S. V Churakov, C. Labbez, Thermodynamics and molecular mechanism of Al incorporation in calcium silicate hydrates, *J. Phys. Chem. C.* 121 (2017) 4412–4419.
- [113] S.-Y. Hong, F.P. Glasser, Alkali sorption by C-S-H and C-A-S-H gels: Part II. Role of alumina, *Cem. Concr. Res.* 32 (2002) 1101–1111.
- [114] C. Roosz, P. Vieillard, P. Blanc, S. Gaboreau, H. Gailhanou, D. Braithwaite, V. Montouillout, R. Denoyel, P. Henocq, B. Madé, Thermodynamic properties of C-S-H, C-A-S-H and M-S-H phases: Results from direct measurements and predictive modelling, *Appl. Geochemistry.* 92 (2018) 140–156.
- [115] A.C.A. Muller, K.L. Scrivener, A.M. Gajewicz, P.J. McDonald, Use of bench-top NMR to measure

References

- the density, composition and desorption isotherm of C-S-H in cement paste, *Microporous Mesoporous Mater.* 178 (2013) 99–103.
- [116] G. Renaudin, J. Russias, F. Leroux, F. Frizon, C. Cau-dit-Coumes, Structural characterization of C-S-H and C-A-S-H samples-Part I: Long-range order investigated by Rietveld analyses, *J. Solid State Chem.* 182 (2009) 3312–3319.
- [117] G. Geng, R.J. Myers, M. Javad, A. Qomi, P.J.M. Monteiro, Densification of the interlayer spacing governs the nanomechanical properties of calcium-silicate-hydrate, *Sci. Rep.* (2017) 1–8.
- [118] G. Geng, R.J. Myers, J. Li, R. Maboudian, C. Carraro, D.A. Shapiro, P.J.M. Monteiro, Aluminum-induced dreierketten chain cross-links increase the mechanical properties of nanocrystalline calcium aluminosilicate hydrate, *Sci. Rep.* 7 (2017) 44032.
- [119] Y.L. Yaphary, D. Lau, F. Sanchez, C.S. Poon, Effects of sodium/calcium cation exchange on the mechanical properties of calcium silicate hydrate (C-S-H), *Constr. Build. Mater.* 243 (2020) 118283.
- [120] I. Lognot, I. Klur, A. Nonae, NMR and Infrared Spectroscopies of C-S-H and Al-Substituted C-S-H Synthesised in Alkaline Solutions, in: *Nucl. Magn. Reson. Spectrosc. Cem. -Based Mater.*, 1998: pp. 189–196.
- [121] P. Nieto, H. Zanni, Polymerization of alkaline-calcium-silicate hydrates obtained by interaction between alkali-silica solutions and calcium compounds. A ^{29}Si nuclear magnetic resonance study, *J. Mater. Sci.* 32 (1997) 3419–3425.
- [122] M.D. Andersen, H.J. Jakobsen, J. Skibsted, A new aluminium-hydrate species in hydrated Portland cements characterized by ^{27}Al and ^{29}Si MAS NMR spectroscopy, *Cem. Concr. Res.* 36 (2006) 3–17.
- [123] M. Daugaard Andersen, H.J. Jakobsen, J. Skibsted, Incorporation of aluminum in the calcium silicate hydrate (C-S-H) of hydrated Portland cements: A high-field ^{27}Al and ^{29}Si MAS NMR investigation, *Inorg. Chem.* 42 (2003) 2280–2287.
- [124] G. Geng, R.N. Vasin, J. Li, M.J.A. Qomi, J. Yan, H.R. Wenk, P.J.M. Monteiro, Preferred orientation of calcium aluminosilicate hydrate induced by confined compression, *Cem. Concr. Res.* 113 (2018) 186–196.
- [125] J. Li, G. Geng, R. Myers, Y.S. Yu, D. Shapiro, C. Carraro, R. Maboudian, P.J.M. Monteiro, The chemistry and structure of calcium (alumino) silicate hydrate: A study by XANES, ptychographic imaging, and wide- and small-angle scattering, *Cem. Concr. Res.* 115 (2019) 367–378.
- [126] J. Li, W. Zhang, K. Garbev, P.J.M. Monteiro, Coordination environment of Si in calcium silicate hydrates, silicate minerals, and blast furnace slags: A XANES database, *Cem. Concr. Res.* 143 (2021) 106376.
- [127] J. Li, W. Zhang, K. Garbev, G. Beuchle, P.J.M. Monteiro, Influences of cross-linking and Al incorporation on the intrinsic mechanical properties of tobermorite, *Cem. Concr. Res.* 136 (2020) 106170.
- [128] T. Runčevski, R.E. Dinnebier, O. V. Magdysyuk, H. Pöllmann, Crystal structures of calcium hemicarboaluminate and carbonated calcium hemicarboaluminate from synchrotron powder diffraction data, *Acta Crystallogr. Sect. B Struct. Sci.* 68 (2012) 493–500.
- [129] E. Tajuelo Rodriguez, K. Garbev, D. Merz, L. Black, I.G. Richardson, Thermal stability of C-S-H phases and applicability of Richardson and Groves' and Richardson C-(A)-S-H(I) models to synthetic C-S-H, *Cem. Concr. Res.* 93 (2017) 45–56.
- [130] R.. Smith, P. Bayliss, Interlayer desorption of CSH(1), *Cem. Concr. Res.* 2 (1972) 634–646.
- [131] P. Bayliss, Further interlayer desorption studies of CSH(1), *Cem. Concr. Res.* 3 (1973) 185–188.
- [132] M.W. Barnes, B.E. Scheetz, The chemistry of Al-tobermorite and its coexisting phases at 175°C,

References

- MRS Proc. 179 (1989) 243–272.
- [133] R.D. Shannon, Revised effective ionic radii and systematic studies of interatomic distances in halides and chalcogenides, *Acta Crystallogr. Sect. A.* 32 (1976) 751–767.
- [134] J. Schreiner, F. Goetz-Neunhoffer, J. Neubauer, D. Jansen, Hydrothermal synthesis of 11 Å tobermorite – Effect of adding metakaolin to the basic compound, *Appl. Clay Sci.* 185 (2020).
- [135] M.D. Jackson, J. Moon, E. Gotti, R. Taylor, S.R. Chae, M. Kunz, A.H. Emwas, C. Meral, P. Guttman, P. Levitz, H.R. Wenk, P.J.M. Monteiro, Material and elastic properties of Al-tobermorite in ancient roman seawater concrete, *J. Am. Ceram. Soc.* 96 (2013) 2598–2606.
- [136] S. Komarneni, D.M. Roy, R. Roy, Al-substituted tobermorite: shows cation exchange, *Cem. Concr. Res.* 12 (1982) 773–780.
- [137] N. Hara, N. Inoue, Thermal behaviour of 11Å tobermorite and its lattice parameters, *Cem. Concr. Res.* 10 (1980) 53–60.
- [138] K. Matsui, J. Kikuma, M. Tsunashima, T. Ishikawa, S.Y. Matsuno, A. Ogawa, M. Sato, In situ time-resolved X-ray diffraction of tobermorite formation in autoclaved aerated concrete: Influence of silica source reactivity and Al addition, *Cem. Concr. Res.* 41 (2011) 510–519.
- [139] Y. Going, C.S. Yim, Influence of alumina on Hydrothermal synthesis of 11 Å tobermorite, *Korean J. Mater. Res.* 15 (2005) 97–105.
- [140] S. Diamond, J.L. White, W.L. Dolch, Effects of isomorphous substitution in hydrothermally-synthesized tobermorite, *Am. Mineral.* 51 (1966) 388–401.
- [141] Y. Yan, S.Y. Yang, G.D. Miron, I.E. Collings, E. L'Hôpital, J. Skibsted, F. Winnefeld, K. Scrivener, B. Lothenbach, Effect of alkali hydroxide on calcium silicate hydrate (C-S-H), *Cem. Concr. Res.* 151 (2022).
- [142] P.F. McMillan, G.H. Wolf, B.T. Poe, Vibrational spectroscopy of silicate liquids and glasses, *Chem. Geol.* 96 (1992) 351–366.
- [143] L. Black, C. Breen, J. Yarwood, K. Garbev, P. Stemmermann, B. Gasharova, Structural features of C-S-H(I) and its carbonation in air-A Raman spectroscopic study. Part II: Carbonated phases, *J. Am. Ceram. Soc.* 90 (2007) 908–917.
- [144] N.Y. Mostafa, A.A. Shaltout, H. Omar, S.A. Abo-El-Enein, Hydrothermal synthesis and characterization of aluminium and sulfate substituted 1.1 nm tobermorites, *J. Alloys Compd.* 467 (2009) 332–337.
- [145] M. Horgnies, J.J. Chen, C. Bouillon, Overview about the use of fourier transform infrared spectroscopy to study cementitious materials, *WIT Trans. Eng. Sci.* 77 (2013) 251–262.
- [146] M. Montes, E. Pato, P.M. Carmona-Quiroga, M.T. Blanco-Varela, Role of tobermorite on the hydration of C3A in the presence and absence of gypsum, in: 15th Int. Congr. Chem. Cem., 2019: pp. 1–8.
- [147] W. Mozgawa, The relation between structure and vibrational spectra of natural zeolites, *J. Mol. Struct.* 596 (2001) 129–137.
- [148] L.W. Finger, R.M. Hazen, R.J. Hemley, BaCuSi₂O₆: a new cyclosilicate with four-membered tetrahedral rings, *Am. Mineral.* 74 (1989) 952–955.
- [149] K. Yasuda, S. Takeya, M. Sakashita, H. Yamawaki, R. Ohmura, Binary ethanol-methane clathrate hydrate formation in the system CH₄-C₂H₅OH-H₂O: confirmation of structure II hydrate formation, *J. Phys. Chem. C.* 113 (2009) 12598–12601.
- [150] D. Li, G.M. Bancroft, M.E. Fleet, X.H. Feng, Y. Pan, Al K-edge XANES spectra of aluminosilicate minerals, *Am. Mineral.* 80 (1995) 432–440.

References

- [151] G. Geng, R.J. Myers, Y.S. Yu, D.A. Shapiro, R. Winarski, P.E. Levitz, D.A.L. Kilcoyne, P.J.M. Monteiro, Synchrotron X-ray nanotomographic and spectromicroscopic study of the tricalcium aluminate hydration in the presence of gypsum, *Cem. Concr. Res.* 111 (2018) 130–137.
- [152] D.A. McKeown, Aluminum X-ray absorption near-edge spectra of some oxide minerals: Calculation versus experimental data, *Phys. Chem. Miner.* 16 (1989) 678–683.
- [153] E. Wieland, R. Dähn, M. Vespa, B. Lothenbach, Micro-spectroscopic investigation of Al and S speciation in hardened cement paste, *Cem. Concr. Res.* 40 (2010) 885–891.
- [154] G. Geng, J. Li, Y.S. Yu, D.A. Shapiro, D.A.L. Kilcoyne, P.J.M. Monteiro, Nanometer-resolved spectroscopic study reveals the conversion mechanism of $\text{CaO}\cdot\text{Al}_2\text{O}_3\cdot 10\text{H}_2\text{O}$ to $2\text{CaO}\cdot\text{Al}_2\text{O}_3\cdot 8\text{H}_2\text{O}$ and $3\text{CaO}\cdot\text{Al}_2\text{O}_3\cdot 6\text{H}_2\text{O}$ at an elevated temperature, *Cryst. Growth Des.* 17 (2017) 4246–4253.
- [155] P. Ildefonse, D. Cabaret, P. Saintavit, G. Calas, A.M. Flank, P. Lagarde, Aluminium X-ray absorption near edge structure in model compounds and earth's surface minerals, *Phys. Chem. Miner.* 25 (1998) 112–121.
- [156] V.O. Özçelik, C.E. White, Nanoscale charge-balancing mechanism in alkali-substituted calcium-silicate-hydrate gels, *J. Phys. Chem. Lett.* 7 (2016) 5266–5272.
- [157] S. Barzgar, Y. Yan, M. Tarik, J. Skibsted, C. Ludwig, B. Lothenbach, The effect of aluminum concentration on Al uptake in C-S-H, *Resour. Conserv. Recycl.* submitted (2022).
- [158] J.R. Houston, R.S. Maxwell, S.A. Carroll, Transformation of meta-stable calcium silicate hydrates to tobermorite: Reaction kinetics and molecular structure from XRD and NMR spectroscopy, *Geochem. Trans.* 10 (2009) 1–14.
- [159] E.T. Rodriguez, I.G. Richardson, L. Black, E. Boehm-Courjault, A. Nonat, J. Skibsted, Composition, silicate anion structure and morphology of calcium silicate hydrates (C-S-H) synthesised by silica-lime reaction and by controlled hydration of tricalcium silicate (C3S), *Adv. Appl. Ceram.* 114 (2015) 362–371.
- [160] R. Zarzuela, M. Luna, L.M. Carrascosa, M.P. Yeste, I. Garcia-Lodeiro, M.T. Blanco-Varela, M.A. Cauqui, J.M. Rodríguez-Izquierdo, M.J. Mosquera, Producing C-S-H gel by reaction between silica oligomers and portlandite: A promising approach to repair cementitious materials, *Cem. Concr. Res.* 130 (2020) 106008.
- [161] A. Kumar, B.J. Walder, A. Kunhi Mohamed, A. Hofstetter, B. Srinivasan, A.J. Rossini, K. Scrivener, L. Emsley, P. Bowen, The atomic-level structure of cementitious calcium silicate hydrate, *J. Phys. Chem. C.* 121 (2017) 17188–17196.
- [162] Y. Yan, B. Ma, G.D. Miron, D.A. Kulik, K. Scrivener, B. Lothenbach, Effect of alkali hydroxide on Al uptake in calcium silicate hydrate (C-S-H) with $\text{Ca/Si} = 1$, 2022.
- [163] K. De Weerd, B. Lothenbach, M.R. Geiker, Comparing chloride ingress from seawater and NaCl solution in Portland cement mortar, *Cem. Concr. Res.* 115 (2019) 80–89.
- [164] E. Bernard, A. Jenni, M. Fisch, D. Grolimund, U. Mäder, Micro-X-ray diffraction and chemical mapping of aged interfaces between cement pastes and Opalinus Clay, *Appl. Geochemistry.* 115 (2020).
- [165] P. Lalan, A. Dauzères, L. De Windt, D. Bartier, J. Sammaljärvi, J.D. Barnichon, I. Techer, V. Detilleux, Impact of a 70 °C temperature on an ordinary Portland cement paste/claystone interface: An in situ experiment, *Cem. Concr. Res.* 83 (2016) 164–178.

Curriculum Vitae

Yiru Yan

Im Grund 5

8600 Dübendorf

Switzerland

Telephone: (+41)0 77 980 6691

E-mail: yiru.yan@empa.ch

Education:

- Since 2018: **PhD at EPFL (Ecole polytechnique fédéral de Lausanne)** - Switzerland and **EMPA (Swiss Federal Laboratories for Materials Science and Technology)** - Dübendorf - Suisse.
- 2014 - 2017: **Master's degree: Materials Science and Engineering at Southeast University** - Nanjing - China.
- 2010 - 2014: **Bachelor's degree: Materials Science and Engineering at Southeast University** - Nanjing - China.

Professional experience:

- Since March 2018: **PhD in Materials science and engineering** - EMPA - Dübendorf, Switzerland.

Effect of alkali, aluminium and equilibration time in calcium silicate hydrate (C-S-H). Thesis director: Karen Scrivener, Co-director: Barbara Lothenbach. Main objectives: Project management, literature review, protocol optimisation of C-S-H synthesis, characterisation and determination of the structure.

- September 2014 - 2018: **Master at Southeast University** (Nanjing - China):

Topic 1: Study on structure and mechanical properties of analogous calcium-silicate-hydrates crystals and calcium-silicate-hydrates

Topic 2: Design of a novel nano-composite for thermal energy storage: a theoretical and experimental study.

Topic 3: Preparation and characterization of a surface modified aqueous silica sol

Topic 4: Study on rubber matrix piezoelectric-damping composite

- December 2012 - June 2014: **Student research project and graduate thesis at Southeast University** (Nanjing - China):

Preparation and performance of high-strength ceramsite lightweight aggregates made of sediment.

Skills:

Characterisation methods: IC, ICP, XRD, TGA, DSC, FTIR, Raman, UV-Visible spectroscopy

Some experience also with: SEM, EDX, DLS, Synchrotron based XANES and zeta potential measurement, mechanical/ thermal testings, first-principles method, density functional theory, molecular dynamics method

Computer skills: Microsoft Office, X'Pert HighScore Plus, Gems, Dmfit, Vesta, Material Studio, VASP, Jade, Origin, Chemical Draw.

Curriculum Vitae

Supervision of trainees: Introduction to laboratory work, materials characterisation, analysis and interpretation of results.

Languages: Chinese: native, English: fluent.

Publications and patent:

1. **Y. Yan**, S.Y. Yang, G.D. Miron, I.E. Collings, E. L'Hôpital, J. Skibsted, F. Winnefeld, K. Scrivener, B. Lothenbach, Effect of alkali hydroxide on calcium silicate hydrate (C-S-H), *Cem. Concr. Res.* 151 (2022) 106636.
2. E. Bernard, **Y. Yan**, B. Lothenbach, Effective cation exchange capacity of calcium silicate hydrates (C-S-H), *Cem. Concr. Res.* 143 (2021) 106393
3. S.-Y. Yang, **Y. Yan**, B. Lothenbach, J. Skibsted, Sodium and tetrahedral aluminium in cementitious calcium-aluminate-silicate hydrate phases (C-A-S-H), *J. Phys. Chem. C.* 125 (2021) 27975–27995
4. G.D. Miron, D.A. Kulik, **Y. Yan**, J. Tits, B. Lothenbach, Extensions of CASH+ thermodynamic solid solution model for the uptake of alkali metals and alkaline earth metals in C-S-H, *Cem. Concr. Res.* 152 (2022) 106667
5. B. Lothenbach, D. Jansen, **Y. Yan**, J. Schreiner, Solubility and characterization of synthesized Al-tobermorite, *Cem. Concr. Res.* under review (2022)
6. S. Barzgar, **Y. Yan**, M. Tarik, J. Skibsted, C. Ludwig, B. Lothenbach, The effect of aluminum concentration on Al uptake in C-S-H, *Resour. Conserv. Recycl.* submitted (2022).
7. **Y. Yan**, B. Ma, G.D. Miron, D.A. Kulik, K. Scrivener, B. Lothenbach, Effect of alkali hydroxide on Al uptake in calcium silicate hydrate (C-S-H) with Ca/Si = 1, *Cem. Concr. Res.* submitted
8. **Y. Yan**, K. Scrivener, B. Lothenbach, Effect of time on Al uptake in calcium silicate hydrate, in preparation
9. J. Jiang, **Y. Yan**, D. Hou, J. Yu, Understanding the deformation mechanism and mechanical characteristics of cementitious mineral analogues from first principles and reactive force field molecular dynamics, *Phys. Chem. Chem. Phys.* 20 (2018) 13920–13933.
10. J. Jiang, Q. Zheng, D. Hou, **Y. Yan**, H. Chen, W. She, S. Wu, D. Guo, W. Sun, Calcite crystallization in the cement system: Morphological diversity, growth mechanism and shape evolution, *Phys. Chem. Chem. Phys.* 20 (2018) 14174–14181.
11. J. Jiang, Q. Zheng, **Y. Yan**, D. Guo, F. Wang, S. Wu, W. Sun, Design of a novel nanocomposite with C-S-H@LA for thermal energy storage: A theoretical and experimental study, *Appl. Energy.* 220 (2018) 395–407
12. J. Jiang, **Y. Yan**, Z. Wang, H. Wang, A Preparation Method of Piezoelectric Rubber

Curriculum Vitae

Damping Composite, CN 104592647 A

Conference proceedings:

13. **Y. Yan**, B. Lothenbach, A. Di Giacomo, K. Scrivener, Structure of synthetic calcium silicate hydrate in presence of aluminium and alkali, in: Mech. Model. Waste / Cem. Interact., Karlsruhe, Germany, 2019: p. 109.
14. **Y. Yan**, B. Lothenbach, A. Di Giacomo, K. Schrivener, Structure of synthetic calcium silicate hydrate (C-S-H) in presence of aluminum and alkalis, in: 15th Int. Congr. Chem. Cem., Prague, Czech Republic, 2019: pp. 3–7.
15. **Y. Yan**, B. Lothenbach, K. Scrivener, Effect of alkali hydroxide on calcium silicate hydrate, in: ERICA-CASH II Conf., Heidelberg, Germany, 2021.